United States
Environmental Protection
Agency

Office of Air Quality
Planning and Standards
Research Triangle Park, NC 27711

EPA-454/R-94-015
April 1994

Air

EPA

DEVELOPMENT AND TESTING OF A DRY DEPOSITION ALGORITHM (Revised)

EPA-454/R-94-015

Development and Testing of a Dry Deposition Algorithm (Revised)

U.S. Environmental Protection Agency
Office of Air Quality Planning and Standards
Technical Support Division
Research Triangle Park, NC 27711

April 1994

This report has been reviewed by the Office of Air Quality Planning and Standards, U.S. Environmental Protection Agency, and has been approved for publication. Any mention of trade names and commercial products is not intended to constitute endorsement or recommendation for use.

EPA-454/R-94-015

ACKNOWLEDGEMENTS

This report has been prepared by Sigma Research Corporation and funded by the U.S. Environmental Protection Agency under Contract No. 68-D90067, with Jawad S. Touma as Work Assignment Manager.

PREFACE

The ability to accurately estimate deposition due to atmospheric releases is important to the modeling community. Limitations of the Industrial Source Complex (ISC2) models (dated 92273) for estimating deposition of small particles have been known for some time. An improved algorithm for estimating deposition for a wide range of pollutants has been developed and tested and is described in this report.

The Environmental Protection Agency must conduct a formal and public review before the Agency can recommend for routine use this new algorithm in regulatory analyses. This report is being released to establish a basis for reviews of the capabilities of this methodology in routine dispersion modeling analyses. This report is one part of a larger set of information on the ISC2 models that must be considered before any formal changes can be adopted.

The report "Development and Testing of a Dry Deposition Algorithm", EPA-454/R-92-017, was issued in May 1993. EPA discovered that a typographical error in a journal paper used as a basis for one of the models (ADOM 2) had propagated to the report. The corrected equation has been re-analyzed. In addition, a revised form of the Stokes number equation, based on Slinn (1982), was used in the re-analysis. Because the performance of the corrected model was significantly different than that originally reported, this new report is being issued as an entire replacement document.

Table of Contents

Section			Page
1.	Introduction		1-1
2.	Dry Deposition		2-1
	2.1 Dry Deposition of Particulate Matter		2-5
	2.1.1	ISC Method	2-7
	2.1.2	CARB Model	2-13
	2.1.3	ADOM Model - Particles	2-21
	2.1.4	UAM-V Model	2-26
	2.2 Dry Deposition of Gaseous Pollutants		2-26
	2.2.1	RADM Model	2-27
	2.2.2	ADOM Model - Gases	2-28
	2.2.3	NOAA/ARL Models	2-31
3.	Plume Depletion Techniques		3-1
	3.1 Source Depletion		3-1
	3.2 Surface Depletion		3-2
	3.3 K-theory Approach		3-2
	3.4 Modified Source Depletion		3-4
4.	Calculation of Meteorological Variables		4-1
	4.1 Unstable/Neutral Conditions		4-1
	4.2 Stable Conditions		4-5
5.	Model Evaluation Protocol		5-1
	5.1 Evaluation Approach		5-1
	5.2 Stratification of Deposition Velocity Datasets		5-2
	5.3 Comparison of Predictions and Observations		5-5
	5.4 Scoring Model Performance Using Composite Measures		5-7
6.	Model Evaluation Data Bases		6-1
	6.1 Particle Data Sets		6-1
	6.2 Gas Data Sets		6-2

Table of Contents - Continued

7. Results of Model Evaluation 7-1
7.1 Particle Deposition Models 7-1
7.1.1 Full Data Sets 7-4
7.1.2 Stratification by Particle Diameter 7-7
7.1.3 Stratification by Roughness Length 7-14
7.1.4 Stratification by Leaf Area Index 7-17
7.1.5 Stratification by Day vs Night 7-19
7.1.6 Stratification by Friction Velocity 7-20
7.1.7 Stratification by Temperature 7-22
7.1.8 Estimation of CPM from Tables 7-25
7.2 Discussion of Model Performance 7-25
7.2.1 Uniform Size Distribution 7-25
7.2.2 Sulfate Particle Distribution 7-29
7.2.3 Model Performance When Zeros are Included 7-29
7.2.4 Cumulative Distribution Results 7-34
7.2.5 Selection of Best Performing Deposition Model 7-34

8. Summary and Conclusions 8-1

9. References 9-1

Appendix A Estimation of ISC Deposition Velocity A-1
Appendix B Supplemental Graphics B-1
Appendix C Observational Particle Deposition Velocity Data Sets C-1
Appendix D Predicted Deposition Velocities vs Particle Diameter D-1
Appendix E Implementation of the Modified Source Depletion Method in ISC2 ..... E-1

List of Figures

Figure 2-1. Summary of observed SO_2 deposition velocities 2-3

Figure 2-2. Observed deposition velocities (v_d) as a function of particle size for 1.5 g/cm^3 density particles. 2-4

Figure 2-3. Predicted deposition velocities for $u_* = 100$ cm/s and particle densities of 1, 4, and 11.5 g/cm^3. 2-6

Figure 2-4. Illustration of the reflection coefficient scheme used in ISC for reflection coefficients of 0.0, 0.5, and 1.0. 2-8

Figure 2-5. Reflection coefficient as a function of the gravitational settling velocity. 2-12

Figure 2-6. Deposition velocity as a function of particle diameter as predicted by the Sehmel/CARB model for three different values of ambient temperature (0°, 60°, 100°F). 2-18

Figure 2-7. Deposition velocity as a function of particle diameter as predicted by the Sehmel/CARB model for surface roughness lengths of 0.001, 0.01, 3, and 10 cm. 2-19

Figure 5-1. Schematic illustration of division of deposition velocity data into subsets. . . . 5-4

Figure 7-1. A summary of absolute value of the fractional bias using all data 7-8

Figure 7-2. A summary of absolute value of the fractional bias averaged over all 12 subsets. 7-9

Figure 7-3a. Co-plot of fractional bias of the standard deviation for each of the deposition models. 7-10

Figure 7-3b. Co-plot of fractional bias of the 11 largest deposition velocities for each of the deposition models. 7-11

Figure 7-3c. Co-plot of fractional bias of the 17 smallest deposition velocities for each of the deposition models. 7-12

Figure 7-3d. Co-plot of fractional bias of the 11 largest and 17 smallest deposition velocities for each of the deposition models. 7-13

Figure 7-4. A summary of the total CFB of the six types of data subsets 7-24

Figure 7-5. A ranking of the models by CPM 7-27

Figure 7-6. A summary of the MCM for each unique model pair. 7-28

Figure 7-7. A ranking of the models by CPM 7-31

Figure 7-8. A summary of the MCM for each unique mode pair 7-32

Figure 7-9. A ranking of the models by CPM 7-33

Figure B-1a. Scatter plot of observed deposition velocity (cm/s) versus model predicted deposition velocity (cm/s) for the complete small particle data set. B-1

Figure B-1b. Scatter plot of observed deposition velocity (cm/s) versus model predicted deposition velocity (cm/s) for the complete small particle data set. B-2

Figure B-1c. Scatter plot of observed deposition velocity (cm/s) versus model predicted deposition velocity (cm/s) for the complete small particle data set. B-3

Figure B-1d. Scatter plot of observed deposition velocity (cm/s) versus model predicted deposition velocity (cm/s) for the complete small particle data set. B-4

List of Figures - Continued

Figure B-1e. Scatter plot of observed deposition velocity (cm/s) versus model predicted deposition velocity (cm/s) for the complete small particle data set. B-5

Figure B-1f. Scatter plot of observed deposition velocity (cm/s) versus model predicted deposition velocity (cm/s) for the complete small particle data set. B-6

Figure B-1g. Scatter plot of observed deposition velocity (cm/s) versus model predicted deposition velocity (cm/s) for the complete small particle data set. B-7

Figure B-1h. Scatter plot of observed deposition velocity (cm/s) versus model predicted deposition velocity (cm/s) for the complete small particle data set. B-8

Figure B-1i. Scatter plot of observed deposition velocity (cm/s) versus model predicted deposition velocity (cm/s) for the complete small particle data set. B-9

Figure B-1j. Scatter plot of observed deposition velocity (cm/s) versus model predicted deposition velocity (cm/s) for the complete small particle data set. B-10

Figure B-2a. Cumulative probability plot of deposition velocity (cm/s) using the complete small particle data set. B-11

Figure B-2b. Cumulative probability plot of deposition velocity (cm/s) using the complete small particle data set. B-12

Figure B-2c. Cumulative probability plot of deposition velocity (cm/s) using the complete small particle data set. B-13

Figure B-2d. Cumulative probability plot of deposition velocity (cm/s) using the complete small particle data set. B-14

List of Figures - Concluded

Figure D-1. Predicted deposition velocity for the CARB-based models for $u_* = 10$ cm/s, $z_o = 10$ cm, LAI = 1.0, $\rho = 1.0$ g/cm^3, and neutral stability. D-1

Figure D-2. Predicted deposition velocity for the ADOM-based models for $u_* = 10$ cm/s, $z_o = 10$ cm, LAI = 1.0, $\rho = 1.0$ g/cm^3, and neutral stability. D-2

Figure D-3. Predicted deposition velocity for the UAM-based models for $u_* = 10$ cm/s, $z_o = 10$ cm, LAI = 1.0, $\rho = 1.0$ g/cm^3, and neutral stability. D-3

Figure E-1. Illustration of the depletion factor FQ and the corresponding profile correction factor P(x,z). E-2

Figure E-2. Vertical profile of concentration before and after applying FQ and P(x,z) shown in Figure E-1. . . . . E-3

List of Tables

Table 1-1 Core Particle Deposition Models and Other Algorithms Included in Study .. 1-3

Table 2-1 Factors Influencing Dry Deposition Rates 2-2

Table 2-2 Typical Surface Roughness Lengths for Various Land Use Types 2-17

Table 2-3 Values of Chemical Input Parameters Required by the RADM Deposition Model 2-29

Table 2-4 Summary of Input Requirements of RADM Deposition Module for Gases 2-30

Table 2-5 Leaf Area Index Values as a Function of Land Use Type and Season 2-32

Table 2-6 Summary of Input Requirements of ADOM-type Deposition Modules for Gases 2-33

Table 4-1 Values of Net Radiation Constants 4-3

Table 4-2 Minimum Values of Monin-Obukhov Length During Stable Conditions for Various Land Use Types .. 4-7

Table 7-1 A Summary of the Model Designations 7-2

Table 7-2 A Summary of the Stratifications Made to the Small Particle Data Set (N = 168) 7-3

Table 7-3 A Summary of the Fractional and Composite Statistical Measures for Each of the 10 Models Examined 7-6

Table 7-4 A Summary of the Fractional and Composite Statistical Measures for Each of the Models Examined 7-15

Table 7-5 A Summary of the Fractional and Composite Statistical Measures for Each of the Models Examined 7-16

List of Tables - Concluded

Table 7-6	A Summary of the Fractional and Normalized Statistical Measures for Each of the Models Examined	7-18
Table 7-7	A Summary of the Fractional and Normalized Statistical Measures for Each of the Models Examined	7-20
Table 7-8	A Summary of the Fractional and Normalized Statistical Measures for Each of the Models Examined	7-21
Table 7-9	A Summary of the Fractional and Normalized Statistical Measures for Each of the Models Examined	7-23
Table 7-10	Summary of Composite Statistical Measures that Illustrate how the CPM Arises for the CARB 1 Model	7-26
Table 7-11	Aerosol Mass Fraction as a Function of Size Distribution for Two Assumed Aged Sulfate Distributions	7-30
Table C-1	Observational Particle Deposition Velocity Data Sets	C-1

1. Introduction

The intermedia transfer of pollutants from the atmosphere to land, water, and vegetation is an increasingly important concern in many regulatory environmental impact analyses. The process of dry deposition is a critical transport route for pollutant movement across the air/surface interface. However, current regulatory modeling tools have limitations in their ability to evaluate dry deposition. For example, the Industrial Source Complex (ISC) model contains an empirical dry deposition algorithm based on reflection coefficients which is appropriate for large particles dominated by gravitational settling (i.e., particle diameters larger than approximately 20 μm). However, this algorithm is not designed for small particles or gaseous pollutants, both of which are of concern for many analyses involving criteria pollutants and toxic air pollutants. Recognizing the need for a generalized, scientifically-credible dry deposition algorithm capable of estimating deposition fluxes for a wide range of pollutants, the U.S. Environmental Protection Agency (EPA) has sponsored a study to develop such an algorithm for use in the ISC model. The primary objectives of the present study are to identify deposition models suitable for regulatory use, evaluate and intercompare several of the techniques, and implement the most appropriate approach into the ISC model.

The dry deposition flux (F) of a pollutant at a reference height above the surface can be defined as the product of the ambient concentration of the pollutant, (χ), and a "deposition velocity" (v_d), i.e., $F = \chi v_d$. Therefore, a model to predict deposition fluxes requires an estimation of both the ambient concentration and deposition velocity. The EPA has established procedures for estimating ambient pollutant concentrations, which can be used for deposition modeling as well. However, an approved procedure for calculating deposition velocities is not established. The focus on this study is the testing and evaluation of algorithms to compute deposition velocities for particulate matter.

The following criteria are being applied in the selection of the dry deposition velocity algorithms for evaluation.

(1) The algorithm should parameterize the important physical/chemical processes known to determine the rate of deposition.

(2) The scheme should require only routinely and/or readily available meteorological, chemical, and physical input data.

(3) The algorithm should have modest computational requirements.

(4) The formulation should be general enough to accommodate, with the proper input parameters, a wide variety of pollutants.

Although the number of models to be tested must be limited, hybrid approaches, consisting of the best components of two or more models, have been constructed for some of the particle deposition velocity models. Various components of these models have been modified or enhanced in order to provide increased generality or to eliminate weaknesses in the approach. Table 1-1 lists the base (core) particle deposition models which have been evaluated in this study along with the gas deposition, plume depletion, and meteorological processing algorithms which have been reviewed.

Because pollutants that are deposited are removed from the plume, there is some feedback between upwind plume depletion and the ambient concentration at a particular receptor. Therefore, a second component of deposition which is reviewed in this study is the method used to track and deplete a pollutant from the plume as it travels downwind and deposits onto the surface. Among the methods which have been proposed to incorporate plume depletion into the Gaussian plume framework are source depletion, surface depletion, modified source depletion, and K-theory methods. Based on a review of the literature, the advantages and disadvantages of these techniques are discussed in Section 3.

Most dry deposition algorithms require as input certain micrometeorological parameters such as the surface friction velocity and Monin-Obukhov length. In order to provide a complete system for modeling deposition, a revised ISC modeling system must include a technique for estimating these parameters. A review of some previous studies which have tested various methods for the computation of friction velocity and Monin-Obukhov length from routinely available meteorological observations is discussed in Section 4.

The model evaluation protocol used in the present study, described in Section 5, is based on the Cox-Tikvart protocol. It represents EPA's recommended approach to the evaluation of model performance. Section 6 contains a summary of the observational particle deposition data bases used in the model evaluation efforts (described in Section 7.1) as well as some gas deposition data for possible use in future evaluation work. A summary of the recommendations and conclusions reached to-date is contained in Section 8.

Table 1-1
Core Particle Deposition Models and Other Algorithms Included in the Study

Type	Model	References
Deposition velocity models (particles)	CARB/Sehmel model	Sehmel and Hodgson (1978) Sehmel (1980)
	ADOM/CALPUFF/CALGRID models	Pleim et al. (1984) Scire et al. (1990) Yamartino et al. (1992)
	UAM-V model	Gray et al. (1991)
	ISC reflection coefficient scheme	Dumbauld et al. (1976) Overcamp (1976) Bowers et al. (1979)
Deposition velocity models (gases)	RADM model	Wesely (1989) Walcek et al. (1986) Shieh et al. (1986)
	ADOM/CALPUFF/CALGRID models	Pleim et al. (1984) Scire et al. (1990) Yamartino et al. (1992)
	NOAA/ARL models	Meyers and Baldocchi (1988) Baldocchi et al. (1987) Meyers (1987) Hicks et al. (1987)
Plume depletion techniques	Source depletion Surface depletion K-theory approach Modified source depletion	Chamberlain (1953) Horst (1977) Rao (1981) Horst (1983)
Meteorological preprocessor	Holtslag and van Ulden technique	Holtslag and van Ulden (1983) van Ulden and Holtslag (1985) Hanna and Chang (1992)

2. Dry Deposition

Many complex processes are involved in the transfer and deposition of pollutants at the surface. Sehmel (1980) compiled a list of the factors known to influence dry deposition rates (see Table 2-1). Although it is not practical to incorporate all of the factors listed in the table into a routinely-applied regulatory deposition model, algorithms with only modest data requirements exist which parameterize many of the processes which typically dominate deposition rates. Among the most important factors included in Table 2-2 are pollutant properties such as the size and density of particles, and the solubility, reactivity, and diffusivity of gases; surface characteristics such as the surface roughness, vegetation type, amount, and physiological state; and atmospheric variables including the stability, friction velocity, and turbulence intensity. Hicks (1982) noted the important differences controlling the deposition of larger particles (e.g., gravitational settling, inertial impaction) and those controlling gases (e.g., turbulence, molecular diffusion). Deposition of small particles is complicated by the fact that because of their intermediate size, they may be influenced by the processes affecting gases and large particles.

Due to the number and variability of the factors influencing dry deposition rates, measured values of deposition velocities exhibit considerable variability. For example, SO_2 deposition velocity observations summarized by Sehmel (1980) range over two orders of magnitude (Figure 2-1). Particle deposition velocities (Slinn et al., 1978) show an even greater variability. This is illustrated in Figure 2-2, which shows the deposition velocity as a function of particle size as measured in two wind tunnel experiments. The deposition velocity ranges from over 10 cm/s (for > 10 μm diameter particles) to less than 0.01 cm/s (0.25 μm diameter particle). Although it is not practical to include in the deposition model all of the variables listed in Table 2-1, it is possible to parameterize many of the most important effects known to control deposition rates in terms of routinely-available variables which describe the state of the atmosphere, surface conditions, and pollutant properties.

The treatment of particle resuspension is not being treated in the current study. The problem of particle resuspension is very complex, involving highly variable and site-specific factors. Sehmel (1984) notes that experimentally-determined resuspension factors vary over eight orders of magnitude (i.e., 10^{-10} to 10^{-2} m^{-1}). Among the factors influencing resuspension rates are soil/surface moisture, mean wind speed, gust intensity, particle/soil/surface properties, and the nature, frequency, and magnitude of mechanical disturbances of the surface. Development of a generalized particle resuspension model would involve a substantial effort beyond the scope of the present study.

Table 2-1
Factors Influencing Dry Deposition Rates
(from Sehmel, 1980)

Micrometeorological Variables	Depositing Material	Surface Variable
Aerodynamic roughness	Particles	Accommodation
- Mass transfer		- Exudates
(a) Particles	Agglomeration	- Trichomes
(b) Gases	Diameter	- Pubescence
- Heat	Density	- Wax
- Momentum	Diffusion	Biotic surfaces
Atmospheric stability	- Brownian	Canopy growth:
Diffusion, effect of:	- Eddy equal to	- Dormant
- Canopy	(a) Particle	- Expanding
- Diurnal variation	(b) Momentum	Senescent
- Fetch	(c) Heat	Canopy structure:
Flow separation:	- Effect of canopy on	- Areal density
- Above canopy	Diffusiophoresis	- Bark
- Below canopy	Electrostatic effects	- Bole
Friction velocity	- Attraction	- Leaves
Inversion layer	- Repulsion	- Porosity
Pollutant concentration	Gravitational settling	- Reproductive structure
Relative humidity	Hygroscopicity	- Soils
Seasonal variation	Impaction	- Stem
Solar radiation	Momentum	- Type
Surface heating	Physical properties	Electrostatic properties
Temperature	Resuspension	Leaf-Vegetation:
Terrain	Shape	- Boundary layer
- Uniform	Size	- Change at high winds
- Nonuniform	Solubility	- Flutter
Turbulence	Thermophoresis	- Stomatal resistance
Wind velocity		Non-biotic surfaces
Zero-plane displacements	Gases	pH effects on:
- Mass transfer		- Reaction
(a) Particles	Chemical activity	- Solubility
(b) Gases	Diffusion:	Pollutant penetration and distribution in canopy
- Heat	- Brownian	Prior deposition loading
- Momentum	- Eddy	Water
	Particle pressure in equilibrium with surface	
	Solubility	

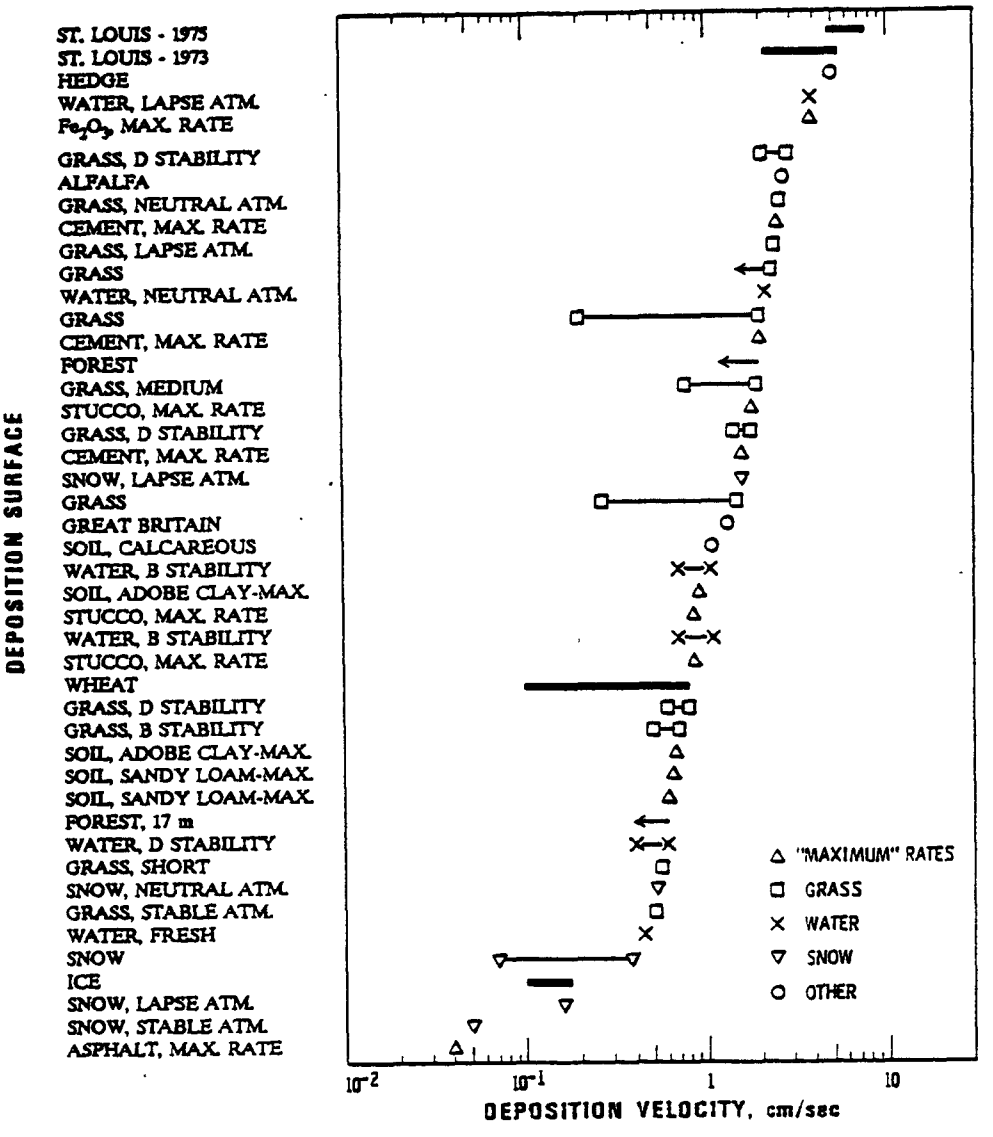

Figure 2-1. Summary of observed SO_2 deposition velocities (Sehmel, 1980).

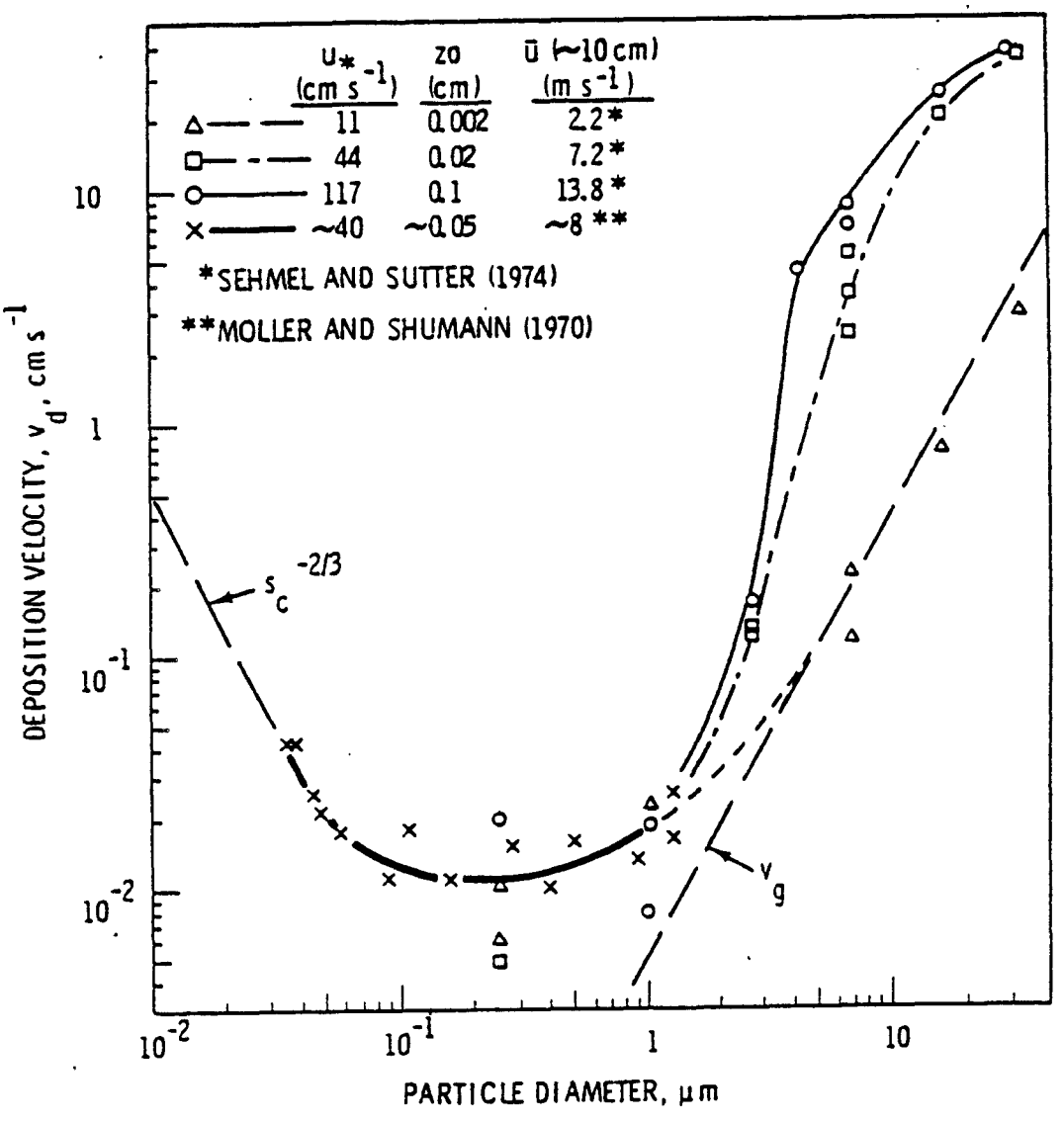

Figure 2-2. Observed deposition velocities (v_d) as a function of particle size for 1.5 g/cm^3 density particles. Measured by Sehmel and Sutter (1974) and Moller and Schumann (1970). Figure from Slinn et al. (1978). The gravitational settling velocity (v_g) is also shown.

2.1 Dry Deposition of Particulate Matter

Many models of dry deposition express the deposition velocity as the inverse of a sum of "resistances" plus, for particles, gravitational settling velocity terms. The resistances represent the opposition to transport of the depositing material from a reference height through the turbulent atmospheric surface layer, and through a quasi-laminar layer just above the surface to the surface itself. The major processes are briefly described below.

Gravitational Settling. The gravitational settling velocity is a function of the particle diameter, shape, and density. Figure 2-3 shows the gravitational settling velocity (v_g) as a function of particle size for several values of the particle density (ρ) for solid spherical particles. In many cases, effective or aerodynamic particle diameters are reported which express the size and shape of the particle as an equivalent diameter for a spherical particle of unit density, which simplifies the input to the deposition model. Note that the gravitational settling velocity represents a lower limit to the deposition velocity. It can be seen that for larger particles, in the range of 20-40 μm diameter and higher, the deposition velocity approaches the gravitational settling velocity, which indicates that the rate of deposition is dominated by the gravitational settling mechanism. The gravitational settling velocity decreases with decreasing particle size. However, for particles smaller than about 20 μm diameter, the deposition velocity curve shows larger and larger deviations from the gravitational settling curve as the particle size decreases. This is due to the effect of other mechanisms, discussed below, in enhancing the deposition rate of smaller particles above that predicted by gravitational settling alone.

Atmospheric Diffusion. The rate of deposition can sometimes be limited by the transfer of pollutant material to the vicinity of the surface by atmospheric turbulence. For example, atmospheric turbulence-limited deposition situations would typically occur during very stable conditions for an elevated plume of material composed of small-sized particles with small gravitational settling. In the lowest layer of the atmosphere, the aerodynamic resistance is used to parameterize the rate of mixing in terms of the wind speed, atmospheric stability, and surface roughness length. The aerodynamic resistance generally decreases (i.e., the deposition velocity will increase) with increasing wind speed and/or surface roughness.

Quasi-laminar Layer. Over smooth surfaces, a thin non-turbulent sublayer develops that can be a significant obstacle to the transfer of the pollutant onto the surface. For rough, real-world surfaces, this sublayer is constantly changing and is likely to be intermittently turbulent. For this reason, Hicks (1982) calls this layer the "quasi-laminar" layer. It is also known as the deposition layer. Small particles (< 0.05 μm diameter) are transported through the quasi-laminar layer primarily by Brownian diffusion. However, Brownian diffusion becomes less efficient as the particle size increases. Particles in the 1-20 μm diameter range tend to penetrate the quasi-laminar layer by inertial impaction. Since particles larger than 20 μm diameter are less efficiently captured, the inertial impaction mechanism is most effective in the 1-20 μm diameter size range. Because particles in the 0.1-1.0 μm diameter size range are not efficiently transported across the quasi-laminar layer by either Brownian diffusion or inertial impaction, particles of this size have the lowest deposition velocities.

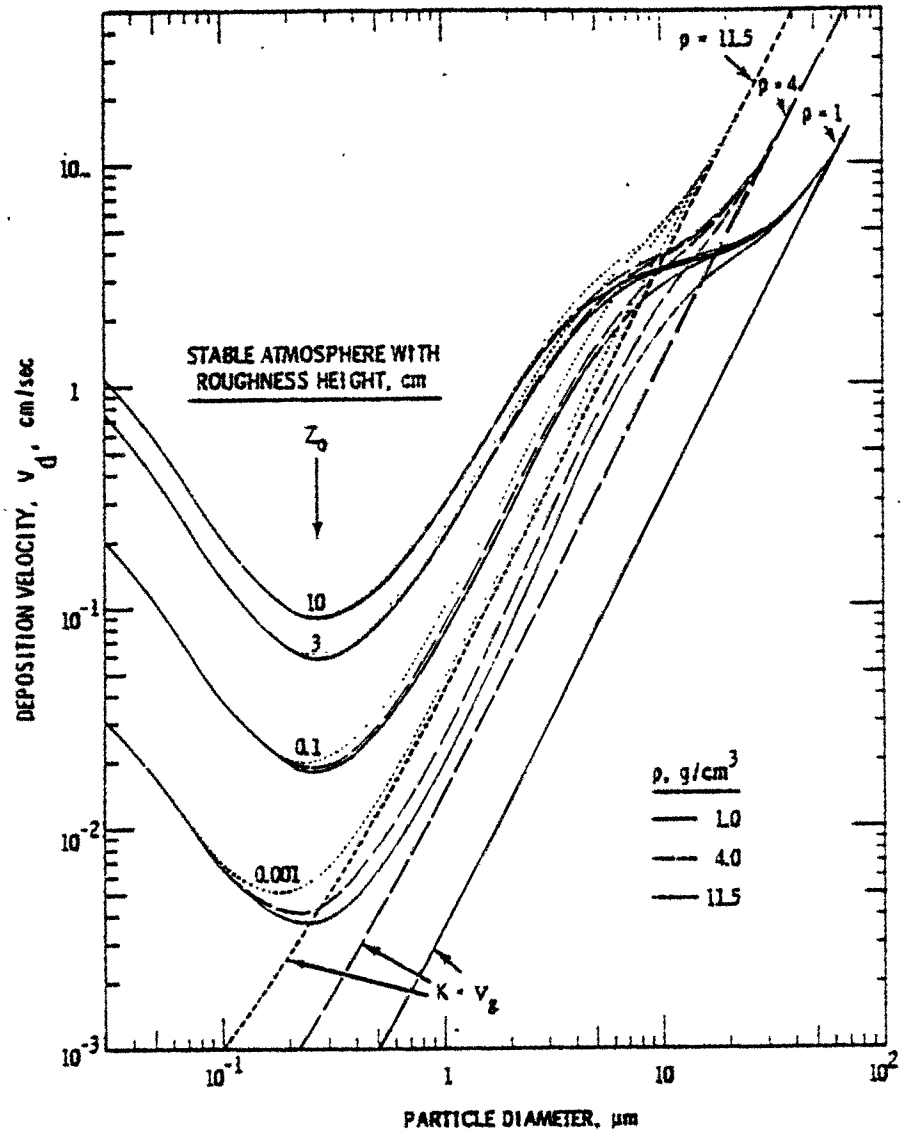

Figure 2-3. Predicted deposition velocities for $u_* = 100$ cm/s and particle densities of 1, 4, and 11.5 g/cm^3. Also shown is the gravitational settling velocity (v_g). Figure from Sehmel (1980).

Based on the discussion above, it is considered essential that the final generalized model selected be able to parameterize, at a minimum, the effects of gravitational settling, which is a dominate effect for large particles (> ~ 20 μm diameter), inertial impaction (dominates in the size range 1.0 to 20 μm diameter), and Brownian motion (important for small particles less than about 0.1 μm diameter).

2.1.1 ISC Method

The basis for the present ISC deposition algorithm is found in Dumbauld et al. (1976) and Overcamp (1976). In the ISC approach, the particles are allowed to move toward the ground by the combined processes of atmospheric turbulence and gravitational settling. At the surface, a portion of the plume determined by a user-specified reflection coefficient, γ_n, is assumed to be reflected from the surface and the remainder $(1 - \gamma_n)$ is assumed to be retained by the surface. The reflection coefficient scheme is illustrated in Figure 2-4 for γ_n = 0.0 (no reflection), 0.5 (partial reflection), and 1.0 (full reflection).

The effect of gravitational settling is assumed to result in a tilted plume with an angle, θ, to the horizontal given by:

$$\theta = \tan^{-1}(v_g/u) \tag{2-1}$$

where v_g is the gravitational settling velocity and u is the wind speed.

The concentration in ISC is given by:

$$\chi = \frac{KQD_tV}{\pi u \sigma_y \sigma_z} \exp\left[-\frac{1}{2}\left(\frac{y}{\sigma_y} \right)^2 \right] \tag{2-2}$$

where, K is an units scaling factor,
Q is the pollutant emission rate,
D_t is the decay term,
V is the vertical term,
σ_y is the standard deviation of the concentration distribution in the horizontal,
σ_z is the standard deviation of the concentration distribution in the vertical,

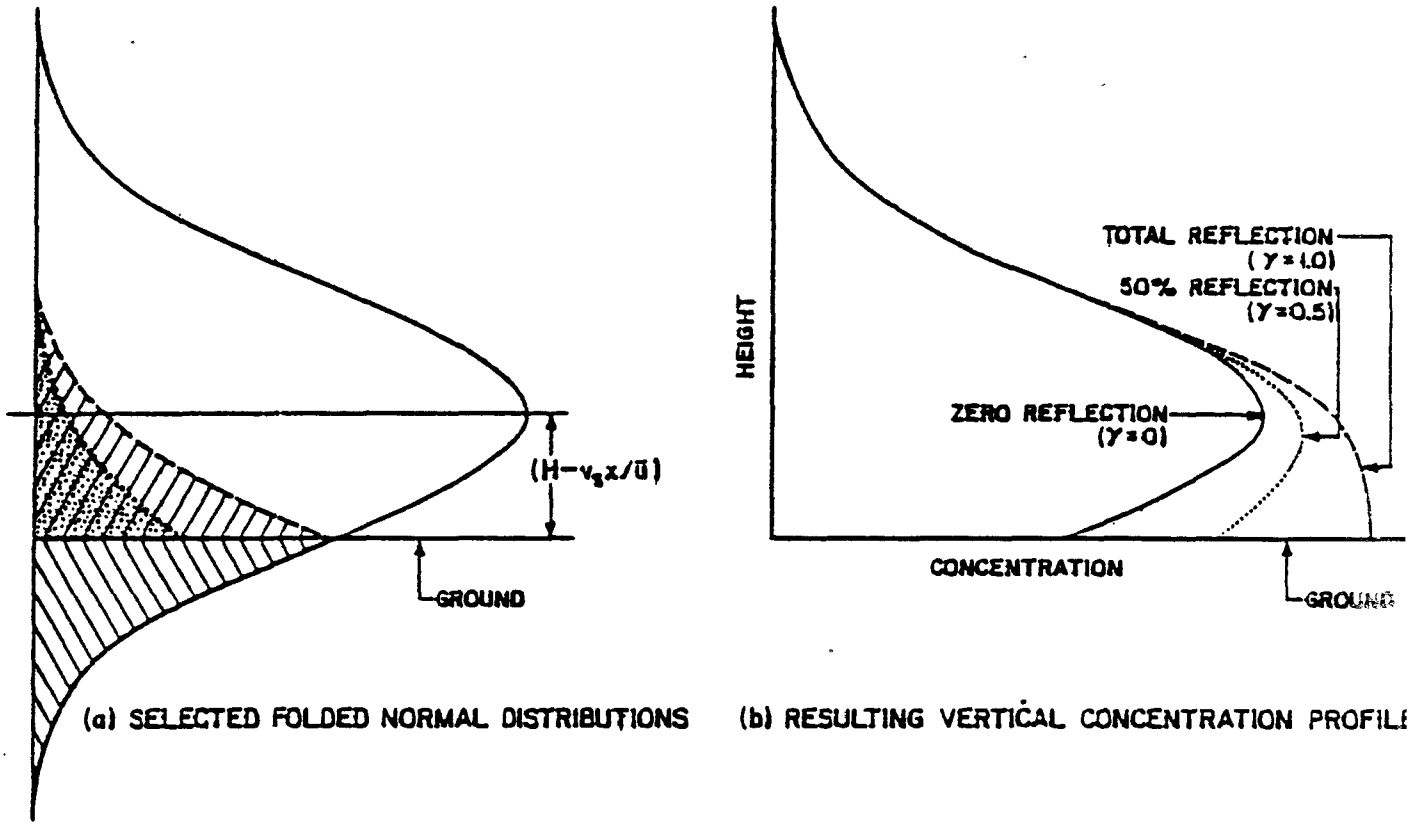

Figure 2-4. Illustration of the reflection coefficient scheme used in ISC for reflection coefficients of 0.0, 0.5, and 1.0. Figure from Bowers et al., 1979.

u is the wind speed, and

y is the crosswind distance from the plume centerline to the receptor.

The user must subdivide the pollutant size distribution into N particle settling categories. A maximum of 20 particle settling categories is allowed. The vertical term for a ground-level receptor involves a summation over all N particle categories.

$$V = \sum_{n=1}^{N} V_n \tag{2-3}$$

where,

$$V_n = 0.5\ \phi_n \left[\sum_{i=0}^{\infty} (A_1 + A_2) + \sum_{i=1}^{\infty} (A_3 + A_4) \right] \tag{2-4}$$

$$A_1 = \gamma_n^{\,i} \exp \left[- 0.5 \left(\frac{2iH_m - H_e + H_v}{\sigma_z} \right)^2 \right] \tag{2-5}$$

$$A_2 = \gamma_n^{\,i+1} \exp \left[- 0.5 \left(\frac{2iH_m + H_e - H_v}{\sigma_z} \right)^2 \right] \tag{2-6}$$

$$A_3 = \gamma_n^{\,i} \exp \left[- 0.5 \left(\frac{2iH_m + H_e - H_v}{\sigma_z} \right)^2 \right] \tag{2-7}$$

$$A_4 = \gamma_n^{\,i-1} \exp \left[- 0.5 \left(\frac{2iH_m - H_e + H_v}{\sigma_z} \right)^2 \right] \tag{2-8}$$

and, ϕ_n is the mass fraction of the pollutant emitted in the nth particle settling category,
γ_n is the reflection coefficient for particles in the nth particle settling category,
H_v is the height lost at the downwind distance x due to the gravitational settling [$H_v = (v_g \cdot x)/u$],
v_g is the gravitational settling velocity,
H_m is the mixing height, and,
H_e is the effective plume height (stack height + plume rise).

The ISC manual suggests the use of the following equation (McDonald, 1960) for calculating the gravitational settling velocity, v_g, in cm/s.

$$v_g = \frac{\rho\, g\, d_p^2}{18\mu} \tag{2-9}$$

where, ρ is the particle density (g/cm^3),
g is the acceleration due to gravity,
d_p is the particle diameter (cm), and
μ is the absolute viscosity of air (ISC manual suggests $\mu \sim 1.83 \times 10^{-4}$ g/cm/s).

The total deposition, D, is summed over all N particle categories, and is given by:

$$D = \sum_{n=1}^{N} D_n \tag{2-10}$$

$$D_n = \frac{K\, Q_t\, V'\, D_t\, (1 - \gamma_n)\, \phi_n}{(2\pi\, \sigma_y\, \sigma_z\, x)} \exp\left(- 0.5 \left(\frac{y}{\sigma_y} \right)^2 \right] \tag{2-11}$$

where the vertical term for deposition, V', is defined as:

$$V' = \left[\bar{b}\, H_e + (1 - \bar{b})H_v \right] \exp\left[-0.5\left(\frac{H_e - H_v}{\sigma_z}\right)^2\right] +$$

$$\sum_{i=1}^{\infty} \left\{ \gamma^{i-1} \left[\bar{b}\,(2iH_m - H_e) - (1 - \bar{b})H_v \right] \exp\left[-0.5\left(\frac{2iH_m - H_e + H_v}{\sigma_z}\right)^2\right] \right. \qquad (2\text{-}12)$$

$$\left. + \gamma^{i} \left[\bar{b}\,(2iH_m + H_e) + (1 - \bar{b})H_v \right] \exp\left[-0.5\left(\frac{2iH_m + H_e - H_v}{\sigma_z}\right)^2\right] \right\}$$

where, Q_t is the total pollutant mass emitted during the time period over which the deposition is calculated, and

$\bar{b}$ is the average value of the exponent b of the σ_z equation ($\sigma_z = ax^b$) for the interval between the source and the downwind distance x.

The ISC deposition method requires that the user specify the following:

(1) mass fraction of pollutant emitted in each particle settling category

(2) reflective coefficients for each particle settling category.

The reflection coefficient is given by Dumbauld et al. (1976) as a function of the particle settling velocity (see Figure 2-5). The settling velocity, which depends on the particle diameter and particle density, must be calculated by the user for each size category and used to determine the reflection coefficient, which is then entered into the model. The reflection coefficients are assumed to be spatially and temporally constant in ISC.

The reflection coefficient approach used to model dry deposition in the ISC model suffers several drawbacks for applications to small particles (< 20 μm diameter) and gases (e.g., see Scire and Wojichowski, 1987). The ISC deposition algorithm was developed for use only with large particles dominated by gravitational settling effects. The empirical reflection coefficients used in ISC are based on data collected and analyzed by Dumbauld et al. (1976). Their experiment consisted of several aircraft releases of two spray carriers: Duphar and No. 2 fuel oil. The size distributions of the particles were heavily weighted with large particles. The mass mean diameter of the particle distributions were 66 μm (for the Duphar releases) and

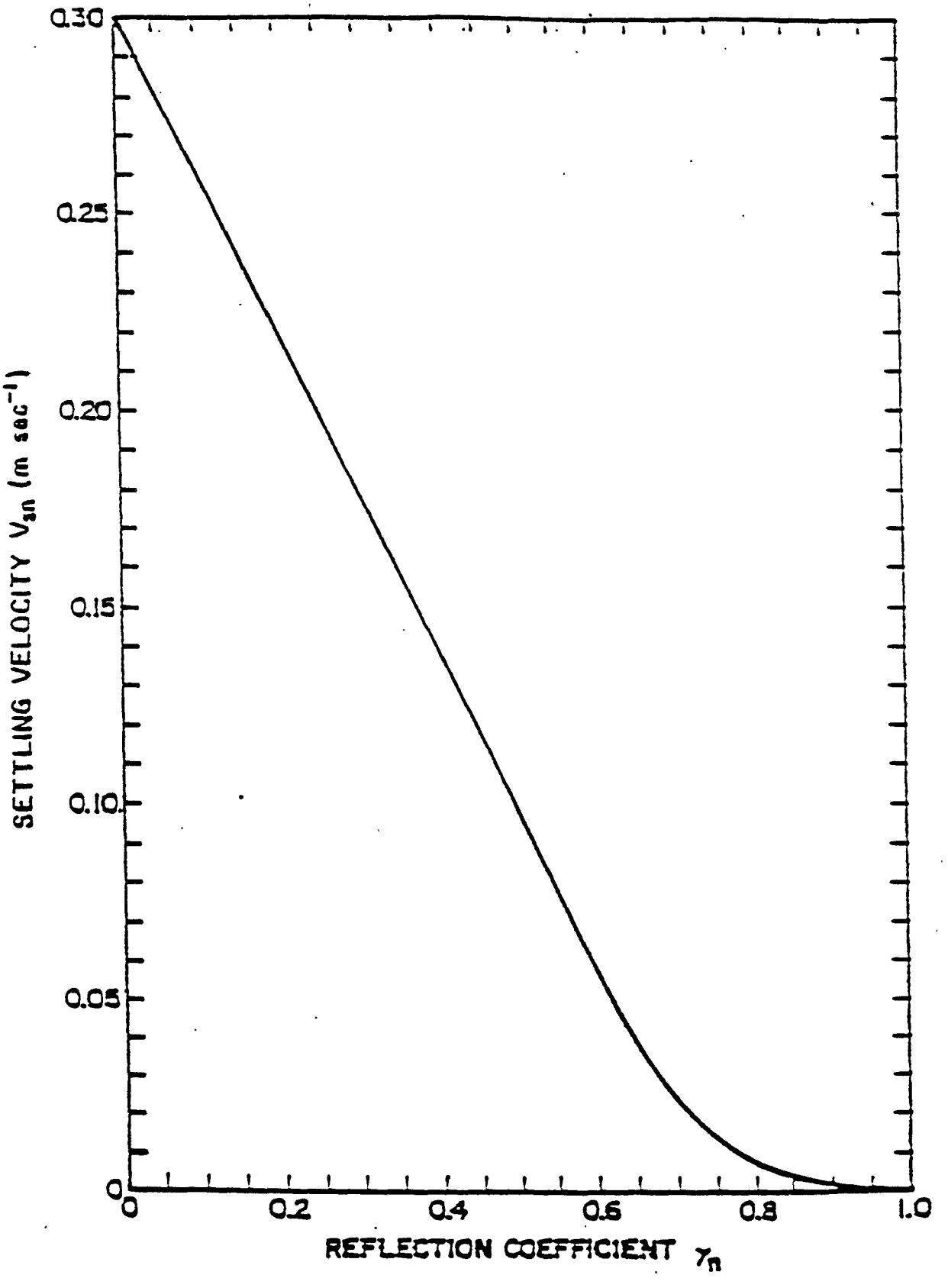

Figure 2-5. Reflection coefficient as a function of the gravitational settling velocity (from Dumbauld et al., 1976).

55 μm diameter (fuel oil releases). Less than 1% of the mass of the Duphar was in particles with diameters < 30 μm. For the fuel oil distribution, less than 1% of the mass was in particles smaller than 20 μm diameter. Particles of this large size are nearly completely controlled by gravitational settling, which, because it is a characteristic of the particle and does not depend on factors such as meteorological conditions and surface characteristics, is compatible with the use of spatially and temporally constant reflection coefficients. However, the deposition of small particles is controlled by other physical processes such as inertial impaction and Brownian motion, which are affected by both meteorological and surface conditions. These effects are not easily parameterized within the framework of a reflection coefficient model.

For small particles, the ISC reflection coefficient curve (Figure 2-5) was derived based on an extrapolation of the gravitational settling-dominated data for larger particles (Dumbauld et al., 1976). The extrapolation led to the assumption that particles with settling velocities less than 0.1 cm/s (approximately 5.7 μm diameter for unit density particles) are completely reflected (i.e., experience no deposition). However, this assumption is not consistent with measurement studies of small particles, as discussed previously, which show significant deposition velocities for particles at and below 5.7 μm diameter (e.g., see Figures 2-2 and 2-3). It was concluded that the ISC scheme could significantly underestimate small particle deposition because several important physical processes are not parameterized in its approach. Therefore, the ISC method is not considered appropriate for small particles. However, it was tested and intercompared with the other approaches to serve as a reference point for the performance of the other models.

2.1.2 CARB Model

Sehmel and Hodgson (1978) and Sehmel (1980) proposed a model for predicting deposition velocities of particles above smooth surfaces. The basis of the model is a set of wind tunnel observations of deposition for monodispersed particles to surfaces such as gravel, artificial grass, brass shim stock, and water. The model consists of empirical equations for transfer resistances derived from a least-squared empirical fit of deposition velocity as a function of particle size, density, surface roughness, and friction velocity. The equations were converted into a computer code by the California Air Resources Board (CARB) and is widely known as the CARB model. It is also used in the Fugitive Dust Model (FDM) (Winges, 1990).

In the CARB model, integrated resistances to mass transfer are computed within two layers. The first layer extends from a reference height of one meter above the surface down to one centimeter above the surface. In this layer, atmospheric turbulence dominates mass transfer. Eddy diffusivities are used to describe the transfer rate. The second layer is the

deposition surface layer within one centimeter of the surface. The integrated resistance within the deposition surface layer is derived from a statistical fit of the wind tunnel particle deposition data. Sehmel and Hodgson express the deposition velocity as:

$$v_d = \frac{v_g}{1. - \exp[-v_g(I_{12} + I_3)/u_*]} \tag{2-13}$$

where, v_d is the deposition velocity (cm/s),
v_g is the gravitational settling velocity (cm/s),
I_{12} is the atmospheric diffusional resistance (dimensionless),
I_3 is the surface resistance integral (dimensionless), and,
u_* is the surface friction velocity (cm/s).

The gravitational settling velocity (cm/s) in the CARB model is calculated as:

$$v_g = \left(1 + \frac{c_1\sqrt{T}}{d_p}\right)(\rho - \rho_{AIR})g\, d_p^2\, \frac{c_2}{18\mu} \tag{2-14}$$

where, d_p is the particle diameter (μm),
ρ is the particle density (g/cm^3),
ρ_{AIR} is the density of air (CARB assumed ρ_{AIR} = 1.2 x 10^{-3} g/cm^3),
T is the air temperature (°K),
μ is the absolute viscosity of air (CARB used μ = 1.78 x 10^{-4} g/cm/s), and
the constants c_1 and c_2 were assigned values of 9.73 X 10^{-3} and 1.0 x 10^{-8}, respectively.

The atmospheric diffusion resistance used by Sehmel and Hodgson (1978) is based on the flux profile relationships of Businger et al. (1971). For neutral or stable conditions,

$$I_{12} = [\ln z_1/z_2) + 4.7(z_1 - z_2)/L]/k \tag{2-15}$$

where, z_1 is the upper limit of the atmospheric diffusional resistance integral (i.e., 100 cm),
z_2 is the lower limit of integral (i.e., 1 cm),
L is the Monin-Obukhov length (cm), and,
k is the von Karman constant (Sehmel used a value of 0.35).

For unstable conditions, the atmospheric diffusional resistance integral is:

$$I_{12} = (\ln\{[(A_{z1} - 1.)(A_{z2} + 1.)]/[(A_{z1} + 1.)(A_{z2} - 1.)]\} + 2.[\tan^{-1}(A_{z1}) - \tan^{-1}(A_{z2})])/k \quad (2\text{-}16)$$

$$A_{z1} = (1. - 15.z_1/L)^{0.25} \quad (2\text{-}17)$$

$$A_{z2} = (1. - 15.z_2/L)^{0.25} \quad (2\text{-}18)$$

The surface resistance integral is an empirical relationship based on the wind tunnel observations. For particles with a diameter ≥ 0.01 μm,

$$I_3 = \exp\{-378.051 + 16.498 \ln(Sc) + \ln(t^+)[-11.818 - 0.2863 \ln(t^+) + 0.3226 \ln(d_p 10^{-4}/z_o) - 0.3385 \ln(D/(z_o u_*))] - 12.804 \ln(d_p 10^{-4})\} \quad (2\text{-}19)$$

where, D is the Brownian diffusion coefficient (cm^2/s),
t^+ is a relaxation time (dimensionless),
Sc is the Schmidt number (dimensionless),
z_o is the surface roughness length (cm), and,
d_p is the particle diameter (μm).

The relaxation time, t^+, is

$$t^+ = 3.156 \times 10^{-13} (d_p u_*)^2 \quad (2\text{-}20)$$

where the constant is defined assuming the units of d_p and u_* are μm and cm/s, respectively.

The Brownian diffusion coefficient is a function of the particle diameter and temperature. Sehmel and Hodgson (1978) express D as:

$$D = \{7.868 \times 10^{-10} T/d_p\} [1 + (2.632 \times 10^{-2}/d_p) * (6.32 + 2.01 e^{(-8.322 d_p)})] \quad (2\text{-}21)$$

where T is the temperature (deg. K).

The data requirements of the model are relatively simple (particle size, density, surface roughness, and routine meteorological parameters to compute the friction velocity and Monin-Obukhov length).

The plots of deposition velocity in Sehmel (1980) (e.g., see Figure 2-3) show a reasonable variation of deposition velocity as a function of model parameters (i.e., density, size, surface roughness, friction velocity). The predicted deposition velocity is close to the gravitational settling velocity for large particles (e.g., greater than about 20 μm diameter), and decreases with decreasing particle size to about 0.1-1.0 μm, where it reaches a minimum. The deposition velocity then increases with decreasing particle size for smaller sized particles. This behavior is consistent with the importance of Brownian motion in enhancing deposition rates for very small particles. The CARB scheme produces increased deposition rates for increased particle density, surface roughness length, and friction velocity, which is expected based on physical considerations.

The main concern about the CARB model deals with the generality of the highly empirical relationship for the surface resistance integral (Eqn. 2-19). I_3 is based on wind tunnel data for relatively smooth surfaces conducted under a limited range of conditions. For example, in order to avoid extrapolation, the CARB implementation of the model does not allow the surface roughness length used in the algorithm to exceed 10 cm, even though most real world surfaces have significantly greater roughness lengths (e.g., see Table 2-2). In addition, sensitivity testing of the model has shown it exhibits some non-physical behavior when the inputs are varied beyond the range of conditions tested in the wind tunnel. For example, the CARB model showed a very strong sensitivity to temperature which is not exhibited by other deposition models. For particles in the 0.1-1.0 μm diameter size, a change on nearly an order of magnitude in deposition velocity was predicted for a temperature change from 0°F to 100°F (see Figure 2-6). This behavior is probably an artifact of the regression equations used to fit the surface resistance integral to the wind tunnel data. The original wind tunnel tests were performed at a constant temperature, and, as a result, application to a realistic range of atmospheric conditions involves extrapolation outside the range on which the model was developed.

A second problem noted from the sensitivity testing is that the deposition velocities show a kink in the curve at about 0.03 μm particle diameter. For particles smaller than about 0.1 μm diameter, the deposition velocity increases with decreasing particle diameter. However, the CARB model shows this trend only to about 0.03 μm diameter, beyond which the deposition velocity is predicted to decrease or level off with decreasing particle diameter (see Figure 2-7). The kink in the curves appears to be another artifact of the regression equations which occurs as a result of extrapolation outside the range of conditions on which the model is based.

Table 2-2
Typical Surface Roughness Lengths for Various Land Use Types
(From Hjelmfelt, 1982)

Land Use	Typical Roughness Length (cm)
Urban - Commercial/Industrial	200
Common residential - single family dwellings	20
Compact residential - multi-family dwelling	50
Metropolitan natural (parks, golf courses)	15
Agricultural - rural	20
Semi-rural	20
Undeveloped, wasteland	5
Forest	100
Bottomland agricultural	15

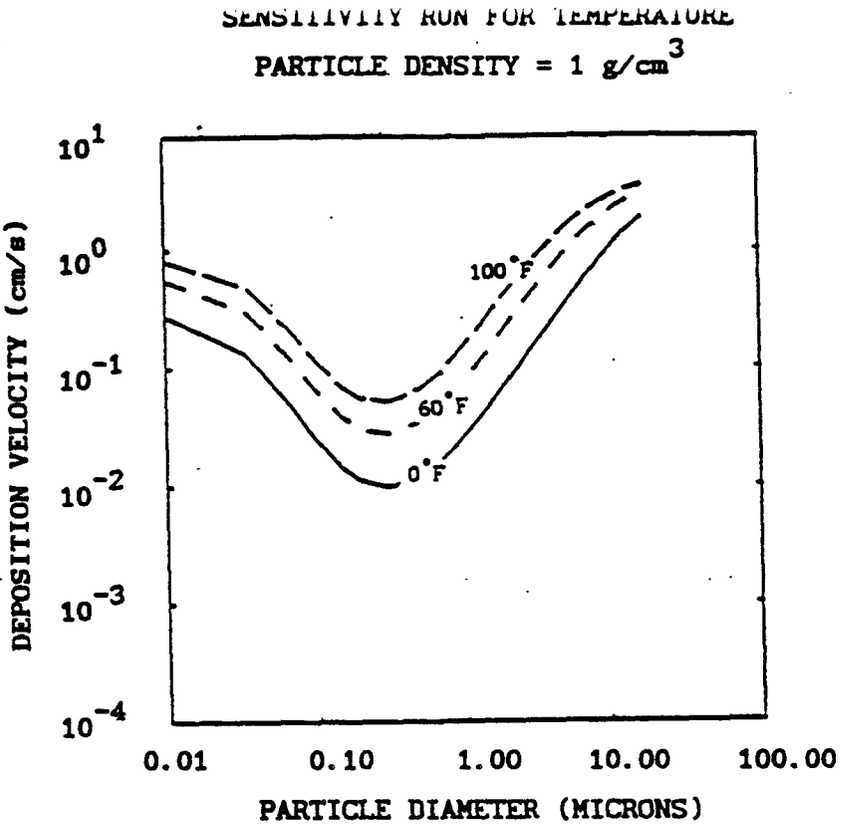

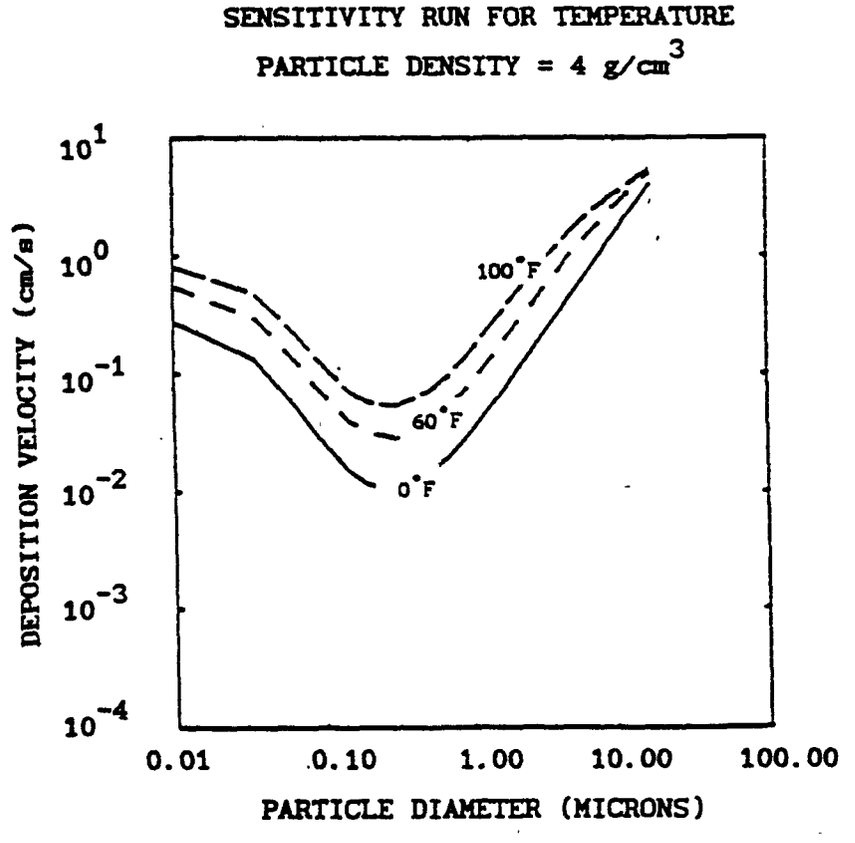

Figure 2-6. Deposition velocity as a function of particle diameter as predicted by the Sehmel/CARB model for three different values of ambient temperature (0°, 60°, 100°F).

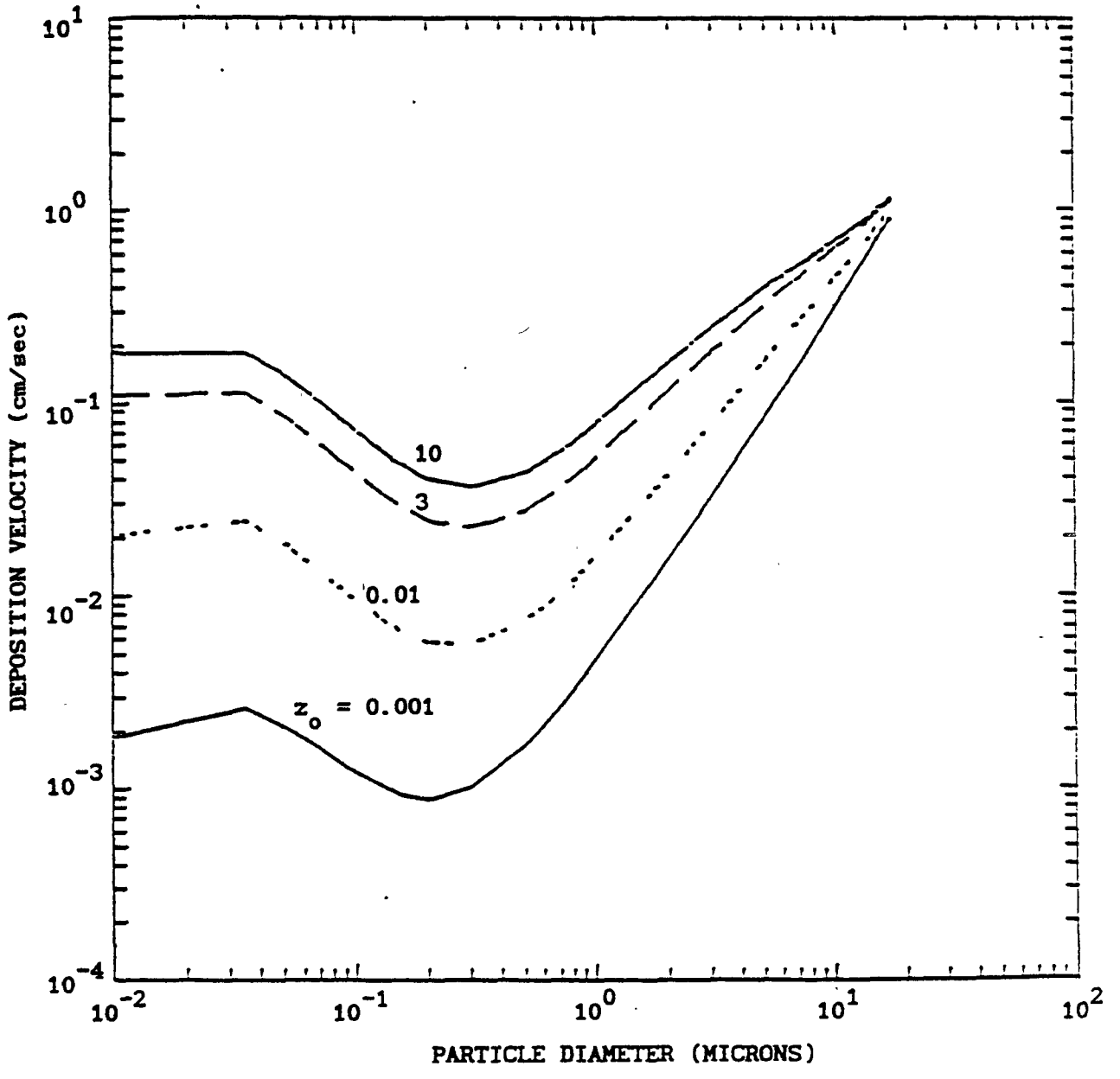

Figure 2-7. Deposition velocity as a function of particle diameter as predicted by the Sehmel/CARB model for surface roughness lengths of 0.001, 0.01, 3, and 10 cm.

In addition to evaluating the basic CARB model, several modifications to the model were made in an attempt to address some of the concerns raised above. In the model evaluation (Section 7), the basic CARB model described by Eqns. (2-13) to (2-21) is designated CARB 1. Three variations of the model were developed and evaluated (CARB 0, CARB 2, and CARB 3). The modifications to each version of the model are described below.

CARB 0 - same as the CARB 1 except the portion of the code which limits the value of z_o to 10 cm was eliminated. Thus, the CARB 0 revision uses actual surface roughness lengths which are allowed to be greater than 10 cm.

CARB 2 - same as CARB 1, except in Eqn. (2-21), a constant temperature of 75°F is always used rather than the actual air temperature. This change was intended to eliminate the temperature sensitivities of the model noted above.

CARB 3 - contains changes to eliminate the temperature dependency (as in CARB 2) and an adjustment to the surface resistance integral, I_3. The value of I_3 used in CARB 3 is that given by Eqn. (2-19) divided by (1.0 + LAI), where LAI is the leaf area index. In addition, a fixed reference length of 0.5 cm is used in CARB 3 in the calculation of the LAI-adjusted I_3 instead of z_o.

The Sehmel and Hodgson (1978) empirical relations are based on simple surfaces. For compound surfaces which are aerodynamically independent, it seems reasonable to expect the deposition velocity to be increased by the additional surface area. The LAI adjustment in CARB 3 is made to test this assumption.

Also, the roughness length in the surface integral resistance, I_3, differs from the traditional roughness length defined by other researchers such as Plate and Quraishi (1965). Rather, it is related to the thickness of the laminar sublayer, which is proportional to the ratio of the molecular diffusivity to the surface friction velocity. The constant of proportionality for an established sublayer is approximately 20. Thus, for a friction velocity of 0.1 m/s and a diffusivity of 2×10^{-5} m^2/s, the resulting sublayer depth is .4 cm, which is close to the largest roughness length used by Sehmel and Hodgson (1978). Thus, for the relatively smooth surfaces tested by Sehmel, z_o may be a good approximation of the sublayer depth length scales, but for the LAI-adjusted I_3, it may be more appropriate to use a constant reference length. A constant value of 0.5 cm is tested in CARB 3.

2.1.3 ADOM Model - Particles

The Acid Deposition and Oxidant Model (ADOM) contains a dry deposition algorithm (Pleim et al., 1984) which has served as the basis for the deposition scheme in several other models, including CALPUFF (Scire et al., 1990) and CALGRID (Yamartino et al., 1992).

The deposition flux, F, is calculated as the product of the concentration, χ, at a reference height and a deposition velocity, v_d.

$$F = \chi \cdot v_d \tag{2-22}$$

The general approach used in the resistance methods such as in the ADOM model is to include explicit parameterizations of the effects of Brownian motion, inertial impaction, and gravitational settling. The deposition velocity is written as the inverse of a sum of resistances to pollutant transfer through various layers, plus gravitational settling terms (Slinn and Slinn, 1980; Pleim et al., 1984).

$$v_d = \frac{1}{r_a + r_d + r_a r_d v_g} + v_g \tag{2-23}$$

where, v_d is the deposition velocity (cm/s),
v_g is the gravitational settling velocity (cm/s),
r_a is the aerodynamic resistance (s/cm), and,
r_d is the deposition layer resistance (s/cm).

Note that for large settling velocities, the deposition velocity approaches the settling velocity ($v_d \rightarrow v_g$), whereas, for small settling velocities, v_d tends to be dominated by the r_a and r_d resistance terms.

The lowest few meters of the atmosphere can be divided into two layers: a fully turbulent region where vertical fluxes are nearly constant, and the thin quasi-laminar sublayer. The resistance to transport through the turbulent, constant flux layer is the aerodynamic resistance. It is usually assumed that the eddy diffusivity for mass transfer within this layer is similar to that for heat. The atmospheric resistance formulation used in ADOM is based on Wesely and Hicks (1977).

$$r_a = \frac{1}{k\,u_*}\left[\ln\left(z_R/z_o\right) - \psi_H\right] \tag{2-24}$$

where, ψ_H is a stability adjustment factor,
u_* is the surface friction velocity (cm/s),
k is the von Karman constant (0.4),
z_R is reference height (m) (= 10 m), and,
z_o is the surface roughness length (m).

$$\psi_H = \begin{cases} -5\ z/L & 0 < z/L < 1 \\ 0 & z/L = 0 \\ 2\ln\left(\dfrac{1 + \sqrt{1 - 16\ z/L}}{2}\right) & -1 < z/L < 0 \end{cases} \tag{2-25}$$

The approach used by Pleim et al. (1984) to parameterize the deposition layer resistance terms is:

$$r_d = \left[Sc^{-2/3} + 10^{-3/St}\right]^{-1} u_*^{-1} \tag{2-26}$$

where, Sc is the Schmidt number (Sc = υ/D) (dimensionless),
υ is the viscosity of air (= 0.15 cm^2/s),
D is the Brownian diffusivity (cm^2/s) of the pollutant in air,
St is the Stokes number [St = $(v_g/g)(u_*^2/\upsilon)$] (dimensionless), and,
g is the acceleration due to gravity (981 cm/s^2).

The gravitational settling velocity (cm/s) in the ADOM model is calculated as:

$$v_g = \frac{(\rho - \rho_{AIR})\ g\ d_p^2\ c_2}{18\mu}\ S_{CF} \tag{2-27}$$

where, ρ is the particle density (g/cm^3),
ρ_{AIR} is the air density (= 1.2×10^{-3} g/cm^3),
d_p is the particle diameter (μm),

μ is the absolute viscosity of air (= 1.81×10^{-4} g/cm/s),
c_2 is air units conversion constant (1×10^{-8} cm^2/μm^2), and
S_{CF} is the slip correction factor, which is computed as:

$$S_{CF} = 1. + \frac{2x_2 \left(a_1 + a_2 e^{-(a_3 d_p/x_2)}\right)}{10^{-4} d_p} \qquad (2\text{-}28)$$

and, x_2, a_1, a_2, a_3 are constants with values of 6.5×10^{-6}, 1.257, 0.4, and 0.55×10^{-4}, respectively.

The diffusivity of the pollutant (in cm^2/s) is computed from the following relationship.

$$D = 8.09 \times 10^{-10} \left[\frac{TS_{CF}}{d_p}\right] \qquad (2\text{-}29)$$

where T is the air temperature (°K).

The first term of Eqn. (2-26), involving the Schmidt number, parameterizes the effects of Brownian motion. This term controls the deposition rate for small particles. The second term, involving the Stokes number, is a measure of the importance of inertial impaction, which tends to dominate for intermediate-sized particles in the 2-20 µm diameter size range.

The data requirements of the ADOM-type deposition model are identical to those of the CARB model. Particle size, particle density, surface roughness length, friction velocity, and Monin-Obukhov length are input parameters used by the model.

The ADOM approaches produce patterns of deposition velocities as a function of particle size, density, etc. similar to those of the CARB model. However, the ADOM algorithm tends to predict somewhat higher deposition velocities in the 5-15 µm diameter size range than the CARB model and lower values in the 0.1-5.0 µm diameter range, although the general shape of the deposition velocity curves are similar. The minimum deposition velocity tends to occur closer to 1.0 µm than 0.1 µm diameter.

The parameterizations of the resistance models for Brownian motion and inertial impaction effects involve empirical factors derived from field studies and wind tunnel experiments. The sensitivity analyses with the ADOM model showed no unusual response to

temperature variations over the range from 0° F to 100°F. The resistance models all showed a steady increase of deposition velocity with decreasing particle diameter in the small particle range (< 0.1 μm diameter).

The basic (core) ADOM model defined by Eqns. (2-23) to (2-29) is designated as ADOM 1. Two sets of changes to the ADOM formulation, described below, were also tested.

The -3/St exponent in the inertial term of Eqn. (2-26) may represent too sharp a cutoff as pointed out by Slinn (1982). Slinn suggests that a better function for the inertial impaction term, E_{IM}, for canopies is:

$$E_{IM} = \frac{St_b^2}{\left(1 + St_b^2\right)} \tag{2-30}$$

where St_b is a bulk the Stokes parameter defined in Slinn (1982) as $St_b = St(\mu U/u_* A)$. At the present time the obstacle scale size A has been set to 1 mm. Note that Slinn (1982) also suggests an explicit parameterization of the interception mechanism. However, due to its reliance on parameters that are not available on a routine basis, it has not been tested in this version of the model.

The power law dependence on the Schmidt number for the Brownian diffusion term is likely to be a function of the surface type, with established laminar layers over a smooth water surface having an exponent closer to -0.5 (Slinn and Slinn, 1980), while for more complex surfaces, the exponent is likely to be nearer -0.7.

Therefore, in the version designated ADOM 2, a hybrid deposition layer resistance was computed as:

$$r_d = \left[Sc^n + \frac{St_b^2}{\left(1 + St_b^2\right)}\right]^{-1} u_*^{-1} \tag{2-31}$$

instead of using Eqn. (2-26), with n = -0.5 for $z_o \leq 10$ cm and n = -0.7 for $z_o > 10$ cm.

A second change in ADOM 2 is an allowance for a small adjustment to the deposition rates to account for possible phoretic effects. Some examples of phoretic effects (Hicks, 1982) are:

THERMOPHORESIS: Particles close to a hot surface experience a force directed away from the surface because, on the average, the air molecules impacting on the side of the particle facing the surface are hotter and more energetic.

DIFFUSIOPHORESIS: Close to an evaporating surface, a particle is more likely to be impacted by water molecules on the side of the particle facing the surface. Since the water molecules have a lower molecular weight than the average air molecule, there is a net force toward the surface, which results in a small enhancement of the deposition velocity of the particle.

A second effect is that the impaction of new water vapor molecules at an evaporating surface displaces a certain volume of air. For example, 18 g of water vapor evaporating from 1 m^2 will displace 22.4 liters of air at standard temperature and pressure (STP) conditions (Hicks, 1982). This effect is called Stefan flow. The Stefan flow effect tends to reduce deposition fluxes from an evaporating surface. Conversely, deposition fluxes to a surface experiencing condensation will be enhanced.

ELECTROPHORESIS: Attractive electrical forces have the potential to assist the transport of small particles through the quasi-laminar deposition layer, and thus could increase the deposition velocity in situations with high local field strengths. However, Hicks (1982) suggests this effect is likely to be small in most natural circumstances.

Phoretic and Stefan flow effects are generally small. However, for particles in the range of 0.1 - 1.0 μm diameter, which have low deposition velocities, these effects may not always be negligible. Therefore, the ability to specify a phoretic term to the deposition velocity is added to ADOM 2 (i.e., $v_d' = v_d + v_{d(phor)}$, where v_d' is the modified deposition velocity and $v_{d(phor)}$ is the phoretic term). Although the magnitude and sign of $v_{d(phor)}$ will vary, a small, constant value of + 0.01 cm/s is used in ADOM 2 for testing purposes.

Another version of the model, ADOM 3, was tested which included the ADOM 2 changes, and a leaf area index (LAI) adjustment to r_d. In ADOM 3, r_d is that given by Eqn. (2-31) divided by (1.0 + LAI).

2.1.4 UAM-V Model

The deposition formulation variable grid version of the Urban Airshed Model (UAM-V) (Gray et al., 1991) is similar to that in ADOM. The deposition velocity is expressed in terms of an aerodynamic resistance (r_a), deposition layer resistance (r_d), and a gravitational settling velocity (v_g) according to Eqn. (2-23). The formulation for r_a in UAM-V is identical to that in ADOM (Eqn. 2-24). The form of the stability adjustment factor, ψ_H, is given by Eqn. (2-25), except the coefficient for positive L is -4.7 in UAM-V instead of -5.

The main difference is in the formulation of the inertial impaction term of the deposition layer resistance.

$$r_d = \left[0.25 \left(Sc^{-2/3} + C_1 \, St \right) \right]^{-1} u_*^{-1} \tag{2-32}$$

where the parameter C_1 is computed each hour to force the Sc and St terms to be equal at a critical diameter of 0.3 μm.

The form of the gravitational settling velocity equation in UAM-V is identical to that in ADOM (i.e., Eqns. 2-27 and 2-28). The values of the constants in the v_g equations are slightly different. The values of x_2, μ, and ρ_{AIR} used in UAM-V are 6.53×10^{-6}, 1.83×10^{-4} g/cm/s, and 1.0×10^{-3} g/cm^3, respectively.

The data input requirements of the UAM-V dry deposition model (particle size, particle diameter, roughness length, friction velocity, and Monin-Obukhov length) are the same as those required by the CARB and ADOM models.

The UAM-V dry deposition algorithm described above is designated as UAM 1 in the model evaluation tests. A second version, called UAM 2, was also evaluated. UAM 2 was modified to include a LAI adjustment to the deposition layer resistance (i.e., r_d in UAM 2 is that given by Eqn. (2-32) divided by (1.0 + LAI)).

2.2 Dry Deposition of Gaseous Pollutants

Many of the available models for predicting dry deposition of gaseous pollutants have a similar structure. The deposition velocity is expressed as the inverse of a sum of resistances.

$$v_d = \left(r_a + r_d + r_c \right)^{-1} \tag{2-33}$$

where, r_a is the aerodynamic resistance (s/m),
r_d is the deposition layer or quasi-laminar layer resistance (s/m), and,
r_c is the bulk canopy resistance (s/m).

The gravitational settling velocity is not a factor for gases, and therefore does not appear in Eqn. (2-33). The aerodynamic resistance for gases is the same as discussed previously for particles, see Eqn. (2-24). It is determined from meteorological and surface parameters and does not depend on the pollutants characteristics. The deposition layer resistance involves transport by molecular diffusion through the thin quasi-laminar sublayer which intermittently exists just above the surface. The deposition layer resistance is a function of the properties of the pollutant (i.e., molecular diffusivity in air) and meteorological conditions. The canopy resistance involves the physical capture or chemical reaction of the pollutant within the vegetative canopy or at the surface. The canopy resistance, r_c is often the controlling resistance determining deposition flux. Therefore, considerable effort is devoted to estimating r_c in many of the deposition models.

There are many models based on this simple resistance concept. Three widely-used techniques appropriate for deposition of gases have been selected for future further evaluation. In some cases, various components of the algorithms are very similar or identical to each other (e.g., the formulation of r_a). However, other important variations exist, especially in the parameterization of r_c which will be intercompared, tested and evaluated. Because the goal of this study is to produce an algorithm which can be used on a routine basis for regulatory applications, top consideration has been given to simpler parameterizations which capture the most significant features of the physical system while requiring modest, readily-available data as input.

The major features of the algorithms selected for the current study are described below. The original references provide a detailed description of the algorithms.

2.2.1 RADM Model

The dry deposition algorithm used in the Regional Acid Deposition Model (RADM) meets all of the model selection criteria listed in Section 1. It has undergone considerable testing and refinement over the past five years. The RADM deposition scheme is described in a series of reports and papers, including Sheih et al., 1986; Walcek et al., 1986; and Wesely, 1989. It has also been incorporated into the latest version of the UAM-V model (Gray et al., 1991).

The early version of the RADM deposition model used fairly standard formulations for r_a and r_d, and look-up tables for r_c based on land use and season. However, the difficulty with the look-up table approach is that detailed r_c tables must be developed for each pollutant of

interest, which can be difficult for many pollutants. The latest version of the model computes r_c based on the bulk surface resistance along several parallel pathways of mass transfer (Wesely, 1989). The equation for r_c is:

$$r_c = \left[\frac{1}{r_s + r_m} + \frac{1}{r_{lu}} + \frac{1}{r_{dc} + r_{cl}} + \frac{1}{r_{ac} + r_{gs}} \right]^{-1} \qquad (2\text{-}34)$$

where, r_s is the bulk canopy stomatal resistance,
r_m is the leaf mesophyll resistance,
r_{lu} is the leaf cuticle resistance,
r_{dc} is the within-canopy aerodynamic resistance to the lower canopy,
r_{cl} is the exposed surface resistance in the lower canopy,
r_{ac} is the within-canopy aerodynamic resistance to the ground, and,
r_{gs} is the ground resistance.

The data requirements of this more sophisticated module include chemical parameters such as solubility, reactivity, and diffusivity. Table 2-3 contains values of these parameters for several gaseous species. Values for other toxic pollutants of concern can be obtained in the literature or estimated based on the properties of the pollutant. Other parameters required include meteorological factors such as solar radiation, friction velocity and Monin-Obukhov length (which can be estimated from routinely-available data), and geophysical data such as surface roughness and land use type. The data requirements of the RADM scheme are summarized in Table 2-4.

The stomatal resistance, r_s is computed as a function of air temperature and solar radiation. The resistance, r_{ac} is specified by Wesely (1989) as a function of the land use type. The resistance, r_{dc} is often small. It can be conservatively estimated based on solar radiation. The other resistances in Eqn. (2-34) are computed by the model using values of solubility and reactivity of the pollutant as shown in Table 2-3.

2.2.2 ADOM Model - Gases

The dry deposition modules in the Acid Deposition and Oxidant model (ADOM) (Pleim et al, 1984), CALPUFF (Scire et al., 1990), and CALGRID (Yamartino et al., 1992) models use the same basic approach, although the CALPUFF/CALGRID models contain a few enhanced features. The parameterization of the aerodynamic resistance is the same as for particles (Eqn. (2-24)). The deposition layer resistances is parameterized in terms of the Schmidt number, Sc.

$$r_d = d_1 \, Sc^{2/3} / (k \, u_*) \qquad (2\text{-}35)$$

Table 2-3

Values of Chemical Input Parameters Required by the RADM Deposition Model
(From Wesely, 1989)

Gaseous species	Symbol	D_{H_2O}/D_x [1]	Solubility[2]	Reactivity[3]
Sulfur dioxide	SO_2	1.9	1×10^5	0
Ozone	O_3	1.6	0.01	1
Nitrogen dioxide	NO_2	1.6	0.01	0.1
Nitric oxide	NO	1.3	2×10^{-3}	0
Nitric acid vapor	HNO_3	1.9	1×10^{14}	0
Hydrogen peroxide	H_2O_2	1.4	1×10^5	1
Acetaldehyde	ALD	1.6	15	0
Formaldehyde	HCHO	1.3	6×10^3	0
Methyl hydroperoxide	OP	1.6	240	0.1
Peroxyacetic acid	PAA	2.0	540	0.1
Formic acid	ORA	1.6	4×10^6	0
Ammonia	NH_3	1.0	2×10^4	0
Peroxyacetyl nitrate	PAN	2.6	3.6	0.1
Nitrous acid	HNO_2	1.6	1×10^5	0.1

(1) Ratio of molecular diffusivity of water to that of the pollutant

(2) Effective Henry's law coefficient (m/atm)

(3) Pollutant reactivity parameter as defined by Wesely (1989)
(0 = nonreactive, 0.1 = slightly reactive, 1 = highly reactive)

Table 2-4
Summary of Input Requirements of RADM Deposition Module
for Gases

Pollutant Characteristics:

- solubility (effective Henry's law coefficient)
- molecular diffusivity
- reactivity class parameter (nonreactive, slightly reactive, or highly reactive)

Geophysical Data:

- surface roughness length
- land use category

Meteorological Variables:

- friction velocity
- Monin-Obukhov length
- air temperature
- solar radiation

---

where d_1 is an empirical constant (~ 2). The Schmidt number is defined as the ratio of the viscosity of air (~ 0.15 cm^2/s) to the molecular diffusivity of the pollutant in air.

The canopy resistance is computed by considering three pathways for uptake of the pollutant within the vegetation or at the surface:

(1) transfer through the stomatal pore and dissolution or reaction in the leaf interior,
(2) reaction with or transfer through the leaf cuticle, and,
(3) transfer into the ground or water surface.

This is expressed as three resistances in parallel.

$$r_c = [LAI/r_f + LAI/r_{cut} + 1/r_g]^{-1} \quad (2\text{-}36)$$

where, LAI is the leaf area index (ratio of leaf surface area divided by ground surface area). The LAI can be estimated from land use type and season (e.g., see Table 2-5),
r_f is the internal foliage resistance,
r_{cut} is the cuticle resistance, and,
r_g is the ground resistance.

SO_2 is used as a reference species because considerable data are available for it. The model inputs for other species are computed by scaling the reference values for SO_2 by the relative adjustment factors for the other compounds. For example, the cuticle resistance for a pollutant twice as reactive as SO_2 is assumed to be one half the reference SO_2 cuticle resistance. Typical input values for many chemical species are described in the ADOM User's Guide.

The data requirements of the ADOM-type deposition models are very similar to those of the advanced RADM deposition model. Table 2-6 lists the required input parameters. All of the geophysical parameters can be derived from a classification of the land use in the area (e.g., urban, agriculture, forest, etc.). The meteorological variables are either observed routinely (e.g., temperature) or can be computed from routinely-available data. The pollutant characteristics can generally be obtained from the literature.

2.2.3 NOAA/ARL Models

A hierarchy of dry deposition models developed by NOAA/ARL are described in papers by Meyers and Baldocchi (1988), Baldocchi et al. (1987), Meyers (1987), Hicks et al. (1987), and

Table 2-5
Leaf Area Index Values as a Function of Land Use Type and Season
(From Scire et al., 1986)

Land Use Type	Vegetative Growing Season*			
	I	II	III	IV
Water	0.00	0.00	0.00	0.00
Deciduous forest	6.00	6.00	0.50	0.40
Coniferous forest	7.00	7.00	7.00	6.00
Swamp	2.00	1.50	1.00	0.50
Cultivated	3.00	1.00	0.20	0.01
Grassland	2.00	1.50	1.00	0.50
Urban	0.30	0.20	0.05	0.01
Desert shrubland	0.10	0.10	0.10	0.05

* Definitions of season categories:

I = peak growing season
II = early growing season
III = non-growing season without snow
IV = non-growing season with snow

Table 2-6
Summary of Input Requirements of ADOM-type Deposition Modules for Gases

---

Pollutant Characteristics:

- solubility (Henry's law coefficient)
- molecular diffusivity
- pollutant reactivity
-aqueous phase dissociation constant

Geophysical Data:

- land use category
- surface roughness length (derived from land category)
- leaf area index (derived from land use category)

Meteorological Variables:

- friction velocity
- Monin-Obukhov length
- air temperature
- solar radiation

---

others. There are four basic models of increasing complexity and sophistication (as well as increasing data requirements and computational cost) referred to as model I through model IV. The simpler two models (I and II) were reviewed in the current project. Model I is known as the "big leaf" model because it treats the plant canopy as a single surface partitioned into shaded and sunlit portions to account for differences in stomatal resistances. The aerodynamic resistance in model I is approximated (Hicks et al., 1987) by:

$$r_a = \begin{cases} 4\left(u\ \sigma_\theta^2\right)^{-1} & \textit{neutral, stable conditions} \\ 9\left(u\ \sigma_\theta^2\right)^{-1} & \textit{unstable conditions} \end{cases} \qquad (2\text{-}37)$$

where, u is the wind speed (m/s), and,

σ_θ is the standard deviation of the horizontal wind direction fluctuations (deg.).

The level II model is similar to model I, except that a somewhat more refined estimate is made of the aerodynamic resistance and canopy resistance. The formulation of r_a in model II may be better suited for regulatory applications because it does not need an estimate of σ_θ, which is not routinely measured at airport meteorological stations. Model II computes r_a based on the surface friction velocity and Monin-Obukhov length.

The deposition layer resistance is parameterized in models I and II as:

$$r_d = \left(\frac{2}{k\ u_*}\right)\left(\frac{D_t}{D_x}\right)^{2/3} \qquad (2\text{-}38)$$

where, D_t is the thermal diffusivity of air (cm^2/s), and,

D_x is the molecular diffusivity of the pollutant (cm^2/s).

The canopy resistance is expressed as a composite resistance composed of several parallel pathways, including transfer to the leaf stomata into the plant tissue, transfer to the leaf cuticle, or transfer directly to the ground or water surface.

The variables used by the model to compute the stomatal resistance include detailed information on vegetation which would not be available for many routine applications. The data and computational requirements of the level III model (K-theory model) and level IV (higher-order closure model) are considered too extensive for routine applications. Therefore, the NOAA/ARL models are not being used as core models in the current study, although the parameterization of some individual resistances may be included in future hybrid versions of the core gas deposition models to be evaluated.

3. Plume Depletion Techniques

Several different approaches to account for the depletion of the pollutant from the plume due to dry deposition processes have been reviewed. The schemes examined include the source depletion method (Chamberlain, 1953), the surface depletion method (Horst, 1977), the K-theory approach (Rao, 1981), and a modified source depletion technique (Horst, 1983). These models determine how the pollutant which is deposited at the surface is removed from the plume.

3.1 Source Depletion

The source depletion technique is the simplest method for removing pollutant material from a Gaussian plume. At each downwind distance, the source term (emission term) of the Gaussian equation is adjusted (decreased) to simulate the effect of increased pollutant removal with distance. At any distance, x, the source strength, Q is:

$$Q(x) = Q_o \exp\left\{ - \int_0^x \frac{v_d}{u} \overline{D}\,(x)\, dx \right\} \qquad (3\text{-}1)$$

where, Q_o is the initial source strength (g/s),
u is the transport wind speed (m/s), and,
$D(x)$ is a cross-wind integrated diffusion function ($\overline{D} = u\,\overline{\chi}/Q_o$) with units of (1/m), and,
$\overline{\chi}$ is the cross-wind integrated concentration (g/m^2).

Although the source depletion method is computationally efficient, it has the drawback that it immediately redistributes any pollutant loss at the ground throughout the entire depth of the plume. This results from making the adjustment for plume depletion only in the source term while retaining the original Gaussian shape of the vertical distribution. This redistribution of plume mass in the vertical results in an overestimation of deposition in the near-field but underestimation at large distances. The source depletion technique would probably be acceptable for determining deposition at the point of maximum impact, but is not recommended for use in the current study, because of the requirement for applicability to a wider range of conditions.

3.2 Surface Depletion

The surface depletion technique (Horst, 1977) allows the pollutant to be depleted in the vicinity of the surface rather than throughout the vertical extent of the plume. Thus, the resultant plume is allowed to assumed a non-Gaussian shape. This is done by treating the ground surface as "negative" sources, representing a sink for the pollutant. The surface depletion equation is:

$$\chi(x,y,z) = Q_o \frac{D(x,y,z,h)}{u} - \int_{-\infty}^{\infty}\int_{o}^{x} \frac{v_d}{u} \chi(\xi,\eta,z_d) D(x-\xi, y-\eta, z,o)\, d\xi\, d\eta \qquad (3\text{-}2)$$

where D is the diffusion function ($D = u\chi/Q_o$),
χ is the concentration at spatial coordinates (x,y,z), and
the other terms have been defined previously.

The surface depletion method is generally considered to be the most accurate solution of plume depletion and is frequently used as a reference method for other techniques. However, the numerical solution of the complex integral requires between 10 and 100 times more computer time than the source depletion technique. The large computational cost of the surface depletion method makes it impractical for routine use. Another drawback of the surface depletion technique for the current application is that its applicability is restricted to pollutants with negligible gravitational settling velocities.

3.3 K-theory Approach

Rao (1981) describes a K-theory model for estimating concentrations in the case of gravitational settling and deposition. The concentration is given by:

$$\chi(x,y,z) = \frac{Q_o}{u} \frac{g_1}{L_y} \frac{g_2'}{L_z} \qquad (3\text{-}3)$$

where $g_1(x,y)$ is the crosswind diffusion function,
$g'_2(x,y)$ is the vertical diffusion function modified for deposition effects, and
L_y, L_z are the length scales of the concentration distribution in the y and z directions.

$$g_1(x,y) = \exp\left(-y^2/2\sigma_y^2\right) \tag{3-4}$$

$$L_y = \sqrt{2\pi}\ \sigma_y \tag{3-5}$$

$$g_2' = \exp\left[\frac{-v_g\,(z-H)r}{2\sigma_z} - \frac{v_g^2 r^2}{g}\right] \cdot \left[\exp\left\{\frac{-(z-H)^2}{2\sigma_z^2}\right\} + \exp\left[\frac{-(z+H)^2}{2\sigma_z^2}\right]\right] \cdot \left(1-\sqrt{2\pi}\,(v_d - v_g/2)\,r\,\exp(\xi^2)\,erfc\ \xi\right)\Big] \tag{3-6}$$

$$r = \frac{2x}{u\sigma_z} \tag{3-7}$$

$$\xi = \frac{z+H}{\sqrt{2}\ \sigma_z} + \frac{(v_d - v_g/2)r}{\sqrt{2}} \tag{3-8}$$

$$L_z = \sqrt{2\pi}\ \sigma_z \tag{3-9}$$

The K-theory model was included in the evaluation study of Doran and Horst (1985). They noted that the K-theory model is valid only when the vertical dispersion coefficient, σ_z, varies as $x^{1/2}$. For more general forms for σ_z (e.g., such as those used in regulatory models such as ISC), the K-theory model does not conserve mass. Doran and Horst developed a method to estimate the missing mass, and then add it back into the plume. Although this correction improved the

performance of the model, it still did not perform quite as well as the modified source depletion technique.

Winges (1990) describes the numerical integration scheme used to compute the mass conservation correction factors for the K-theory method in the Fugitive Dust Model (FDM). A least squares fit to computed values of the correction factors was calculated for the various combinations of 6 wind speeds, 6 stability classes, 6 particle size classes, and 5 release heights (i.e., 1080 values), and entered into the FDM code in data statements. Winges (1992, personal communication) has indicated that in a new release of FDM, an external disk file with a much larger number of the correction factors is supplied with FDM to cover a wider range of wind speeds, size classes and release heights than the previous version of the model.

The lack of mass conservation in the unmodified K-theory model or alternatively, the need to store large numbers of pre-computed mass conservation correction coefficients are viewed as the major drawbacks to the K-theory scheme, especially since alternatives without these liabilities are available.

3.4 Modified Source Depletion

Horst (1983) describes modifications to the source depletion technique to account for the change in the vertical distribution of the pollutant due to deposition at the surface. In the modified source depletion method, a profile correction factor, P (x,z) is defined and applied to the diffusion function to account for plume depletion effects.

$$\begin{aligned} C(x,z) &= Q(x)\, D'(x,z,h) \\ &= Q(x)\, D_o'(x,z,h)\; P(x,z) \end{aligned} \tag{3-10}$$

where C(x,z) is the crosswind integrated concentration,
D′(x,z,h) is the crosswind integrated diffusion function,
D_o'(x,z,h) is D′ for a nondepositing pollutant, and
P(x,z) is the profile correction factor.

For $\sigma_z = ax$,

$$R(z,z_d) = \sqrt{\frac{2}{\pi}\,\frac{1}{au}}\,\ln(z/z_d) \tag{3-11}$$

$$P(x,z) = \left\{ 1 + \frac{v_d}{u} \sqrt{\frac{2}{\pi}} \frac{1}{a} \left[\ln(\sigma_z/z_d) - 1 \right] \right\}^{-1} \tag{3-12}$$

where the resistance, R, is defined such that

$$C(x,z) = C(x,z_d) \left[1 + v_d R(z,z_d) \right] \tag{3-13}$$

and z_d is the reference height.

Horst (1983) provides equations for other forms of σ_z as well, including ax^b, $ax(1 + bx)^{-1/2}$, and $ax(1 + bx)^{-1}$. However, he does not provide solutions for the form $ax(1 + bx)^{1/2}$, which is needed for McElroy-Pooler coefficients under A and B stability conditions.

The modified source depletion method has been shown to produce results in close agreement with the exact surface depletion method (Horst, 1984), but only required a small fraction of the computer resources. In fact, its computational requirements were found to be comparable to the source depletion method. In the dual tracer study of Doran and Horst (1985), the modified source depletion model produced the best agreement with observations of any of the plume depletion models tested. They used dual tracer field observations of a depositing aerosol (ZnS) and a non-depositing gas (SF_6) in their evaluation.

In summary, the modified source depletion method has been shown to produce accurate results compared to both the exact surface depletion method and field observations. In addition, its formulation is well-suited for use in a Gaussian model, it can treat gravitational settling effects and plume tilt, it is computationally efficient, and it conserves mass exactly. For these reasons, the modified source depletion method of Horst (1983) was selected as the approach to use in the deposition module for assessing plume depletion.

The Horst (1983) method was implemented in ISC2 during a later phase of this study. Extensions to the method that were required are described in Appendix E.

4. Calculation of Meteorological Variables

Nearly all of the deposition models require estimates of the surface friction velocity (u_*), Monin-Obukhov length (L), and solar radiation. The methods of Holtslag and van Ulden (1983) are widely-used to estimate solar radiation and surface sensible heat flux from routinely-available meteorological and surface (land use) data. The Holtslag-van Ulden scheme has been implemented into the HPDM model (Hanna and Chang, 1991a), extensively compared and tested with field data (e.g., Hanna and Chang, 1992), and has been shown to produce reasonable results. Therefore, the techniques used in the HPDM meteorological preprocessor are used to produce the micrometeorology variables required in the deposition calculations.

4.1 Unstable/Neutral Conditions

The energy balance at the surface can be written as:

$$Q_* + Q_f = Q_h + Q_e + Q_g \tag{4-1}$$

where Q_* is the net all-wave radiation,
Q_f is the anthropogenic heat flux,
Q_h is the sensible heat flux,
Q_e is the latent heat flux, and
Q_g is the ground/storage heat flux.

Holtslag and van Ulden (1983) provide the following parameterization of the net radiation term:

$$Q_* = \frac{(1-A)Q_{sw} + c_1 T^6 + c_2 N - \sigma T^4}{1 + c_3} \tag{4-2}$$

$$Q_{sw} = (a_1 \sin\phi + a_2)(1 + b_1 N^{b2}) \tag{4-3}$$

$$c_3 = 0.38 \left[\frac{(1-\alpha)(S)+1}{S+1} \right] \qquad (4\text{-}4)$$

where T is the measured air temperature (deg. K),

A is the albedo,

σ is the Stefan-Boltzmann constant (5.67×10^{-8} W/m^2/deg. K^4),

N is the fraction of the sky covered by clouds,

ϕ is the solar elevation angle (deg.),

α is an empirical surface moisture parameter, and,

S is the slope of the saturation enthalpy curve [$S = s/\gamma$], where

$s = \partial(q_s)/\partial(T)$ and $\gamma = c_p/L$,

λ is the latent heat of water vaporization,

q_s is the saturation specific humidity, and,

c_p is the specific heat at constant pressure.

The four terms in the numerator of Eqn. (4-2) account for absorption of short-wave radiation at the surface, incoming long-wave radiation from gaseous components of the atmosphere (e.g., water vapor and carbon dioxide), incoming long-wave radiation due to clouds, and outgoing long-wave radiation from the surface, respectively. The factor in the denominator $(1+c_3)$, results from the use of air temperature rather than the more difficult-to-determine surface radiation temperature in the equation. The term in the first set of parentheses in Eqn. (4-3) represents short-wave solar radiation in the absence of clouds. The second term $(1+b_1N^{b2})$, accounts for the reduction of incoming solar radiation due to clouds (b_1 is negative). The values for the empirical constants c_1, c_2, a_1, a_2, b_1, and b_2 suggested by Holtslag and van Ulden (1983) are shown in Table 4-1.

The flux of heat into the ground or storage in surface materials, Q_g, is usually parameterized during the daytime as a fraction of the net radiation (e.g., DeBruin and Holtslag, 1982; Oke, 1978).

$$Q_g = c_g Q_* \qquad (4\text{-}5)$$

where c_g is an empirical coefficient which depends on the properties of the surface. Holtslag and van Ulden (1983) obtained a value of c_g of 0.1 for a grass covered surface in the Netherlands. Oke (1982) indicates that typical ranges for c_g are 0.05 to 0.25 in rural areas, 0.20 to 0.25 in suburban areas, and 0.25 to 0.30 in urban regions and suggests that typical values of c_g are 0.15, 0.22, and 0.27 for rural, suburban, and urban areas, respectively.

Table 4-1
Values of Net Radiation Constants
(Holtslag and van Ulden, 1983)

Constant	Value
a_1	990 W/m^2
a_2	-30 W/m^2
b_1	-0.75
b_2	3.4
c_1	5.31×10^{-13} $W/m^2/deg.\ K^6$
c_2	60 W/m^2

The anthropogenic heat flux, Q_f, can usually be neglected, except in highly urbanized areas. Hanna and Chang (1991b) contains a table listing typical values of Q_f for various cities.

The sensible heat flux, Q_h and latent heat flux are determined by Holtslag and van Ulden (1983) as:

$$Q_h = \left[\frac{(1-\alpha)+S}{S+1}\right](Q_* + Q_f - Q_g) - (\alpha)(\beta') \tag{4-6}$$

$$Q_e = \left[\frac{\alpha}{S+1}\right](Q_* + Q_f - Q_g) + (\alpha)(\beta') \tag{4-7}$$

where β' is an empirical coefficient (= 20 W/m^2).

Typical values of α, based on empirical data of Holtslag and van Ulden and summarized by Hanna and Chang (1991b) are:

α = 0.2 (arid rural areas)
α = 0.5 (urban areas, some parks, crops and fields during mid-summer when rain has not fallen for several days)
α = 0.8 (crops, fields, or forest with sufficient moisture)
α = 1.0 (normal wet grass in a moderate climate)

In neutral and unstable conditions, the following relationship developed by Wang and Chen (1980) is used in HPDM and other models such as MESOPUFF II to compute the friction velocity.

$$u_* = \frac{ku}{\ln[(z-d)/z_o]}\left[1 + d_1 \ln(1 + d_2\, d_3)\right] \tag{4-8}$$

where

$$d_1 = \begin{cases} 0.128 + 0.005\ln(z_o/z) & z_o/z \le 0.01 \quad (4\text{-}9) \\ 0.107 & z_o/z > 0.01 \quad (4\text{-}10) \end{cases}$$

$$d_2 = 1.95 + 32.6(z_o/z)^{0.45} \quad (4\text{-}11)$$

$$d_3 = \frac{Q_h}{\rho c_p} \frac{kgz}{T u_{*n}^3} \quad (4\text{-}12)$$

The term $d_1\ln(1 + d_2d_3)$ represents the correction due to instability, $u_{*n} = ku/[\ln(z - d)/z_o]$, k is the von Karman constant (~ 0.4), and d is the displacement height.

Hanna and Chang (1990, 1992) tested the analytical formula against values produced by the iterative solution of u_* and L. They found that the Wang and Chen (1980) expression produced values within 10% of the results determined by the iterative solution for z = 10 m, d = 0, z_o = 1 m, and a large value of Q_h (400 W/m^2). Better agreement was found for smaller roughness elements and smaller sensible heat fluxes. In addition, the analytical solution was computationally significantly faster.

The Monin-Obukhov length can then be computed directly from its definition once u_* is determined from Eqn. (4-8) and Q_h from Eqn. (4-6).

$$L = \frac{-u_*^3 T \rho c_p}{k g Q_h} \quad (4\text{-}13)$$

4.2 Stable Conditions

The Weil and Brower (1983) method for estimating u_* is applied in HPDM during stable conditions. A first estimate of the scaling temperature, θ_*, is calculated using Holtslag and Van Ulden's (1983) equation:

$$\theta_{*1} = 0.09(1 - 0.5N^2) \quad (4\text{-}14)$$

where N is the total fractional cloud cover and θ_* has units of °K. Another estimate of θ_* is made from the profile equation for temperature:

$$\theta_{*2} = \frac{T C_{dn} u^2}{18.8 z g} \qquad (4\text{-}15)$$

where the neutral drag coefficient C_{dn} is defined as $k/\ln[(z - d)/z_o]$.

Then, θ_* is set equal to the smaller of θ_{*1} and θ_{*2}.

The sensible heat flux, Q_h, is defined during stable conditions as:

$$Q_h = - \rho c_p u_* \theta_* \qquad (4\text{-}16)$$

For large values of u (or u_*), θ_{*1} (which depends only on cloud cover) is smaller than θ_{*2}, but an additional check on the product $u_*\theta_*$ must be made, since Q_h does not keep increasing indefinitely with higher wind speeds. In HPDM, the value of θ_* is not allowed to exceed $0.05/u_*$, where the numerator has units of °K m/s and denominator has units of m/sec. This limit is estimated from observations of heat fluxes during high-wind, stable conditions.

The friction velocity, u_*, can be calculated from:

$$u_* = \frac{C_{dn} u}{2} \left[1 + \left(1 - \left(\frac{2 u_o}{C_{dn}^{1/2} u} \right)^2 \right)^{1/2} \right] \qquad (4\text{-}17)$$

where $u_o = (4.7 z g \theta_* / T)^{1/2}$.

Because θ_* is set equal to the smaller of θ_{*1} and θ_{*2}, the following condition is always met:

$$\frac{2 u_o}{C_{dn}^{1/2} u} \leq 1 \qquad (4\text{-}18)$$

During stable conditions, Hanna and Chang (1992) suggest a lower limit on L in recognition of the fact that the atmosphere is less stable over urban areas than over rural surfaces. Their suggested values for use for the various land use categories defined in the Auer (1978) scheme are shown in Table 4-2.

Table 4-2
Minimum Values of Monin-Obukhov Length
During Stable Conditions
for Various Land Use Types
(From Hanna and Chang, 1992)

Auer (1978)	Class	Description	Minimum L
C1	Commercial	> 40 story buildings	150 m
		10-40 story buildings	100 m
		< 10 story buildings	50 m
I1, I2	Industrial		50 m
R3	Compact Residential		50 m
R1, R2	Residential		25 m
A	Agricultural		2 m

5. Model Evaluation Protocol

The major objective of the evaluation exercise is the development and implementation of an objective model evaluation and scoring methodology that allows good-performing and poor-performing models to be distinguished, so that an appropriate dry deposition technique representing the current state-of-the-science may be selected. This protocol outlines an evaluation approach which allows, to the extent possible, an objective model performance scoring and selection process which results in the selection of a deposition model for gases and another for particles. We have adopted the EPA's model statistical approach to model evaluation as described by Cox and Tikvart (1990).

The accuracy of a model performance evaluation is dependent upon the accuracy and representativeness of both the observations used for comparison and the model input data used to produce predictions. Estimates of dry deposition rates presently suffer from numerous sources of uncertainty (Hosker and Lindberg, 1982) leading to the situation where there is a wide spread of overlap for sets of deposition velocity observations even under similar experimental conditions. As a consequence, it is expected that, given the small size of the deposition velocity data sets and uncertainties present in the measurements and model input data, the resulting uncertainties present in both observations and predictions of deposition velocity will make it difficult in many cases to distinguish between the statistical performance of some models. An exact quantitative description of the uncertainties is not possible for many of the data sets due to limited information on the reported observed data.

5.1 Evaluation Approach

The model evaluation focused on a comparison of observed and predicted deposition velocities. Since the ISC model uses reflective coefficients instead of deposition velocities, the effective deposition velocity for the ISC scheme had to be estimated. Appendix A contains a description of the method used to convert the reflective coefficients into effective deposition velocities for use in the model evaluation effort.

In the present study we combined all the particle deposition data from the various observational studies, many of which had less than 10 observations, into one large data set of 168 data points that have sufficient concurrent data for inputs to the deposition models. Several subsets of deposition data were created based on one or more stratification criteria. On each subset model performance statistics were calculated. These statistics were used to estimate a composite measure of performance where the most accurate model produces the smallest

composite measure based on the EPA's Cox-Tikvart approach utilizing fractional bias. In summary, the model evaluation exercise consisted of the following steps:

1) Stratification of the observed deposition velocity data into subsets based on several criteria such as physical and chemical properties, surface characteristics, meteorological conditions, etc.

2) Direct statistical and graphical comparison of observations versus predictions of deposition velocity for each subset using the EPA's Cox-Tikvart protocol (Cox and Tikvart, 1990).

3) Ranking of model performance using a composite performance measure (CPM) and selection of the best performing model based on rank and uncertainty in the CPM.

The models which were evaluated and scored were discussed in Section 2. In addition to core models, several hybrid models were created for performance evaluation based on our review of the physics represented by the models, and on the outcome of the sensitivity analysis. The technical review provided indications of which components of the various core models are superior, and which may have some unrealistic characteristics. We created several hybrid models from the core models in order to offer the U.S. EPA the best performing model (instead of several that perform about the same and which may have one or more flaws that can create problems in the context of the wide ranging applications seen by ISC). The hybrid models were exercised in the same manner as the core models and received the same statistical treatment and scoring as the core models.

5.2 Stratification of Deposition Velocity Datasets

The complete data set of observed deposition velocities includes observations for several chemical species plus particles made over a variety of surfaces and under a wide range of meteorological conditions and sampling times. Model performance was expected to vary significantly between chemicals or particle sizes, and for different surfaces and meteorological conditions. As a result we divided the complete data set into subsets based on the following criteria:

1) physical and chemical characteristics
2) surface conditions
3) meteorological conditions

Figure 5-1 illustrates these subdivisions that were made in the data. A primary division is made depending whether the substance is a particle or a gas since the physical deposition processes are different for gases than particles. Further subdivision of the data was made in such a manner that a minimum number of observations was lost to datasets with sample sizes less than 10. The stratification criteria that appear to provide large enough sample sets and which are informative and nonredundant are the following:

> Physical characteristics
  a) Particles
    1) 2 size ranges (diameters less than 0.1 micron and between 0.1 and 20 microns),
  b) Gases
    1) Chemical species (SO_2 and O_3 are only two species with sample sizes in the hundreds)

> Surface Characteristics
  a) Particles and Gases
    1) rough/smooth surface based on surface roughness length
    2) dense/sparse vegetation density based on leaf area index

> Meteorological Conditions
  a) Particles and gases
    1) day/night based on time of day
    2) large/small atmospheric diffusion based on friction velocity
    3) hot/cold based on ambient temperature

Division criteria were selected in order to (1) provide a logical break between two conditions (e.g., night = 000-600 1800-2400, day = 600-1800) and (2) provide a breakdown of the data set into subsets of approximately the same size.

The evaluation effort of particle deposition has focused on smaller particles (< 20 μm diameter) because this size range is where the most significant differences among the deposition models occurs. For particles above 20 μm diameter, the deposition velocity predictions for all of the models tend to quickly approach the gravitational settling velocity. Appendix D contains plots of deposition velocities as a function of particle diameter which illustrates this point.

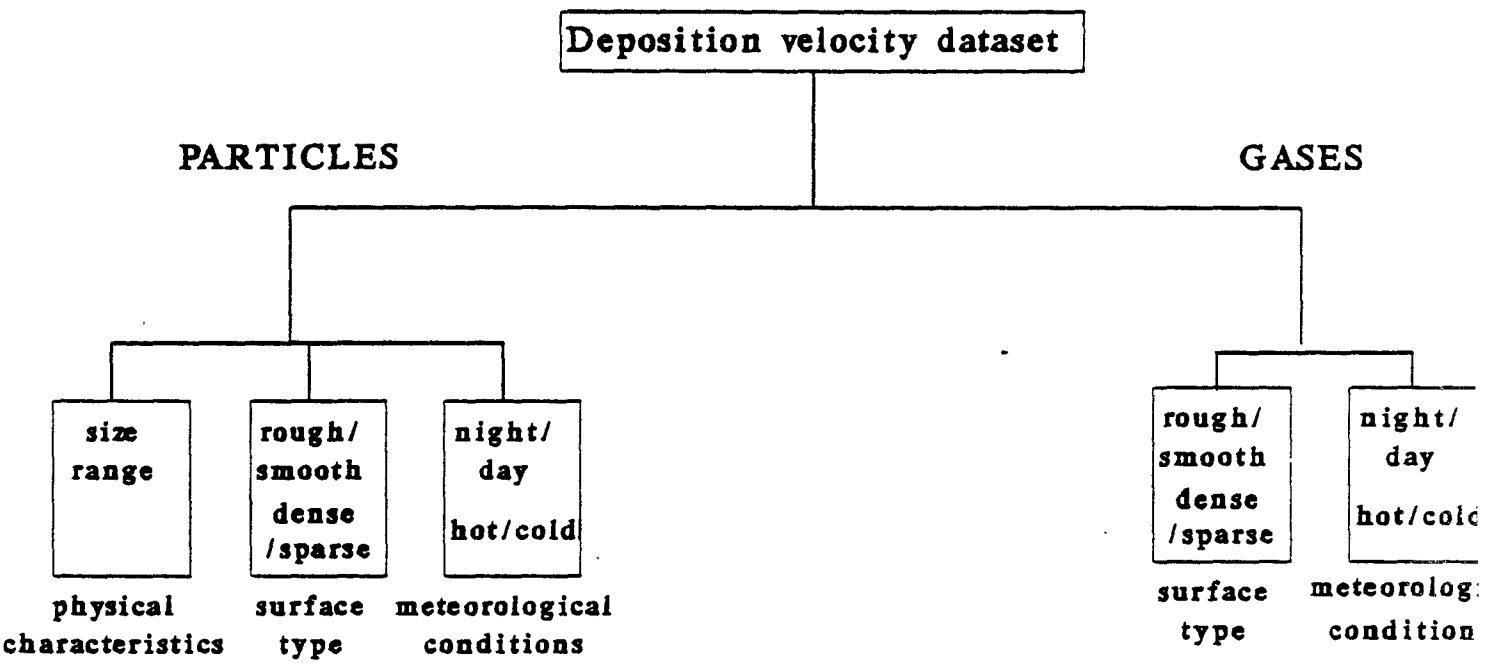

Figure 5-1. Schematic illustration of division of deposition velocity data into subsets.

5.3 Comparison of Predictions and Observations

For paired comparisons, the performance measures for the previously described subsets are based on an analysis of deposition velocity residuals either paired in time, paired in space, or paired in both space and time. Since deposition velocities are dependent on local surface conditions, pairings only by time would not be appropriate for the present study. Likewise, due to (1) limited simultaneous monitoring and (2) variations in sampling time between data sets, the use of pairing only by space does not seem to be appropriate either. Consequently the focus of the present study is on fully paired (space and time) data.

A number of traditional performance measures such as bias, variance, gross variability, and average absolute residuals suffer from the lack of ability to intercompare across the deposition velocity data subsets. Furthermore, other statistical measures utilized by the EPA (e.g., Cox and Tikvart, 1990) possess similar information on bias and precision, and are normalized in a manner that allows data set intercomparison and composite scoring of model performance. We utilized four types of normalized statistical measures including:

1) fractional bias of arithmetic averages (FBA)
2) fractional bias of arithmetic standard deviations (FBSD)
3) fractional bias of robust extreme statistic for the n smallest values (FBSE)
4) fractional bias of robust extreme statistic for the n largest values (FBLE)

These four measures all possess the same metric (e.g., have the same range bounding and limits) and consequently are directly intercomparable. The fractional bias of the average (FBA) is defined as:

$$FBA = 2\frac{(\overline{O} - \overline{P})}{(\overline{O} + \overline{P})} \tag{5-1}$$

where the average is given by:

$$\overline{O} = \frac{1}{N}\sum_{i}^{N} O_i \tag{5-2}$$

The fractional bias of the standard deviation (FBSD) is defined as:

$$FBSD = 2\frac{(\sigma_o - \sigma_p)}{(\sigma_o + \sigma_p)} \tag{5-3}$$

where the standard deviation is given by:

$$\sigma_o = \left[\frac{1}{(N-1)} \sum_{i}^{N} (O_i - \overline{O})^2 \right]^{1/2} \tag{5-4}$$

The FBA is useful to quantify the degree of model over or underprediction. FBSD is useful to determine if model predictions have more or less variability than observations.

Deposition velocity minimums are an important factor in estimating maximum ambient concentrations, while maximum deposition velocities are important when estimating maximum exposure (due to deposited material) estimates. Thus estimating a robust extreme statistic for both the n set of largest and smallest deposition velocities is important.

The robust extreme statistic (RES) for maximum deposition velocities is expected to follow an exponential tailed distribution like that of concentration. For such a distribution the RES is estimated via the relation:

$$O(RES) = O(n) + (\overline{O} - O(n)) \log \left[\frac{3n - 1}{2} \right] \tag{5-5}$$

where the average $\overline{O}$ is over the n - 1 largest values and O(n) is the nth largest value. There is also a need to estimate a similar robust statistic for the smallest deposition velocities. Development of a similar robust statistic for small deposition velocities is difficult since:

1) the functional form of the probability density function (pdf) is relatively unknown for the tail of the distribution representing the smallest deposition velocities,

2) considerable uncertainty is present in observations of small deposition velocities due to both uncertainty in measurement and interference by resuspension processes, and

3) the presence of a lower bound (zero) insures asymmetry in the distribution of extremes, meaning the same measure estimated using Eqn. (5-5) for the unbounded maximum deposition velocities cannot be used as a lower bound measure.

Because of the problems cited above we elected to use the average of the smallest 10% of the deposition velocities. In an effort to avoid a lack of robustness due to small sample size

we estimated the extreme statistics for only the overall data set and not for the subsets in the study.

The fractional bias of the extreme statistic is given by:

$$FB(LE \text{ or } SE) = 2\frac{(O(RES) - P(RES))}{(O(RES) - P(RES))} \tag{5-6}$$

The FBLE provides an indication of the degree of over- or underprediction in the largest values while FBSE does the same for the smallest values.

5.4 Scoring Model Performance Using Composite Measures

A composite performance measure (CPM) is calculated for each model as a weighted linear combination of the individual absolute fractional bias components. Each of the four fractional bias measures previously defined are combined as a weighted linear sum. The compensatory effect of sign (over- or underprediction) is removed by taking the absolute value of each bias measure. The resulting sum which serves as a composite fractional bias (CFB) is defined for both the overall data set

$$CFB_o = w_1|FBA_o| + w_2|FBSD_o| + w_3|FBSE_o| + w_4|FBLE_o| \tag{5-7}$$

and for each of the stratification subsets. The CFB for kth subdivision is defined as:

$$CFB_k = w_1|FBA_k| + w_2|FBSD_k| \tag{5-8}$$

All measures are assumed to be equally important and the weights serve merely as an average, e.g.,

$$w_1 = w_2 = w_3 = w_4 = \frac{1}{4} \tag{5-9}$$

The CFB_k is averaged over all subsets (assuming each subset is equally important).

$$\overline{CFB} = \frac{1}{n}\sum_{k=1}^{M} CFB_k \tag{5-10}$$

where in the present case there are 12 subsets (M = 12). The average is then combined with the CFB_o resulting from the overall data in order to produce the composite measure (CPM).

$$CPM = \frac{1}{2}\overline{CFB} + \frac{1}{2}CFB_o \tag{5-11}$$

The CPM thus contains information about both overall model performance as well as performance under specific sets of conditions. The use of the CPM to select an appropriate model reduces the possibility that model performance biases under specific sets of conditions (which may be over represented in the complete data) will unduly influence model selection. A perfect model will produce a CPM of zero. The CPM is independent of whether the model over- or underpredicts. The model with the smallest CPM is selected as a winner if it can be shown that the CPM is lower than other models in a statistically significant sense (e.g., different at the 95% confidence level).

In the present study we estimate the 95% confidence interval of the CPM for each model. The confidence interval is used to establish how robust our selection process may be based on our single estimate of CPM. A model could have the smallest CPM but if it is not very different from that of another model, or if the estimate is relatively uncertain, then the model should not be selected.

The difference in the CPM between all pairs of models is estimated in order to determine if differences between models are significant. The difference between the performance of one model and another is the model comparison measure (MCM), defined as;

$$MCM(A,B) = CPM(A) - CPM(B) \tag{5-12}$$

where, CPM(A) = Composite performance measure for Model A, and
CPM(B) = Composite performance measure for Model B

The MCM is used to judge the statistical significance of the apparent superiority of any one model over another. If the MCM is not significant from zero at the 95% confidence level then the two models cannot be said to perform in a significantly different manner.

The bootstrap resampling technique is used to estimate confidence intervals on the various measures described above. In applying the bootstrap procedure, observed and predicted data pairs are resampled. Sampling is done with replacement, so some data points are represented more than once. This process is repeated 1000 times so that sufficient samples are

available to calculate the standard error of each measure. The resampling recognizes the stratifications made on each of the model input variables as individual blocks. This assures that each of the 1000 variants of the original dataset retained the same number of samples from each stratification. Had we not blocked the data in this way, one of the 1000 variants might, for example, only consist of a few samples associated with say the largest friction velocity (repeated many times). The bootstrap resampling method allows the standard deviation, s_{pm}, of any performance measure to be estimated, from which a confidence interval can be calculated. The actual CPM or MCM for each model or model pair is assumed to have a 95% chance of lying within the range given as

$$CPM - cs_{pm} < CPM_{actual} < CPM + cs_{pm} \tag{5-13}$$

where c is a multiplier for a specific percentage level of confidence.

The standard error of the estimate is simply the standard deviation of the measure over all of the bootstrap-generated outcomes. If the measure involves a single comparison, such as CPM for a single model, then the value of c can be set equal to the student-t parameter.

Difference measures such as the MCM require that simultaneous confidence intervals be found for each pair of models in order to ensure an adequate confidence level and to protect against falsely concluding that two models are different. The method of Cleveland and McGill (1984) is used to calculate c. In this method, c is found such that for 95 percent of the 1,000 bootstrap i-tuples,

$$\frac{|\Delta_{ij} - \Delta_{ijk}|}{s_{ij}(\Delta_{ijk})} \leq c \tag{5-14}$$

where, Δ_{ij} = model comparison difference measure for model pair i,j,
Δ_{jkl} = model comparison difference measure for model pair i,j and bootstrap replication k, and
s_{ij} = standard deviation of all the Δ_{ijk} values.

The 95% confidence intervals for CPM and MCM for each model and pair of models is presented. The confidence intervals on the MCM are critical to this study since if the range that the actual MCM may be found in does not include zero, then the two model's performance statistics can be said to be statistically different.

Model selection was based on model rank, and if the model MCM was significantly non zero for all other models. Models with overlapping confidence intervals (MCM that are not significant from zero) were grouped. Models clustered within groups were treated as having the same model performance.

Summary of Scoring Scheme

In summary, the steps taken in providing a scoring of each model analyzed are as follows:

(1) For each model calculate the FB's for the observed and predicted deposition velocities paired by time and location over all data and for each stratification (block). Calculate the CPM with confidence limits and summarize the model performance by category using CFB's. The smaller the CFB's and the CPM, the better the overall performance of the model.

(2) Rank CPM from smallest to largest. Calculate confidence intervals for each CPM to determine if clearly superior or inferior model performance occurs based on ranking and confidence interval.

(3) Calculate the MCM with confidence intervals for each possible model pairing. Rank MCM's and determine which model pairs have a significantly non zero difference.

6. Model Evaluation Data Bases

A list of observational data sets of particle deposition used in the evaluation of the particle deposition models described in Section 2.1 is presented below. The observational deposition velocity data are reproduced in Appendix C.

6.1 Particle Data Sets

(1) *Doran and Horst (1985).* This paper reports on the results of a field experiment involving dual tracers. Simultaneous releases were conducted of ZnS, a polydisperse aerosol, and nondepositing SF_6. Deposition velocities of the particles were computed and are summarized in the paper. The study used the data to compare four different plume-depletion models.

(2) *Lorenz and Murphy (1989).* The aerodynamic profile method was used to determine deposition rates of 1.0 μm diameter particles to a rough vegetated surface. Figures showing deposition velocities as a function of meteorological parameters are contained in the paper. Tables summarizing the mean deposition velocity as a function of particle size contain 61 data points.

(3) *Nicholson and Davies (1987).* The profile method was used to derive dry deposition rates of particulate sulfate over a rural site in England. Approximately 170 observations were made over a one year period. Of these, 78 data points remained after application of a set of stringent quality criteria. Tabulated values of deposition velocities and meteorological conditions are presented in the report.

(4) *Sehmel (1980), Sehmel and Hodgson (1978).* These studies contain the results of wind tunnel measurements of particles in the size range from 0.03 μm to 29 μm diameter. Low roughness surfaces were used in the experiments, ranging from smooth brass to gravel (z_o up to 0.6 cm). Least squared techniques were used to develop a set of equations fitting the data points. Graphs are provided in the papers showing deposition velocities predicted by the least squared fit equations (though not the original data points) as a function of roughness length, friction velocity, and particle diameter. The predictions from the Sehmel and Hodgson regression equations (as coded in the CARB model) were plotted and intercompared with the other deposition models.

(5) *Hicks et al. (1986).* Eight data points for the dry deposition particulate sulfur were obtained from this study which also measured gaseous fluxes. Measured meteorological parameters included temperature, wind speed, and friction velocity.

(6) *Garland (1982).* This paper summarizes the dry deposition rates of small particles to grass in field and wind tunnel experiments. Deposition velocities for lead are presented as a function of particle diameter. Additional data for an oxide of iron is presented. These data show similar results from measurements in the field and wind tunnel.

(7) *Wesely et al. (1982).* Eddy correlation measurements were used to estimate the dry deposition of particulate sulfur. Approximately 19 data points are available including measurements of sensible heat and friction velocity. The data points were gathered over short grass during drought conditions in eastern Texas. Summaries of eddy-correlation experiments over other surfaces are also presented.

(8) *Wesely et al., (1983).* Observations of submicron particle deposition velocities were made in a deciduous forest during winter over the course of a week. A fine particle sensor was used to measure particles in the 0.01 to 2 micron size range. Approximately a dozen eddy correlation estimates of deposition velocities were reported. Micrometeorological turbulence data was collected simultaneously with the deposition data.

6.2 Gas Data Sets

The observational data sets of gas deposition which have been collected for use in the future evaluation of gas deposition models are summarized below.

(1) *Meyers and Baldocchi (1988).* Direct eddy correlation measurements of SO_2 and O_3 fluxes are summarized for both well-watered and water-stressed conditions. Deposition velocities and meteorological data are presented for approximately 31 periods during two experiments. The study discusses a comparison of the observations to a hierarchy of deposition models from simple to highly complex.

(2) *McMillen et al. (1987).* This report contains measurements of dry deposition of SO_2 to a forested site in Germany. The measurements were made using the eddy correlation method. A tabular listing of the meteorological and deposition data are presented in an Appendix of the report. The report discusses limitations to the data and conditions under which the results are considered usable. Basically, good results were obtained when SO_2 concentrations exceeded about 1 ppb.

(3) *Hicks et al. (1989).* Data are summarized from an intensive field study of dry deposition of SO_2 to a variety of crops at a site in Pennsylvania. Conservative quality-assurance guidelines were used to screen the raw data base and produce about 22 useful data points. The report contains tabular listings of the meteorological data and deposition results from the study.

(4) *Harrison et al. (1989).* A gradient technique was used to determine deposition velocities of HNO_3 and HCl over a variety of vegetative surfaces. Approximately 34 data points are provided for the deposition velocity along with selected meteorological parameters, including the surface friction velocity for each run.

(5) *Meyers et al. (1989).* The deposition velocity of HNO_3 over a fully leafed deciduous forest was estimated using a gradient technique. The observations were compared to the predictions of a detailed canopy turbulence model. Heat flux and friction velocities are provided for each experiment. Approximately 10 data points are listed in tables in the paper.

(6) *Godowitch (1990).* Vertical ozone fluxes were measured from aircraft over several different land use types, including agricultural crops and forested areas. An analysis was performed to derive ozone deposition velocities for each experiment. Measurements of selected meteorological parameters are also provided.

(7) *Wesely et al., (1983).* Eddy correlation measurements of ozone fluxes were performed above a leafless deciduous forest. Measurements of fine particles with a diameter of approximately 0.1 μm were also performed. Ranges of deposition velocities and meteorological parameters are tabulated in the paper. The results of 19 half-hour averaged measurements are also provided for both ozone and particulate sulfur deposition, although the particle data contain a low signal-to-noise ratio. However, at least the ozone measurements (10 points) appear to be usable.

(8) *Wesely et al., (1978).* An eddy correlation technique was used to determine vertical fluxes of ozone above both mature and senescent maize canopies. The results of approximately 26 runs are tabulated. Both deposition velocities and meteorological measurements (e.g., friction velocity, heat flux) are provided.

(9) *Wesely et al., (1981).* Measurements of ozone deposition velocity over snow, wet bare soil, and water were made using the eddy correlation technique. Over 60 data points are listed. Meteorological data during each experiment is provided. An interesting component of this study is the importance of evaporation (Stefan flow) in influencing the deposition rate.

(10) *Hicks et al., (1986).* Eddy correlation measurements of vertical fluxes of gaseous and particulate sulfur compounds were conducted over two different surface types. Tables of meteorological conditions and deposition velocities are provided for 26 different time periods. Data is also presented for NO_x fluxes, but it is highly variable due to a low signal-to-noise ratio in the NO_x measurement system. It appears that 8 points of SO_2 deposition are usable.

(11) *Fowler and Cape (1982).* The eddy correlation method was used to calculate SO_2 fluxes over a Scots pine forest during daytime hours. Tables of flux, deposition velocity, and sensible heat are presented for 20 points. Dry deposition rates ranged from 0.5 to 10 mm/sec.

(12) *Davies and Mitchell (1982).* This paper presents dry deposition rates for SO_2 based on gradient method measurements over grass in rural eastern England during a period of relatively constant atmospheric conditions. Twenty-five data points are available including wind speed, friction velocity, sensible heat flux, and Monin-Obukhov length.

(13) *Huebert (1982).* A modified Bowen Ratio method was used to measure nitric acid fluxes in this study. Measurements were made over a pasture near Champaign, Illinois. Meteorological parameters measured include wind speed and friction velocity. The results of the study showed that dry deposition is capable of depositing HNO_3 at a rate comparable to that of wet deposition measured in previous experiments.

(14) *Padro et al. (1991).* In this paper, the ADOM dry deposition model was compared to observed ozone deposition velocities taken over a fully leafed mixed deciduous forest during July and August of 1988. Meteorological data collected during the study include wind speed, wind direction, temperature, dew point, solar radiation, net radiation, friction velocity, sensible heat flux, latent heat flux, and stability. Dr. Padro has kindly supplied us with the data from this experiment on a floppy diskette.

7. Results of Model Evaluation

7.1 Particle Deposition Models

For identification purposes the model designations listed in Table 7-1 identifies each of the ten models and describes the differences between the models. The modifications adopted for the hybrid models are summarized in the table.

The particle data set consists of 168 cases in total where non-zero observations of deposition velocity were made and for which sufficient concurrent meteorological data exists to exercise each deposition model. Assumptions needed to be made regarding the size distributions of the particles that were measured during some experiments where only an average size or a range of particle sizes were reported. For some particles that are formed in situ such as sulfate particles there may be a reason for selecting an a priori distribution. For primary particle sources there may not be a reason for selecting any particular distribution. In our initial analyses we have assumed a uniform particle size distribution. Later we introduce a particle size distribution that is peaked in the 'accumulation' size range centered around 0.2 microns in order to see if model performance characteristics would change for 'aged' particle distributions. A total of twelve data subsets were developed in order to learn if model performance biases and imprecision appeared systematically in the data. Table 7-2 summarizes the stratifications made, along with the stratification criteria. For each of the stratifications there are greater than 10 cases, sufficient for minimal performance statistics. In each of the following sections we discuss the results for each stratification.

The resulting composite performance measures depend on several factors including:

- particle size distribution assumed
- random numbers used and number of replications
- number of sample points in extremes
- treatment of zero and negative observed deposition velocity

In the present study we present model performance and selection results for both a uniformly distributed particle distribution and a more realistic peaked particle distribution for sulfate particle observations. In the present study we use 1000 replications for bootstrap estimation of confidence intervals. Tests show little sensitivity to sources of random numbers. The extremes are represented by a sample of the 11 largest velocities and 17 smallest velocities (lowest 10 percentile). Due to issues of robustness related to sufficient sample size the RES was estimated for only the overall data set (168 cases). Initially all zero or negative observations were thrown

Table 7-1
A Summary of the Model Designations

Model Name	Description of Model
CARB 1*	Unmodified CARB model
CARB 0	Removal of CARB roughness length restriction of z_o < 10 cm
CARB 2	Same as CARB 1 except uses fixed temperature (T = 75 degrees F)
CARB 3	Uses fixed temperature (as in CARB 2), a LAI adjustment to I_3, and a constant reference length of 0.5 cm in I_3
ADOM 1*	ADOM dry deposition algorithm
ADOM 2	Modified Stokes/Schmidt relations and phoretic effects term
ADOM 3	Changes made to ADOM 2 + LAI adjustment to r_d
UAM 1*	Unmodified UAM-V model
UAM 2	Contains LAI adjustment to r_d
ISC*	ISC model with boundary layer estimator for H_e/x

* Core (unmodified) models

Table 7-2
A Summary of the Stratifications Made To the Small Particle Data Set (N = 168)

Stratifying Variable	Definition Threshold(s)	Threshold Selection	Sample Size
Particle Diameter (microns)	≤ 0.1	non inertial	13
	0.1 < d < 20.0	inertial	155
Roughness Length (m)	≤ 0.25	simple canopy	97
	> 0.25	complex canopy	71
Leaf Area Index	≤ 3.0	nonforest	105
	> 3.0	forest	63
Day/Night Insolation	night	-	42
	day	-	51
Friction Velocity (m/s)	≤ 0.25	sample size	58
	> 0.25	sample size	110
Temperature (deg K)	≤ 290.0	sample size	62
	> 290.0	sample size	106

out since relative measurement uncertainty is large for small deposition velocities, and factors like resuspension could become important. We examined the potential bias caused by dropping such data by assigning a minimum velocity of 0.005 cm/s.

7.1.1 Full Data Sets

One of the first steps in the model performance evaluation exercise was to examine the scatter plots of the observed versus the predicted deposition velocities. A complete set of scatter plots for each of the ten models is presented in Appendix B as Figures B-1a through B-1j. From these scatter plots we can note that the observed deposition velocity ranges through nearly three orders of magnitude. Most of the models with the exception of ISC also reproduce the wide range of variation. There appears to be a tendency for the original model algorithms (CARB 1, ADOM 1, UAM 1, and ISC) to underpredict the deposition velocity. The scatter plots also indicate that there is a very wide range of scatter through most ranges of observed deposition velocity. The major exception that can be noted is a tendency for the scatter to decrease with increasing deposition velocity, suggesting that the fractional (percentage) error decreases with increasing deposition velocity.

The scatter plots indicate that there appears to be a significant decrease in average bias in the hybrid model results compared with the original model formulations. For example, comparing B-1a with B-1d, or B-1e with B-1g, or B-1h with B-1i we find that several groups of observation which were originally underpredicted in a significant manner, are predicted significantly better by the hybrid model formulation.

Several of the models such as ADOM 1 (Figure B-1e) exhibit a tendency to underpredict in the mid-range of observed deposition velocity. The underpredictions are sometimes by as much as an order of magnitude. The range of observed deposition velocities extend over a factor of several hundred and are plotted on a logarithmic scale which visually understates the contribution of the largest deposition velocities. Caution should be exercised in interpreting the scatter plots since some models do rather well at either extreme (or both) and the various performance measures which are designed to describe a specific characteristic of performance can produce a conflicting picture of performance which can reduce the discriminating power of the composite measure.

A purely qualitative survey of the scatter plots in Figures B-1a through B-1j suggests that models such UAM 2 (Figure B-1i) and CARB 3 (Figure B-1d) appear to have similar scatter over all ranges of observed deposition velocity and appear to do the best job of predicting. Of these two models the UAM 2 appears to be better at predicting the very smallest observed deposition velocities. The ADOM 1 model appears to perform well at the extremes, but considerably less well in the mid-range. The hybrid model ADOM 2 does not significantly

improve the mid-range underprediction bias and in fact causes the predicted range of deposition velocities to shrink by causing small deposition velocities to be overpredicted and large deposition velocities to be underpredicted.

The ISC model exhibits the most unique scatter plot signature in Figure B-1j. Due to the fact that small particles with a settling velocity of less than 0.1 cm/s are assumed to have a reflection coefficient equal to one, a majority of particles have essentially a zero deposition velocity (small values in Figure B-1j are lower bounds that are set so that the deposition velocity does not identically equal zero). The non-zero values of the predicted deposition velocity in Figure B-1j are strongly underpredicted due to the fact that the deposition velocity components are multiplied by one minus the reflection factor, α, which is generally smaller than 0.1.

All of the fractional and several composite statistical performance measures are summarized in Table 7-3. The UAM 2 model (with CARB 3 a distant second) appears to predict the average deposition velocity the best. The bias in the standard deviation is best predicted by the ADOM 1 model, with the UAM 2 model a close second. The CARB 3 model's overpredictions of the largest observed deposition velocities offsets its good performance in other areas. These overpredictions made by CARB 3 appear to be due to the LAI modification of the deposition velocities as evidence by an improvement in performance when LAI is not considered as in the case of CARB 2 in Table 7-3. The ADOM 2 model appears to most accurately predict the smallest deposition velocities while the ADOM 1 model shows a tendency to overpredict them. The LAI modification of the deposition velocities produces overpredictions of the smallest deposition velocities for both the CARB 3 and ADOM 3 models. The largest deposition velocities appear to be most accurately predicted by the ADOM 1 model with the UAM 2 model coming in second.

The composite fractional bias for the 168 cases is shown in Table 7-3. The best performing models in order of rank are UAM 2, CARB 3, and ADOM 1. The UAM 2 model appears to have the most well rounded performance since the fractional bias was at or nearly the smallest bias for all of the four bias measures. The ADOM 1 model on the other hand was helped significantly by the fact that what it lost in performance by overpredicting the smallest deposition velocities, it gained back by producing an appropriate estimate of the variation in deposition velocity. In all cases the ISC model performed significantly poorer than all other models and so was ranked last in terms of performance.

The composite measure of fractional bias for each of the subsets was computed using only the fractional bias of the average and the standard deviation. The average of the composite factional bias was averaged over all twelve subsets and the complete data set and is

Table 7-3

A summary of the fractional and composite statistical measures for each of the 10 models examined. The $<CFB_k>$ is the composite fractional bias measure estimated as the fractional bias of the average and standard deviation averaged over all 12 subsets. The overall sample size is 168. The largest extreme sample size is 11; the smallest extreme sample size is 17. A uniform particle size distribution is assumed.

Model Name	FBA	FBSD	FBSE	FBLE	$<CFB_k>$	CFB_o
CARB 0	0.991	0.852	0.815	1.090	1.137	0.937
CARB 1	1.070	0.846	0.815	1.090	1.031	0.955
CARB 2	0.976	0.764	0.366	1.013	0.991	0.780
CARB 3	0.800	0.815	-0.276	0.907	0.986	0.700
ADOM 1	1.005	0.448	0.999	0.494	1.023	0.736
ADOM 2	1.146	0.944	0.071	1.094	1.160	0.814
ADOM 3	0.895	0.886	-0.892	0.987	0.937	0.915
UAM 1	0.992	0.604	0.784	0.858	1.121	0.810
UAM 2	0.609	0.539	0.383	0.686	0.829	0.554
ISC	1.854	1.719	1.976	1.773	1.854	1.831

presented in Table 7-3 as well. This composite measure indicates that UAM 2, CARB 3, and ADOM 3 have the best average performance as measured by the smallness of the average composite.

Figure 7-1 shows the fractional biases present in the data taken as a single data set. The results indicate that UAM 2 has the smallest bias in the mean and standard deviation. According to FBSE, the smallest deposition velocities appear to be best predicted by the ADOM 2 as noted earlier in Table 7-3. According to the FBLE the largest deposition velocities are predicted best by the ADOM 1 model. The confidence intervals on these measures for the entire data set are rather large, sometimes being as large as 50% of the measure. In order to reduce this wide error bar an average was taken over all data stratifications, reducing the confidence interval by over a factor of 3. The resulting averaged composite measures are graphically summarized in Figure 7-2. This figure indicates UAM 2 is the best performer for average bias and CARB 0 and ADOM 3 are nearly tied runners up. The ISC model is clearly the poorest performing model out of the 10 models.

The scatter plots of the fractional measures of model performance for the overall data set are presented in Figures 7-3a through 7-3d. A co-plot of the fractional bias in the average and standard deviations is shown in Figure 7-3a. This plot indicates that model performance for all of the models except UAM 2 and ISC are clumped outside the factor of two box in the upper right hand quadrant where underpredictions of both the average and standard deviation occur. The UAM2 model also underpredicts both measures and lies just inside the factor of two box. The ISC model is an outlier and underpredicts both measures in an extreme sense. The co-plot of the fractional bias in the average of the entire data set versus that of the 11 largest deposition velocities in Figure 7-3b shows a similar pattern as that of Figure 7-3a. When the average bias of the RSE of the 17 smallest deposition velocities is co-plotted with the fractional bias of the average for the entire data set (Figure 7-3c) the UAM 2 and CARB 2 and 3 models appear to best predict small deposition velocities. The ADOM 3 model significantly overpredicts while ISC significantly underpredicts. The co-plot of the fractional bias in the 17 smallest and 11 largest deposition velocities (Figure 7-3d), indicates that only UAM 2 prediction of deposition velocities fall within a factor of 2 for both extremes.

7.1.2 Stratification by Particle Diameter

The stratification by particle diameter is important in order to see which models perform best for intermediate sized particles that behave neither as rapidly sedimenting particles or as a gas. Thus we will be evaluating model performance for very small particles (< 0.1 microns) versus intermediate size particles of size 0.1 through 20 microns.

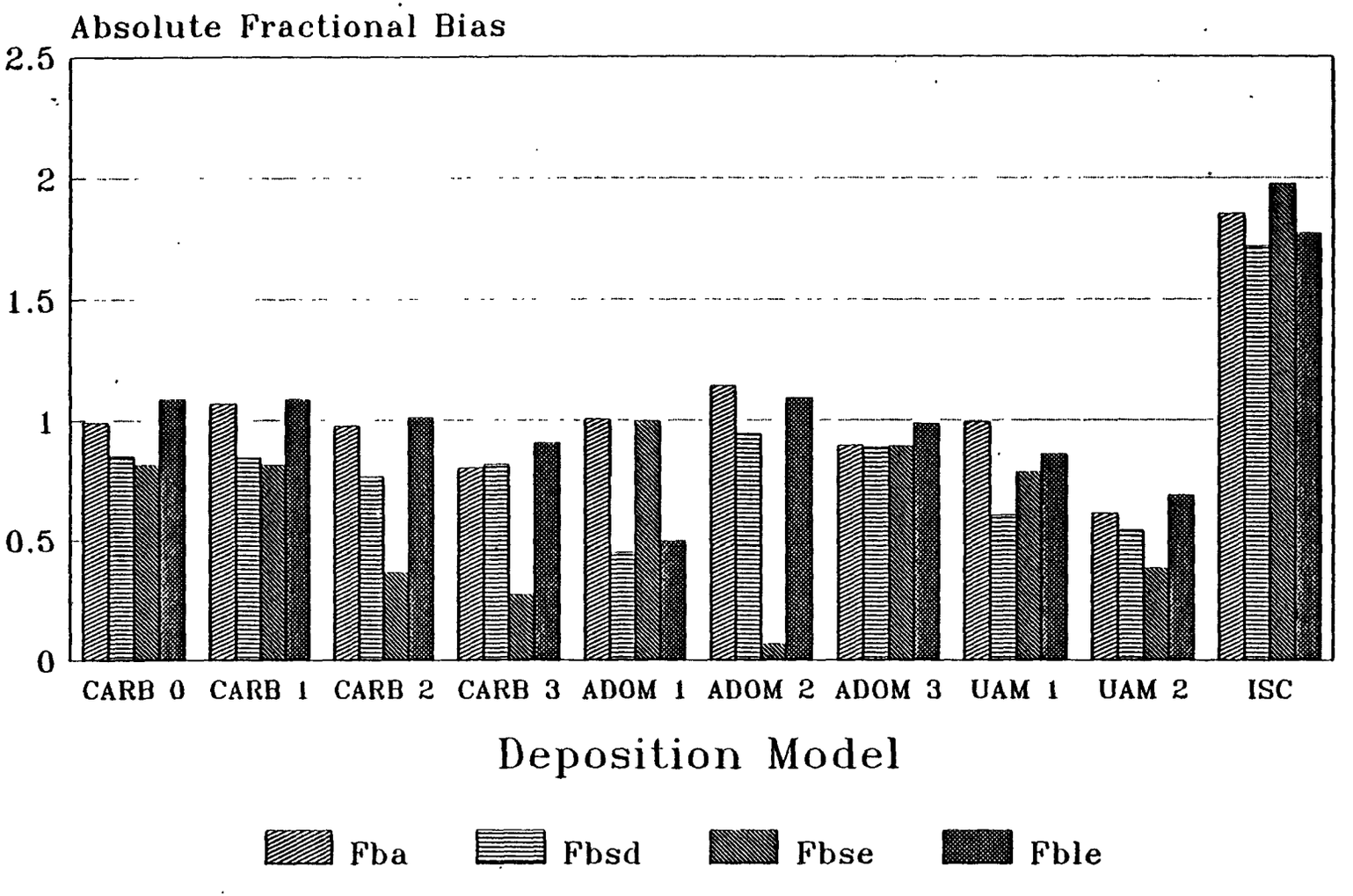

n = 168

Figure 7-1. A summary of the absolute value of the fractional bias using all data.

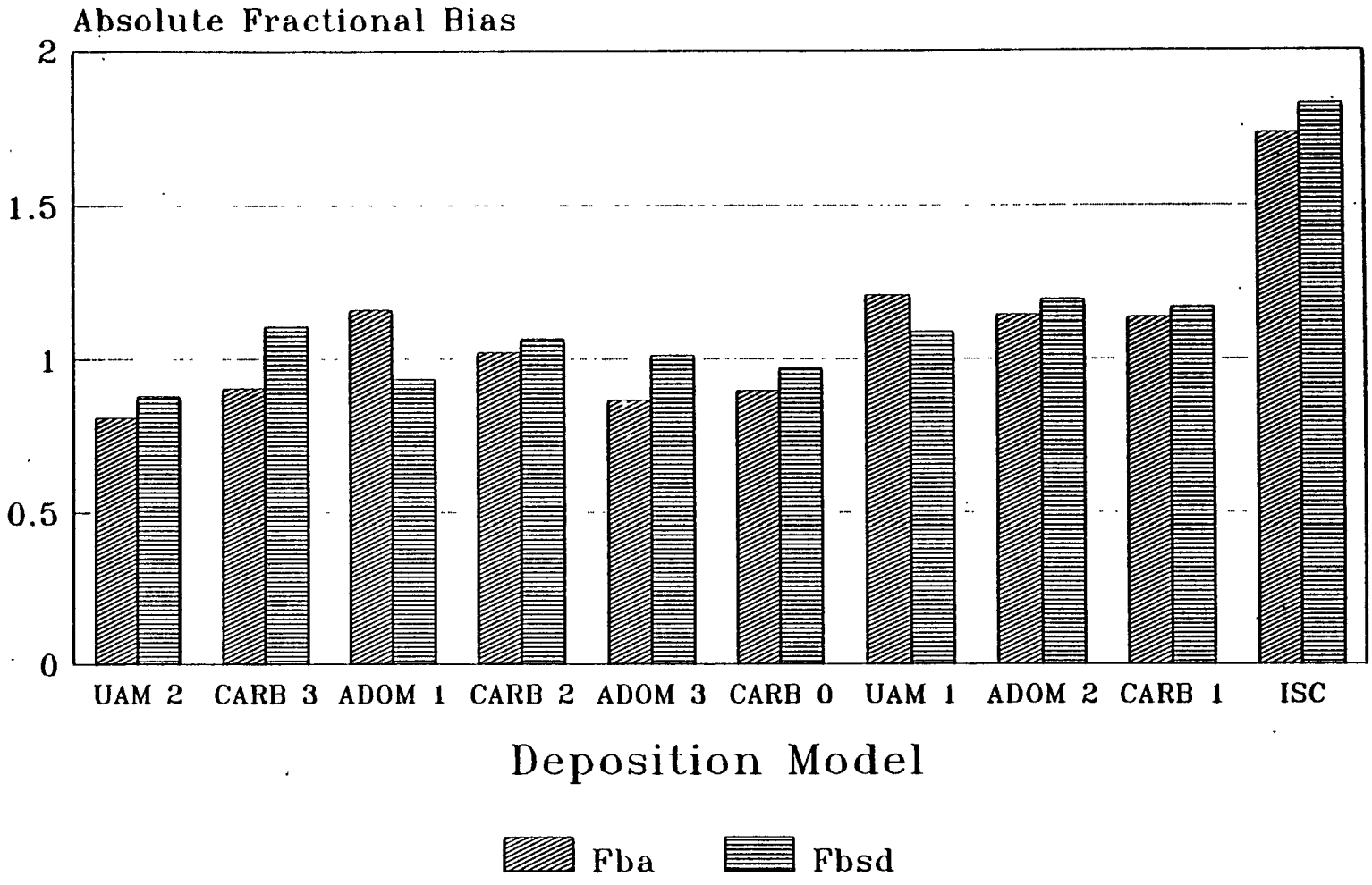

Figure 7-2. A summary of the absolute value of the fractional bias averaged over all 12 subsets.

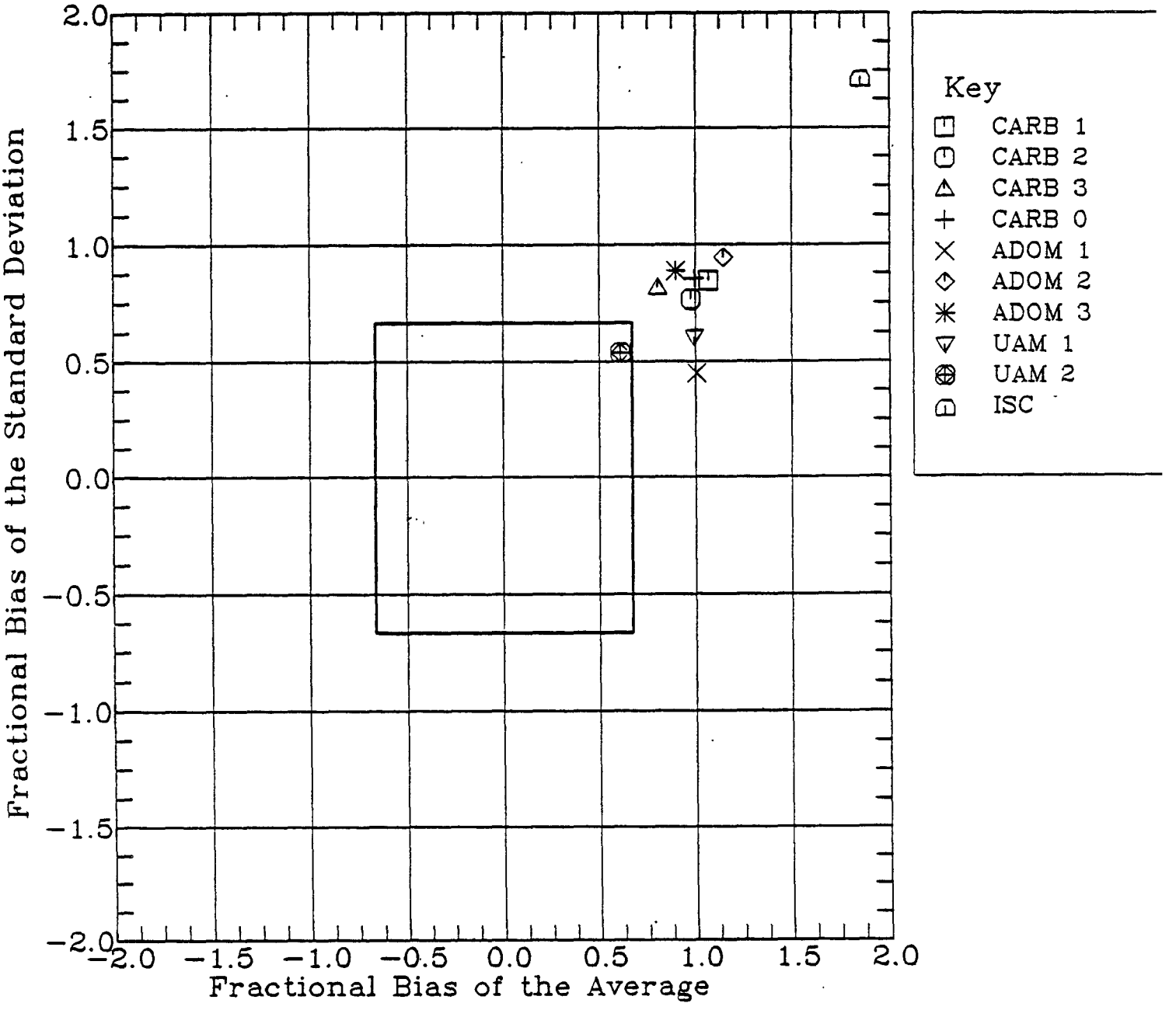

Figure 7-3a. Co-plot of fractional bias of the standard deviation for each of the deposition models. The sample set includes all data points. The box indicates the region within which the predictions are within a factor of 2 of observations.

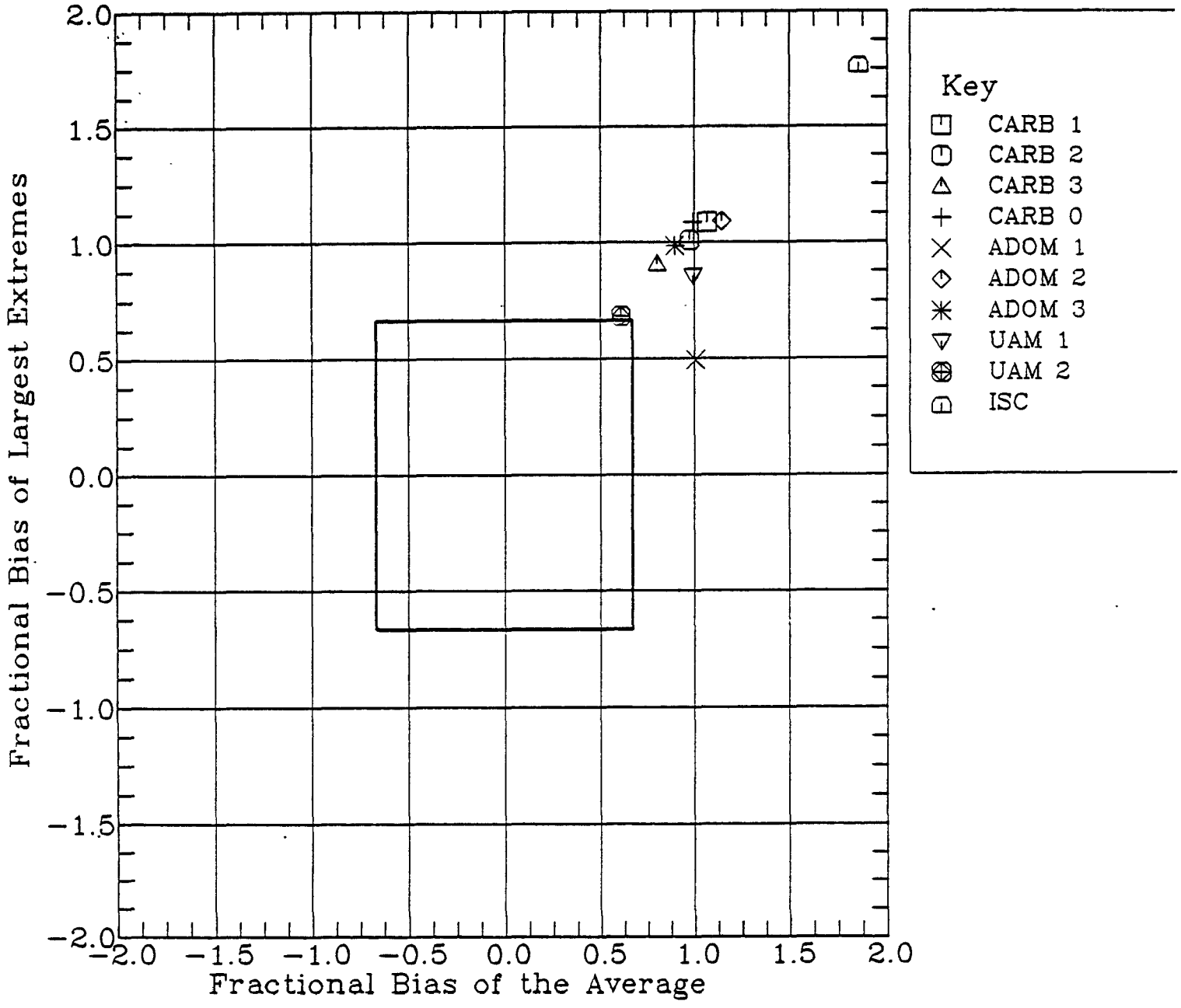

Figure 7-3b. Co-plot of fractional bias of the 11 largest deposition velocities for each of the deposition models. The sample set includes all data points. The box indicates the region within which the predictions are within a factor of 2 of observations.

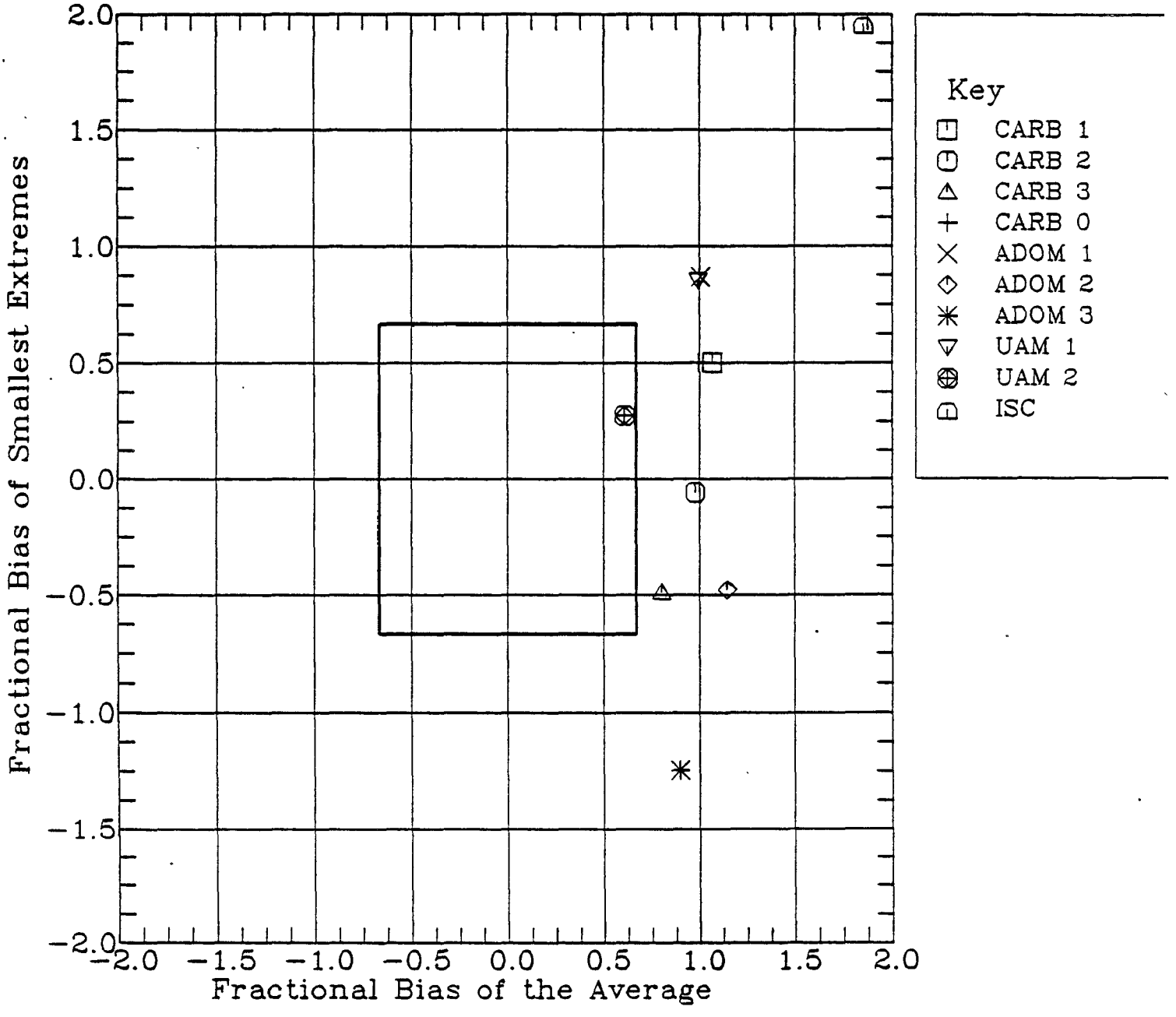

Figure 7-3c. Co-plot of fractional bias of the 17 smallest deposition velocities for each of the deposition models. The sample set includes all data points. The box indicates the region within which predictions are within a factor of 2 of observations.

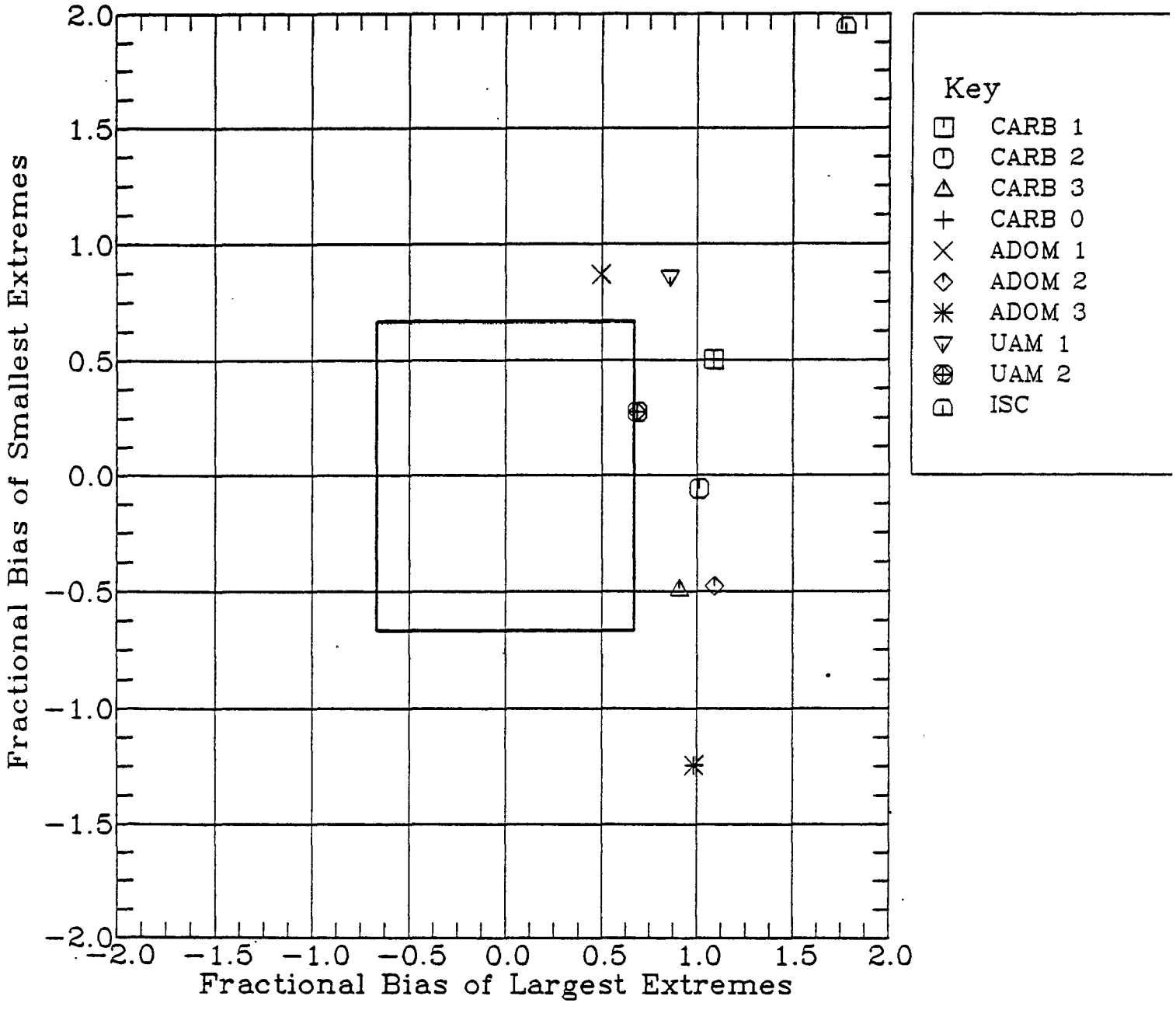

Figure 7-3d. Co-plot of fractional bias of the 11 largest and 17 smallest deposition velocities for each of the deposition models. The sample set includes all data points. The box indicates the region within which predictions are within a factor of 2 of observations.

The results of the performance evaluation are quantitatively summarized by Table 7-4. The most notable points to be drawn from this table are the following:

1) The CFB suggest that the ADOM 2, ADOM 3 and CARB 0 models are the most accurate models for small particles however the CARB model variants do perform poorer for intermediate sized particles due to significant underpredictions.

2) The overall most accurate model with the smallest CFB for larger particles seems to be the UAM 2 and ADOM 1 models which seem to treat larger particles considerably better than small ones.

3) All measures indicate that the ISC model consistently performs the worst of all of the models with significant underpredictions of the deposition velocity.

Table 7-4 indicates that no single model does well for both small and larger particles. The ADOM 3 model appears to do best for small particle diameters, while UAM 2 does the best for larger particles. Both models provide significantly small fractional biases for both the average and standard deviation. All models underpredict all measures of bias. The ISC model cannot predict deposition for particles smaller than 0.1 microns since the deposition velocity is basically set equal to zero by setting the reflection coefficient equal to 1. This effect results in the extremely large CFB in Table 7-4 for the ISC model.

7.1.3 Stratification by Roughness Length

The roughness length figures prominently in most of the deposition models undergoing evaluation. For small roughness lengths where a complex canopy is not present the models would be expected to perform at their best. The fractional and composite performance statistics which are presented in Table 7-5 indicate the following points:

1) According to the CFB, the UAM 2 model performs in a superior manner regardless of the underlying surface. The model produces underpredictions on the average.

2) The statistical measures indicate that all models perform poorer over rough surfaces than smooth ones as might be expected.

Table 7-4

A summary of the fractional and composite statistical measures for each of the models examined. The first row is for particle diameters less than 0.1 microns, the second is for particles in the range 0.1 to 20 microns. The rank is by CFB and the particle distribution is for a uniform distribution.

Model Name	Samples	FBA	FBSD	CFB_k	Rank
CARB 0	13	0.100	1.435	0.768	2
	155	1.042	0.846	0.944	7
CARB 1	13	0.899	1.827	1.363	6
	155	1.077	0.839	0.958	8
CARB 2	13	0.641	1.669	1.155	4
	155	0.991	0.756	0.874	5
CARB 3	13	1.186	1.591	1.388	7
	155	0.787	0.815	0.801	4
ADOM 1	13	0.971	1.622	1.297	5
	155	1.006	0.439	0.723	2
ADOM 2	13	0.925	0.856	0.891	3
	155	1.156	0.942	1.049	9
ADOM 3	13	0.443	0.232	0.337	1
	155	0.916	0.895	0.905	6
UAM 1	13	1.673	1.895	1.784	9
	155	0.970	0.601	0.786	3
UAM 2	13	1.500	1.761	1.630	8
	155	0.583	0.542	0.562	1
ISC	13	1.998	2.000	1.999	10
	155	1.849	1.717	1.783	10

Table 7-5

A summary of the fractional and composite statistical measures for each of the models examined. The first row is for roughness lengths less than 0.25 m, the second is for roughness lengths greater than 0.25 m. The rank is by CFB and the particle size distribution is for a uniform distribution.

Model Name	Samples	FBA	FBSD	CFB_k	Rank
CARB 0	97	0.902	0.846	0.874	8
	71	1.196	1.263	1.229	3
CARB 1	97	0.902	0.846	0.874	7
	71	1.490	1.765	1.628	6
CARB 2	97	0.813	0.763	0.788	4
	71	1.385	1.631	1.508	4
CARB 3	97	0.800	0.793	0.796	5
	71	0.800	1.356	1.078	2
ADOM 1	97	0.732	0.446	0.589	2
	71	1.795	1.614	1.705	7
ADOM 2	97	0.916	0.970	0.943	9
	71	1.766	1.747	1.756	8
ADOM 3	97	0.687	0.925	0.806	6
	71	1.453	1.700	1.577	5
UAM 1	97	0.725	0.616	0.671	3
	71	1.761	1.920	1.840	9
UAM 2	97	0.571	0.521	0.546	1
	71	0.691	1.068	0.879	1
ISC	97	1.789	1.720	1.754	10
	71	1.999	2.000	1.999	10

3) All measures indicate that the ISC model consistently performs poorest of all models, regardless of surface, and always produces significant underpredictions as noted from the large positive FB's.

The average deposition velocity for both rough and smooth surfaces is predicted best by UAM 2. The UAM 2 also predicts the variance of the deposition velocities under rough surfaces the best, while ADOM 1 does this best for smooth surfaces. All models underpredict all measures.

7.1.4 Stratification by Leaf Area Index

Several hybrid models possess an explicit dependence of deposition velocity on Leaf Area Index (LAI). The LAI for each observation was separated into complex surfaces (e.g., forests) where the LAI is 3 or greater and simple surface ceases where the LAI is less than 3 (e.g., grass). If LAI represents an appropriate increase in collection area, then adding a adjustment for LAI should, in principle, improve model predictions. The normalized performance measures summarized in Table 7-6.

From Table 7-6 we can note the following:

1) The UAM 2 model produces superior composite performance according to the CFB regardless of LAI.

2) The CFB indicates that all models tend to perform poorer under large LAI situations with a consequent increase in the average magnitude of model residuals (e.g., FBA).

3) The ISC model consistently performs the worst of all of the models regardless of LAI

Both the average and standard deviations of the deposition velocity distribution are underpredicted by all models. The UAM and ADOM family of models exhibit an improvement for both small and large LAI samples. The results for the CARB family is mixed, with there being no improvement for small LAI samples, but for large LAI samples the improvement is dramatic.

Table 7-6

A summary of the fractional and composite statistical measures for each of the models examined. The first row is for leaf area index (LAI) less than 3.0, the second is for LAI greater than 3.0. The rank is by CFB and the particle size distribution is for a uniform distribution.

Model Name	Samples	FBA	FBSD	CFB_k	Rank
CARB 0	105	0.844	0.856	0.850	7
	63	1.422	1.800	1.611	4
CARB 1	105	0.902	0.850	0.876	8
	63	1.572	1.867	1.720	6
CARB 2	105	0.804	0.769	0.787	4
	63	1.499	1.847	1.673	5
CARB 3	105	0.826	0.790	0.808	5
	63	0.738	1.552	1.145	2
ADOM 1	105	0.743	0.449	0.596	2
	63	1.915	1.979	1.947	9
ADOM 2	105	0.935	0.968	0.951	9
	63	1.817	1.861	1.839	8
ADOM 3	105	0.711	0.918	0.814	6
	63	1.469	1.616	1.543	3
UAM 1	105	0.760	0.612	0.686	3
	63	1.765	1.912	1.838	7
UAM 2	105	0.609	0.515	0.562	1
	63	0.610	1.237	0.923	1
ISC	105	1.798	1.719	1.759	10
	63	1.999	2.000	1.999	10

7.1.5 Stratification by Day vs Night

The particle deposition velocity is dependent on the degree of atmospheric turbulence which in turn is dependent on the atmospheric stability. Atmospheric stability generally undergoes a significant diurnal variation. At night turbulent transport is generally conducted under neutral or stable conditions. Any day-night difference in performance is likely to be directly connected with the aerodynamic resistance formulation utilized. From Table 7-7 which summarizes the normalized and composite performance statistics, the following points can be noted:

1) The CFB indicates that during the night the ADOM 1 model is the best performing model while during the day the ADOM 3 model is best.

2) Models tend to perform better during the night than during the day. During the day even typically good performing models such as UAM 2 perform markedly poorer.

The fractional bias measures compiled in Table 7-7 suggests that ADOM 1 does quite well for night samples for both the average and the standard deviation. During the day the CARB 0 model has the smallest bias in the standard deviation, while the ADOM 3 model has the smallest bias in the average. The ISC model performed the worst, and during the day essentially showed no predictive skill.

7.1.6 Stratification by Friction Velocity

Friction velocity is related directly to the vertical turbulent transport of momentum. In addition, the friction velocity plays a role in determining the laminar boundary layer near the surface. Consequently the friction velocity is a relatively important determinant of deposition velocity. We have stratified the small particle cases into high and low friction velocity sets with a threshold set to divide the sample into halves. The model performance statistics are presented in Table 7-8. From this table we can make the following observations;

1) Based on CFB the UAM 2 model is the best performing model regardless of friction velocity while ISC is the worst

2) CARB 3 is the next best performing model with its best performance occurring under low friction velocity conditions.

Table 7-7

A summary of the fractional and composite statistical measures for each of the models examined. The first row is for night, the second is for day. The rank is by CFB and the particle size distribution is for a uniform distribution.

Model Name	Samples	FBA	FBSD	CFB_k	Rank
CARB 0	42	0.987	0.994	0.991	8
	51	1.001	0.703	0.852	2
CARB 1	42	0.987	0.994	0.991	7
	51	1.380	1.410	1.395	5
CARB 2	42	0.893	0.904	0.899	4
	51	1.243	1.207	1.225	3
CARB 3	42	1.014	1.087	1.051	9
	51	1.272	1.717	1.495	7
ADOM 1	42	0.665	0.493	0.579	1
	51	1.558	1.396	1.477	6
ADOM 2	42	0.946	1.021	0.984	6
	51	1.069	1.648	1.358	4
ADOM 3	42	0.853	1.041	0.947	5
	51	0.481	1.067	0.774	1
UAM 1	42	0.787	0.779	0.783	3
	51	1.739	1.876	1.808	9
UAM 2	42	0.741	0.759	0.750	2
	51	1.493	1.729	1.611	8
ISC	42	1.766	1.737	1.752	10
	51	1.998	2.000	1.999	10

Table 7-8

A summary of the fractional and composite statistical measures for each of the models examined. The first row is for friction velocity less than 0.25 m/s, the second is for friction velocity greater than 0.25 m/s. The rank is by CFB and the particle size distribution is for a uniform distribution.

Model Name	Samples	FBA	FBSD	CFB_k	Rank
CARB 0	58	1.116	0.773	0.944	6
	110	0.966	0.859	0.913	7
CARB 1	58	1.135	0.772	0.954	7
	110	1.056	0.843	0.949	8
CARB 2	58	1.036	0.670	0.853	3
	110	0.964	0.764	0.864	5
CARB 3	58	0.806	0.769	0.787	2
	110	0.799	0.821	0.810	4
ADOM 1	58	1.522	1.047	1.285	9
	110	0.914	0.406	0.660	2
ADOM 2	58	1.103	1.001	1.052	8
	110	1.155	0.925	1.040	9
ADOM 3	58	0.770	1.011	0.890	5
	110	0.923	0.867	0.895	6
UAM 1	58	1.151	0.604	0.878	4
	110	0.960	0.590	0.775	3
UAM 2	58	0.801	0.511	0.656	1
	110	0.572	0.550	0.561	1
ISC	58	1.933	1.798	1.865	10
	110	1.838	1.709	1.774	10

Of the core models ADOM 1 performs rather well under large friction velocity conditions, but is the next to worst performer under small friction velocity conditions. The UAM 2 fractional bias for both the average and standard deviation was the smallest of all models evaluated.

7.1.7 Stratification by Temperature

The dependence of deposition velocity model performance on temperature was examined. The observed data was broken up into 'hot' and 'cold' subsets based on a 17°C threshold which was applied to split the overall data set up into two large subsets. While most particle deposition algorithm do not have an explicit temperature dependence, the original CARB formulation (CARB 1) does. The resulting model normalized performance statistics and performance scores are summarized in Table 7-9. The resulting fractional bias and composite performance measures indicate that:

1) The CFB indicates that the UAM 2 model is the best performer under warm temperatures and is the second best performer under cool temperatures. The model always underpredicted the observed deposition velocities.

2) The CFB indicates that the ADOM 1 model is the best performer under cool temperatures, while the CARB 3 model is the second best performer under warm temperatures.

3) All measures consistently show the ISC model as the worst performing model regardless of temperature.

Under warm temperatures the UAM 2 shows significantly smaller fractional bias measures for both the average and the standard deviation. Under cool temperatures the ADOM 1 model produces the smallest fractional biases for both the average and the standard deviation.

The results of the findings or each model and for each subset is summarized by the model specific bar chart of CFB in Figure 7-4. This figure shows the composite fractional bias averaged over the high low categories. This figure indicates that the UAM 2 is the best performing model (smallest CFB) over many of the stratifications while the ISC model is the worst performed over all stratifications. The runners up for best performance are the ADOM 3 and the CARB 3 models. The performance of these two models alternate in ranking from subset to subset. For example from Figure 7-4 for the two stratifications that UAM 2 does poorly on, namely the particle size and day/night stratifications, the best performing model was ADOM 3 in both cases.

Table 7-9

A summary of the fractional and composite statistical measures for each of the models examined. The first row is for temperatures less than 290.0 deg K, the second is for temperatures greater than 290.0 deg K. The rank is by CFB and the particle size distribution is for a uniform distribution.

Model Name	Samples	FBA	FBSD	CFB_k	Rank
CARB 0	62	0.987	1.064	1.025	7
	106	0.994	0.661	0.827	6
CARB 1	62	1.115	1.067	1.091	8
	106	1.045	0.648	0.847	7
CARB 2	62	0.972	0.952	0.962	5
	106	0.979	0.587	0.783	5
CARB 3	62	1.091	1.116	1.104	9
	106	0.659	0.595	0.627	2
ADOM 1	62	0.811	0.481	0.646	1
	106	1.127	0.411	0.769	4
ADOM 2	62	0.972	1.014	0.993	6
	106	1.253	0.870	1.062	9
ADOM 3	62	0.796	1.012	0.904	3
	106	0.953	0.757	0.855	8
UAM 1	62	0.999	0.817	0.908	4
	106	0.988	0.410	0.699	3
UAM 2	62	0.932	0.793	0.863	2
	106	0.457	0.340	0.398	1
ISC	62	1.820	1.737	1.779	10
	106	1.874	1.697	1.786	10

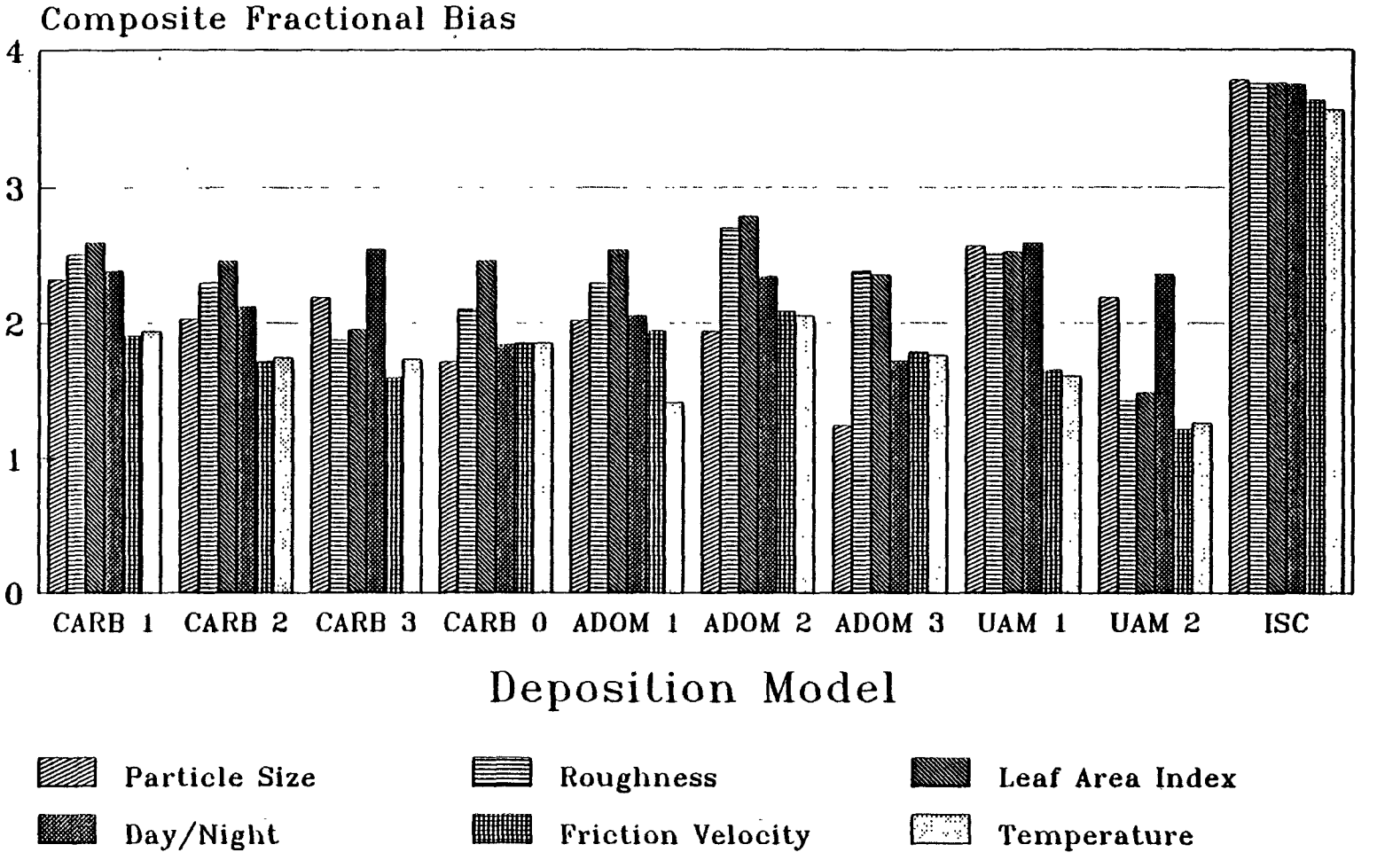

Figure 7-4. A summary of the total CFB for the six types of data subsets. The total represents a sum over both high and low categories for each subdividing variable.

7.1.8 Estimation of CPM from Tables

The estimate of a CPM can be conducted from the statistics presented in the tables. The CFB's for CARB 1 will serve as an illustrative example. Table 7-10 illustrates how one can extract fractional bias information from the tables to estimate the CPM.

7.2 Discussion of Model Performance

The composite performance measure (CPM) defined by Equation (5-11) was used to rank the models. The model with the smallest CPM is ranked highest. The 95 percent confidence interval indicates how much the estimated CPM might vary if measurements and predictions of deposition velocity were repeated under identical meteorological and site conditions. Model performance was determined using the reported size distribution except for the experiments involving sulfates where size distribution were not reported. In those cases, two different particle distributions assumed for those data sets involving sulfate: a predicted distribution with most of the mass between 0.16 to 0.29 μm diameter (Richards et al., 1989) and a second distribution with the sulfate uniformly distributed between 0.1 - 1.0 μm diameter. In the following sections the results of the statistical analysis is summarized.

7.2.1 Uniform Size Distribution

Figure 7-5 illustrates the top to bottom ranking for the 10 models assuming a uniform size distribution. With the exception of ISC all models fall within a narrow range of CPM. The three top ranked models are UAM 2, CARB 3, and ADOM 1. The first two models represent a hybrid variant of core models with an LAI adjustment. The only core model in the top three ranked models is the ADOM 1 model. The confidence intervals suggest that none of the three models has any obvious performance advantages. The other core models themselves appear to have essentially the same composite performance. The only exception is ISC which appears as an outlier with a confidence interval that is narrowed by the many zero predictions it produces.

The overlap of the confidence intervals on the CPM in Figure 7-5 suggests that most models have performance indistinguishable from their ranked neighbors. The model comparison measure (MCM) defined by Equation 5-12 is an appropriate measure to compare one model versus another. If the difference is not significant from zero at the 95% confidence level the two models can be said to be statistically identical. Figure 7-6 ranks the MCM for all unique model pairings. The MCM's reveal that over 50% of the MCM confidence intervals cross zero thereby indicating a lack of significant difference in performance. There is no significant difference among UAM 2, CARB 3, and ADOM 1 regardless of pairing. There are significant

Table 7-10
Summary of Composite Statistical Measures that Illustrate how the CPM Arises for the CARB 1 Model

Stratification	Source	CFB
Particle Size	Table 7-4	
small		1.27
large		1.01
Roughness Length	Table 7-5	
< 25		1.01
> 25		1.53
Leaf Area Index	Table 7-6	
< 3		0.99
> 3		1.56
Sunlight	Table 7-7	
night		1.25
day		1.41
Friction Velocity	Table 7-8	
< 25 cm/s		0.99
> 25 cm/s		1.00
Temperature	Table 7-9	
< 290°K		1.06
> 290°K		0.93
Average		1.17
CPM_o	Table 7-3	0.99
CPM		1.08 (Table 7-3 = 1.08)

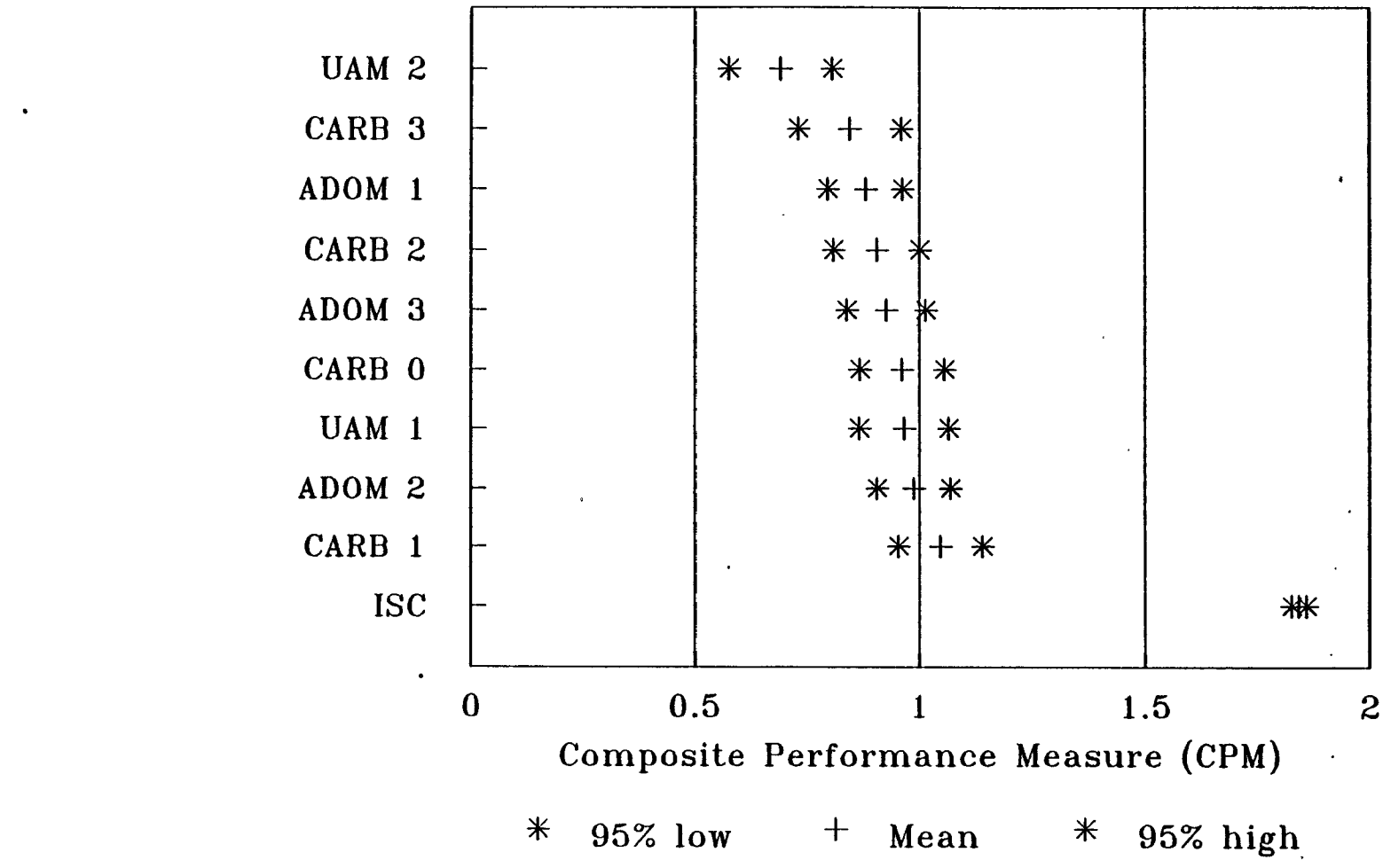

Figure 7-5. A ranking of the models by CPM estimated from Equation 5-11. The smallest CPM represents the best performance. The CPM is for a uniform particle size distribution.

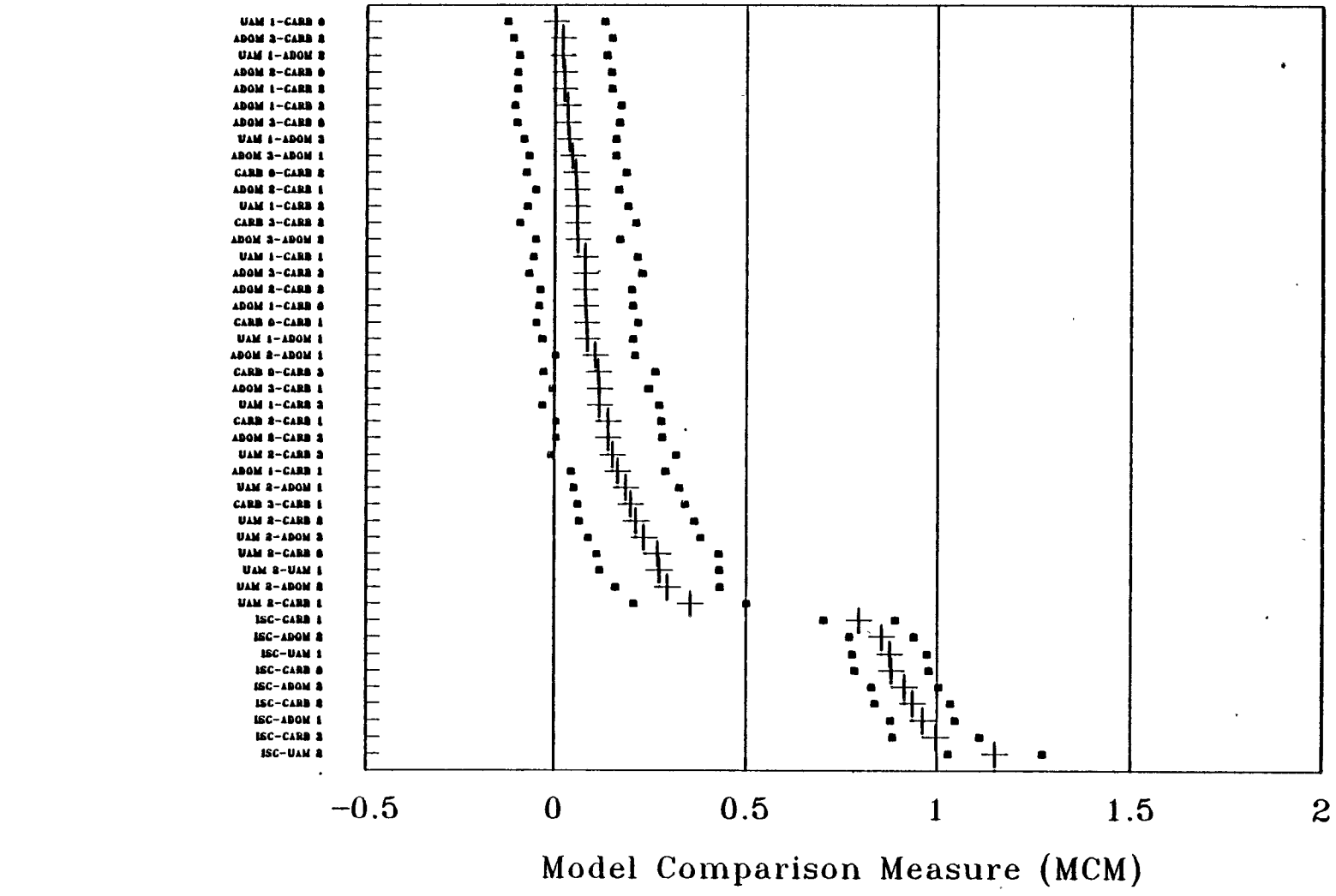

Figure 7-6. A summary of the MCM for each unique model pair. The MCM was computed using predictions made assuming a uniform particle size distribution.

differences among ISC and the other models and certain model pairs, usually involving one of the core (unmodified) models (e.g., CARB 1, ADOM 1, UAM 1).

7.2.2 Sulfate Particle Distribution

The performance evaluation exercise was repeated using a more realistic distribution for the experiment data sets where sulfate particle deposition was observed. Aerosol observations such as those reported by Hidy (1984) and Richards et al. (1989) generally exhibit a multi-peaked mass distribution as a function of mean particle diameter. Peaks have been observed in the mass fraction at 0.2, 1-2, and 6-10 microns. Each of these peaks are associated with a particular pathway of particle emission and/or formation. Many of the particle experiments observed aged sulfate aerosol with a mass fraction peak at 0.2 microns. The model performance evaluation statistics may be sensitive to changing assumptions of the size distribution of the particle mass fraction. To address this concern the model performance evaluation exercise was repeated with a size distribution taken from Richards et al. (1989) and which is summarized in Table 7-11. The mass fraction peak occurs at 0.2 microns and is nearly twice the value of the uniform distribution for a 0.1 micron size range.

The CPM for the sulfate particle distribution case is illustrated in Figure 7-7. The model results are presented in top to bottom ranking by CPM with the highest ranked (most favored) model having the smallest CPM. The ranking indicates that the top three models, CARB 3, UAM 2, and ADOM 1 identified previously remain as the top ranked models. Figure 7-8 shows that the MCM and its confidence interval indicates that there is in fact no statistically significant difference between any combination of the top three models. The results of the performance evaluation and selection exercises are relatively unaffected by the changes tested in particle distribution.

7.2.3 Model Performance When Zeroes are Included

A test that was performed was to examine the model performance statistics if negative or zero observed deposition velocities were retained in the data base as small positive values. Five such cases out of 173 observations with valid meteorological data were noted. The effects of these five cases were examined by setting the deposition velocity equal to a minimum of 0.005 cm/s. Figure 7-9 illustrates the results of ranking the models top-to-bottom by CPM. The sulfate particle distribution was used for this exercise due to its greater realism. Two of the same models CARB 3 and UAM 2 remain as the top ranked models and are separated by relatively small differences in CPM. The only notable change is that the hybrid ADOM 3 model succeeds the core model ADOM 1 as the third best performer.

Table 7-11
Aerosol Mass Fraction as a Function of Size Distribution for Two Assumed Aged Sulfate Distributions

Diameter (Microns)	Mass Fraction (Uniform)	Mass Fraction (Richards et al. 1989)
0.10	0.083	0.053
0.13	0.083	0.095
0.16	0.083	0.144
0.19	0.083	0.189
0.23	0.083	0.161
0.29	0.083	0.111
0.36	0.083	0.053
0.44	0.083	0.046
0.54	0.083	0.053
0.66	0.083	0.062
0.81	0.083	0.035
1.00	0.083	0.000

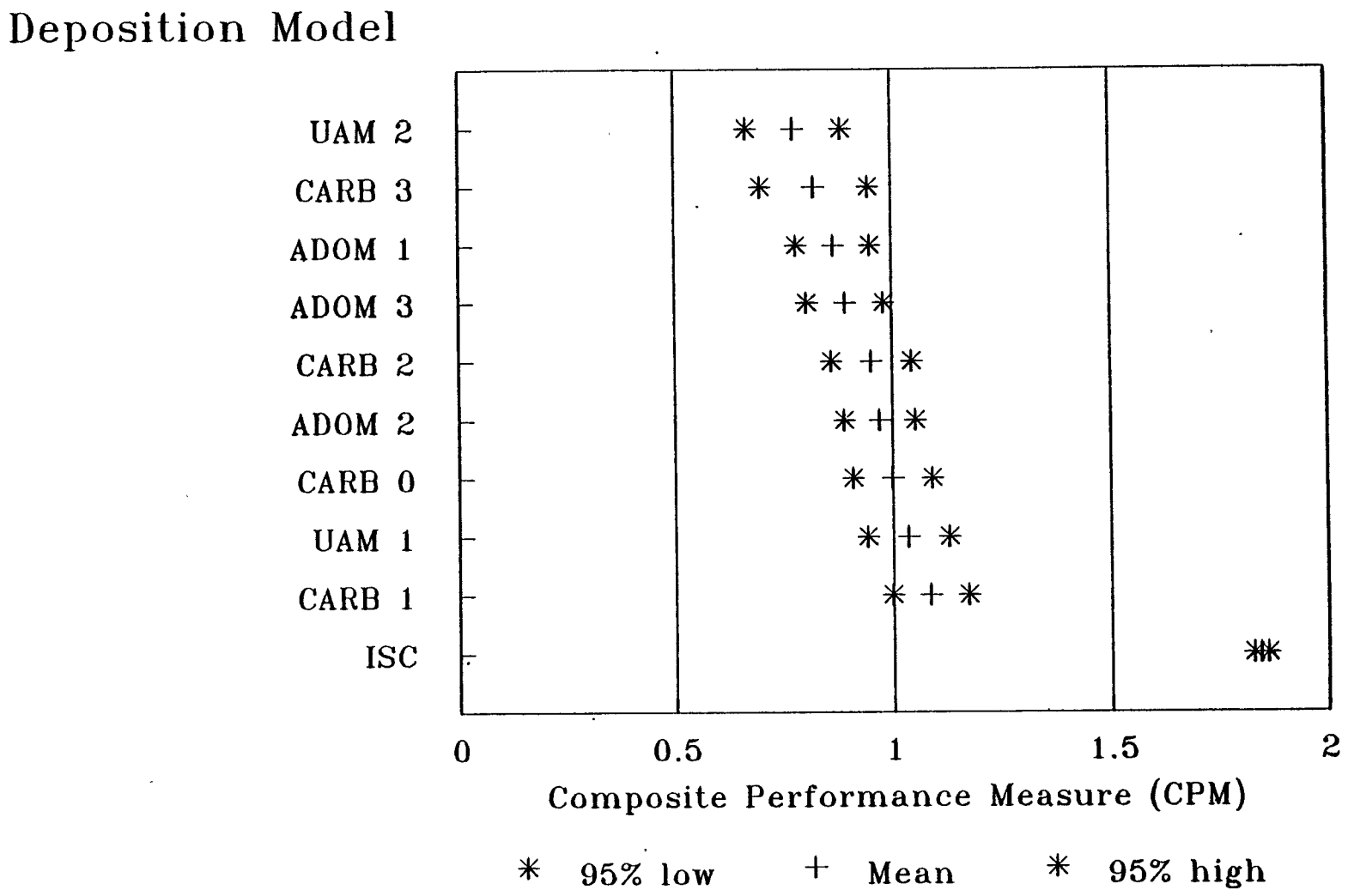

Figure 7-7. A ranking of the models by CPM. The smallest CPM represents the best performance. The CPM is for a peaked particle size distribution.

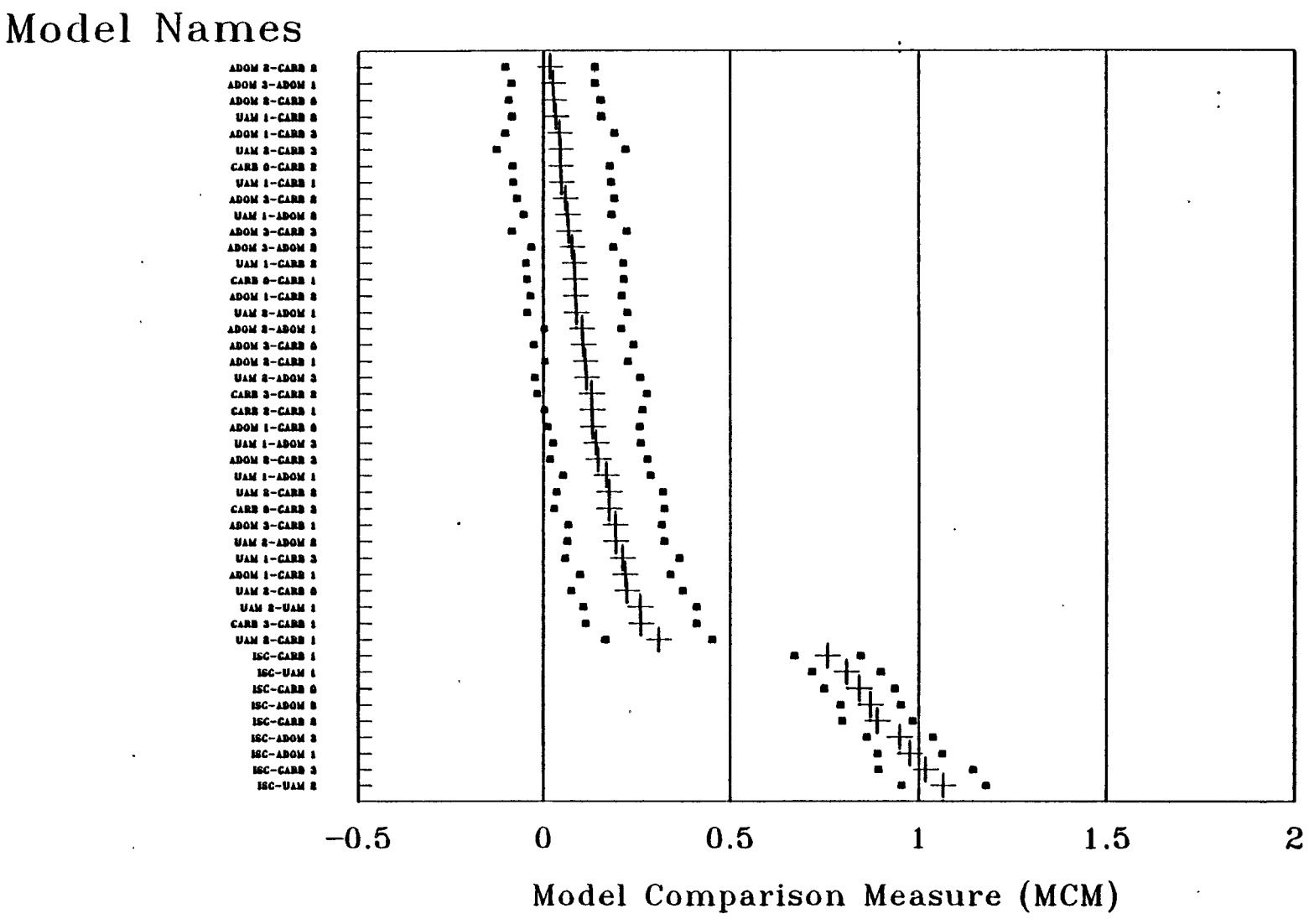

Figure 7-8. A summary of the MCM for each unique model pair. The MCM was computed using predictions made assuming a peaked particle size distribution.

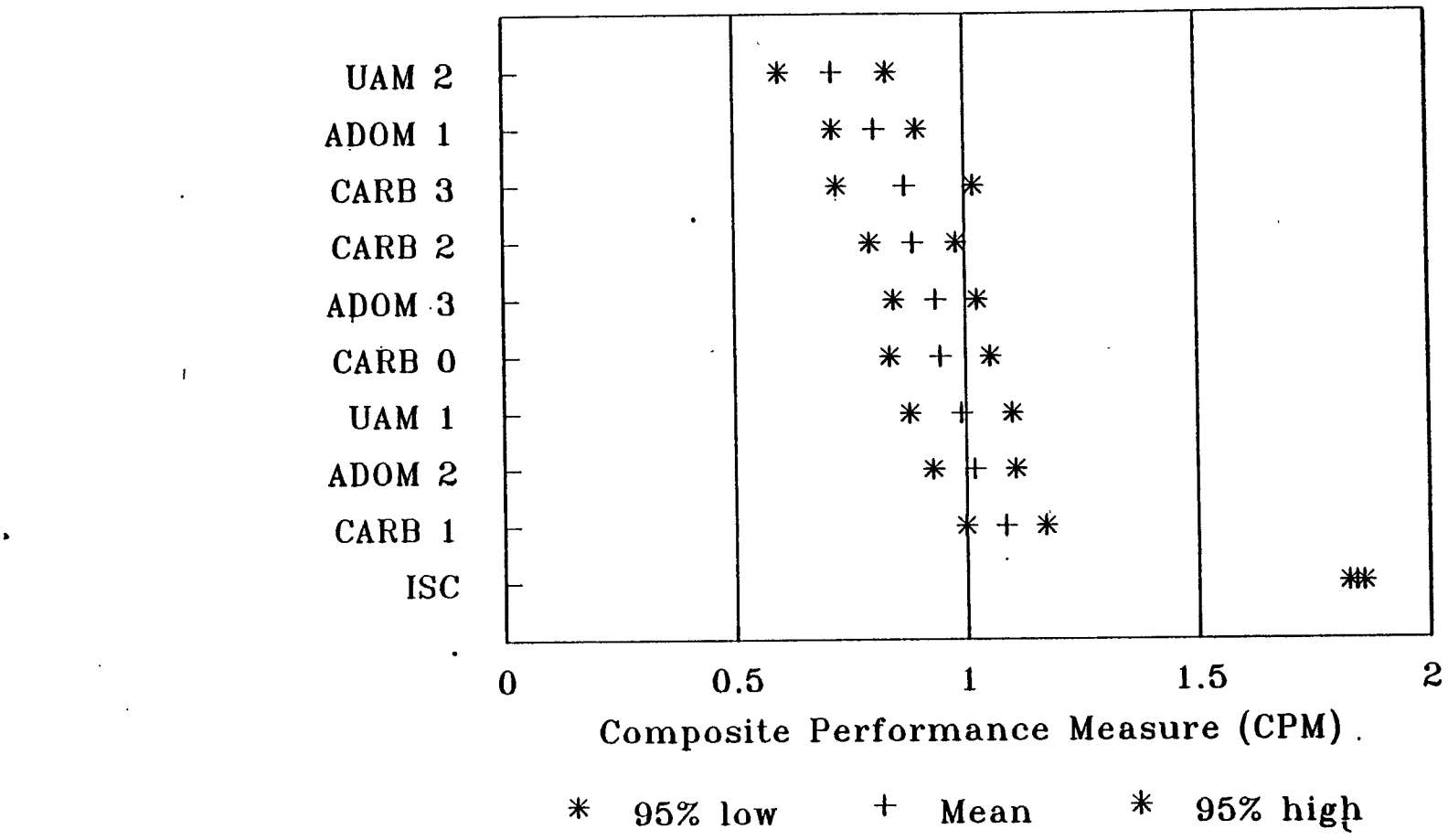

Figure 7-9. A ranking of the models by CPM. The smallest CPM represents the best performance. The CPM is for a uniform particle size distribution with the observed zeros set to 0.005 cm/s.

This result was not unexpected since ADOM 1 previously performed the best for the smallest deposition velocities, and the larger range of observations due to the small deposition cutoff enables ADOM 3 to predict the standard deviation better. The similarity of the ranking of models and the magnitude of the CPM for each model suggests that the presence of the five cases of minimal deposition velocity does not result in a major change in the results presented in previous sections.

7.2.4 Cumulative Distribution Results

The Cumulative Distribution Function (CDF) plots presented in Appendix B illustrate how the models tend to perform over the range of deposition velocities. Figure B-2a in the appendix shows the performance of the core models. The curves indicate that all models underpredict deposition velocities less than 0.2 cm/s, but did much better for larger deposition velocities. The ISC model is the notable exception. The CDF of the CARB series of models are illustrated in Figure B-2b. For small deposition velocities the CARB 3 hybrid model appears to track the observed CDF most closely. However for deposition velocities greater than 0.5 cm/s there seems to be no appreciable difference between the model variants. Figure B-2c shows the closely matching CDF's of the observations and UAM 2 and the poor match obtained with ISC. The improvement in UAM due to the addition of the LAI influence is best illustrated by Figure B-2c. The overprediction tendency of the UAM 1 model is significantly lessened in the UAM 2 model, although both models perform similarly for the largest deposition velocities.

7.2.5 Selection of Best Performing Deposition Models

The results indicate that two hybrid models with an LAI adjustment perform best. Three models, CARB 3, UAM 2, and ADOM 1 have approximately the same overall composite performance. Although any of the three best performing models is a substantial improvement in the predictive ability over the current scheme in ISC, each of the new methods has drawbacks and limitations. For example, the CARB formulation is empirical which raises questions on its generality outside the limits of particle size and surface roughness on which it is based. The UAM 2 formulation is based on the assumed equivalence of the Schmidt number term and the Stokes number term in the resistance equation for particles of 0.3 μm diameter, which is an assumption not fully supported or documented with data. Finally, ADOM 1 shows a distinct trend for underpredicting deposition velocities for particle size ranges which may be important for many combustion sources. However, although additional improvements in modeling deposition will undoubtedly be made in the future, a significant benefit can be realized by replacing the scheme in ISC now with one of the best performing schemes (CARB 3, UAM 2, or ADOM 1).

8. Summary and Conclusions

The purpose of this study was to review, refine, and test dry deposition techniques that are suitable for use in regulatory models such as the Industrial Source Complex (ISC) model. Dry deposition is the process by which particulate matter and gaseous pollutants are transferred from the air to land, water, and vegetative surfaces through "dry" (i.e., non-precipitation) mechanisms. Because indirect risk assessment pathways such as fish, food chain, and water ingestion, commonly dominate total intake and exposure to many pollutants, an accurate estimate of dry deposition is an important element of many regulatory analyses. Dry deposition may also be important for a refined estimate of air quality concentrations for sources subject to significant plume depletion.

The dry deposition flux can be written as $F = \chi v_d$, where F is the flux ($g/m^2/s$), χ is the ambient pollutant concentration (g/m^3), and v_d is the deposition velocity (m/s), all defined at a reference height. Standard procedures can be used for estimating the concentration term of the flux equation, with appropriate modifications made to account for plume depletion effects. The main focus of this study was the testing and evaluation of various methods for computing the deposition velocity.

A review of the technical literature identified several models that are suitable for predicting the dry deposition velocity within the framework of a regulatory model. These models are listed in Section 1 and described in more detail in Section 2. Three resistance-based particle deposition models were identified which fit the required criteria of this study (i.e., methods of sound technical basis that are suitable for regulatory use for both large and small particles). The technical literature suggested that certain parameterizations in these models could be improved. Therefore, several modifications and enhancements to the core models were developed and tested in this study. As a result, a total of ten deposition velocity models were evaluated (see Section 7).

A second literature review identified observational data sets which could be used to test deposition velocity algorithms. Based on this review, eight datasets for particulate matter and fourteen datasets for gases were assembled in a database. Although the ultimate goal is to evaluate dry deposition for both particulate matter and gases, only particulate matter deposition was evaluated in this study. Appendix C lists the observational particle deposition velocity datasets. One of the recommendations of the study is that additional evaluation efforts be conducted to test the dry deposition models for gases (see Section 2.2) with the datasets listed in Section 7.

As explained in Section 2.1, large particles (i.e., above ~ 20 μm diameter for unit density particles) tend to be dominated by gravitational settling effects. The concept of gravitational settling is incorporated into the deposition velocity relationship described in Section 2.1.3 as well as the reflection coefficient scheme used in the current ISC model. Particles in the size range from 1.0 to 20.0 μm diameter are significantly influenced by inertial effects, which enhance the rate of deposition over that obtained by considering gravitational settling alone. The deposition of very small particles (< ~ 0.1 μm diameter) are dominated by Brownian diffusion. This process increases in importance as the size of the particles decreases. Particles in the size range from 0.1 to 1.0 μm diameter show a minimum in the deposition velocity because they are not efficiently deposited by any of the processes described above. Although the deposition velocity database consists of particles in the range from 0.1 to 20 μm diameter sizes, the resistance-based modeling techniques tested in this study apply to larger particle as well. For all of the models, the deposition velocity approaches the same gravitational settling velocity as the size of the particle becomes large. Therefore, the recommended deposition model is considered to be applicable to the full range of particle sizes of interest as might be encountered in typical regulatory studies.

Two related components necessary for a complete deposition model are (1) a method for tracking mass conservation and plume depletion, and (2) a meteorological module for estimating the micrometeorological parameters required by the deposition model. In Section 3, four algorithms for computing plume depletion (source depletion, surface depletion, K-theory method, and modified source depletion) were reviewed. As discussed in Section 3, the modified source depletion model of Horst (1983) is recommended as the overall best approach for use in a regulatory model. Although evaluations of plume depletion algorithms in the literature against field data are very limited, one such study (the dual tracer study of Doran and Horst, 1985) and intercomparisons of the various techniques with the reference surface depletion method support the use of the modified source depletion technique. This algorithm is computationally efficient, conserves mass, and can account for gravitational settling effects. In Appendix E, implementation issues associated with the use of the modified source depletion method are discussed.

Methods suitable for estimating the necessary micrometeorological parameters for the dry deposition model are outlined in Section 4. As required for regulatory applications, these data must be obtained from routinely available observations. In particular, the dry deposition models require an estimate of the surface friction velocity (u_*) and the Monin-Obukhov length (L). The meteorological literature contains several techniques for estimating these input parameters. The techniques selected here have been shown to produce reasonable results. Although other mathematical relationships may eventually be used when the deposition

algorithm is incorporated in the ISC model, the effects of the change are likely to be minimal since experience shows that differences among the most commonly-used techniques are small for most conditions.

An objective model evaluation methodology was used to distinguish between the performance of the various models for predicting particle deposition velocities. Only those models deemed from the scientific review to parameterize the major known processes affecting deposition of small and large particles, as discussed in Section 2, were considered for recommendation as the preferred model. The model evaluation approach, discussed in Section 5, is based on the EPA's statistical model evaluation protocol. This approach was used because it has been successfully demonstrated for many other regulatory model evaluation studies.

The results of the model evaluation exercise described in section 7 was inconclusive in picking a single model with statistically significant (e.g. at the 95% confidence level) superior overall performance. Three models (UAM 2, ADOM 1, and CARB 3 described in section 2) appeared to have one or more performance characteristics that were superior to the rest of the models. The addition of a factor to account for increased deposition area due to leaf area index (LAI) appears to consistently improve core model performance.

The recommended procedures for computing the deposition velocity, plume depletion, and meteorological variables have been implemented in a revised version of the ISC2 dispersion model and a companion meteorological processor. Modified versions of both the short term (ISC2ST) and long term (ISC2LT) models and the meteorological processor will be made available through the EPA's SCRAM bulletin board system. Draft revisions to the user's guide and model formulation documents will also be made available for the purposes of public review and comment.

In future work, it is recommended that an analysis be made to compare the revised version of the ISC model to the previous version of the model to determine likely changes in modeled design concentrations. It is also recommended that some additional analysis be conducted to examine the combined sensitivity of the recommended deposition velocity model and the modified source depletion model to various input variables. This can be done within the new ISC model, since both models have been included in the revised code. For example, the relative sensitivity of the deposition fluxes to the particle size distribution, particle density, surface characteristics (e.g., surface roughness) and meteorological conditions should be assessed.

9. References

Auer, A.H. Jr., 1978: Correlation of land use and cover with meteorological anomalies. *J. Appl. Meteor.*, 17, 636-643.

Baldocchi, D.D., B.B. Hicks and P. Camara, 1987: A canopy stomatal resistance model for gaseous deposition to vegetated surfaces. *Atmos. Environ.*, 21, 91-101.

Bowers, J.F., J.R. Bjorklund and C.S. Cheney, 1979: Industrial Source Complex (ISC) Dispersion Model User's Guide. Volume I. EPA-450/4-79-030, U.S. Environmental Protection Agency, Research Triangle Park, NC.

Businger, J.A., J.C. Wyngaard, Y. Izumi and E.F. Bradley, 1971: Flux-profile relationships in the atmospheric surface layer. *J. Atmos. Sci.*, 28, 181-189.

Chamberlain, A.C., 1953: Aspects of travel and deposition of aerosol and vapor clouds. Atomic Energy Research Establishment, HP/R 1261.

Cleveland, W.S. and R. McGill, 1984: Graphical Perception: Theory, Experimentation, and Application to the Development of Graphical Methods. *J. Am. Stat. Assoc.*, 79, 531-444.

Cox, W.M. and J.A. Tikvart, 1990: A Statistical Procedure for Determining the Best Performing Air Quality Simulation Model. *Atmos. Environ.*, 24, 2387-2395.

Davies, T.D. and J.R. Mitchell, 1982: Dry deposition of sulfur dioxide onto grass in rural eastern England (with some comparisons with other forms of sulfur deposition). *Proceedings of the Fourth International Conference on Precipitation Scavenging, Dry Deposition, and Resuspension*, Volume 2, Santa Monica, CA, 29 November-3 December.

DeBruin, H.A.R. and A.A.M. Holtslag, 1982: A simple parameterization of the surface fluxes of sensible and latent heat during daytime compared with the Penman-Monteith concept. *J. Clim. Appl. Meteor.*, 21, 1610-1621.

Doran J.C. and T.W. Horst, 1985: An evaluation of Gaussian plume-depletion models with dual-tracer field measurements. *Atmos. Environ.*, 19, 939-951.

Dumbauld, R.K., J.E. Rafferty and H.E. Cramer, 1976: Dispersion-deposition from aerial spray releases. *Proceedings of the Third Symposium on Atmospheric Turbulence, Diffusion, and Air Quality*, October 19-22, Raleigh, NC.

Fowler, D. and J.N. Cape, 1982: Dry deposition of SO_2 onto a Scots pine forest. *Proceedings of the Fourth International Conference on Precipitation Scavenging, Dry Deposition, and Resuspension*, Volume 2, Santa Monica, CA, 29 November-3 December.

Garland, J.A., 1982: Dry deposition of small particles to grass in field conditions. *Proceedings of the Fourth International Conference on Precipitation Scavenging, Dry Deposition, and Resuspension*, Volume 2, Santa Monica, CA, 29 November-3 December.

Godowitch, J.M., 1990: Vertical ozone fluxes and related deposition parameters over agricultural and forested landscapes. *Boundary-Layer Meteorol.*, 50, 375-404.

Gray, H.A., M.P. Ligocki, G.E. Moore, C.A. Emery, R.C. Kessler, J.P. Cohen, C.C. Chang, S.I. Balestrini, S.G. Douglas, R.R. Schulhof, J.P. Killus, C.S. Burton, 1991: Deterministic Modeling in the Navajo Generating Station Visibility Study. Volume II. Appendix E (Description of deposition algorithms). Systems Applications, International, San Rafael, CA.

Hanna, S.R. and J.C. Chang, 1990: Modification of the Hybrid Plume Dispersion Model (HPDM) for urban conditions and its evaluation using the Indianapolis data set. Vol. III. Analysis of urban boundary layer data. Sigma Research Corp., Concord, MA.

Hanna, S.R. and J.C. Chang, 1991a: Modification of the Hybrid Plume Dispersion Model (HPDM) for urban conditions and its evaluation using the Indianapolis data set. Vol. I. User's guide for HPDM-Urban. Sigma Research Corp., Concord, MA.

Hanna, S.R. and J.C. Chang, 1991b: SIGPRO - A meteorological preprocessor for dispersion model applications to stack plumes in urban areas. Seventh Joint AMS-AWMA Conf. on Appl. of Air Poll. Meteor., New Orleans, LA, Jan., 1991.

Hanna, S.R. and J.C. Chang, 1992: Boundary-layer parameterizations for applied dispersion modeling over urban areas. *Boundary-Layer Meteorology*, 58, 229-259.

Harrison, R.M., S. Rapsomanikis and A. Turnbull, 1989: Land-surface exchange in a chemically-reactive system: Surface fluxes of HNO_3, HCl and NH_3. *Atmos. Environ.*, 23, 1795-1800.

Hicks, B.B., 1982: Critical assessment document on acid deposition. ATDL Contrib. File No. 81/24, Atmos. Turb. and Diff. Laboratory, Oak Ridge, TN.

Hicks, B.B., D.D. Baldocchi, T.P. Meyers, R.P. Hosker, Jr. and D.R. Matt, 1987: A preliminary multiple resistance routine for deriving dry deposition velocities from measured quantities. *Water, Air, and Soil Poll.*, **36**, 311-330.

Hicks, B.B., D.R. Matt and R.T. McMillen, 1989: A micrometeorological investigation of surface exchange of trace gases: A case study. NOAA Tech. Memo. ERL ARL-172, Air Resources Laboratory, Silver Spring, MD.

Hicks, B.B., M.L. Wesely, R.L. Coulter, R.L. Hart, J.L. Durham, R. Speer and D.H. Stedman, 1986: An experimental study of sulfur and NO_x fluxes over grassland. *Boundary-Layer Meteorol.*, **34**, 103-121.

Hidy, G.M., 1984: *Aerosols: An Industrial and Environmental Science*. Academic Press, Inc., New York, NY.

Hjelmfelt, M.R., 1982: Numerical simulation of the effects of St. Louis on mesoscale boundary-layer airflow and vertical air motion: Simulations of urban vs. non-urban effects. *J. Appl. Meteor.*, **21**, 1239-1257.

Holtslag A.A.M. and A.P. van Ulden, 1983: A simple scheme for daytime estimates of the surface fluxes from routine weather data. *J. Clim. and Appl. Meteor.*, **22**, 517-529.

Horst, T.W., 1977: A surface depletion model for deposition from a Gaussian plume. *Atmos. Environ.*, **11**, 41-46.

Horst, T.W., 1983: A correction to the Gaussian source-depletion model. In *Precipitation Scavenging, Dry Deposition and Resuspension*, H.R. Pruppacher, R.G. Semonin, W.G.N. Slinn, eds., Elsevier, NY.

Horst, T.W., 1984: The modification of plume models to account for dry deposition. *Boundary-Layer Meteor.*, **30**, 413-430.

Hosker, R.P. and S.E. Lindberg, 1982: Review: Atmospheric Deposition and Plant Assimilation of Gases and Particles. *Atmos. Environ.*, 16, 889-910.

Huebert, B.J., 1982; Measurements of the dry-deposition flux of nitric acid vapor to grasslands and forest. *Proceedings of the Fourth International Conference on Precipitation Scavenging, Dry Deposition, and Resuspension*, Volume 2, Santa Monica, CA, 29 Nov.-3 Dec.

Lorenz, R. and C.E. Murphy, Jr., 1989: Dry deposition of particles to a pine plantation. *Boundary-Layer Meteorol.*, 46, 355-366.

McDonald, J.E., 1960: An aid to computation of terminal fall velocities of spheres. *J. Met.*, 17, 463.

McMillen R.T., D.R. Matt, B.B. Hicks and J.D. Womack, 1987: Dry deposition measurements of sulfur dioxide to a spruce-fir forest in the Black Forest: A data report. NOAA Tech. Memo. ERL ARL-152, Air Resources Laboratory, Silver Spring, MD.

Meyers, T.P., 1987: The sensitivity of modeled SO_2 fluxes and profiles to stomatal and boundary layer resistances. *Water, Air, and Soil Poll.*, 35, 261-278.

Meyers, T.P. and D.D. Baldocchi, 1988: A comparison of models for deriving dry deposition fluxes of O_3 and SO_2 to a forest canopy. *Tellus*, 40B, 270-284.

Meyers, T.P., B.J. Huebert, and B.B. Hicks, 1989: HNO_3 deposition to a deciduous forest. *Boundary-Layer Meteorol.*, 49, 395-410.

Moller U. and G. Schumann, 1970: Mechanisms of transport from the atmosphere to the earth's surface. *J. Geophy. Res.*, 75, 3013-3019.

Nicholson, K.W. and T.D. Davies, 1987: Field Measurements of the dry deposition of particulate sulphate. *Atmos. Environ.*, 21, 1561-1571.

Oke, T.R., 1978: *Boundary Layer Climates*. John Wiley & Sons, New York, NY.

Oke, T.R., 1982: The energetic basis of the urban heat island. *Quart. J.R. Meteor. Soc.*, 108, 1-24.

Overcamp, T.J., 1976: A general Gaussian diffusion-deposition model for elevated point sources. *J. Appl. Meteor.*, 15, 1167-1171.

Padro, J., G. den Hartog, and H.H. Neumann, 1991: An investigation of the ADOM dry deposition module using summertime O_3 measurements above a deciduous forest. *Atmos. Environ.*, 25A, 1689-1704.

Plate, E. and A.A. Quraishi, 1965: Modeling of velocity distribution inside and above tall crops. *J. Appl. Meteorol.*, 4, 400-408.

Pleim, J., A. Venkatram and R. Yamartino, 1984: ADOM/TADAP model development program. Volume 4. The dry deposition module. Ontario Ministry of the Environment, Rexdale, Ontario.

Rao, K. S., 1981: Analytical solutions of a gradient-transfer model for plume deposition and sedimentation. NOAA Tech. Memo. ERL ARL-109, Air Resources Laboratory, Silver Spring, MD.

Richards, L.W., J.A. Anderson, D.L. Blumenthal, J.A. McDonald, P.S. Bhardwaja, R.B. Candelaria and D.W. Moon, 1989: Nitrogen and sulfur chemistry and aerosol formation in a western coal-fired power plant plume. AWMA/EPA International Specialty Conference. Ester Park, CO, October, 1989.

Scire J.S., F.W. Lurmann, P. Karamchandani, A. Venkatram, R. Yamartino, J. Young and J. Pleim, 1986: ADOM/TADAP model development program. Volume 9. ADOM/TADAP User's Guide. Ontario Ministry of the Environment, Rexdale, Ontario, Canada.

Scire, J.S., D.G. Strimaitis and R.J. Yamartino, 1990: Model formulation and user's guide for the CALPUFF dispersion model. Sigma Research Corp., Concord, MA.

Scire, J.S. and D.L. Wojichowski, 1987: Modeling deposition and dispersion in an urban environment. M.A.S.S.-APCA 33rd Anniv. Technical Conference, November 3-6, Atlantic City, NJ.

Sehmel, G.A., 1980: Particle and gas dry deposition: A review. *Atmos. Environ.*, 14, 983-1011.

Sehmel, G.A., 1984: Deposition and Resuspension. Chapter 12 in *Atmospheric Science and Power Production*, DOE/TIC-27601. U.S. Department of Energy, D. Randerson, Ed.

Sehmel, G.A. and W.H. Hodgson, 1978: A model for predicting dry deposition of particles and gases to environmental surfaces. PNL-SA-6721, Battelle Pacific Northwest Laboratory.

Sehmel, G.A. and S.L. Sutter, 1974: Particle deposition rates on a water surface as a function of particle diameter and air velocity. *J. Rechs. Atmos.*, III, 911-918.

Shieh, C.M., M.L.Wesely and C.J. Walcek, 1986: A dry deposition module for regional acid deposition. EPA/600/3-86/037, U.S. Environmental Protection Agency, Research Triangle Park, NC.

Slinn, W.G.N., L. Hasse, B.B. Hicks, A.W. Hogan, D. Lal, P.S. Liss, K.O. Munnich, G.A. Sehmel and O. Vittori, 1978: Some aspects of the transfer of atmospheric trace constituents past the air-sea interface. *Atmos. Environ.*, 12, 2055-2087.

Slinn, S.A. and W.G.N. Slinn, 1980: Predictions for particle deposition on natural waters. *Atmos. Environ.*, 14, 1013-1016.

Slinn, W.G.N., 1982: Predictions for particle deposition to vegetative canopies. *Atmos. Environ.*, 16, 1785-1794.

van Ulden, A.P. and A.A.M. Holtslag, 1985: Estimation of atmospheric boundary layer parameters for diffusion applications. *J. Appl. Meteor.*, 24, 1196-1207.

Walcek, C.J., R.A. Brost, J.S. Chang and M.L. Wesely, 1986: SO_2, sulfate, and HNO_3 deposition velocities computed using regional land use and meteorological data. *Atmos. Environ.*, 20, 949-964.

Wang, I.T. and P.C. Chen, 1980: Estimations of heat and momentum fluxes near the ground. *Proc. 2nd Joint Conf. on Applications of Air Poll. Meteor.*, American Meteorological Society, Boston, MA, 764-769.

Weil, J.C. and R.P. Brower, 1983: *Estimating Convective Boundary Layer Parameters for Diffusion Application*. Draft Report prepared by Environmental Center, Martin Marietta Corp., for Maryland Dept. of Natural Resources.

Wesely, M.L., 1989: Parameterization of surface resistances to gaseous dry deposition in regional-scale numerical models. *Atmos. Environ.*, 23, 1293-1304.

Wesely, M.L., D.R. Cook, and R.M. Williams, 1981: Field measurement of small ozone fluxes to snow, wet bare soil, and lake water. *Boundary-Layer Meteorol.*, 20, 459-471.

Wesely, M.L., D.R. Cook and R.L. Hart, 1983: Fluxes of gases and particles above a deciduous forest in wintertime. *Boundary-Layer Meteorol.*, 27, 237-255.

Wesley, M.L., D.R. Cook, R.L. Hart, B.B. Hicks, J.L. Durham, R.E. Speer, D.H. Stedman and R.J. Tropp, 1982: Eddy-correlation measurements of the dry deposition of particulate sulfur and submicron particles. *Proceedings of the Fourth International Conference on Precipitation Scavenging, Dry Deposition, and Resuspension*, Volume 2, Santa Monica, CA, 29 November-3 December.

Wesely, M.L., J.A. Eastman, D.R. Cook and B.B. Hicks, 1978: Daytime variations of ozone eddy fluxes to maize. *Boundary-Layer Meteorol.*, 15, 361-373.

Wesely, M.L. and B.B. Hicks, 1977: Some factors that affect the deposition rates of sulfur dioxide and similar gases on vegetation. *J. Air Poll. Control Assoc.*, 27, 1110-1116.

Winges, K.D., 1990: User's guide for the Fugitive Dust Model (FDM) (revised). Volume 1: User's Instructions. EPA-910/9-88-202R. U.S. EPA, Region 10, Seattle, WA.

Winges, K.D., 1992: Personal communication to J. Scire.

Yamartino, R.J., J.S. Scire, S.R. Hanna, G.R. Carmichael and Y.S. Chang, 1992: The CALGRID mesoscale photochemical grid model. Volume I. Model formulation. *Atmos. Environ.*, 26A, 1493-1512.

Appendix A

Estimation of ISC Deposition Velocity

Estimation of ISC Deposition Velocity

The basis for the present ISC deposition algorithm is found in Dumbauld et al. (1976) and in Overcamp (1976). In this approach the particles are assumed to move towards the ground with a total velocity equal to the sum of the gravitational settling velocity and an average turbulent velocity which determines the rate of plume spreading. This turbulent velocity is given by

$$v_t = (uH_e - v_g x) \frac{d\ln\sigma_z}{dx} \tag{A-1}$$

where u is the stack height wind speed, H_e is the effective plume height, v_g is the gravitational settling velocity, x is the downwind distance, and the vertical dispersion coefficient, σ_z, is given by the relation:

$$\sigma_z = Ax^B \tag{A-2}$$

The coefficients A and B are stability dependent, and are treated as average values in the ISC deposition model. By differentiating Equation A-2 and substituting into Equation A-1 we have:

$$v_t = \overline{B}\left(\frac{uH_e}{x} - v_g\right) \tag{A-3}$$

The turbulent velocity is thus a function of the ratio of the plume centerline height to the downwind distance. For small particles, the uH_e/x term is much larger than the settling velocity which can be ignored.

In nearly all of the small particle experiments there is no specific plume-receptor information in order to directly estimate an H_e/x. Furthermore, in some experiments it is possible that several sources may be contributing to the deposition fluxes. How then does one estimate an H_e/x that will be appropriate and consistent with the information provided to the other deposition velocity models?

The other deposition models estimate a turbulent velocity near the surface as being equal to the inverse of the aerodynamic resistance, r_a. Thus the H_e/x term can be estimated from the relation:

$$H_e/x = \frac{1 + v_g r_a \bar{B}}{u r_a \bar{B}} \tag{A-4}$$

where the aerodynamic resistance is given by:

$$r_a = \frac{\left[\ln\left(\frac{z - d}{z_o}\right) - \psi\left(\frac{z}{L}\right) \right]}{k u_*} \tag{A-5}$$

which is a formulation common to the ADOM and UAM models. Using the information on Pasquill Gifford Turner stability class and the friction velocity and Monin-Obukhov length, and assuming a reference height of 10 m, a displacement plane height of zero and using the given surface roughness length and wind speed we estimated the equivalent H_e/x needed by the ISC model.

The actual deposition velocity used in the ISC model is, following Overcamp (1976), equal to:

$$v_d = \left[\frac{1 - \alpha}{1 + \alpha} \right] (v_g + v_t) \tag{A-6}$$

The settling velocity used in ISC, v_g, is given by the Stokes relation:

$$v_g = \frac{\rho g d^2}{18\mu} \tag{A-7}$$

where ρ is the particle density, g is the acceleration due to gravity, d is the particle diameter, and μ is the absolute viscosity of air ($\mu = 1.83 \times 10^{-4}$ g cm^{-1} s^{-1}).

The reflection coefficient, α, in Equation A-6 is the fraction of the image plume source remaining. In the limit of a fully reflecting plume the image plume experiences no depletion and α approaches one. The Dumbauld et al. (1976) paper indicates that when the settling velocity drops below 0.1 cm/s the reflection coefficient is set equal to 1. As a result, ISC will predict a zero deposition velocity for many of the cases in the small particle dataset. This limit on deposition velocity especially affects sulfate particulate matter since the size range for such particulate matter peaks in the submicron diameter range.

Appendix B

Supplemental Graphics

Series 1: Scatter plots of Observed Versus Model Predicted Deposition Velocities

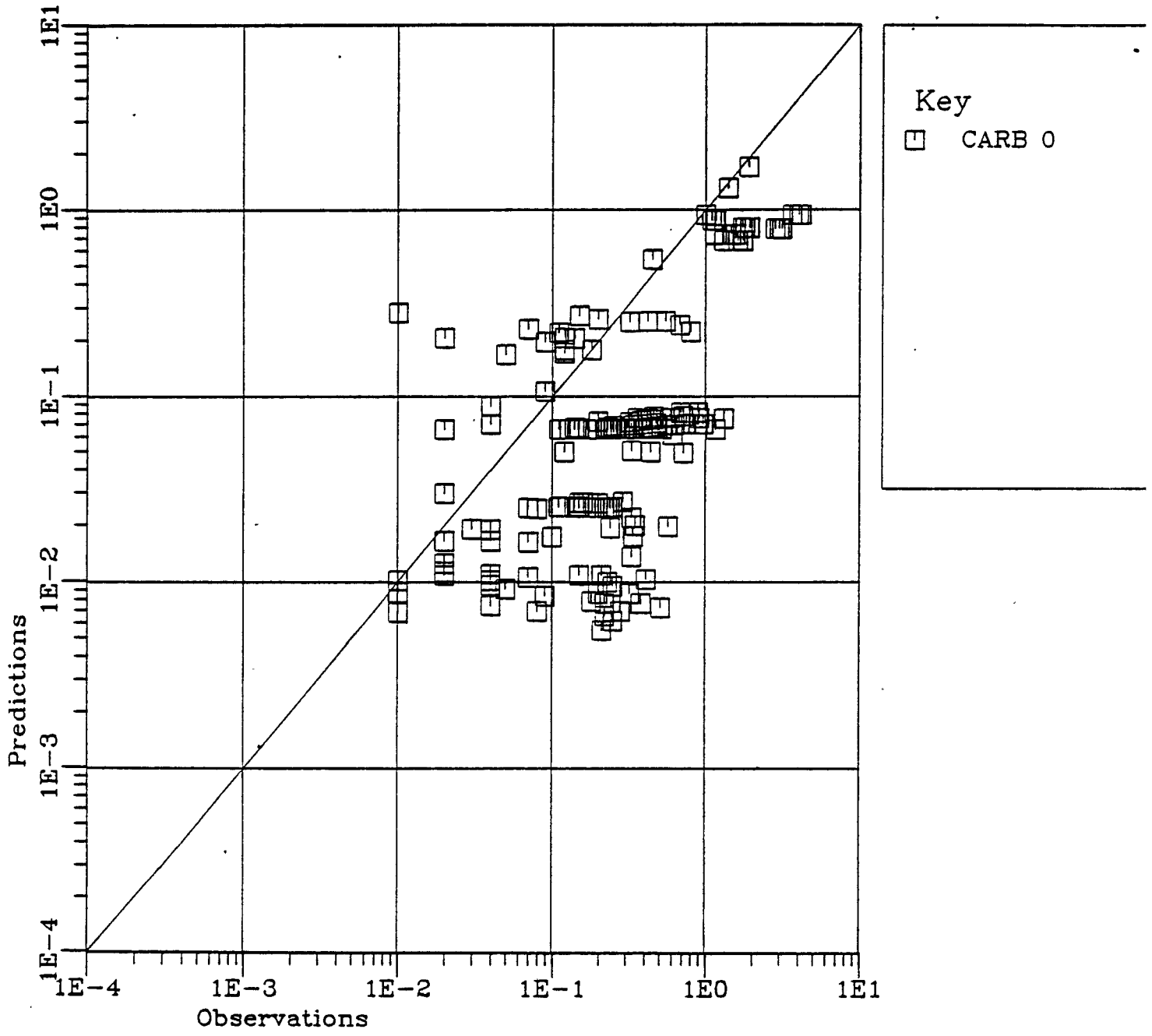

Figure B-1a. Scatter plot of observed deposition velocity (cm/s) versus model predicted deposition velocity (cm/s) for the complete small particle data set.

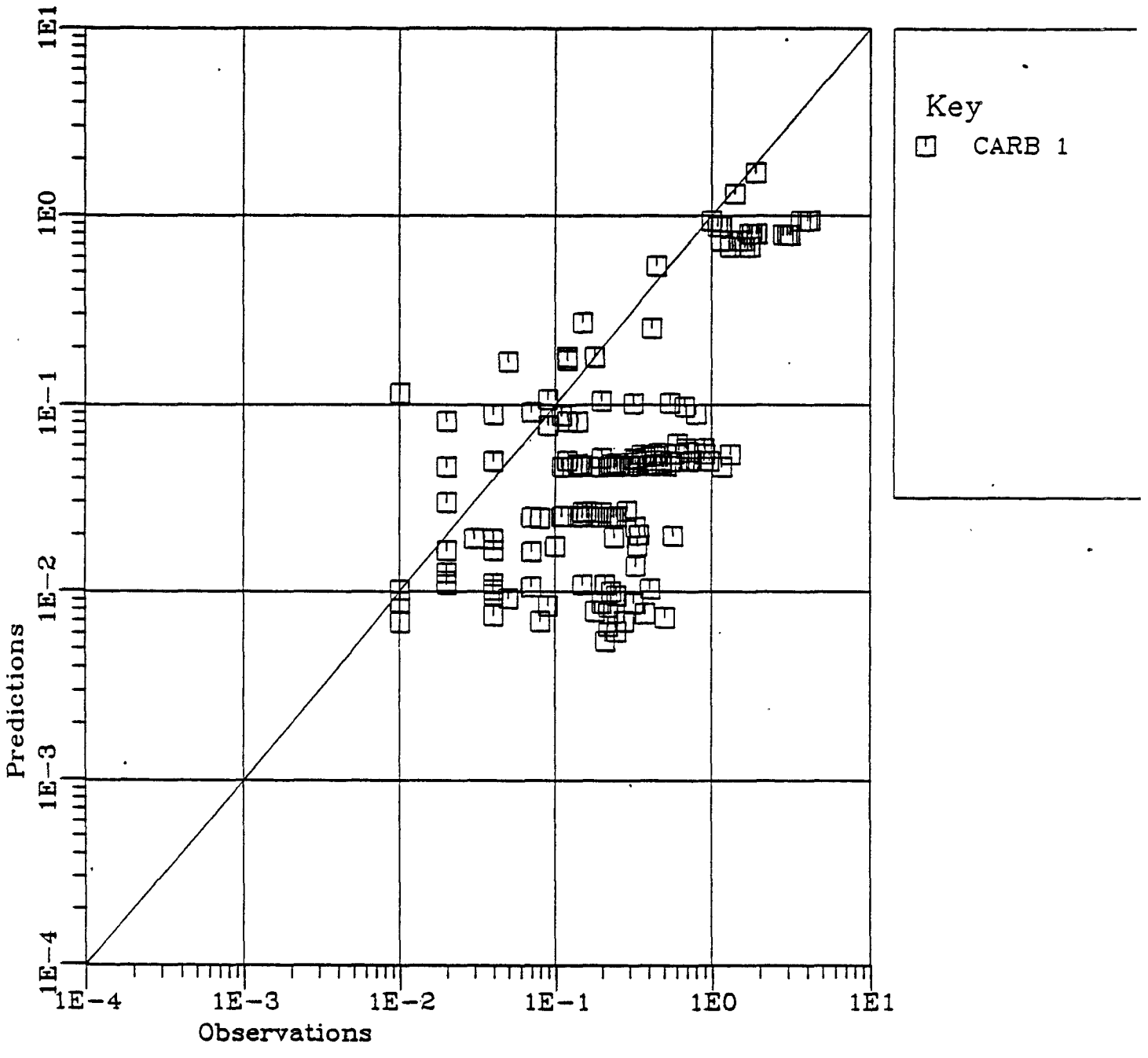

Figure B-1b. Scatter plot of observed deposition velocity (cm/s) versus model predicted deposition velocity (cm/s) for the complete small particle data set.

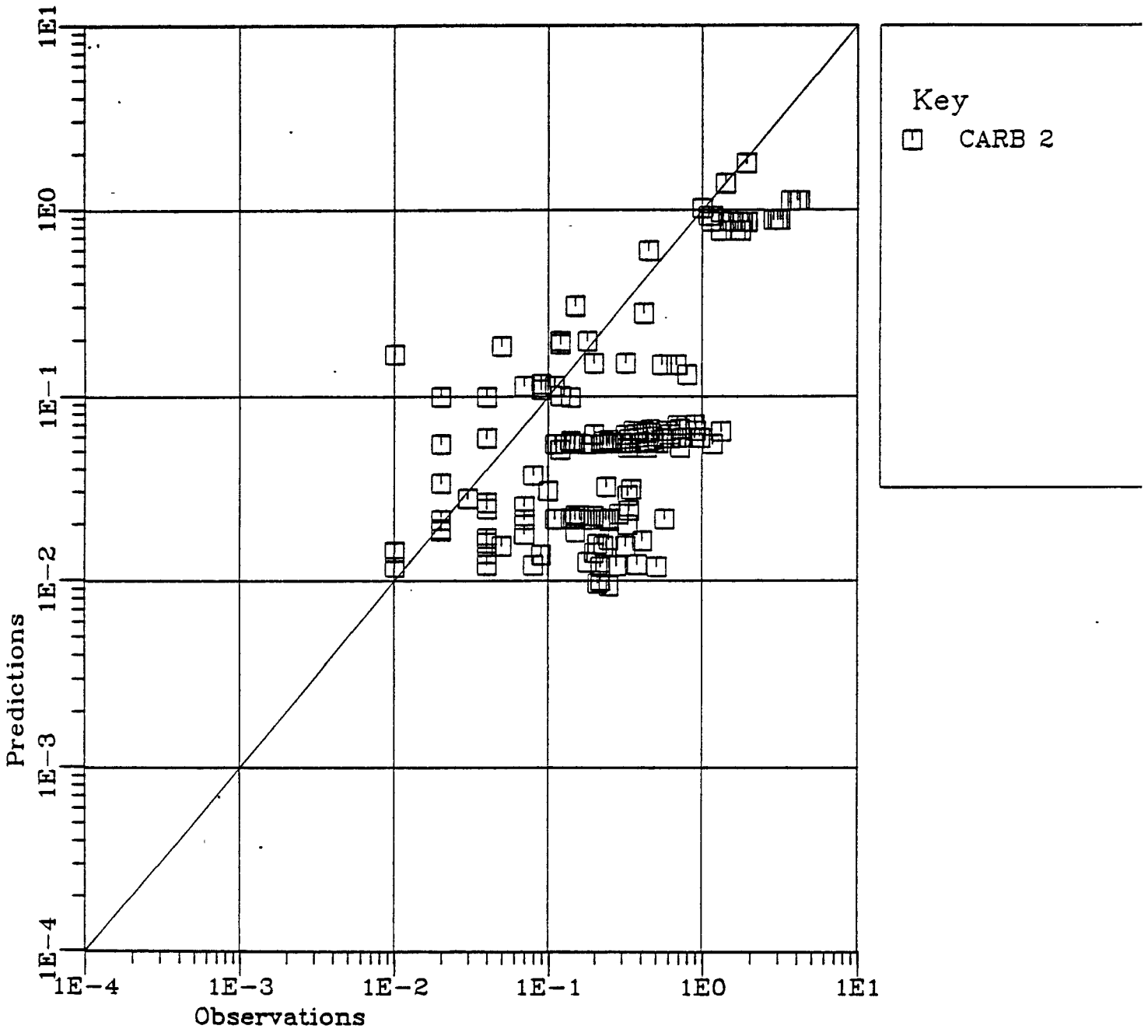

Figure B-1c. Scatter plot of observed deposition velocity (cm/s) versus model predicted deposition velocity (cm/s) for the complete small particle data set.

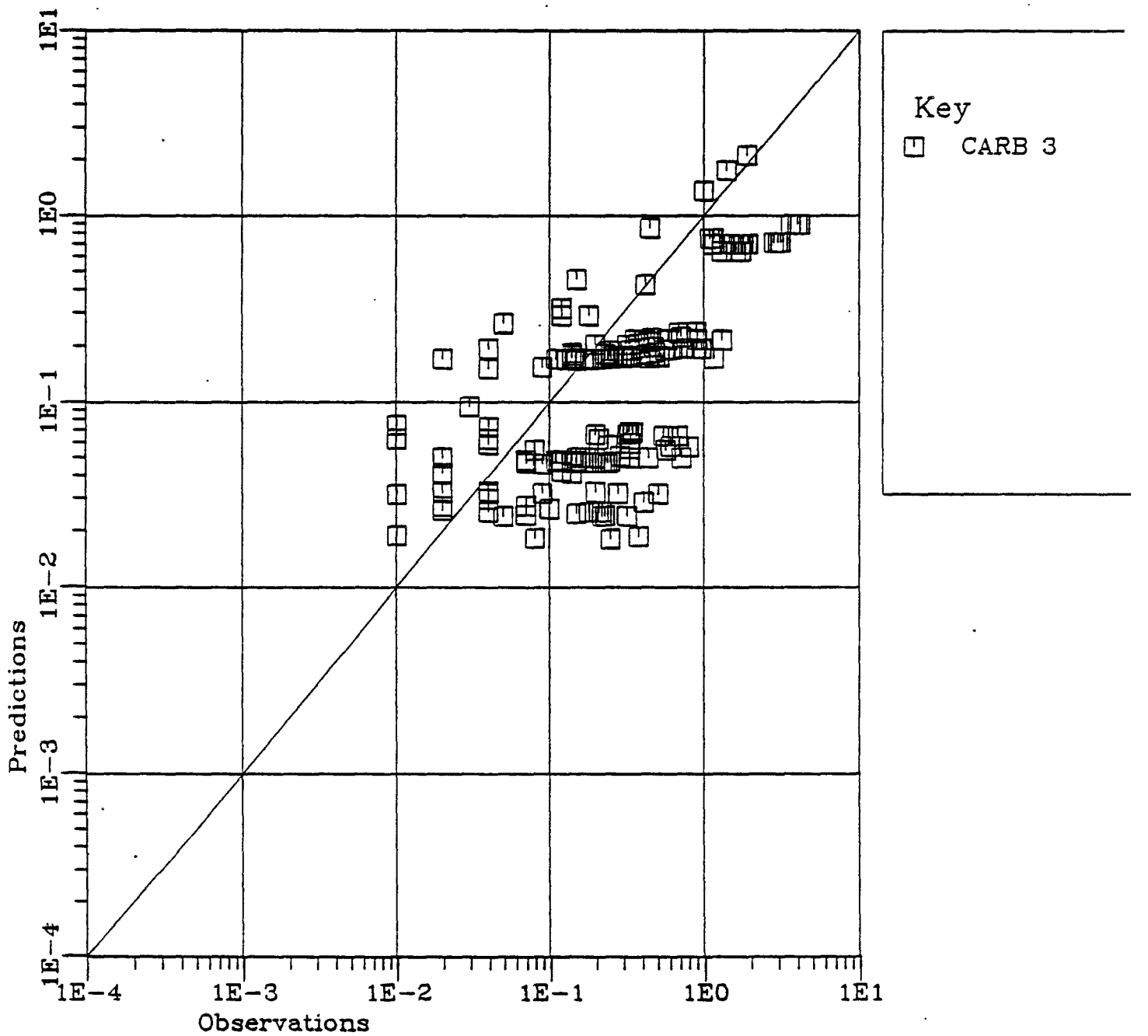

Figure B-1d. Scatter plot of observed deposition velocity (cm/s) versus model predicted deposition velocity (cm/s) for the complete small particle data set.

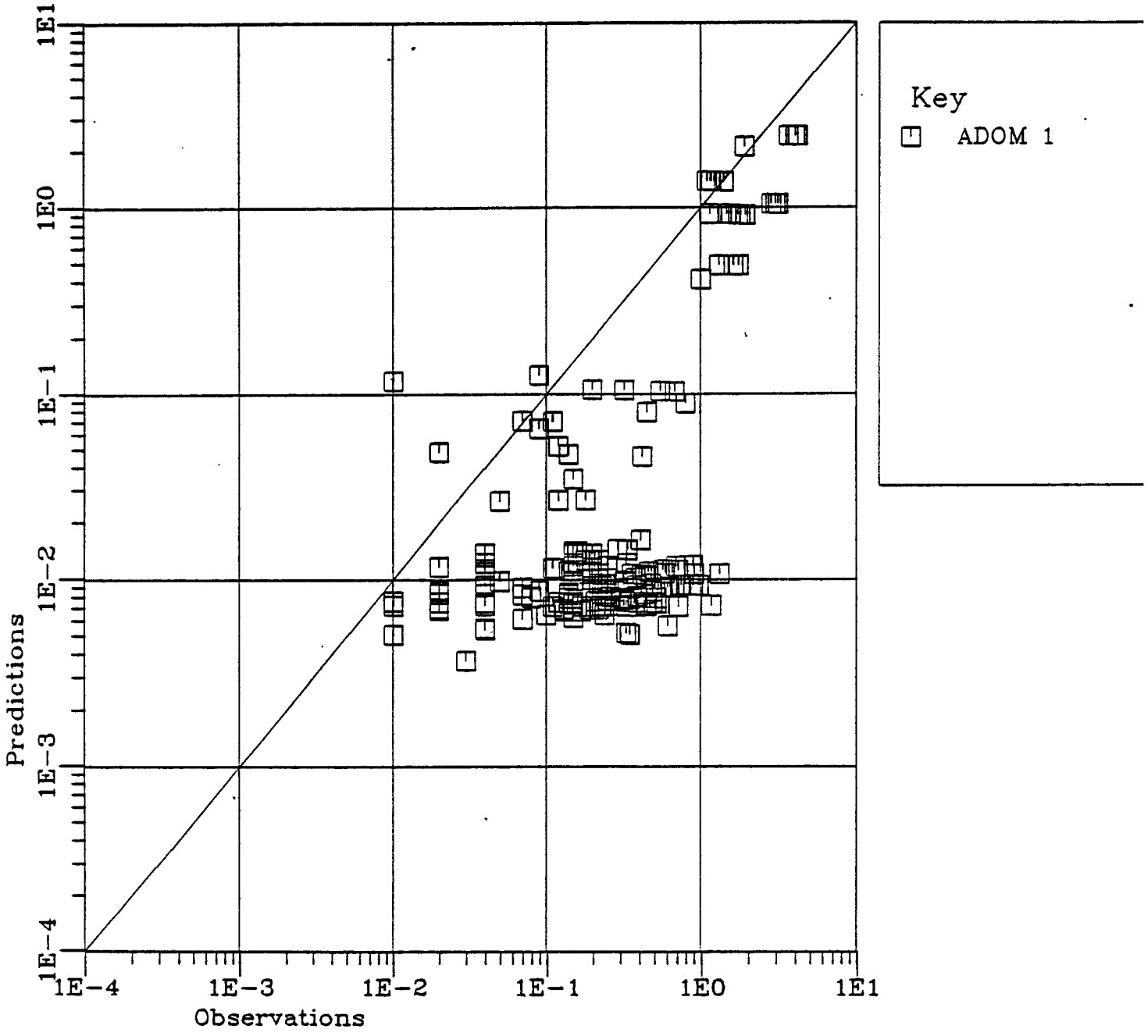

Figure B-1e. Scatter plot of observed deposition velocity (cm/s) versus model predicted deposition velocity (cm/s) for the complete small particle data set.

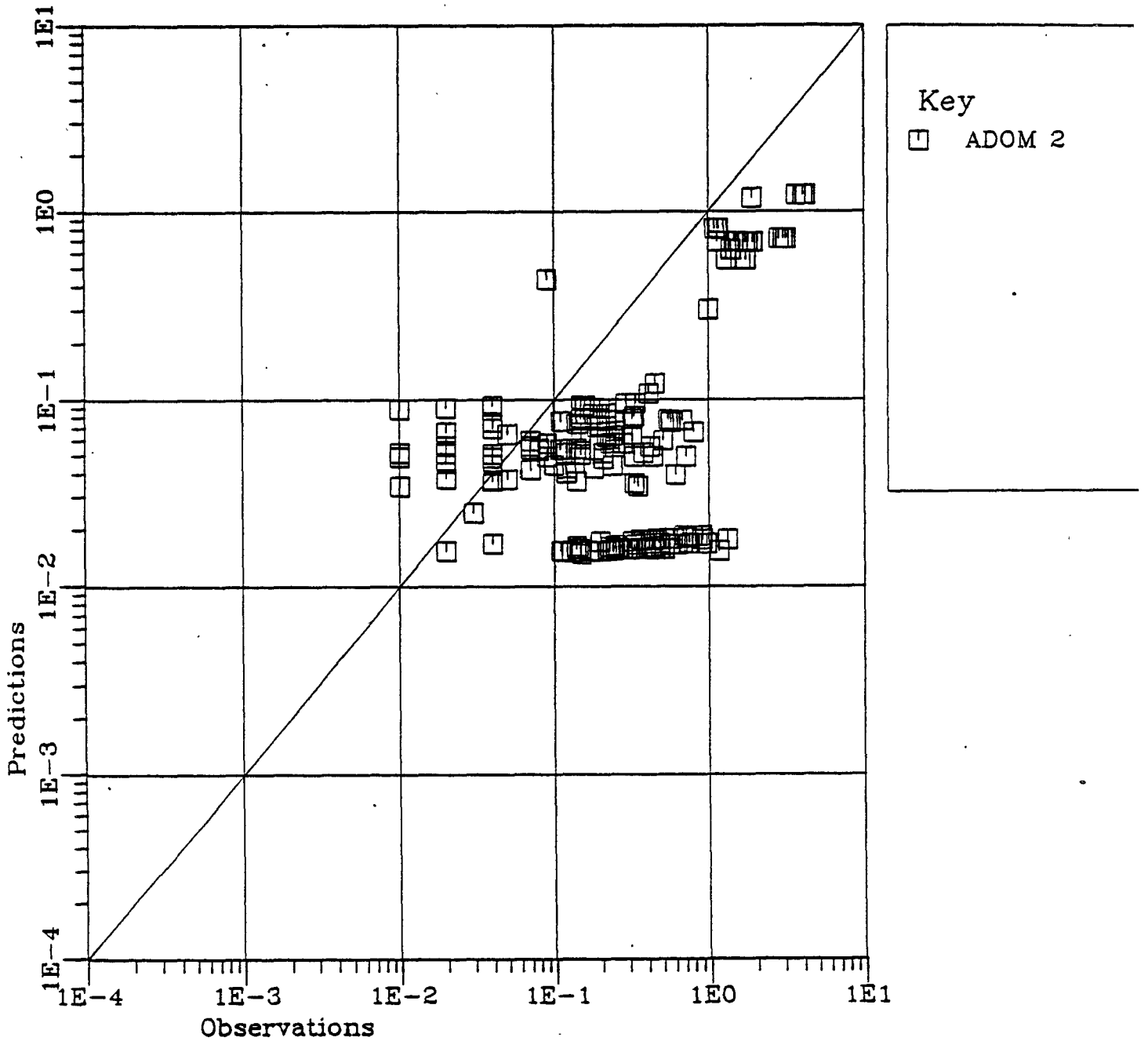

Figure B-1f. Scatter plot of observed deposition velocity (cm/s) versus model predicted deposition velocity (cm/s) for the complete small particle data set.

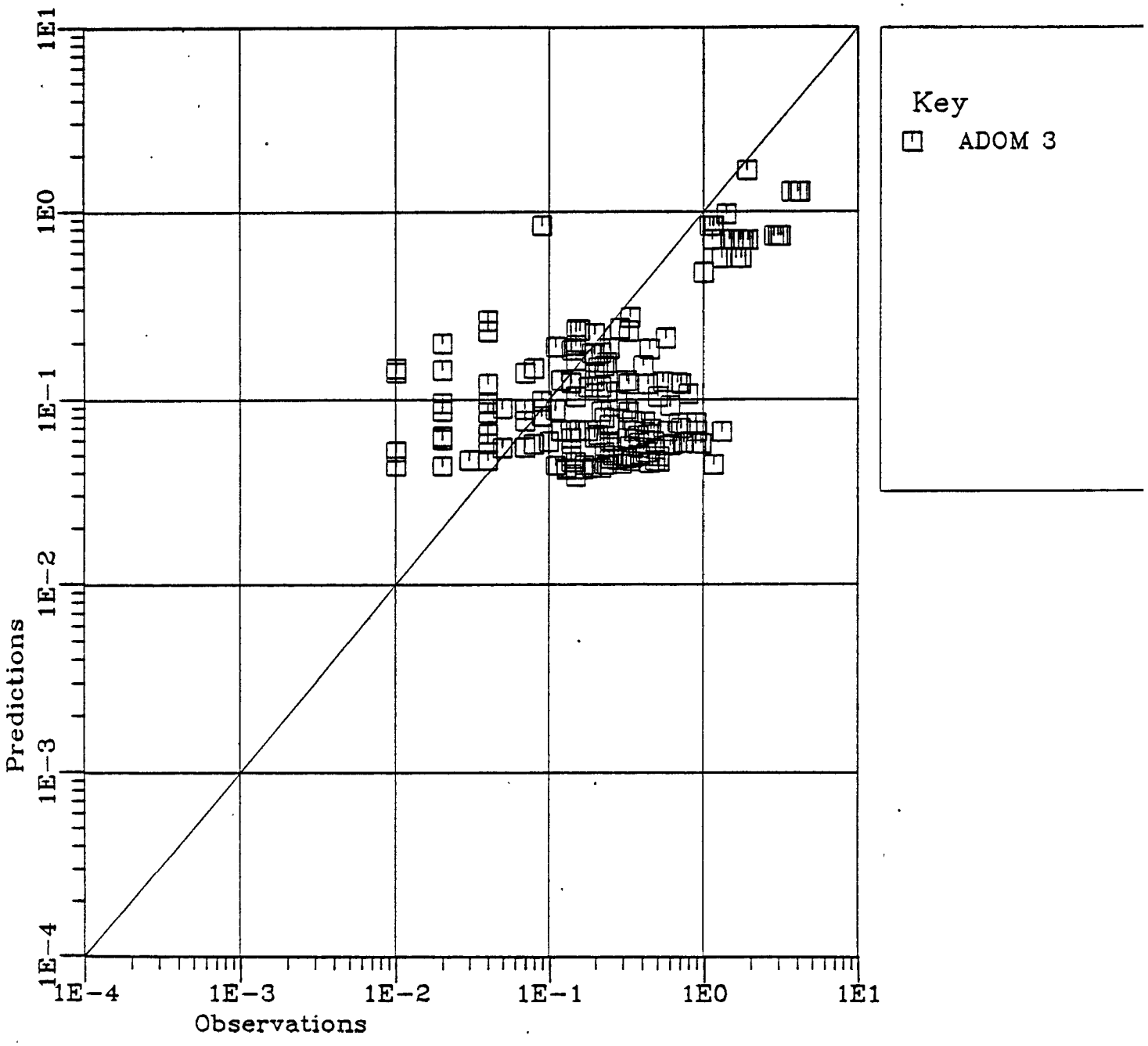

Figure B-1g. Scatter plot of observed deposition velocity (cm/s) versus model predicted deposition velocity (cm/s) for the complete small particle data set.

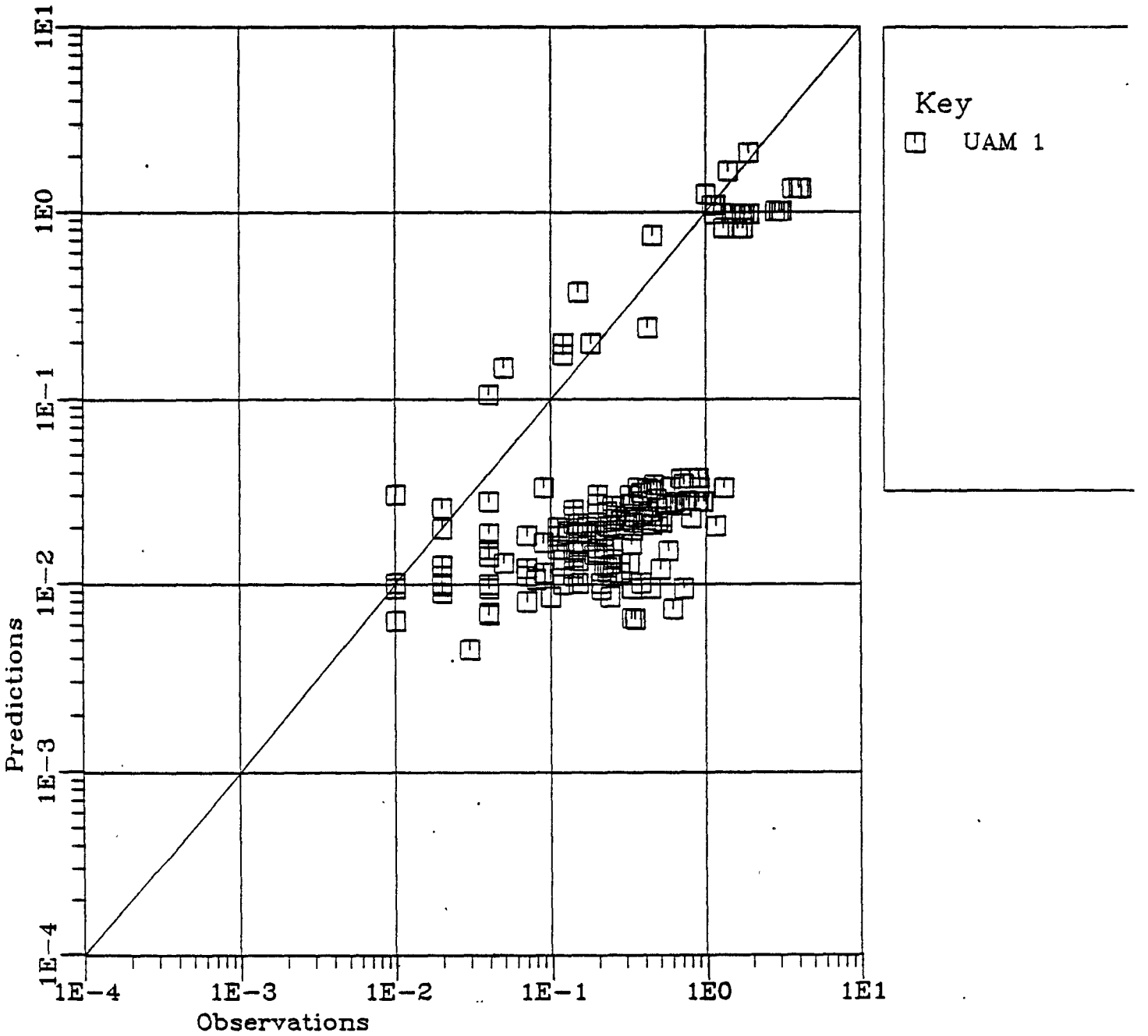

Figure B-1h. Scatter plot of observed deposition velocity (cm/s) versus model predicted deposition velocity (cm/s) for the complete small particle data set.

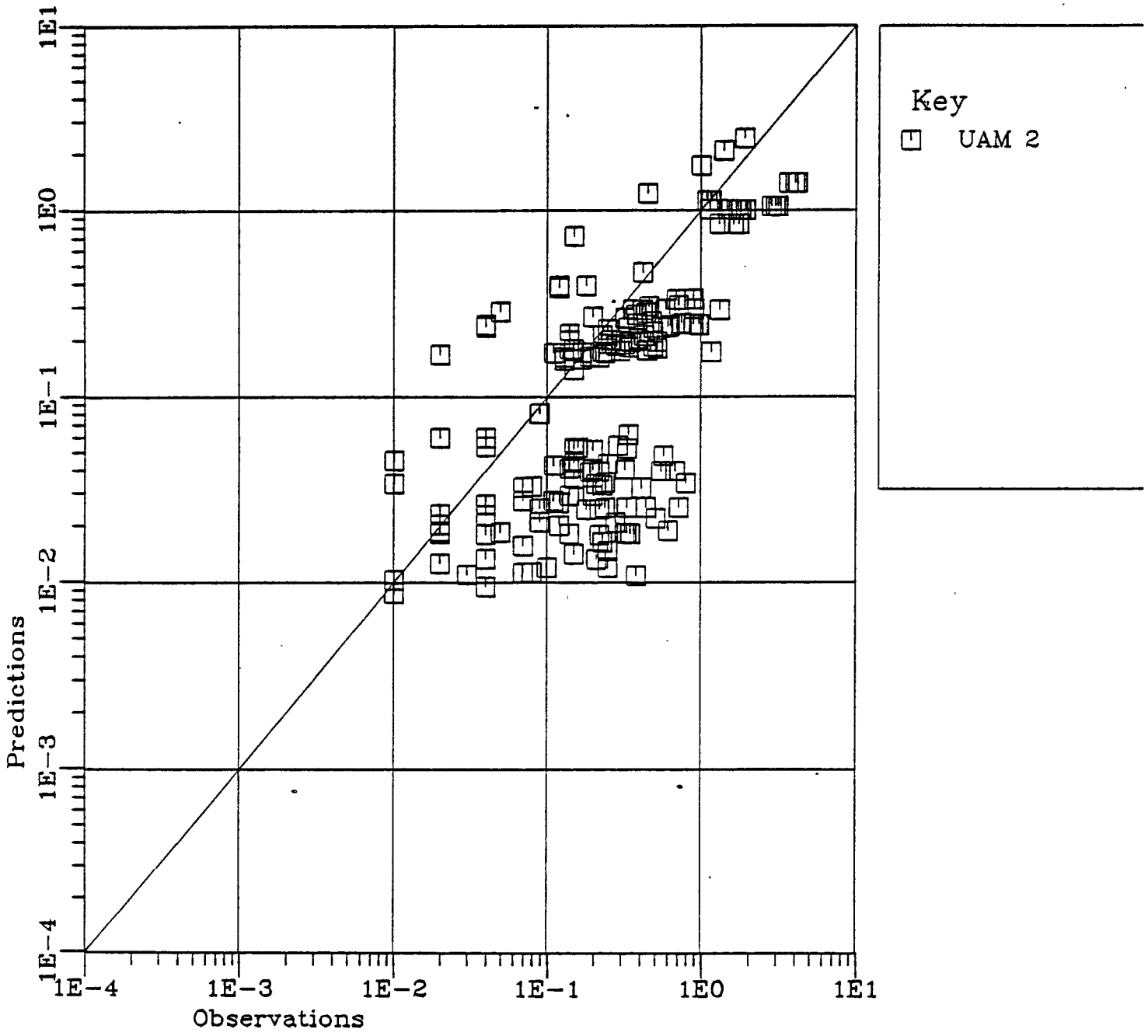

Figure B-1i. Scatter plot of observed deposition velocity (cm/s) versus model predicted deposition velocity (cm/s) for the complete small particle data set.

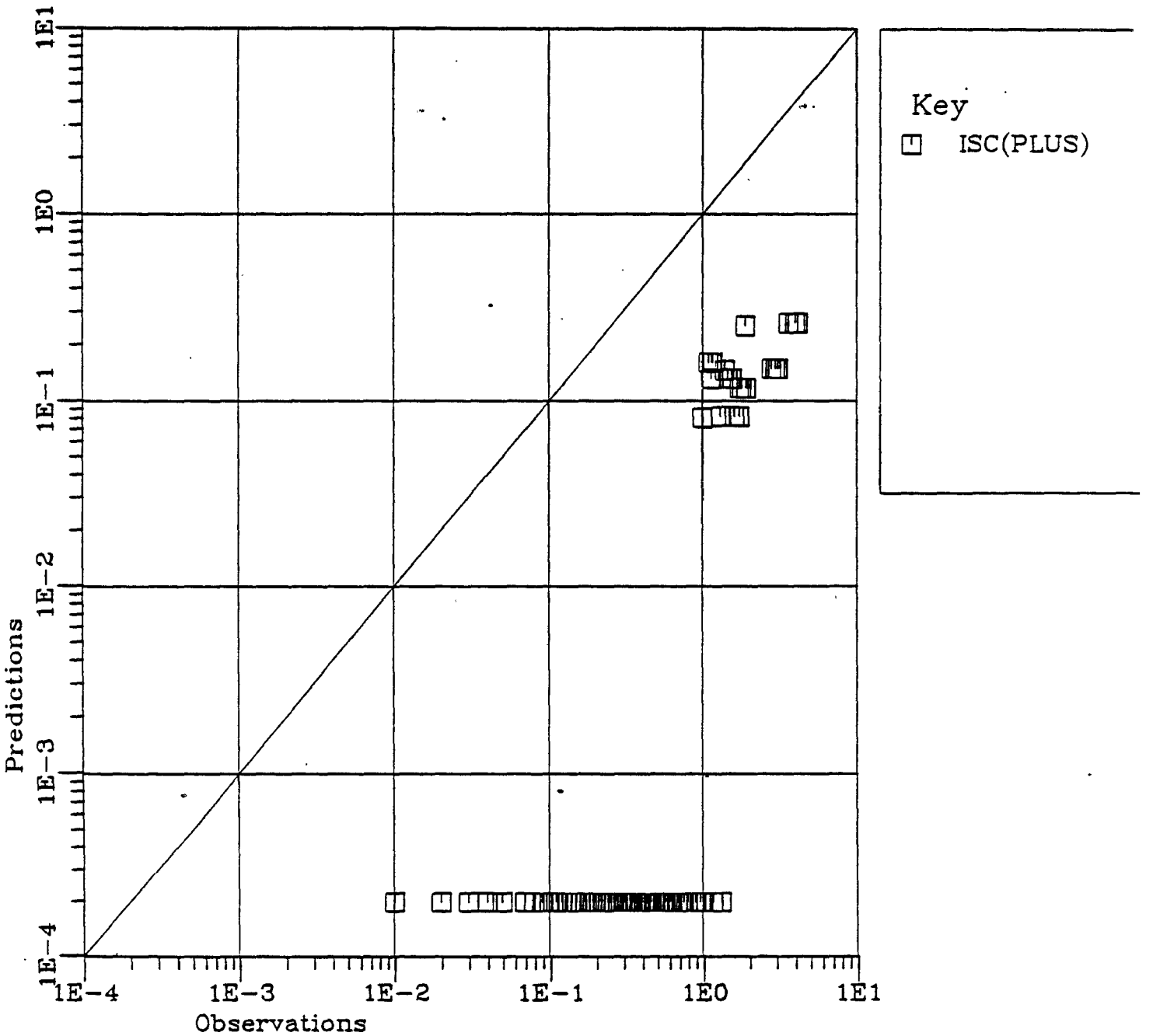

Figure B-1j. Scatter plot of observed deposition velocity (cm/s) versus model predicted deposition velocity (cm/s) for the complete small particle data set.

Series 2: Cumulative Distribution Function (CDF) Plots for Observations and Model Predictions of Deposition Velocity

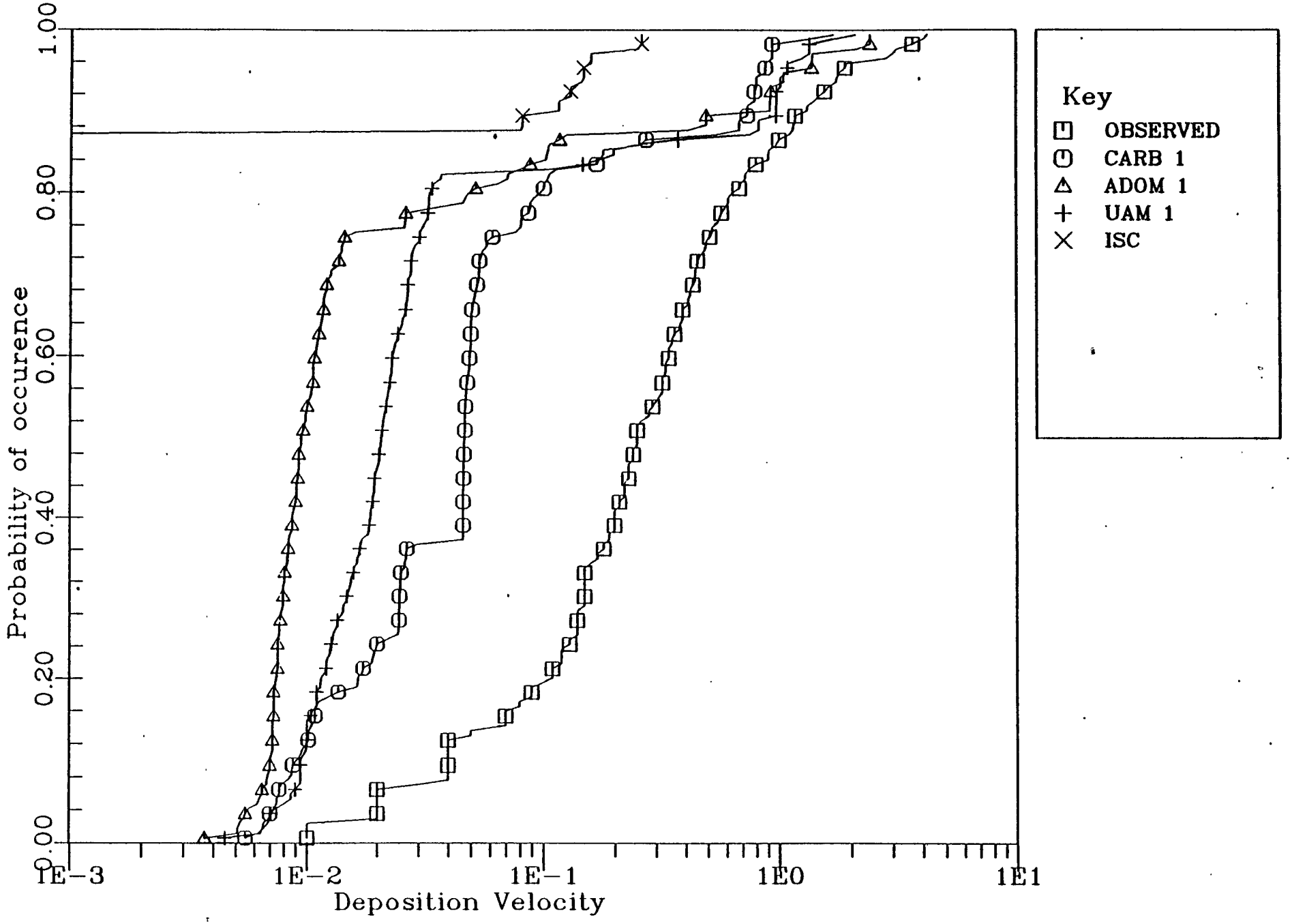

Figure B-2a. Cumulative probability plot of deposition velocity (cm/s) using the complete small particle data set.

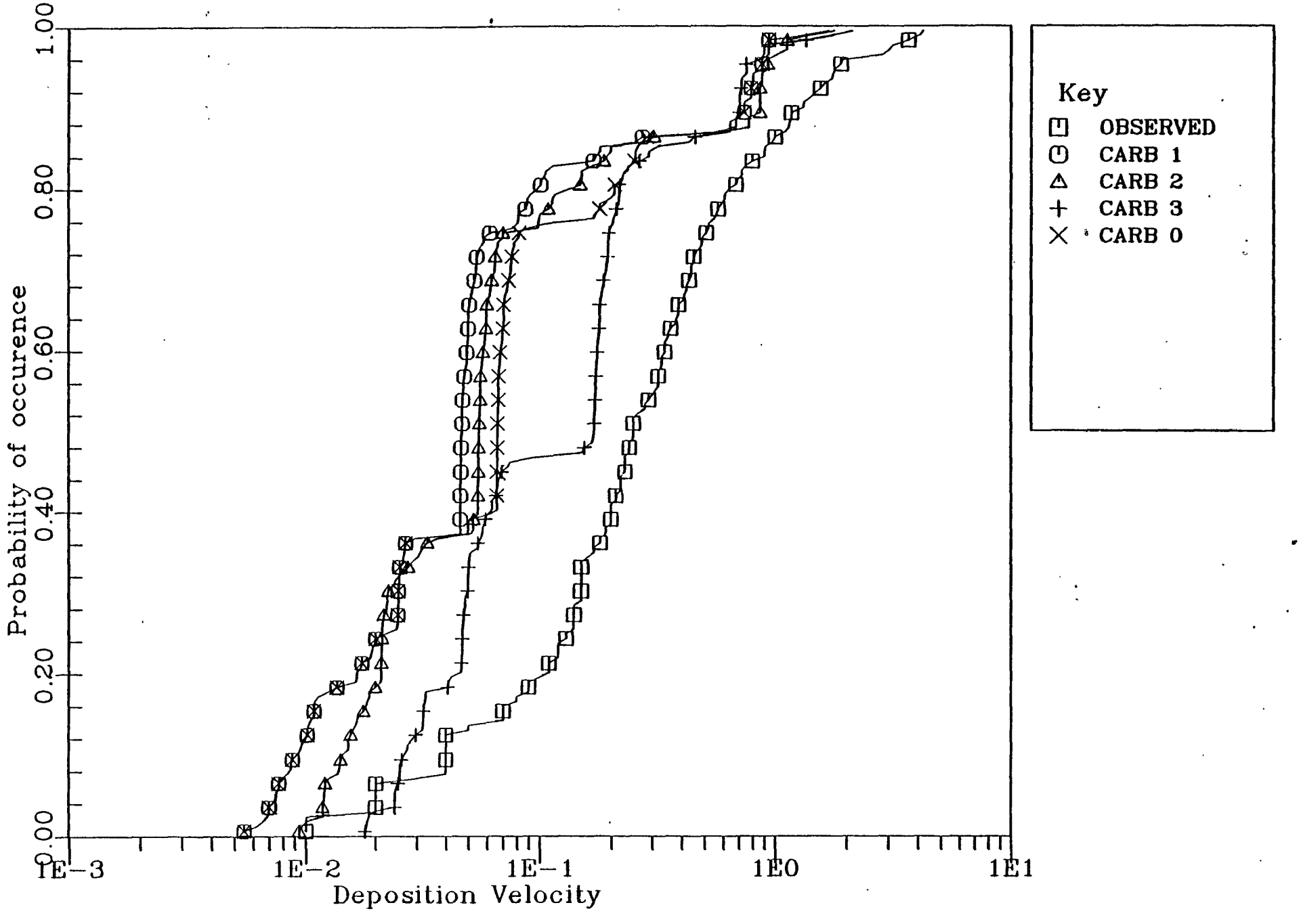

Figure B-2b. Cumulative probability plot of deposition velocity (cm/s) using the complete small particle data set

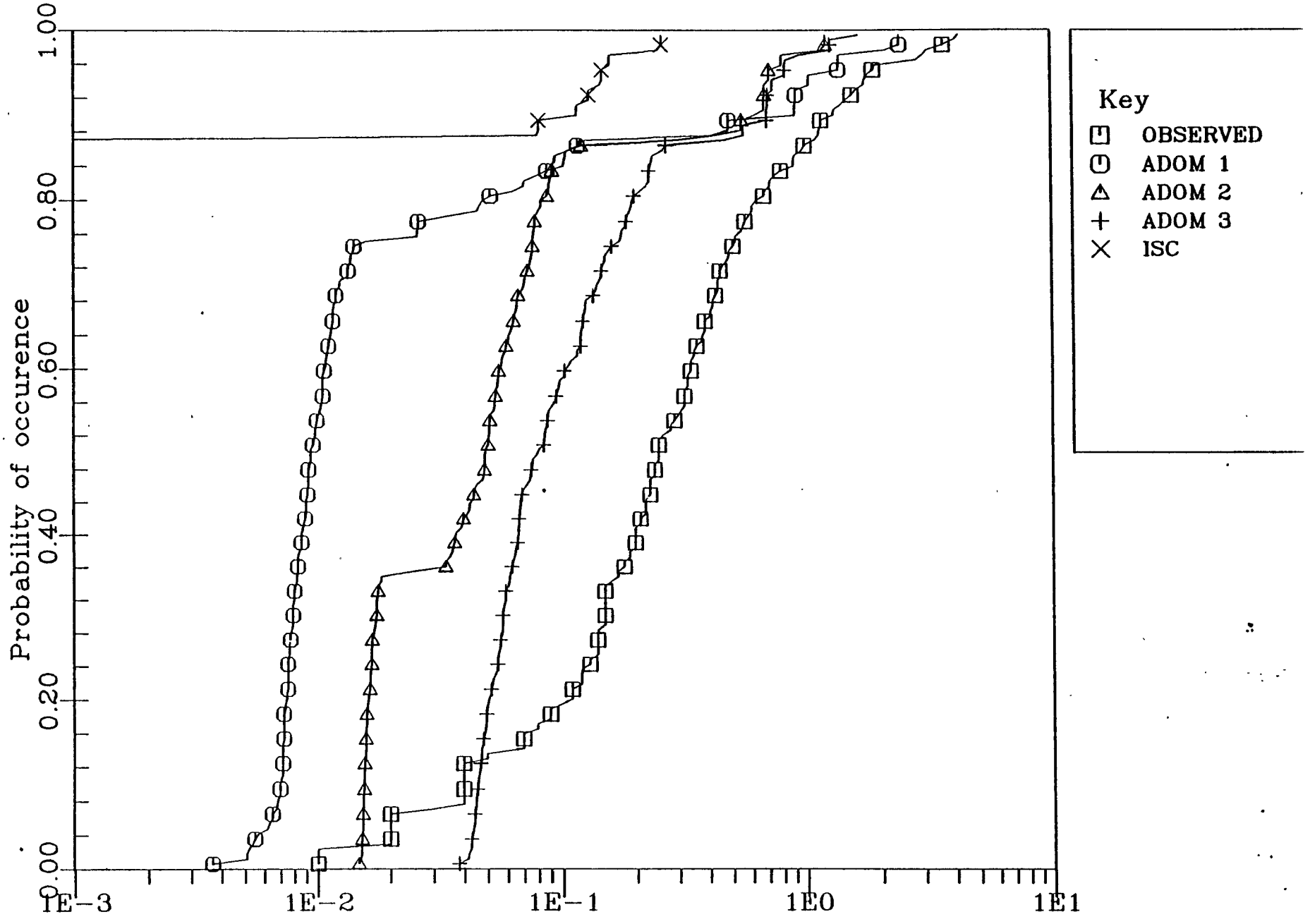

Figure B-2c. Cumulative probability plot of deposition velocity (cm/s) using the complete small particle data set.

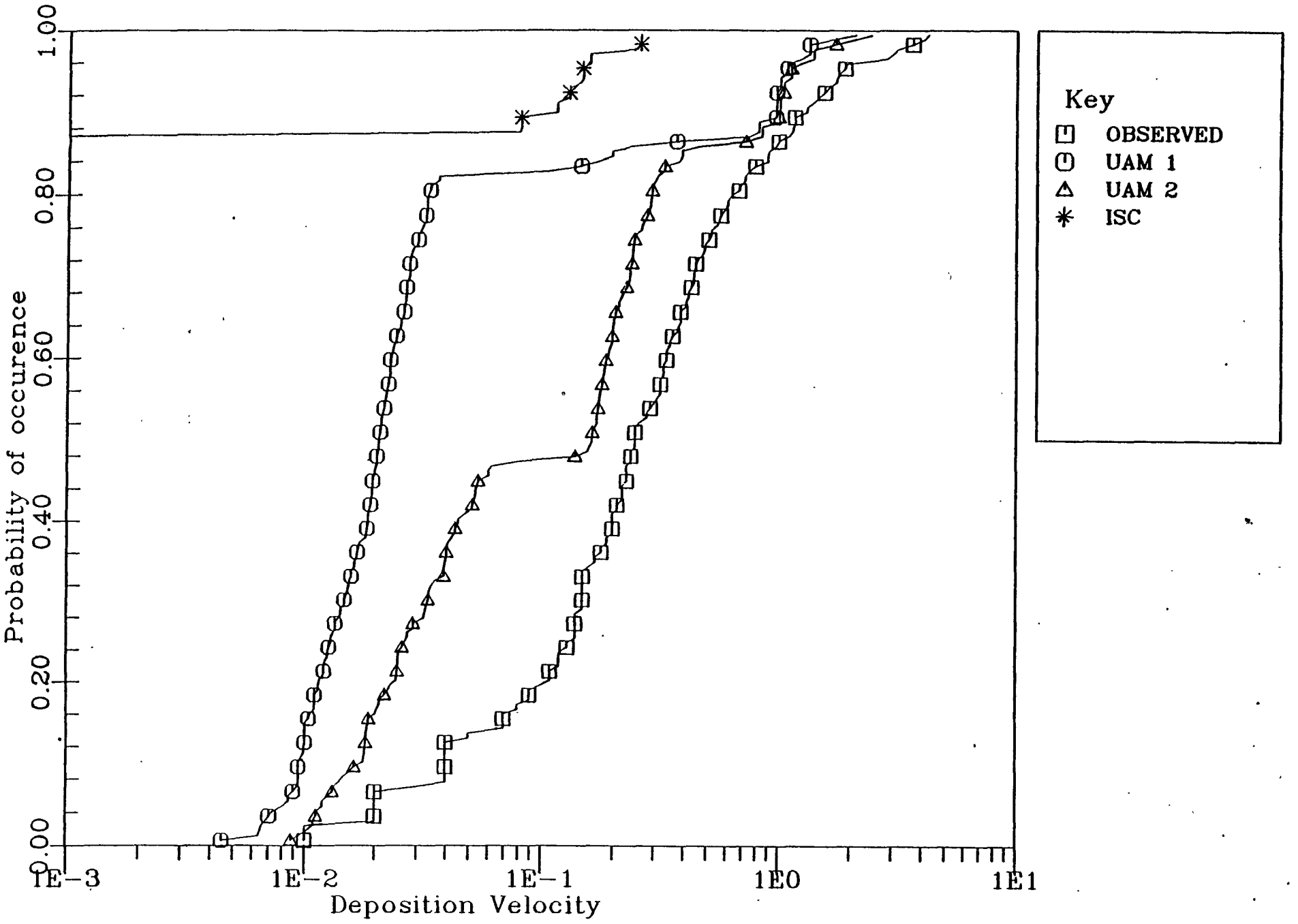

Figure B-2d. Cumulative probability plot of deposition velocity (cm/s) using the complete small particle data set.

Appendix C

Observational Particle Deposition Velocity Data Sets

Technical Note

Description of Particle Deposition Velocity Data Sets

There are 24 original data sets altogether which are used in the data analysis. These data sets are read into the fortran program PARTVD and are analyzed and processed in the manner shown schematically in Figure C-1. The PARTVD software reads in each observed deposition velocity case in one of two formats. If the global roughness length z0 is present it is used for the entire data set and data on Richardson number (Ri) and nondimensional fluxes of heat and momentum are assumed to NOT be present. If the global roughness length is set to -999.7 then this data is assumed to be present for each observed deposition velocity present in the sample. One can note this difference when comparing sample sets numbers 1 and 2. If the reference height for wind speed is missing a default value of 10 m is used which is typical of the assumptions made in applications of the deposition models. If the leaf area index is missing a value is assigned based on the the land use type (vegetation state), or whether is is a special wind tunnel study. The effects of nonuniform particle size distributions is input as a fractional mass weight for each size range. Presently this is done for only the sulfate particle samples. In cases where case specific Ri, phim, and phih are assigned -999.9 there is NOT sufficient information to generate deposition velocity estimates for all models and these cases are dropped. For example the fifth case in sample set number 3 would be dropped. Only samples with positive deposition velocities are kept.

The PARTVD program produces a set of 173 predictions for 9 models. In addition to the 9 model predictions, a number of additional meteorological variables are also output so as to provide a means of stratifying the deposition velocity data. This data set is read in and used to produce estimates of deposition velocity for ISC which becomes the 10th model prediction set and is added to the input data set and written out. These data sets are displayed in Table C-1 for the uniform particle size distribution and Table C-2 for the sulfate peaked particle distribution. Footnotes provide definitions for each column in the tables.

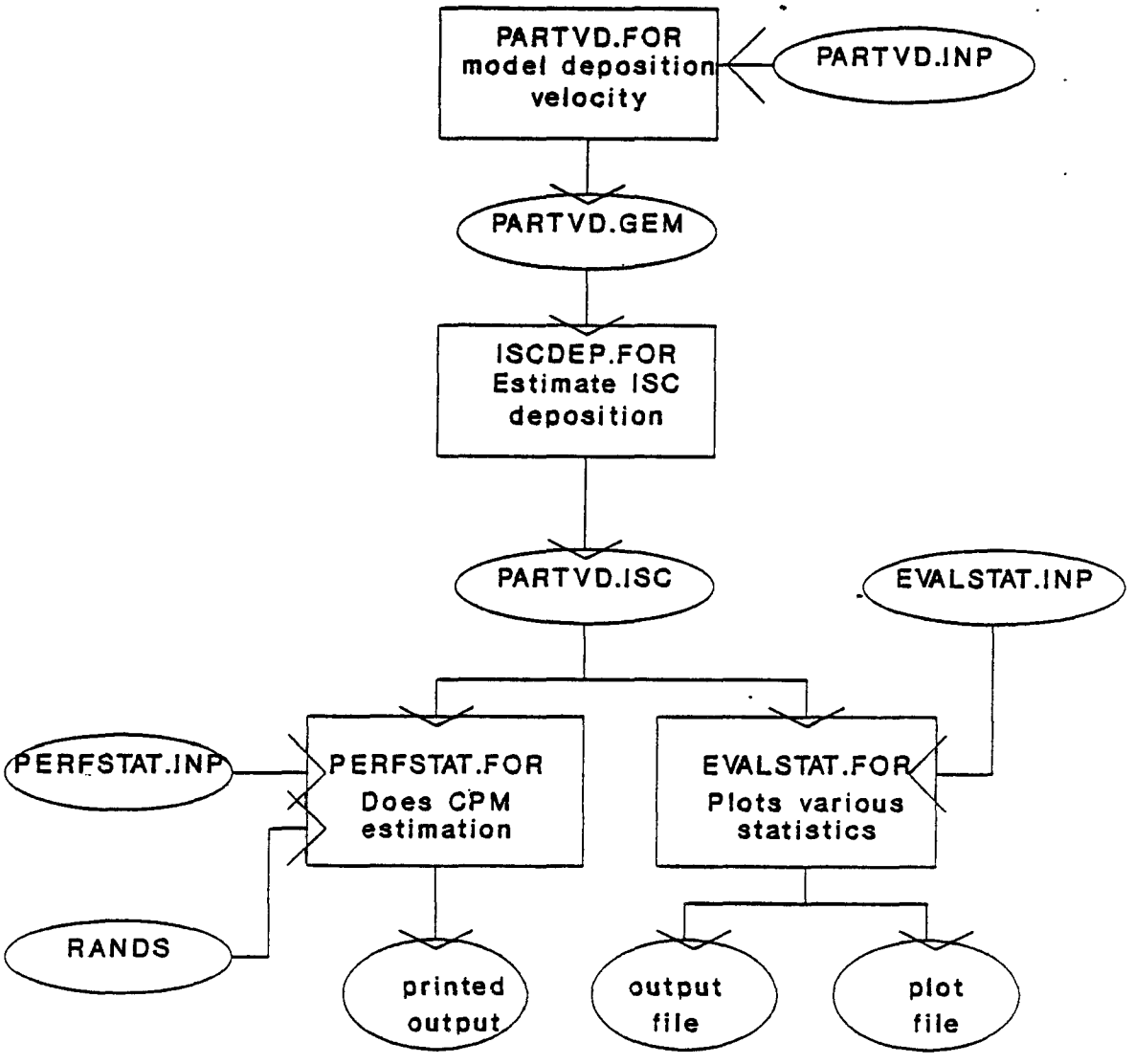

Figure C-1.

Schematic diagram of
data processing

Table C-1. The data making up the overall dataset for a uniform particle distribution. The data set contains 173 data points including observed zero deposition velocities which have been set to a lower limit of 0.005 cm/s. The footnotes define the variable A thru X.

Deposition Model

OBS	CARB 1	CARB 2	CARB 3	CARB 0	ADOM 1	ADOM 2	ADOM 3	UAM 1	UAM 2	ISC	A	B	C	D
4.2100	0.9370	1.1215	0.8954	0.9370	2.4305	1.2241	1.2772	1.3454	1.4027	0.2612	5	18	83	ZnS
4.0500	0.9370	1.1215	0.8954	0.9370	2.4305	1.2241	1.2772	1.3454	1.4027	0.2612	5	18	83	ZnS
3.6500	0.9370	1.1215	0.8954	0.9370	2.4305	1.2241	1.2772	1.3454	1.4027	0.2612	5	18	83	ZnS
1.9300	0.8016	0.8596	0.7043	0.8016	0.9154	0 6852	0 7050	0.9724	1.0057	0.1169	5	26	83	ZnS
1.8000	0.8016	0.8596	0.7043	0.8016	0.9154	0.6852	0.7050	0.9724	1.0057	0.1169	5	26	83	ZnS
1.7400	0.8016	0.8596	0.7043	0.8016	0.9154	0.6852	0.7050	0.9724	1.0057	0.1169	5	26	83	ZnS
3.1400	0.7904	0.8774	0.7165	0.7904	1.0436	0.7185	0.7409	1.0131	1.0496	0.1490	6	5	83	ZnS
3.0200	0.7904	0.8774	0.7165	0.7904	1.0436	0.7185	0.7409	1.0131	1.0496	0.1490	6	5	83	ZnS
2.8400	0.7904	0.8774	0.7165	0.7904	1.0436	0.7185	0.7409	1.0131	1.0496	0.1490	6	5	83	ZnS
1.7500	0.6808	0.7706	0.6434	0.6808	0.4911	0.5564	0.5663	0.8207	0.8449	0.0822	6	12	83	ZnS
1.6200	0.6808	0.7706	0.6434	0.6808	0.4911	0.5564	0.5663	0.8207	0.8449	0.0822	6	12	83	ZnS
1.3100	0.6808	0.7706	0.6434	0.6808	0.4911	0.5564	0.5663	0.8207	0.8449	0.0822	6	12	83	ZnS
1.5600	0.7357	0.8606	0.7048	0.7357	0.9248	0.6887	0.7089	0.9787	1.0129	0.1314	6	24	83	ZnS
1.4700	0.7357	0.8606	0.7048	0.7357	0.9248	0.6887	0.7089	0.9787	1.0129	0.1314	6	24	83	ZnS
1.1400	0.7357	0.8606	0.7048	0.7357	0.9248	0.6887	0.7089	0.9787	1.0129	0.1314	6	24	83	ZnS
1.1700	0.8752	0.9275	0.7524	0.8752	1.3838	0.8085	0.8371	1.0860	1.1266	0.1601	6	27	83	ZnS
1.1500	0.8752	0.9275	0.7524	0.8752	1.3838	0 8085	0.8371	1.0860	1.1266	0.1601	6	27	83	ZnS
1.1000	0.8752	0.9275	0.7524	0.8752	1.3838	0.8085	0.8371	1.0860	1.1266	0.1601	6	27	83	ZnS
0.0400	0.0190	0.0243	0.0732	0.0190	0.0054	0.0370	0.0948	0.0070	0.0228	0.0001	6	4	79	SO4
0.3300	0.0136	0 0199	0.0691	0.0136	0.0051	0.0353	0.0858	0.0065	0.0183	0.0001	6	21	79	SO4
0.5700	0.0197	0.0213	0.0550	0.0197	0.0112	0.0752	0.2120	0.0151	0.0481	0.0001	6	21	79	SO4
0.0300	0.0191	0 0276	0.0943	0.0191	0.0036	0 0246	0.0473	0.0044	0.0109	0.0001	6	21	79	SO4
0.3300	0.0220	0.0287	0.0563	0.0220	0.0121	0.0815	0.2306	0.0164	0 0526	0.0001	7	18	79	SO4
0.0200	0.0125	0.0210	0.0327	0.0125	0.0075	0.0512	0.0865	0.0100	0.0183	0.0001	2	19	80	SO4
0.2000	0.0086	0.0140	0.0326	0.0086	0.0115	0.0773	0 1359	0.0155	0.0291	0.0001	2	20	80	SO4
0.0900	0.0083	0.0137	0.0319	0.0083	0.0086	0.0578	0.0980	0.0114	0.0210	0.0001	2	21	80	SO4
0.0400	0.0074	0.0120	0.0320	0.0074	0.0104	0.0699	0.1212	0.0140	0.0261	0.0001	2	22	80	SO4
0.0400	0.0165	0.0261	0.0592	0.0165	0.0137	0.0923	0.2625	0.0187	0.0603	0.0001	10	17	79	SO4
0.2100	0.0194	0.0319	0.0585	0.0194	0.0064	0.0441	0.1102	0.0085	0.0252	0.0001	10	18	79	SO4
0.3400	0.0174	0.0237	0.0600	0.0174	0 0143	0.0954	0.2722	0.0195	0.0628	0.0001	10	19	79	SO4
0.0800	0.0246	0.0370	0.0550	0.0246	0.0080	0.0545	0.1467	0.0106	0 0328	0 0001	10	19	79	SO4
0.1000	0.0173	0.0303	0.0264	0.0173	0.0064	0.0444	0.0596	0.0085	0.0119	0.0001	11	21	79	SO4
0.0700	0.0105	0.0177	0.0244	0.0105	0.0082	0.0562	0.0768	0.0110	0.0157	0.0001	11	22	79	SO4
0.1500	0.0108	0.0181	0.0249	0.0108	0.0075	0.0508	0.0684	0.0100	0.0141	0.0001	11	27	79	SO4
0.0500	0.0091	0.0152	0.0241	0.0091	0.0097	0.0651	0.0894	0.0129	0.0185	0.0001	11	29	79	SO4
0.0200	0 0108	0.0188	0.0258	0.0108	0.0068	0.0458	0.0611	0.0089	0 0126	0.0001	11	29	79	SO4
0.3200	0.0086	0.0152	0.0241	0.0086	0.0096	0.0647	0.0888	0.0129	0 0184	0.0001	12	3	79	SO4
0.0700	0.0163	0.0250	0.0273	0.0163	0.0061	0.0418	0.0555	0.0080	0.0112	0.0001	12	6	79	SO4
0.2300	0.0099	0.0152	0.0242	0.0099	0.0087	0.0584	0.0798	0.0115	0.0164	0.0001	12	7	79	SO4
0.1800	0.0078	0.0125	0.0254	0.0078	0.0126	0.0837	0.1164	0.0170	0.0246	0.0001	12	12	79	SO4
0.4100	0.0102	0.0163	0.0286	0.0102	0.0162	0.1077	0 1514	0.0221	0.0322	0.0001	1	22	80	SO4
0.0400	0 0095	0.0168	0.0297	0.0095	0.0053	0.0364	0 0473	0.0068	0.0094	0.0001	1	23	80	SO4
0.0100	0.0068	0.0118	0.0316	0.0068	0.0050	0.0340	0.0438	0.0063	0 0087	0.0001	1	24	80	SO4
0 2100	0 0054	0.0096	0.0253	0.0054	0.0071	0.0481	0.0646	0.0093	0.0132	0.0001	1	28	80	SO4
0.2200	0.0076	0.0118	0.0241	0.0076	0.0094	0.0629	0 0861	0.0125	0.0179	0.0001	1	29	80	SO4
0.2200	0.0065	0.0099	0.0254	0.0065	0.0126	0.0838	0.1163	0.0171	0.0247	0.0001	1	30	80	SO4
0.0400	0 0101	0.0159	0.0253	0.0101	0.0072	0.0488	0.0656	0.0094	0 0133	0 0001	1	30	80	SO4
0.0050	0.0073	0.0118	0.0241	0.0073	0.0093	0.0627	0.0859	0.0124	0 0178	0.0001	2	14	80	SO4
0.2800	0.0069	0.0119	0.0319	0.0069	0.0086	0.0578	0 0986	0 0114	0 0209	0 0001	3	5	80	SO4
0.5100	0.0072	0.0118	0.0318	0.0072	0.0090	0 0604	0.1036	0.0119	0 0220	0.0001	3	6	80	SO4
0.0400	0.0074	0.0121	0.0327	0.0074	0.0075	0.0509	0.0853	0.0099	0.0180	0.0001	3	6	80	SO4
0.0200	0.0113	0.0188	0.0321	0.0113	0.0083	0.0560	0.0956	0.0110	0.0203	0 0001	3	11	80	SO4
0.0800	0.0069	0.0120	0.0183	0.0069	0.0079	0.0535	0.0574	0.0104	0.0113	0.0001	1	25	80	SO4
0.2500	0.0061	0.0093	0.0182	0.0061	0.0083	0.0555	0 0596	0.0110	0 0119	0.0001	2	15	80	SO4
0.0100	0.0087	0.0143	0.0188	0.0087	0.0072	0.0491	0 0527	0.0094	0 0102	0 0001	2	27	80	SO4
0 3800	0.0076	0.0121	0.0186	0.0076	0.0075	0.0515	0.0552	0.0100	0.0108	0.0001	2	29	80	SO4
0 2500	0.0094	0.0165	0.0180	0.0094	0.0100	0 0676	0.0728	0 0135	0 0147	0.0001	3	10	80	SO4
0.3500	0.0200	0.0310	0.0682	0.0200	0.0050	0.0341	0 0768	0.0064	0.0181	0.0001	10	21	79	SO4
0.0100	0.0101	0.0141	0.0630	0.0101	0.0076	0.0515	0.1466	0.0100	0.0338	0 0001	6	9	80	SO4
0 0400	0 0109	0.0139	0.0629	0.0109	0.0113	0.0759	0.2313	0.0153	0 0539	0.0001	6	10	80	SO4
0 2100	0.0108	0.0156	0.0630	0.0108	0.0076	0 0516	0.1483	0 0100	0 0338	0.0001	6	12	80	SO4
0.6100	0.0617	0 0622	0.0574	0.0617	0.0056	0 0393	0.0923	0 0073	0 0189	0.0001	9	17	79	S
0.7200	0.0495	0.0527	0.0499	0.0495	0 0071	0.0493	0.1209	0.0094	0 0251	0.0001	9	25	79	S
0.4400	0 0501	0.0526	0.0499	0.0501	0 0071	0 0493	0 1207	0 0094	0.0251	0 0001	9	25	79	S
0.3300	0.0508	0.0526	0.0499	0.0508	0.0071	0 0493	0 1208	0 0094	0 0251	0.0001	9	25	79	S
0.1200	0 0500	0 0513	0.0489	0 0500	0.0075	0 0517	0 1268	0 0099	0 0266	0 0001	9	25	79	S
0.0050	0.0513	0.0526	0.0498	0.0513	0.0071	0.0493	0.1204	0.0094	0.0251	0.0001	9	25	79	S
0.0050	0.0512	0.0525	0.0498	0 0512	0.0071	0 0491	0 1188	0 0094	0.0250	0 0001	9	25	79	S
1.9000	1 6989	1.7923	2.1277	1.6989	2.1279	1.1775	1 6644	2 1045	2 4431	0 2520	0	0	0	Pb
1.4000	1.3043	1.3966	1.7508	1 3043	1 3767	0.6268	0 9671	1.6724	2 0935	0.1458	0	0	0	Pb
1.0000	0 9363	1.0180	1.3551	0.9363	0.4128	0 3031	0 4725	1 2507	1 7413	0 0809	0	0	0	Pb
0.4500	0 5418	0 5990	0.8560	0.5418	0.0800	0 1220	0 1854	0 7495	1 2383	0 0001	0	0	0	Pb
0.1500	0 2726	0 3046	0.4563	0.2726	0 0346	0 0615	0 1037	0 3724	0 7257	0 0001	0	0	0	Pb
0.0400	0 0886	0.0994	0 1517	0 0886	0 0122	0 0446	0 0967	0 1060	0 2376	0 0001	0	0	0	Pb

OBS	E	F	G	H	I	J	K	L	M	N	O	P	Q	R	S	T	U	V
4.2100	22 48	23 18	7.61	14.70	-999.90	0.40	0.166E+03	-999.900	3.00	1	6.00	6.00	4.00	-999.90	0.1	1.0	11	1
4.0500	22 48	23 18	8.53	14.70	-999.90	0.40	0.166E+03	-999.900	3.00	1	6.00	6.00	4.00	-999.90	0.1	1.0	11	1
3.6500	22 48	23 18	9.43	14.70	-999.90	0.40	0.166E+03	-999.900	3.00	1	6.00	6.00	4.00	-999.90	0.1	1.0	11	1
1.9300	23 24	23 54	3.23	19.50	-999.90	0.26	0.440E+02	-999.900	3.00	1	6.00	6.00	4.00	-999.90	0.1	1.0	11	1
1.8000	23 24	23 54	3.59	19.50	-999.90	0.26	0.440E+02	-999.900	3.00	1	6.00	6.00	4.00	-999.90	0.1	1.0	11	1
1.7400	23 24	23 54	3.83	19.50	-999.90	0.26	0.440E+02	-999.900	3.00	1	6.00	6.00	4.00	-999.90	0.1	1.0	11	1
3.1400	22 10	22 40	4.74	17.50	-999.90	0.27	0.770E+02	-999.900	3.00	1	6.00	6.00	4.00	-999.90	0.1	1.0	11	1
3.0200	22 10	22 40	5.40	17.50	-999.90	0.27	0.770E+02	-999.900	3.00	1	6.00	6.00	4.00	-999.90	0.1	1.0	11	1
2.8400	22 10	22 40	6.32	17.50	-999.90	0.27	0.770E+02	-999.900	3.00	1	6.00	6.00	4.00	-999.90	0.1	1.0	11	1
1.7500	22 43	23 13	3.00	14.90	-999.90	0.20	0.340E+02	-999.900	3.00	1	6.00	6.00	4.00	-999.90	0.1	1.0	11	1
1.6200	22 43	23 13	3.39	14.90	-999.90	0.20	0.340E+02	-999.900	3.00	1	6.00	6.00	4.00	-999.90	0.1	1.0	11	1
1.3100	22 43	23 13	3.75	14.90	-999.90	0.20	0.340E+02	-999.900	3.00	1	6.00	6.00	4.00	-999.90	0.1	1.0	11	1
1.5600	23 6	23 28	3.07	14.10	-999.90	0.26	0.590E+02	-999.900	3.00	1	6.00	6.00	4.00	-999.90	0.1	1.0	11	1
1.4700	23 6	23 28	3.24	14 10	-999.90	0.26	0.590E+02	-999.900	3.00	1	6.00	6.00	4.00	-999.90	0.1	1.0	11	1
1.1400	23 6	23 28	3.46	14.10	-999.90	0.26	0.590E+02	-999 900	3.00	1	6.00	6.00	4.00	-999.90	0.1	1.0	11	1
1.1700	21 31	22 1	3.17	20.50	-999.90	0.30	0.710E+02	-999 900	3.00	1	6.00	6.00	4.00	-999.90	0.1	1.0	11	1
1.1500	21 31	22 1	3.80	20.50	-999.90	0.30	0.710E+02	-999.900	3.00	1	6.00	6.00	4.00	-999.90	0.1	1.0	11	1
1.1000	21 31	22 1	4.37	20.50	-999.90	0.30	0.710E+02	-999.900	3.00	1	6.00	6.00	4.00	-999.90	0.1	1.0	11	1
0.0400	6 0	0 0	1.71	14.20	-999.90	0.11	0.144E+02	-999.900	0.80	10	0.10	1.00	1.00	1.00	3.0	1.0	2	2
0.3300	2 36	0 0	1.23	8.80	-999.90	0.10	-0.183E+02	-999.900	0.40	10	0.10	1.00	1.00	1.00	2.5	1.0	10	3
0.5700	0 0	4 0	2.53	21.20	-999.90	0.26	-0.237E+02	-999.900	1.00	10	0.10	1.00	1.00	1.00	2.5	1.0	10	3
0.0300	3 55	0 0	1.64	8.30	-999.90	0.06	0.557E+01	-999.900	0.30	10	0.10	1.00	1.00	1.00	2.5	1.0	10	3
0.3300	0 0	3 43	2.69	14.40	-999.90	0.29	0.900E+10	-999.900	2.20	10	0.10	1.00	1.00	1.00	2.5	1.0	10	3
0.0200	11 23	0 0	2.15	4.40	-999.90	0.17	0.573E+02	-999.900	0.90	10	0.10	1.00	1.00	1.00	1.0	1.0	3	4
0.2000	0 0	4 40	3.73	5.90	-999.90	0.28	-0.101E+03	-999.900	0.30	10	0.10	1.00	1.00	1.00	1.0	1.0	3	4
0.0900	9 55	0 0	3.13	5.00	-999.90	0.20	0.385E+02	-999.900	0.30	10	0.10	1.00	1.00	1.00	1.0	1.0	3	4
0.0400	0 0	4 20	3.81	6.00	-999.90	0.25	0.900E+10	-999.900	0.20	10	0.10	1.00	1.00	1.00	1.0	1.0	3	4
0.0400	6 54	0 0	3.53	7.80	-999 90	0.34	0.245E+03	-999.900	1.50	10	0.10	1.00	1.00	1.00	2.5	1.0	10	5
0.2100	7 0	0 0	1.53	5.10	-999.90	0.14	0.204E+02	-999.900	2.30	10	0.10	1.00	1.00	1.00	2.5	1.0	10	5
0.3400	0 0	4 38	3.84	13.00	-999.90	0.35	-0.333E+03	-999.900	1.10	10	0.10	1.00	1.00	1.00	2.5	1.0	10	5
0.0800	6 58	0 0	1.50	8.80	-999.90	0.18	0.943E+02	-999.900	4.30	10	0.10	1.00	1.00	1.00	2.5	1.0	10	5
0.1000	10 50	0 0	1.48	2.90	-999.90	0.14	0.858E+02	-999.900	2.00	10	0.10	1.00	1.00	1.00	0.5	1.0	10	5
0.0700	0 0	2 55	2.30	4.50	-999.90	0.19	-0.167E+03	-999.900	0.60	10	0.10	1.00	1.00	1.00	0.5	1.0	10	5
0.1500	10 53	0 0	2.52	4.50	-999.90	0.17	0.243E+02	-999.900	0.60	10	0.10	1.00	1.00	1.00	0.5	1.0	10	5
0.0500	0 0	4 7	2.31	5.20	-999.90	0.23	0.661E+02	-999.900	0.40	10	0.10	1.00	1.00	1.00	0.5	1.0	10	5
0.0200	11 1	0 0	2.41	3.10	-999.90	0.15	0.175E+02	-999.900	0.60	10	0.10	1.00	1.00	1.00	0.5	1.0	10	5
0.3200	11 9	0 0	3.45	2.90	-999.90	0.23	0.446E+02	-999.900	0.40	10	0.10	1.00	1.00	1.00	0.5	1.0	10	5
0.0700	11 12	0 0	1.78	7 60	-999.90	0.13	0.241E+02	-999.900	1.10	10	0.10	1.00	1.00	1.00	0.5	1.0	10	5
0.2300	0 0	2 35	2 81	8.00	-999.90	0.20	0.120E+03	-999.900	0.40	10	0.10	1.00	1.00	1.00	0.5	1.0	10	5
0.1800	11 20	0 0	4.72	6.70	-999.90	0.31	0.120E+03	-999.900	0.20	10	0.10	1.00	1.00	1.00	0.5	1.0	10	5
0.4100	0 0	3 18	6.03	7.70	-999.90	0.41	0.245E+03	-999.900	0.30	10	0.10	1.00	1.00	1.00	0.5	1.0	10	5
0.0400	10 59	0 0	2.07	1.70	-999 90	0 11	0.152E+02	-999.900	0.30	10	0.10	1.00	1.00	1.00	0.5	1.0	10	5
0.0100	11 3	0 0	2.19	1.40	-999.90	0.10	0.176E+02	-999.900	0.10	10	0.10	1.00	1.00	1.00	0.5	1.0	10	5
0 2100	0 0	5 4	2.75	1.20	-999.90	0.16	0.858E+02	-999.900	0.10	10	0.10	1.00	1.00	1.00	0.5	1.0	10	5
0.2200	10 42	0 0	3.47	7.30	-999.90	0.22	0.245E+03	-999.900	0.20	10	0.10	1.00	1.00	1.00	0.5	1.0	10	5
0.2200	0 0	4 7	5.02	8.20	-999.90	0.31	0.900E+10	-999.900	0.10	10	0.10	1.00	1.00	1.00	0.5	1.0	10	5
0.0400	10 49	0 0	2.40	6.70	-999.90	0.16	0.505E+02	-999.900	0.40	10	0.10	1.00	1.00	1.00	0.5	1.0	10	5
0.0050	11 22	0 0	3 46	5.90	-999.90	0.22	0.162E+03	-999.900	0.20	10	0.10	1.00	1.00	1.00	0.5	1.0	10	5
0.2800	9 59	0 0	3.12	3.20	-999.90	0.20	0.194E+03	-999.900	0.20	10	0.10	1.00	1.00	1.00	0.5	1.0	10	5
0.5100	0 0	4 36	3.23	5.30	-999.90	0.21	0.900E+10	-999 900	0.20	10	0.10	1.00	1.00	1.00	1.0	1.0	10	5
0.0400	9 56	0 0	2 70	4.70	-999.90	0.17	0.779E+02	-999.900	0.20	10	0.10	1.00	1.00	1.00	1.0	1.0	10	5
0.0200	10 3	0 0	2.52	5.20	-999.90	0.19	0.952E+02	-999.900	0.70	10	0.10	1.00	1.00	1.00	1.0	1.0	10	5
0.0800	0 0	4 56	2.53	2.90	-999.90	0.18	-0.630E+02	-999.900	0 20	10	0.10	1.00	1.00	1.00	0.1	1.0	8	6
0.2500	0 0	5 39	3.10	7 40	-999.90	0.19	0.120E+03	-999.900	0.10	10	0.10	1.00	1.00	1.00	0.1	1.0	8	6
0.0100	0 0	4 52	2.06	5.10	-999.90	0.16	-0.418E+02	-999.900	0.30	10	0.10	1.00	1.00	1.00	0.1	1.0	8	6
0 3800	0 0	4 4	2.30	5.90	-999.90	0.17	-0.289E+02	-999.900	0.20	10	0.10	1.00	1.00	1.00	0.1	1.0	8	6
0 2500	9 59	0 0	3.04	3.60	-999.90	0.24	0.245E+03	-999.900	0.50	10	0.10	1.00	1.00	1.00	0.1	1.0	8	6
0.3500	6 52	0 0	1.77	6.60	-999 90	0.10	0.886E+01	-999.900	1.30	10	0.10	1.00	1.00	1.00	2.5	1.0	10	7
0.0100	5 11	0 0	2 45	11 20	-999.90	0.17	0.162E+03	-999.900	0.30	10	0.10	1.00	1.00	1.00	3.0	1.0	2	8
0 0400	0 0	5 5	3 58	14.70	-999.90	0.27	-0 988E+02	-999.900	0.30	10	0.10	1.00	1.00	1.00	3.0	1.0	2	8
0 2100	5 12	0 0	2 28	10.00	-999.90	0.17	0 900E+10	-999.900	0.40	10	0.10	1.00	1.00	1.00	3.0	1.0	2	8
0.6100	15 5	15 30	1.83	23.60	-999.90	0 11	-0.256E+01	51.000	9.40	10	0.10	1.00	1.00	7.00	2.0	1.0	3	9
0.7200	11 35	12 0	1.28	21.50	-999.90	0 15	-0.373E+01	88 000	9.40	10	0.10	1.00	1 00	7.00	2.0	1.0	3	9
0.4400	12 5	12 30	1 44	22.00	-999.90	0.15	-0.470E+01	70.000	9.40	10	0.10	1.00	1.00	7.00	2.0	1.0	3	9
0.3300	12 35	13 0	1.34	22 50	-999 90	0 15	-0.471E+01	70.000	9.40	10	0.10	1.00	1.00	7.00	2.0	1.0	3	9
0.1200	13 5	13 30	1.29	22 90	-999.90	0.16	-0 977E+01	41 000	9.40	10	0.10	1.00	1.00	7.00	2.0	1.0	3	9
0.0050	14 35	15 0	1 57	22 90	-999.90	0.15	-0 622E+01	53 000	9.40	10	0.10	1.00	1.00	7.00	2.0	1.0	3	9
0.0050	15 35	16 0	1.53	22 90	-999.90	0.15	-0.150E+02	22.000	9.40	10	0.10	1.00	1.00	7.00	2.0	1.0	3	9
1.9000	0 0	0 0	-999.90	20.00	-999.90	0.35	0.900E+10	-999 900	2 00	1	13.00	13.00	1.00	-999.90	1.5	1.0	3	10
1.4000	0 0	0 0	-999 90	20.00	-999.90	0.35	0.900E+10	-999 900	2.00	1	10.00	10.00	1.00	-999.90	1 5	1.0	3	11
1.0000	0 0	0 0	-999.90	20.00	-999.90	0.35	0.900E+10	-999 900	2.00	1	7.50	7.50	1.00	-999.90	1.5	1.0	3	12
0.4500	0 0	0 0	-999 90	20.00	-999 90	0 35	0.900E+10	-999 900	2 00	1	5 00	5.00	1.00	-999.90	1.5	1.0	3	13
0.1500	0 0	0 0	-999 90	20 00	-999.90	0 35	0 900E+10	-999 900	2.00	1	3.20	3 20	1 00	-999.90	1.5	1.0	3	14
0.0400	0 0	0 0	-999 90	20 00	-999 90	0 35	0 900E+10	-999 900	2.00	1	1 60	1.60	1.00	-999.90	1.5	1.0	3	15

0.0200	0.0297	0.0333	0.0501	0.0297	0.0086	0.0667	0.1440	0.0257	0.0603	0.0001	0	0	0	Pb	0	0	0	0	-999.90	20.00	-999.90	0.35	0.900E+10	-999.900	2.00	1	0.75	0.75	1.00	-999.90	1.5	1.0	3	16
0.0200	0.0165	0.0184	0.0272	0.0165	0.0116	0.0904	0.2000	0.0097	0.0232	0.0001	0	0	0	Pb	0	0	0	0	-999.90	20.00	-999.90	0.35	0.900E+10	-999.900	2.00	1	0.40	0.40	1.00	-999.90	1.5	1.0	3	17
0.0900	0.1068	0.1167	0.1546	0.1068	0.1267	0.4353	0.8437	0.0332	0.0812	0.0001	0	0	0	Pb	0	0	0	0	-999.90	20.00	-999.90	0.35	0.900E+10	-999.900	2.00	1	0.04	0.04	1.00	-999.90	1.5	1.0	3	18
0.0500	0.1687	0.1862	0.2642	0.1687	0.0261	0.0372	0.0551	0.1479	0.2861	0.0001	5	21	81	FECOH	0	0	0	0	2.50	20.00	-999.90	0.16	0.900E+10	0.000	2.00	1	2.80	2.80	1.00	10.00	1.5	1.0	3	19
0.1200	0.1725	0.1911	0.3175	0.1725	0.0263	0.0399	0.0686	0.1731	0.3841	0.0001	9	23	81	FECOH	0	0	0	0	3.00	20.00	-999.90	0.19	0.900E+10	0.000	2.00	1	2.80	2.80	1.00	10.00	2.0	1.0	3	19
0.1800	0.1790	0.1988	0.2907	0.1790	0.0265	0.0426	0.0682	0.1982	0.3925	0.0001	6	1	81	FECOH	0	0	0	0	3.50	20.00	-999.90	0.23	0.900E+10	0.000	2.00	1	2.80	2.80	1.00	10.00	1.5	1.0	3	20
0.1200	0.1790	0.1988	0.2907	0.1790	0.0265	0.0426	0.0682	0.1982	0.3925	0.0001	8	17	81	FECOH	0	0	0	0	3.50	20.00	-999.90	0.23	0.900E+10	0.000	2.00	1	2.80	2.80	1.00	10.00	1.5	1.0	3	20
0.4200	0.2539	0.2779	0.4282	0.2539	0.0461	0.0557	0.0758	0.2395	0.4645	0.0001	9	30	82	FECOH	0	0	0	0	2.40	20.00	-999.90	0.15	0.900E+10	0.000	2.00	1	3.80	3.80	1.00	10.00	2.0	1.0	3	21
0.0100	0.1147	0.1676	0.0750	0.2835	0.1183	0.0886	0.1398	0.0303	0.0454	0.0001	1	26	81	Fine Prt	10	0	10	30	4.00	9.20	-999.90	0.64	-0.499E+03	49.000	100.00	6	0.05	0.10	1.00	39.00	0.5	1.0	4	22
0.0200	0.0814	0.0991	0.0412	0.2073	0.0487	0.0375	0.0634	0.0125	0.0187	0.0001	1	26	81	Fine Prt	17	30	18	0	2.10	15.40	-999.90	0.26	0.105E+03	-16.000	100.00	6	0.05	0.10	1.00	39.00	0.5	1.0	4	22
0.1200	0.0814	0.1007	0.0421	0.2073	0.0523	0.0402	0.0674	0.0135	0.0201	0.0001	1	26	81	Fine Prt	18	0	18	30	2.50	14.80	-999.90	0.28	0.104E+03	-20.000	100.00	6	0.05	0.10	1.00	39.00	0.5	1.0	4	22
0.1100	0.0873	0.1133	0.0484	0.2213	0.0712	0.0539	0.0881	0.0182	0.0273	0.0001	1	27	81	Fine Prt	10	30	11	0	2.50	13.20	-999.90	0.38	-0.610E+02	85.000	100.00	6	0.05	0.10	1.00	39.00	0.5	1.0	4	22
0.0700	0.0913	0.1133	0.0484	0.2308	0.0714	0.0541	0.0883	0.0183	0.0274	0.0001	1	27	81	Fine Prt	11	30	12	0	2.60	15.00	-999.90	0.38	-0.932E+02	56.000	100.00	6	0.05	0.10	1.00	39.00	0.5	1.0	4	22
0.1400	0.0807	0.0986	0.0409	0.2058	0.0471	0.0362	0.0617	0.0121	0.0181	0.0001	1	27	81	Fine Prt	12	30	13	0	1.80	15.20	-999.90	0.25	-0.572E+02	26.000	100.00	6	0.05	0.10	1.00	39.00	0.5	1.0	4	22
0.6800	0.0973	0.1481	0.0655	0.2431	0.1032	0.0774	0.1231	0.0265	0.0396	0.0001	1	28	81	Fine Prt	10	30	11	0	3.60	7.50	-999.90	0.56	-0.378E+03	43.000	100.00	6	0.05	0.10	1.00	39.00	0.5	1.0	4	22
0.3200	0.1012	0.1504	0.0666	0.2523	0.1054	0.0790	0.1256	0.0270	0.0404	0.0001	1	28	81	Fine Prt	11	30	12	0	2.70	8.40	-999.90	0.57	-0.824E+02	209.000	100.00	6	0.05	0.10	1.00	39.00	0.5	1.0	4	22
0.8000	0.0889	0.1310	0.0571	0.2239	0.0888	0.0668	0.1074	0.0227	0.0340	0.0001	1	28	81	Fine Prt	12	0	12	30	2.90	8.50	-999.90	0.48	-0.116E+03	89.000	100.00	6	0.05	0.10	1.00	39.00	0.5	1.0	4	22
0.5500	0.1018	0.1481	0.0655	0.2540	0.1038	0.0779	0.1239	0.0266	0.0398	0.0001	1	28	81	Fine Prt	12	30	13	0	3.30	9.20	-999.90	0.56	-0.709E+02	231.000	100.00	6	0.05	0.10	1.00	39.00	0.5	1.0	4	22
0.2000	0.1047	0.1505	0.0666	0.2608	0.1058	0.0793	0.1261	0.0271	0.0405	0.0001	1	28	81	Fine Prt	13	0	13	30	2.80	9.70	-999.90	0.57	-0.730E+02	237.000	100.00	6	0.05	0.10	1.00	39.00	0.5	1.0	4	22
0.0900	0.0771	0.1089	0.0463	0.1969	0.0650	0.0494	0.0813	0.0167	0.0249	0.0001	1	28	81	Fine Prt	15	0	15	30	1.50	9.70	-999.90	0.35	-0.728E+02	55.000	100.00	6	0.05	0.10	1.00	39.00	0.5	1.0	4	22
0.2200	0.0249	0.0211	0.0471	0.0249	0.0106	0.0714	0.1777	0.0143	0.0394	0.0001	8	25	78	S	11	18	11	48	-999.90	30.00	-999.90	0.24	-0.961E+01	144.000	1.00	10	0.10	1.00	1.00	39.00	2.0	1.0	3	23
0.1400	0.0250	0.0212	0.0473	0.0250	0.0110	0.0738	0.1841	0.0148	0.0409	0.0001	8	25	78	S	11	48	12	18	-999.90	30.00	-999.90	0.25	-0.116E+02	135.000	1.00	10	0.10	1.00	1.00	39.00	2.0	1.0	3	23
0.1100	0.0251	0.0213	0.0475	0.0251	0.0114	0.0763	0.1911	0.0154	0.0425	0.0001	8	25	78	S	12	18	12	48	-999.90	30.00	-999.90	0.26	-0.113E+02	156.000	1.00	10	0.10	1.00	1.00	39.00	2.0	1.0	3	23
0.1500	0.0263	0.0222	0.0500	0.0263	0.0136	0.0911	0.2307	0.0186	0.0519	0.0001	8	25	78	S	12	48	13	18	-999.90	30.00	-999.90	0.32	-0.193E+02	170.000	1.00	10	0.10	1.00	1.00	39.00	2.0	1.0	3	23
0.2300	0.0250	0.0213	0.0471	0.0250	0.0091	0.0616	0.1514	0.0122	0.0331	0.0001	8	25	78	S	13	18	13	48	-999.90	30.00	-999.90	0.20	-0.463E+01	173.000	1.00	10	0.10	1.00	1.00	39.00	2.0	1.0	3	23
0.2400	0.0249	0.0212	0.0469	0.0249	0.0094	0.0639	0.1572	0.0127	0.0346	0.0001	8	25	78	S	13	48	14	18	-999.90	30.00	-999.90	0.21	-0.828E+01	112.000	1.00	10	0.10	1.00	1.00	39.00	2.0	1.0	3	23
0.1500	0.0248	0.0211	0.0469	0.0248	0.0098	0.0661	0.1617	0.0132	0.0361	0.0001	8	25	78	S	14	18	14	48	-999.90	30.00	-999.90	0.22	-0.237E+02	45.000	1.00	10	0.10	1.00	1.00	39.00	2.0	1.0	3	23
0.1500	0.0266	0.0224	0.0505	0.0266	0.0140	0.0933	0.2358	0.0191	0.0534	0.0001	8	25	78	S	14	48	15	18	-999.90	30.00	-999.90	0.33	-0.343E+02	105.000	1.00	10	0.10	1.00	1.00	39.00	2.0	1.0	3	23
0.1900	0.0249	0.0211	0.0471	0.0249	0.0106	0.0713	0.1768	0.0143	0.0393	0.0001	8	25	78	S	15	18	15	48	-999.90	30.00	-999.90	0.24	-0.136E+02	102.000	1.00	10	0.10	1.00	1.00	39.00	2.0	1.0	3	23
0.1500	0.0252	0.0214	0.0478	0.0252	0.0117	0.0785	0.1953	0.0159	0.0439	0.0001	8	25	78	S	15	48	16	18	-999.90	30.00	-999.90	0.27	-0.299E+02	66.000	1.00	10	0.10	1.00	1.00	39.00	2.0	1.0	3	23
0.1600	0.0266	0.0224	0.0505	0.0266	0.0140	0.0931	0.2340	0.0191	0.0533	0.0001	8	25	78	S	16	18	16	48	-999.90	30.00	-999.90	0.33	-0.692E+02	52.000	1.00	10	0.10	1.00	1.00	39.00	2.0	1.0	3	23
0.2900	0.0268	0.0227	0.0511	0.0268	0.0144	0.0952	0.2388	0.0196	0.0547	0.0001	8	25	78	S	16	48	17	18	-999.90	30.00	-999.90	0.34	-0.262E+03	15.000	1.00	10	0.10	1.00	1.00	39.00	2.0	1.0	3	23
0.2000	0.0263	0.0222	0.0500	0.0263	0.0136	0.0901	0.2236	0.0185	0.0515	0.0001	8	25	78	S	17	18	17	48	-999.90	30.00	-999.90	0.32	0.234E+03	-14.000	1.00	10	0.10	1.00	1.00	39.00	2.0	1.0	3	23
0.2000	0.0250	0.0212	0.0472	0.0250	0.0109	0.0725	0.1747	0.0148	0.0404	0.0001	8	25	78	S	17	48	18	18	-999.90	30.00	-999.90	0.25	0.539E+02	-29.000	1.00	10	0.10	1.00	1.00	39.00	2.0	1.0	3	23
0.2500	0.0252	0.0214	0.0477	0.0252	0.0117	0.0773	0.1874	0.0158	0.0435	0.0001	8	25	78	S	18	18	18	48	-999.90	30.00	-999.90	0.27	0.481E+02	-41.000	1.00	10	0.10	1.00	1.00	39.00	2.0	1.0	3	23
0.1500	0.0254	0.0215	0.0481	0.0254	0.0121	0.0799	0.1947	0.0164	0.0451	0.0001	8	25	78	S	18	48	19	18	-999.90	30.00	-999.90	0.28	0.610E+02	-36.000	1.00	10	0.10	1.00	1.00	39.00	2.0	1.0	3	23
0.0700	0.0249	0.0212	0.0469	0.0249	0.0090	0.0598	0.1388	0.0121	0.0324	0.0001	8	25	78	S	19	18	19	48	-999.90	30.00	-999.90	0.20	0.229E+02	-35.000	1.00	10	0.10	1.00	1.00	39.00	2.0	1.0	3	23
0.1400	0.0253	0.0216	0.0474	0.0253	0.0082	0.0544	0.1230	0.0110	0.0291	0.0001	8	25	78	S	19	48	20	18	-999.90	30.00	-999.90	0.18	0.139E+02	-42.000	1.00	10	0.10	1.00	1.00	39.00	2.0	1.0	3	23
0.1500	0.0468	0.0554	0.1666	0.0670	0.0062	0.0148	0.0382	0.0168	0.1400	0.0001	0	0	0	PART	0	0	0	0	1.84	17.80	-999.90	0.21	0.900E+10	0.000	28.00	6	0.50	1.00	1.00	9.80	9.0	1.0	5	24
0.0200	0.0464	0.0551	0.1706	0.0662	0.0070	0.0153	0.0436	0.0199	0.1686	0.0001	0	0	0	PART	0	0	0	0	2.22	17.80	-999.90	0.25	0.900E+10	0.000	28.00	6	0.50	1.00	1.00	9.80	9.0	1.0	5	24
0.0400	0.0498	0.0596	0.1942	0.0705	0.0092	0.0168	0.0579	0.0279	0.2436	0.0001	0	0	0	PART	0	0	0	0	3.22	17.80	-999.90	0.36	0.900E+10	0.000	28.00	6	0.50	1.00	1.00	9.80	9.0	1.0	5	24
0.1300	0.0464	0.0550	0.1686	0.0663	0.0067	0.0151	0.0414	0.0187	0.1573	0.0001	0	0	0	PART	0	0	0	0	2.07	17.80	-999.90	0.23	0.900E+10	0.000	28.00	6	0.50	1.00	1.00	9.80	9.0	1.0	5	24
0.1300	0.0463	0.0550	0.1698	0.0662	0.0069	0.0152	0.0427	0.0194	0.1641	0.0001	0	0	0	PART	0	0	0	0	2.16	17.80	-999.90	0.24	0.900E+10	0.000	28.00	6	0.50	1.00	1.00	9.80	9.0	1.0	5	24
0.1100	0.0464	0.0551	0.1713	0.0662	0.0071	0.0154	0.0441	0.0202	0.1716	0.0001	0	0	0	PART	0	0	0	0	2.26	17.80	-999.90	0.25	0.900E+10	0.000	28.00	6	0.50	1.00	1.00	9.80	9.0	1.0	5	24
0.1700	0.0463	0.0550	0.1690	0.0662	0.0067	0.0152	0.0419	0.0189	0.1595	0.0001	0	0	0	PART	0	0	0	0	2.10	17.80	-999.90	0.24	0.900E+10	0.000	28.00	6	0.50	1.00	1.00	9.80	9.0	1.0	5	24
0.2200	0.0463	0.0550	0.1698	0.0662	0.0069	0.0152	0.0427	0.0194	0.1641	0.0001	0	0	0	PART	0	0	0	0	2.16	17.80	-999.90	0.24	0.900E+10	0.000	28.00	6	0.50	1.00	1.00	9.80	9.0	1.0	5	24
0.1900	0.0463	0.0550	0.1699	0.0662	0.0069	0.0153	0.0429	0.0195	0.1648	0.0001	0	0	0	PART	0	0	0	0	2.17	17.80	-999.90	0.24	0.900E+10	0.000	28.00	6	0.50	1.00	1.00	9.80	9.0	1.0	5	24
0.1700	0.0464	0.0552	0.1716	0.0662	0.0071	0.0154	0.0444	0.0203	0.1731	0.0001	0	0	0	PART	0	0	0	0	2.28	17.80	-999.90	0.26	0.900E+10	0.000	28.00	6	0.50	1.00	1.00	9.80	9.0	1.0	5	24
0.1400	0.0466	0.0554	0.1735	0.0664	0.0074	0.0156	0.0460	0.0212	0.1813	0.0001	0	0	0	PART	0	0	0	0	2.39	17.80	-999.90	0.27	0.900E+10	0.000	28.00	6	0.50	1.00	1.00	9.80	9.0	1.0	5	24
0.1500	0.0466	0.0554	0.1733	0.0663	0.0073	0.0156	0.0459	0.0211	0.1806	0.0001	0	0	0	PART	0	0	0	0	2.38	17.80	-999.90	0.27	0.900E+10	0.000	28.00	6	0.50	1.00	1.00	9.80	9.0	1.0	5	24
0.2400	0.0464	0.0552	0.1714	0.0662	0.0071	0.0154	0.0443	0.0203	0.1723	0.0001	0	0	0	PART	0	0	0	0	2.27	17.80	-999.90	0.26	0.900E+10	0.000	28.00	6	0.50	1.00	1.00	9.80	9.0	1.0	5	24
0.2300	0.0464	0.0552	0.1721	0.0662	0.0072	0.0155	0.0449	0.0206	0.1753	0.0001	0	0	0	PART	0	0	0	0	2.31	17.80	-999.90	0.26	0.900E+10	0.000	28.00	6	0.50	1.00	1.00	9.80	9.0	1.0	5	24
0.3000	0.0465	0.0553	0.1724	0.0663	0.0072	0.0155	0.0451	0.0207	0.1768	0.0001	0	0	0	PART	0	0	0	0	2.33	17.80	-999.90	0.26	0.900E+10	0.000	28.00	6	0.50	1.00	1.00	9.80	9.0	1.0	5	24
0.3400	0.0467	0.0555	0.1743	0.0665	0.0075	0.0156	0.0466	0.0215	0.1843	0.0001	0	0	0	PART	0	0	0	0	2.43	17.80	-999.90	0.27	0.900E+10	0.000	28.00	6	0.50	1.00	1.00	9.80	9.0	1.0	5	24
0.2800	0.0468	0.0557	0.1753	0.0666	0.0076	0.0157	0.0473	0.0219	0.1881	0.0001	0	0	0	PART	0	0	0	0	2.48	17.80	-999.90	0.28	0.900E+10	0.000	28.00	6	0.50	1.00	1.00	9.80	9.0	1.0	5	24
0.3200	0.0469	0.0559	0.1763	0.0667	0.0077	0.0158	0.0480	0.0223	0.1918	0.0001	0	0	0	PART	0	0	0	0	2.53	17.80	-999.90	0.28	0.900E+10	0.000	28.00	6	0.50	1.00	1.00	9.80	9.0	1.0	5	24
0.2500	0.0469	0.0559	0.1765	0.0668	0.0077	0.0158	0.0481	0.0224	0.1926	0.0001	0	0	0	PART	0	0	0	0	2.54	17.80	-999.90	0.29	0.900E+10	0.000	28.00	6	0.50	1.00	1.00	9.80	9.0	1.0	5	24
0.1400	0.0472	0.0563	0.1787	0.0671	0.0079	0.0159	0.0496	0.0232	0.2001	0.0001	0	0	0	PART	0	0	0	0	2.64	17.80	-999.90	0.30	0.900E+10	0.000	28.00	6	0.50	1.00	1.00	9.80	9.0	1.0	5	24
0.1400	0.0481	0.0574	0.1843	0.0682	0.0084	0.0163	0.0529	0.0251	0.2173	0.0001	0	0	0	PART	0	0	0	0	2.87	17.80	-999.90	0.32	0.900E+10	0.000	28.00	6	0.50	1.00	1.00	9.80	9.0	1.0	5	24
0.3500	0.0471	0.0561	0.1776	0.0669	0.0078	0.0159	0.0489	0.0228	0.1963	0.0001	0	0	0	PART	0	0	0	0	2.59	17.80	-999.90	0.29	0.900E+10	0.000	28.00	6	0.50	1.00	1.00	9.80	9.0	1.0	5	24
0.3100	0.0472	0.0563	0.1787	0.0671	0.0079	0.0159	0.0496	0.0232	0.2001	0.0001	0	0	0	PART	0	0	0	0	2.64	17.80	-999.90	0.30	0.900E+10	0.000	28.00	6	0.50	1.00	1.00	9.80	9.0	1.0	5	24
0.2600	0.0473	0.0564	0.1791	0.0672	0.0080	0.0160	0.0499	0.0234	0.2016	0.0001	0	0	0	PART	0	0	0	0	2.66	17.80	-999.90	0.30	0.900E+10	0.000	28.00	6	0.50	1.00	1.00	9.80	9.0	1.0	5	24
0.2300	0.0478	0.0571	0.1828	0.0679	0.0083	0.0162	0.0520	0.0246	0.2128	0.0001	0	0	0	PART	0	0	0	0	2.81	17.80	-999.90	0.32	0.900E+10	0.000	28.00	6	0.50	1.00	1.00	9.80	9.0	1.0	5	24
0.2500	0.0489	0.0584	0.1889	0.0693	0.0088	0.0165	0.0553	0.0264	0.2301	0.0001	0	0	0	PART	0	0	0	0	3.04	17.80	-999.90	0.34	0.900E+10	0.000	28.00	6	0.50	1.00	1.00	9.80	9.0	1.0	5	24
0.2000	0.0518	0.0620	0.2044	0.0731	0.0099	0.0172	0.0625	0.0304	0.2676	0.0001	0	0	0	PART	0	0	0	0	3.54	17.80	-999.90	0.40	0.900E+10	0.000	28.00	6	0.50	1.00	1.00	9.80	9.0	1.0	5	24
0.4500	0.0465	0.0553	0.1723	0.0662	0.0072	0.0155	0.0450	0.0207	0.1761	0.0001	0	0	0	PART	0	0	0	0	2.32	17.80	-999.90	0.26	0.900E+10	0.000	28.00	6	0.50	1.00	1.00	9.80	9.0	1.0	5	24
0.4400	0.0465	0.0553	0.1730	0.0663	0.0073	0.0155	0.0456	0.0210	0.1791	0.0001	0	0	0	PART	0	0	0	0	2.36	17.80	-999.90	0.27	0.900E+10	0.000	28.00	6	0.50	1.00	1.00	9.80	9.0	1.0	5	24
0.5200	0.0466	0.0555	0.1739	0.0664	0.0074	0.0156	0.0463	0.0214	0.1828	0.0001	0	0	0	PART	0	0	0	0	2.41	17.80	-999.90	0.27	0.900E+10	0.000	28.00	6	0.50	1.00	1.00	9.80	9.0	1.0	5	24
0.4900	0.0467	0.0556	0.1749	0.0665	0.0075	0.0157	0.0470	0.0218	0.1866	0.0001	0	0	0	PART	0	0	0	0	2.46	17.80	-999.90	0.28	0.900E+10	0.000	28.00	6	0.50	1.00	1.00	9.80	9.0	1.0	5	24
0.5200	0.0472	0.0562	0.1782	0.0671	0.0079	0.0159	0.0493	0.0231	0.1986	0.0001	0	0	0	PART	0	0	0	0	2.62	17.80	-999.90	0.29	0.900E+10	0.000	28.00	6	0.50	1.00	1.00	9.80	9.0	1.0	5	24
0.4100	0.0472	0.0562	0.1785	0.0671	0.0079	0.0159	0.0494	0.0231	0.1993	0.0001	0	0	0	PART	0	0	0	0	2.63	17.80	-999.90	0.30	0.900E+10	0.000	28.00	6	0.50	1.00	1.00	9.80	9.0	1.0	5	24
0.3900	0.0474	0.0565	0.1801	0.0674	0.0080	0.0160	0.0504	0.0237	0.2046	0.0001	0	0	0	PART	0	0	0	0	2.70	17.80	-999.90	0.30	0.900E+10	0.000	28.00	6	0.50	1.00	1.00	9.80	9.0	1.0	5	24
0.3900	0.0475	0.0566	0.1806	0.0675	0.0081	0.0160	0.0507	0.0239	0.2061	0.0001	0	0	0	PART	0	0	0	0	2.72	17.80	-999.90	0.31	0.900E+10	0.000	28.00	6	0.50	1.00	1.00	9.80	9.0	1.0	5	24
0.4300	0.0478	0.0570	0.1825	0.0679	0.0083	0.0162	0.0519	0.0245	0.2121	0.0001	0	0	0	PART	0	0	0	0	2.80	17.80	-999.90	0.32	0.900E+10	0.000	28.00	6	0.50	1.00	1.00	9.80	9.0	1.0	5	24
1.1700	0.0464	0.0552	0.1719	0.0662	0.0072	0.0154	0.0447	0.0205	0.1746	0.0001	0	0	0	PART	0	0	0	0	2.30	17.80	-999.90	0.26	0.900E+10	0.000	28.00	6	0.50	1.00	1.00	9.80	9.0	1.0	5	24
0.4900	0.0484	0.0578	0.1862	0.0687	0.0086	0.0164	0.0539	0.0256	0.2226	0.0001	0	0	0	PART	0	0	0	0	2.94	17.80	-999.90	0.33	0.900E+10	0.000	28.00	6	0.50	1.00	1.00	9.80	9.0	1.0	5	24
0.5600	0.0493	0.0589	0.1912	0.0698	0.0090	0.0166	0.0564	0.0271	0.2361	0.0001	0	0	0	PART	0	0	0	0	3.12	17.80	-999.90	0.35	0.900E+10	0.000	28.00	6	0.50	1.00	1.00	9.80	9.0	1.0	5	24
0.6100	0.0493	0.0590	0.1915	0.0699	0.0090	0.0166	0.0566	0.0271	0.2368	0.0001	0	0	0	PART	0	0	0	0	3.13	17.80	-999.90	0.35	0.900E+10	0.000	28.00	6	0.50	1.00	1.00	9.80	9.0	1.0	5	24
0.6300	0.0497	0.0595	0.1936	0.0704	0.0091	0.0167	0.0576	0.0277	0.2421	0.0001	0	0	0	PART	0	0	0	0	3.20	17.80	-999.90	0.36	0.900E+10	0.000	28.00	6	0.50	1.00	1.00	9.80	9.0	1.0	5	24
0.7500	0.0502	0.0600	0.1960	0.0710	0.0093	0.0169	0.0587	0.0283	0.2481	0.0001	0	0	0	PART	0	0	0	0	3.28	17.80	-999.90	0.37	0.900E+10	0.000	28.00	6	0.50	1.00	1.00	9.80	9.0	1.0	5	24
0.9000	0.0499	0.0597	0.1945	0.0706	0.0092	0.0168	0.0580	0.0279	0.2443	0.0001	0	0	0	PART	0	0	0	0	3.23	17.80	-999.90	0.36	0.900E+10	0.000	28.00	6	0.50	1.00	1.00	9.80	9.0	1.0	5	24
0.9700	0.0498	0.0596	0.1942	0.0705	0.0092	0.0168	0.0579	0.0279	0.2436	0.0001	0	0	0	PART	0	0	0	0	3.22	17.80	-999.90	0.36	0.900E+10	0.000	28.00	6	0.50	1.00	1.00	9.80	9.0	1.0	5	24
0.3400	0.0492	0.0588	0.1906	0.0697	0.0089	0.0166	0.0562	0.0269	0.2346	0.0001	0	0	0	PART	0	0	0	0	3.10	17.80	-999.90	0.35	0.900E+10	0.000	28.00	6	0.50	1.00	1.00	9.80	9.0	1.0	5	24
0.3900	0.0500	0.0598	0.1951	0.0707	0.0092	0.0168	0.0583	0.0281	0.2458	0.0001	0	0	0	PART	0	0	0	0	3.25	17.80	-999.90	0.37	0.900E+10	0.000	28.00	6	0.50	1.00	1.00	9.80	9.0	1.0	5	24
0.4800	0.0505	0.0605	0.1979	0.0714	0.0094	0.0169	0.0596	0.0288	0.2526	0.0001	0	0	0	PART	0	0	0	0	3.34	17.80	-999.90	0.38	0.900E+10	0.000	28.00	6	0.50	1.00	1.00	9.80	9.0	1.0	5	24
0.3200	0.0515	0.0617	0.2031	0.0727	0.0098	0.0172	0.0619	0.0301	0.2646	0.0001	0	0	0	PART	0	0	0	0	3.50	17.80	-999.90	0.39	0.900E+10	0.000	28.00	6	0.50	1.00	1.00	9.80	9.0	1.0	5	24
0.3800	0.0524	0.0628	0.2078	0.0740	0.0101	0.0174	0.0639	0.0312	0.2751	0.0001	0	0	0	PART	0	0	0	0	3.64	17.80	-999.90	0.41	0.900E+10	0.000	28.00	6	0.50	1.00	1.00	9.80	9.0	1.0	5	24
0.4400	0.0530	0.0636	0.2110	0.0748	0.0103	0.0175	0.0652	0.0319	0.2818	0.0001	0	0	0	PART	0	0	0	0	3.73	17.80	-999.90	0.42	0.900E+10	0.000	28.00	6	0.50	1.00	1.00	9.80	9.0	1.0	5	24
0.4200	0.0538	0.0646	0.2149	0.0758	0.0105	0.0177	0.0668	0.0328	0.2901	0.0001	0	0	0	PART	0	0	0	0	3.84	17.80	-999.90	0.43	0.900E+10	0.000	28.00	6	0.50	1.00	1.00	9.80	9.0	1.0	5	24
0.3600	0.0541	0.0649	0.2164	0.0762	0.0106	0.0177	0.0674	0.0331	0.2931	0.0001	0	0	0	PART	0	0	0	0	3.88	17.80	-999.90	0.44	0.900E+10	0.000	28.00	6	0.50	1.00	1.00	9.80	9.0	1.0	5	24
0.4600	0.0552	0.0662	0.2216	0.0776	0.0109	0.0179	0.0694	0.0342	0.3036	0.0001	0	0	0	PART	0	0	0	0	4.02	17.80	-999.90	0.45	0.900E+10	0.000	28.00	6	0.50	1.00	1.00	9.80	9.0	1.0	5	24
0.5900	0.0543	0.0651	0.2171	0.0764	0.0107	0.0178	0.0677	0.0333	0.2946	0.0001	0	0	0	PART	0	0	0	0	3.90	17.80	-999.90	0.44	0.900E+10	0.000	28.00	6	0.50	1.00	1.00	9.80	9.0	1.0	5	24
0.9100	0.0542	0.0650	0.2168	0.0763	0.0106	0.0177	0.0675	0.0332	0.2938	0.0001	0	0	0	PART	0	0	0	0	3.89	17.80	-999.90	0.44	0.900E+10	0.000	28.00	6	0.50	1.00	1.00	9.80	9.0	1.0	5	24

```
0.7200  0.0556  0.0668  0.2239  0.0783  0.0111  0.0180  0 0703  0 0347  0.3081  0 0001  0  0  0 PART     0  0  0  0   4.08  17.80  -999.90   0.46 0.900E+10      0.000  28.00  6  0.50  1.00  1.00  9.80  9.0  1.0  5 24
0.6900  0.0582  0 0699  0.2363  0.0817  0.0117  0.0185  0.0748  0 0372  0.3314  0 0001  0  0  0 PART     0  0  0  0   4.39  17.80  -999.90   0.49 0.900E+10      0.000  28.00  6  0.50  1.00  1.00  9.80  9.0  1.0  5 24
1.3200  0 0539  0 0647  0.2153  0.0759  0.0106  0.0177  0 0670  0 0329  0 2908  0.0001  0  0  0 PART     0  0  0  0   3.85  17.80  -999.90   0.43 0.900E+10      0.000  28 00  6  0.50  1.00  1.00  9.80  9.0  1.0  5 24
0.9000  0.0583  0.0701  0 2372  0.0819  0.0118  0.0185  0.0751  0.0371  0.3329  0.0001  0  0  0 PART     0  0  0  0   4.41  17.80  -999.90   0.50 0 900E+10      0.000  28.00  6  0.50  1.00  1.00  9.80  9.0  1.0  5 24
0.0050  0.0478  0.0571  0.1828  0.0679  0.0083  0.0162  0.0520  0.0246  0.2128  0 0001  0  0  0 PART     0  0  0  0   2.81  17 80  -999.90   0.32 0.900E+10      0.000  28.00  6  0.50  1.00  1.00  9.80  9.0  1.0  5 24
0.0050  0.0508  0.0608  0.1995  0.0718  0.0096  0.0170  0.0603  0 0292  0.2563  0.0001  0  0  0 PART     0  0  0  0   3.39  17.80  -999.90   0.38 0.900E+10      0.000  28.00  6  0.50  1.00  1.00  9.80  9.0  1.0  5 24
```

A = month
B = day
C = year
D = pollutant
E = beginning hour
F = ending hour
G = wind speed
H = temperature
I = solar radiation
J = friction velocity
K = Monin-Obukhov length
L = mixing height
M = roughness length
N = number of diameters
O = smallest diameter
P = largest diameter
Q = density
R = reference height
S = leaf area index
T = LAI correction exponent
U = land use type
V = sample set number

Table C-2. The data making up the overall dataset for a sulfate peaked particle distribution. The data set contains 173 data points including observed zero deposition velocities which have been set to a lower limit of 0.005 cm/s. The footnotes define the variable A thru X.

Deposition Model

OBS	CARB 1	CARB 2	CARB 3	CARB 0	ADOM 1	ADOM 2	ADOM 3	UAM 1	UAM 2	ISC	A	B	C	D	E	F	G	H	I	J	K	L	M	N	O	P	Q	R	S	T	U	V
4.2100	0.9370	1.1215	0.8954	0.9370	2.4305	1.2241	1 2772	1.3454	1.4027	0.2612	5	18	83	ZnS	22	48	23	18	7 61	14.70	-999.90	0.40	0.166E+03	-999.900	3.00	1	6.00	6.00	4.00-999.90	0.1	1.0	11	1
4.0500	0.9370	1.1215	0.8954	0.9370	2.4305	1.2241	1.2772	1.3454	1.4027	0.2612	5	18	83	ZnS	22	48	23	18	8.53	14.70	-999.90	0.40	0.166E+03	-999.900	3.00	1	6.00	6.00	4.00-999.90	0.1	1.0	11	1
3.6500	0.9370	1.1215	0.8954	0.9370	2.4305	1.2241	1.2772	1.3454	1.4027	0.2612	5	18	83	ZnS	22	48	23	18	9.43	14.70	-999.90	0.40	0.166E+03	-999.900	3.00	1	6.00	6.00	4.00-999.90	0.1	1.0	11	1
1.9300	0.8016	0.8596	0.7043	0.8016	0.9154	0.6852	0.7050	0.9724	1.0057	0.1169	5	26	83	ZnS	23	24	23	54	3.23	19.50	-999.90	0.26	0.440E+02	-999.900	3.00	1	6.00	6.00	4.00-999.90	0.1	1.0	11	1
1.8000	0 8016	0.8596	0.7043	0.8016	0.9154	0.6852	0.7050	0.9724	1.0057	0.1169	5	26	83	ZnS	23	24	23	54	3.59	19.50	-999.90	0.26	0.440E+02	-999.900	3.00	1	6.00	6.00	4.00-999.90	0.1	1.0	11	1
1.7400	0.8016	0.8596	0.7043	0.8016	0.9154	0.6852	0.7050	0.9724	1.0057	0.1169	5	26	83	ZnS	23	24	23	54	3.83	19.50	-999.90	0.26	0.440E+02	-999.900	3.00	1	6.00	6.00	4.00-999.90	0.1	1.0	11	1
3.1400	0.7904	0.8774	0.7165	0.7904	1.0436	0.7185	0.7409	1.0131	1.0496	0.1490	6	5	83	ZnS	22	10	22	40	4.74	17.50	-999.90	0.27	0.770E+02	-999.900	3.00	1	6.00	6.00	4.00-999.90	0.1	1.0	11	1
3.0200	0.7904	0.8774	0.7165	0.7904	1.0436	0.7185	0.7409	1.0131	1.0496	0.1490	6	5	83	ZnS	22	10	22	40	5.40	17.50	-999 90	0.27	0.770E+02	-999.900	3.00	1	6.00	6.00	4.00-999.90	0.1	1.0	11	1
2.8400	0.7904	0.8774	0.7165	0.7904	1 0436	0.7185	0.7409	1.0131	1.0496	0.1490	6	5	83	ZnS	22	10	22	40	6.32	17.50	-999.90	0.27	0.770E+02	-999.900	3.00	1	6.00	6.00	4.00-999.90	0.1	1.0	11	1
1.7500	0.6808	0.7706	0.6434	0.6808	0.4911	0.5564	0.5663	0.8207	0.8449	0.0822	6	12	83	ZnS	22	43	23	13	3.00	14.90	-999.90	0.20	0.340E+02	-999.900	3 00	1	6.00	6.00	4.00-999.90	0.1	1.0	11	1
1.6200	0.6808	0.7706	0.6434	0.6808	0.4911	0.5564	0.5663	0.8207	0.8449	0.0822	6	12	83	ZnS	22	43	23	13	3.39	14.90	-999.90	0.20	0.340E+02	-999.900	3.00	1	6.00	6.00	4.00-999.90	0.1	1.0	11	1
1.3100	0.6808	0.7706	0.6434	0.6808	0.4911	0.5564	0.5663	0.8207	0.8449	0.0822	6	12	83	ZnS	22	43	23	13	3.75	14.90	-999.90	0.20	0.340E+02	-999.900	3.00	1	6.00	6.00	4.00-999.90	0.1	1.0	11	1
1.5600	0.7357	0.8606	0.7048	0.7357	0.9248	0.6887	0.7089	0.9787	1.0129	0.1314	6	24	83	ZnS	23	6	23	28	3.07	14 10	-999.90	0.26	0.590E+02	-999.900	3.00	1	6.00	6.00	4.00-999.90	0.1	1.0	11	1
1.4700	0.7357	0.8606	0.7048	0.7357	0.9248	0.6887	0.7089	0.9787	1.0129	0.1314	6	24	83	ZnS	23	6	23	28	3.24	14.10	-999.90	0.26	0.590E+02	-999.900	3.00	1	6.00	6.00	4.00-999.90	0.1	1.0	11	1
1.1400	0.7357	0.8606	0.7048	0.7357	0.9248	0.6887	0.7089	0.9787	1.0129	0.1314	6	24	83	ZnS	23	6	23	28	3.46	14.10	-999.90	0.26	0.590E+02	-999.900	3.00	1	6.00	6.00	4.00-999.90	0.1	1.0	11	1
1.1700	0.8752	0.9275	0.7524	0.8752	1.3838	0.8085	0.8371	1.0860	1.1266	0.1601	6	27	83	ZnS	21	31	22	1	3.17	20.50	-999.90	0.30	0.710E+02	-999.900	3.00	1	6.00	6.00	4.00-999.90	0.1	1.0	11	1
1.1500	0.8752	0.9275	0.7524	0.8752	1.3838	0.8085	0.8371	1.0860	1.1266	0.1601	6	27	83	ZnS	21	31	22	1	3.80	20.50	-999.90	0.30	0.710E+02	-999.900	3.00	1	6.00	6 00	4.00-999.90	0.1	1.0	11	1
1.1000	0.8752	0.9275	0.7524	0.8752	1.3838	0.8085	0.8371	1.0860	1.1266	0.1601	6	27	83	ZnS	21	31	22	1	4.37	20.50	-999.90	0.30	0.710E+02	-999.900	3.00	1	6.00	6.00	4.00-999.90	0.1	1.0	11	1
0.0400	0.0144	0.0182	0.0560	0.0144	0.0066	0.0460	0.1216	0.0034	0.0118	0.0001	6	4	79	SO4	6	0	0	0	1.71	14.20	-999.90	0.11	0.144E+02	-999.900	0.80	12	0.10	1.00	1.00 1.00	3.0	1.0	2	2
0.3300	0.0102	0.0147	0.0530	0.0102	0.0060	0.0438	0.1121	0.0031	0.0094	0.0001	6	21	79	SO4	2	36	0	0	1.23	8.80	-999.90	0.10	-0.183E+02	-999.900	0.40	12	0.10	1.00	1.00 1.00	2.5	1.0	10	3
0.5700	0.0142	0.0152	0.0395	0.0142	0.0153	0.0996	0.2854	0.0075	0 0247	0.0001	6	21	79	SO4	0	0	4	0	2.53	21.20	-999.90	0.26	-0.237E+02	-999 900	1.00	12	0.10	1.00	1.00 1.00	2.5	1.0	10	3
0.0300	0.0148	0.0211	0.0773	0.0148	0.0037	0.0286	0.0575	0.0020	0.0057	0.0001	6	21	79	SO4	3	55	0	0	1.64	8.30	-999.90	0.06	0.557E+01	-999.900	0.30	12	0.10	1.00	1.00 1.00	2.5	1.0	10	3
0.3300	0.0162	0.0209	0.0402	0.0162	0.0168	0.1084	0.3105	0.0082	0.0271	0.0001	7	18	79	SO4	0	0	3	43	2.69	14.40	-999.90	0.29	0.900E+10	-999.900	2.20	12	0.10	1.00	1.00 1.00	2.5	1.0	10	3
0.0200	0.0093	0.0154	0.0238	0 0093	0.0098	0.0660	0.1141	0 0049	0.0092	0.0001	2	19	80	SO4	11	23	0	0	2.15	4.40	-999.90	0.17	0.573E+02	-999.900	0.90	12	0.10	1.00	1.00 1.00	1.0	1.0	3	4
0.2000	0.0059	0.0096	0.0231	0.0059	0.0158	0.1024	0.1824	0.0077	0.0149	0.0001	2	20	80	SO4	0	0	4	40	3.73	5.90	-999.90	0.28	-0.101E+03	-999.900	0.30	12	0.10	1.00	1.00 1.00	1.0	1.0	3	4
0.0900	0.0058	0.0096	0.0230	0.0058	0.0114	0.0750	0.1295	0.0056	0.0107	0.0001	2	21	80	SO4	9	55	0	0	3.13	5 00	-999.90	0.20	0.385E+02	-999.900	0.30	12	0.10	1.00	1.00 1.00	1.0	1.0	3	4
0.0400	0.0051	0.0081	0.0228	0.0051	0.0142	0.0919	0.1617	0.0069	0 0133	0.0001	2	22	80	SO4	0	0	4	20	3.81	6.00	-999.90	0.25	0.900E+10	-999 900	0.20	12	0.10	1.00	1.00 1.00	1.0	1.0	3	4
0.0400	0.0120	0.0187	0.0419	0.0120	0.0193	0.1235	0.3532	0.0094	0.0311	0.0001	10	17	79	SO4	6	54	0	0	3.53	7.80	-999.90	0.34	0.245E+03	-999.900	1.50	12	0.10	1.00	1.00 1.00	2.5	1.0	10	5
0.2400	0.0150	0.0243	0.0438	0.0150	0.0081	0.0559	0.1442	0.0041	0.0130	0.0001	10	18	79	SO4	7	0	0	0	1.53	5.10	-999.90	0.14	0.204E+02	-999.900	2.30	12	0.10	1.00	1.00 1.00	2.5	1.0	10	5
0.3400	0.0124	0.0168	0.0424	0.0124	0.0200	0.1279	0.3664	0.0097	0.0324	0.0001	10	19	79	SO4	0	0	4	38	3.84	13.00	-999.90	0.35	-0.333E+03	-999.900	1.10	12	0.10	1.00	1.00 1.00	2.5	1.0	10	5
0.0800	0.0191	0.0283	0.0404	0.0191	0.0105	0.0708	0.1958	0.0052	0.0168	0.0001	10	19	79	SO4	6	58	0	0	1.50	8.80	-999.90	0.18	0.943E+02	-999.900	4.30	12	0.10	1.00	1.00 1.00	2.5	1.0	10	5
0.1000	0.0134	0.0230	0.0194	0.0134	0.0081	0.0565	0.0775	0.0041	0.0059	0.0001	11	21	79	SO4	10	50	0	0	1.48	2.90	-999.90	0.14	0.858E+02	-999.900	2.00	12	0.10	1.00	1.00 1.00	0.5	1.0	10	5
0.0700	0.0076	0.0127	0.0176	0.0076	0.0109	0.0730	0.1013	0.0054	0.0078	0.0001	11	22	79	SO4	0	0	2	55	2.30	4.50	-999.90	0.19	-0.167E+03	-999.900	0.60	12	0.10	1.00	1.00 1.00	0.5	1.0	10	5
0.1500	0.0079	0.0131	0.0180	0.0079	0.0097	0.0652	0.0892	0.0049	0 0070	0.0001	11	27	79	SO4	10	53	0	0	2 52	4.50	-999 90	0.17	0.243E+02	-999.900	0.60	12	0.10	1.00	1.00 1.00	0.5	1.0	10	5
0.0500	0.0065	0.0106	0.0172	0.0065	0.0131	0.0852	0.1185	0.0064	0.0093	0 0001	11	29	79	SO4	0	0	4	7	2.31	5.20	-999.90	0.23	0.661E+02	-999.900	0.40	12	0.10	1.00	1.00 1.00	0.5	1.0	10	5
0.0200	0.0080	0.0137	0.0188	0.0080	0.0086	0.0583	0.0791	0.0043	0.0062	0.0001	11	29	79	SO4	11	1	0	0	2.41	3.10	-999.90	0.15	0.175E+02	-999.900	0.60	12	0.10	1.00	1.00 1.00	0.5	1.0	10	5
0.3200	0.0061	0.0106	0.0172	0.0061	0.0130	0.0847	0.1176	0.0064	0 0093	0.0001	12	3	79	SO4	11	9	0	0	3.45	2.90	-999.90	0.23	0.446E+02	-999.900	0.40	12	0.10	1.00	1.00 1.00	0.5	1.0	10	5
0.0700	0.0124	0 0187	0.0201	0.0124	0.0076	0.0527	0.0714	0.0039	0.0055	0.0001	12	6	79	SO4	11	12	0	0	1.78	7.60	-999.90	0.13	0.241E+02	-999.900	1.10	12	0.10	1.00	1.00 1.00	0.5	1.0	10	5
0.2300	0.0071	0.0107	0.0174	0.0071	0.0115	0.0760	0.1052	0.0057	0.0082	0.0001	12	7	79	SO4	0	0	2	35	2.81	8.00	-999.90	0.20	0.120E+03	-999.900	0.40	12	0.10	1.00	1.00 1.00	0.5	1.0	10	5
0.1800	0.0053	0.0085	0.0178	0.0053	0.0175	0.1112	0.1557	0.0085	0.0125	0.0001	12	12	79	SO4	11	20	0	0	4.72	6.70	-999.90	0.31	0.120E+03	-999.900	0.20	12	0.10	1.00	1.00 1.00	0.5	1.0	10	5
0.4100	0.0070	0.0110	0.0198	0.0070	0.0231	0.1447	0.2045	0.0111	0.0161	0 0001	1	22	80	SO4	0	0	3	18	6.03	7.70	-999.90	0.41	0.245E+03	-999.900	0.30	12	0.10	1.00	1.00 1.00	0.5	1.0	10	5
0.0400	0.0070	0.0122	0.0222	0.0070	0.0064	0.0451	0.0599	0.0033	0.0047	0.0001	1	23	80	SO4	10	59	0	0	2.07	1.70	-999.90	0.11	0.152E+02	-999.900	0.30	12	0.10	1.00	1.00 1.00	0.5	1.0	10	5
0.0100	0.0048	0.0083	0.0238	0.0048	0.0059	0.0417	0.0550	0.0030	0.0043	0.0001	1	24	80	SO4	11	3	0	0	2.19	1.40	-999.90	0.10	0.176E+02	-999.900	0.10	12	0.10	1.00	1.00 1.00	0.5	1.0	10	5
0.2100	0.0037	0.0065	0.0184	0.0037	0.0091	0.0615	0.0839	0.0046	0.0066	0.0001	1	28	80	SO4	0	0	5	4	2.75	1.20	-999.90	0.16	0.858E+02	-999.900	0.10	12	0.10	1.00	1.00 1.00	0.5	1.0	10	5
0.2200	0.0053	0.0081	0.0172	0.0053	0.0126	0.0821	0.1139	0.0062	0.0090	0.0001	1	29	80	SO4	10	42	0	0	3.47	7.30	-999 90	0.22	0.245E+03	-999.900	0.20	12	0.10	1.00	1.00 1.00	0.5	1.0	10	5
0.2200	0.0043	0.0065	0.0178	0.0043	0.0175	0.1112	0.1556	0.0085	0.0125	0.0001	1	30	80	SO4	0	0	4	7	5.02	8.20	-999.90	0.31	0.900E+10	-999.900	0.10	12	0.10	1.00	1.00 1.00	0.5	1.0	10	5
0.0400	0.0073	0.0113	0.0184	0.0073	0.0093	0.0625	0.0855	0.0046	0.0067	0.0001	1	30	80	SO4	10	49	0	0	2.40	6 70	-999.90	0 16	0.505E+02	-999.900	0.40	12	0.10	1.00	1.00 1.00	0.5	1.0	10	5
0.0050	0.0051	0.0081	0.0172	0.0051	0.0125	0.0819	0 1135	0.0062	0.0090	0.0001	2	14	80	SO4	11	22	0	0	3.46	5.90	-999.90	0.22	0.162E+03	-999 900	0.20	12	0.10	1.00	1.00 1.00	0.5	1.0	10	5
0.2800	0.0048	0.0082	0.0230	0.0048	0.0114	0 0751	0.1304	0.0056	0.0107	0.0001	3	5	80	SO4	9	59	0	0	3.12	3.20	-999.90	0.20	0.194E+03	-999.900	0.20	12	0.10	1.00	1.00 1.00	1.0	1.0	10	5
0.5100	0.0050	0.0081	0.0229	0.0050	0.0120	0.0788	0.1374	0.0059	0.0112	0.0001	3	6	80	SO4	0	0	4	36	3.23	5.30	-999.90	0.21	0.900E+10	-999.900	0.20	12	0.10	1.00	1.00 1.00	1.0	1.0	10	5
0.0400	0.0052	0.0084	0.0238	0.0052	0.0098	0.0654	0.1120	0.0049	0.0091	0 0001	3	6	80	SO4	9	56	0	0	2.70	4.70	-999 90	0 17	0.779E+02	-999.900	0.20	12	0.10	1.00	1.00 1.00	1.0	1.0	10	5
0.0200	0.0083	0.0135	0.0232	0.0083	0.0109	0.0727	0.1267	0.0054	0.0103	0.0001	3	11	80	SO4	10	3	0	0	2.52	5.20	-999.90	0.19	0.952E+02	-999.900	0.70	12	0.10	1.00	1.00 1.00	1.0	1.0	10	5
0.0800	0.0048	0.0083	0.0131	0.0048	0 0103	0 0691	0.0745	0.0051	0.0056	0.0001	1	25	80	SO4	0	0	4	56	2.53	2.90	-999 90	0.18	-0.630E+02	-999.900	0.20	12	0.10	1.00	1.00 1.00	0.1	1.0	8	6
0.2500	0.0041	0.0063	0.0130	0.0041	0.0109	0.0718	0.0774	0 0054	0.0059	0.0001	2	15	80	SO4	0	0	5	39	3.10	7 40	-999 90	0 19	0.120E+03	-999.900	0.10	12	0.10	1.00	1.00 1.00	0.1	1.0	8	6
0.0100	0.0062	0.0101	0.0136	0.0062	0.0092	0.0631	0.0680	0.0046	0.0050	0.0001	2	27	80	SO4	0	0	4	52	2.06	5.10	-999.90	0.16	-0.418E+02	-999 900	0.30	12	0.10	1.00	1.00 1.00	0.1	1.0	8	6
0.3800	0.0053	0.0084	0.0133	0.0053	0.0098	0 0664	0 0715	0 0049	0.0053	0.0001	2	29	80	SO4	0	0	4	4	2 30	5.90	-999.90	0 17	-0.289E+02	-999.900	0.20	12	0.10	1.00	1.00 1.00	0.1	1.0	8	6
0.2500	0 0067	0.0116	0.0127	0.0067	0.0136	0.0888	0 0961	0 0067	0 0073	0.0001	3	10	80	SO4	9	59	0	0	3 04	3 60	-999.90	0 21	0.245E+03	-999.900	0.50	12	0.10	1.00	1.00 1.00	0.1	1.0	8	6
0.3500	0.0156	0.0238	0.0525	0.0156	0.0059	0.0419	0.0976	0 0031	0.0093	0 0001	10	21	79	SO4	6	52	0	0	1 77	6.60	-999 90	0.10	0.886E+01	-999 900	1.30	12	0.10	1.00	1.00 1.00	2.5	1.0	10	7
0.0100	0.0072	0.0099	0.0466	0.0072	0.0099	0.0663	0.1925	0.0049	0.0178	0.0001	6	9	80	SO4	5	11	0	0	2.45	11.20	-999.90	0.17	0.162E+03	-999.900	0.30	12	0.10	1.00	1.00 1.00	3.0	1.0	2	8
0.0400	0.0075	0.0096	0 0452	0.0075	0.0156	0.1004	0.3077	0.0076	0.0283	0.0001	6	10	80	SO4	0	0	5	5	3.58	13.70	-999 90	0.27	-0.988E+02	-999 900	0 30	12	0.10	1.00	1.00 1.00	3.0	1.0	2	8
0.2100	0 0078	0.0111	0 0466	0.0078	0.0099	0.0665	0.1954	0.0049	0 0177	0.0001	6	12	80	SO4	5	12	0	0	2.28	10.00	-999 90	0 17	0.900E+10	-999 900	0.40	12	0.10	1.00	1.00 1.00	3.0	1.0	2	8
0.6100	0.0198	0.0501	0.0434	0 0198	0.0068	0.0497	0.1236	0.0035	0.0094	0.0001	9	17	79	S	15	5	15	30	1.83	23.60	-999.90	0.11	-0.256E+01	51.000	9.10	12	0 10	1.00	1.00 7.00	2.0	1.0	3	9
0.7200	0.0392	0.0416	0.0369	0 0392	0.0091	0 0637	0 1635	0.0045	0.0126	0.0001	9	25	79	S	11	35	12	0	1 28	21.50	-999.90	0.15	-0.373E+01	88 000	9.40	12	0.10	1.00	1.00 7.00	2.0	1.0	3	9
0.4400	0.0397	0.0416	0.0369	0.0397	0.0091	0 0637	0 1631	0 0045	0.0126	0.0001	9	25	79	S	12	5	12	30	1 44	22 00	-999.90	0 15	0 470E+01	70.000	9.40	12	0.10	1.00	1 00 7.00	2.0	1.0	3	9
0.3300	0.0402	0 0416	0.0369	0.0402	0.0091	0 0637	0.1632	0 0045	0 0126	0.0001	9	25	79	S	12	35	13	0	1 34	22 50	-999.90	0.15	-0.471E+01	70 000	9 40	12	0.10	1.00	1.00 7.00	2.0	1.0	3	9
0.1200	0.0394	0.0404	0.0360	0.0394	0.0097	0 0670	0 1713	0 0048	0.0134	0.0001	9	25	79	S	13	5	13	30	1.29	22.90	-999 90	0.16	-0.977E+01	41.000	9 40	12	0.10	1.00	1.00 7.00	2.0	1.0	3	9
0 0050	0.0406	0 0416	0 0369	0.0406	0 0091	0 0637	0 1625	0 0045	0 0126	0.0001	9	25	79	S	14	35	15	0	1 57	22 90	-999.90	0.15	-0.622E+01	53 000	9.40	12	0.10	1.00	1.00 7.00	2.0	1.0	3	9
0.0050	0.0405	0.0415	0.0369	0.0405	0.0091	0 0633	0.1599	0 0045	0 0126	0.0001	9	25	79	S	15	35	16	0	1 53	22.90	-999.90	0.15	-0.150E+02	22.000	9.10	12	0 10	1.00	1.00 7.00	2.0	1.0	3	9
1.9000	1 6989	1.7923	2.1277	1.6989	2 1279	1 1775	1 6644	2 1045	2.4431	0 2520	0	0	0	Pb	0	0	0	0-999.90	20 00	-999.90	0.35	0 900E+10	-999.900	2.00	1	13.00	13.00	1.00-999.90	1.5	1.0	3	10
1.4000	1.3043	1 3966	1.7508	1 3043	1.3767	0.6268	0 9671	1 6724	2 0935	0 1458	0	0	0	Pb	0	0	0	0-999 90	20.00	-999.90	0 35	0.900E+10	-999 900	2 00	1	10.00	10.00	1.00-999.90	1.5	1.0	3	11
1 0000	0.9363	1 0180	1 3551	0 9363	0 4128	0.3031	0.4725	1.2507	1.7413	0.0809	0	0	0	Pb	0	0	0	0-999 90	20.00	-999 90	0.35	0.900E+10	-999.900	2.00	1	7.50	7.50	1.00-999.90	1.5	1.0	3	12
0.4500	0.5418	0.5990	0 8560	0.5418	0 0800	0.1220	0.1851	0.7195	1.2383	0 0001	0	0	0	Pb	0	0	0	0-999.90	20 00	-999 90	0 35	0 900E+10	-999 900	2 00	1	5.00	5 00	1.00-999.90	1 5	1.0	3	13
0.1500	0.2726	0 3046	0.4563	0.2726	0.0346	0.0615	0 1037	0 3724	0 7257	0 0001	0	0	0	Pb	0	0	0	0-999.90	20 00	-999 90	0 35	0 900E+10	-999 900	2 00	1	3.20	3.20	1.00-999.90	1.5	1.0	3	14
0.0100	0 0886	0 0994	0 1517	0.0886	0.0122	0 0446	0.0967	0 1060	0 2376	0 0001	0	0	0	Pb	0	0	0	0-999.90	20 00	-999.90	0.35	0.900E+10	-999 900	2 00	1	1.60	1.60	1.00-999.90	1.5	1.0	3	15

```
0.0200  0.0297  0.0333  0.0501  0.0297  0.0086  0.0667  0.1440  0 0257  0 0603  0 0001  0  0  0 Pb          0  0  0  0-999.90  20.00  -999.90  0.35 0.900E+10  -999.900  2.00  1  0.75  0.75  1.00-999.90  1.5  1.0  3 16
0.0200  0.0165  0.0184  0.0272  0.0165  0.0116  0.0904  0.2000  0.0097  0 0232  0 0001  0  0  0 Pb          0  0  0  0-999.90  20.00  -999.90  0.35 0.900E+10  -999.900  2.00  1  0.40  0.40  1.00-999.90  1.5  1.0  3 17
0.0900  0.1068  0.1167  0.1546  0.1068  0.1267  0.4353  0.8437  0.0332  0.0812  0 0001  0  0  0 Pb          0  0  0  0-999.90  20.00  -999.90  0.35 0.900E+10  -999.900  2.00  1  0.04  0.04  1.00-999.90  1.5  1.0  3 18
0.0500  0.1687  0.1862  0.2642  0.1687  0.0261  0.0372  0.0551  0.1479  0.2861  0.0001  5 21  81 FECCH     0  0  0  0  2.50  20.00  -999.90  0.16 0.900E+10  0.000  2.00  1  2.80  2.80  1.00  10.00  1.5  1.0  3 18
0.1200  0.1725  0.1911  0.3175  0.1725  0.0263  0.0399  0.0686  0.1731  0.3841  0.0001  9 23  81 FECOH     0  0  0  0  3.00  20.00  -999.90  0.19 0.900E+10  0.000  2.00  1  2.80  2.80  1.00  10.00  1.5  1.0  3 19
0.1800  0.1790  0.1988  0.2907  0.1790  0.0265  0.0426  0.0682  0.1982  0.3925  0.0001  6  1  81 FECOH     0  0  0  0  3.50  20.00  -999.90  0.23 0.900E+10  0.000  2.00  1  2.80  2.80  1.00  10.00  2.0  1.0  3 19
0.1200  0.1790  0.1988  0.2907  0.1790  0.0265  0.0426  0.0682  0.1982  0 3925  0.0001  8 17  81 FECOH     0  0  0  0  3.50  20.00  -999.90  0.23 0.900E+10  0.000  2.00  1  2.80  2.80  1.00  10.00  1.5  1.0  3 20
0.4200  0.2539  0.2779  0.4282  0.2539  0 0461  0.0557  0 0758  0.2395  0.4645  0.0001  9 30  82 FECCH     0  0  0  0  2.40  20.00  -999.90  0.15 0.900E+10  0.000  2.00  1  2.80  2.80  1.00  10.00  1.5  1.0  3 20
0.0100  0.1147  0.1677  0.0750  0.2837  0.1184  0.0886  0 1398  0.0304  0.0454  0 0001  1 26  81 Fine Prt  10  0 10 30  4.00  9.20  -999.90  0.64-0.499E+03  49.000  100.00  6  0.05  0.10  1.00  39.00  0.5  1.0  4 22
0.0200  0.0814  0.0991  0.0412  0.2074  0.0487  0.0375  0.0634  0.0125  0 0187  0.0001  1 26  81 Fine Prt  17 30 18  0  2.10  15.40  -999.90  0.26 0.105E+03  -16.000  100.00  6  0.05  0.10  1.00  39.00  0.5  1.0  4 22
0.1200  0.0814  0.1008  0.0421  0.2074  0.0524  0.0402  0.0674  0.0135  0.0202  0.0001  1 26  81 Fine Prt  18  0 18 30  2.50  14.80  -999.90  0.28 0.104E+03  -20 000  100.00  6  0.05  0.10  1.00  39.00  0.5  1.0  4 22
0.1100  0.0874  0.1134  0.0485  0.2214  0.0712  0.0540  0.0881  0.0182  0.0273  0.0001  1 27  81 Fine Prt  10 30 11  0  2.50  13.20  -999.90  0.38-0.610E+02  85.000  100.00  6  0.05  0.10  1.00  39.00  0.5  1.0  4 22
0.0700  0.0914  0.1134  0.0485  0.2309  0.0714  0.0542  0.0884  0.0183  0.0278  0 0001  1 27  81 Fine Prt  11 30 12  0  2.60  15.00  -999.90  0.38-0.932E+02  56 000  100.00  6  0.05  0.10  1.00  39.00  0.5  1.0  4 22
0.1400  0 0807  0.0986  0.0409  0.2059  0.0471  0.0363  0.0617  0.0121  0.0181  0 0001  1 27  81 Fine Prt  12 30 13  0  1.80  15.20  -999.90  0.25-0.572E+02  26.000  100 00  6  0.05  0.10  1.00  39.00  0.5  1.0  4 22
0.6800  0.0974  0.1482  0.0655  0.2432  0.1032  0 0775  0 1232  0.0265  0 0396  0.0001  1 28  81 Fine Prt  10 30 11  0  3.60  7.50  -999.90  0.56-0 378E+03  43.000  100.00  6  0.05  0.10  1.00  39.00  0.5  1.0  4 22
0.3200  0.1012  0.1505  0.0666  0.2524  0.1055  0.0791  0.1257  0.0270  0.0404  0.0001  1 28  81 Fine Prt  11 30 12  0  2.70  8.40  -999.90  0.57-0.824E+02  209.000  100.00  6  0.05  0.10  1.00  39.00  0.5  1.0  4 22
0.8000  0.0889  0.1311  0.0571  0.2240  0.0888  0.0669  0.1074  0.0228  0 0341  0.0001  1 28  81 Fine Prt  12  0 12 30  2.90  8 50  -999.90  0.48-0.116E+03  89.000  100.00  6  0.05  0.10  1.00  39.00  0.5  1.0  4 22
0.5500  0.1019  0.1482  0.0655  0.2541  0.1039  0.0779  0 1239  0.0266  0.0398  0 0001  1 28  81 Fine Prt  12 30 13  0  3.30  9.20  -999.90  0.56-0.709E+02  231 000  100.00  6  0.05  0.10  1.00  39.00  0.5  1.0  4 22
0.2000  0.1048  0.1505  0.0666  0.2609  0.1058  0.0794  0.1261  0.0271  0.0406  0.0001  1 28  81 Fine Prt  13  0 13 30  2.80  9.70  -999.90  0.57-0.730E+02  237.000  100.00  6  0.05  0.10  1.00  39.00  0.5  1.0  4 22
0.0900  0.0772  0.1090  0.0463  0.1970  0.0650  0.0494  0 0813  0.0167  0.0249  0.0001  1 28  81 Fine Prt  15  0 15 30  1.50  9.70  -999.90  0.35-0.728E+02  55.000  100.00  6  0.05  0.10  1.00  39.00  0.5  1.0  4 22
0.2200  0.0178  0.0152  0.0339  0.0178  0.0145  0.0944  0.2399  0.0071  0.0201  0.0001  8 25  78 S        11 18 11 48-999 90  30.00  -999.90  0.24-0.961E+01  144.000  1.00 12  0.10  1.00  1.00  39.00  2.0  1.0  3 23
0.1400  0.0178  0.0152  0.0339  0.0178  0.0150  0.0978  0.2486  0.0073  0.0209  0.0001  8 25  78 S        11 48 12 18-999.90  30 00  -999.90  0.25-0.116E+02  135.000  1.00 12  0.10  1.00  1.00  39.00  2.0  1.0  3 23
0.1100  0.0179  0.0152  0.0340  0.0179  0.0156  0.1013  0 2582  0.0076  0.0217  0.0001  8 25  78 S        12 18 12 48-999.90  30.00  -999.90  0 26-0.113E+02  156.000  1.00 12  0.10  1.00  1.00  39.00  2.0  1.0  3 23
0.1500  0.0185  0.0158  0.0354  0.0185  0.0191  0.1219  0 3124  0.0093  0.0266  0.0001  8 25  78 S        12 48 13 18-999.90  30.00  -999.90  0.32-0.193E+02  170.000  1.00 12  0.10  1.00  1.00  39.00  2.0  1.0  3 23
0.2300  0.0181  0.0155  0.0342  0.0181  0.0121  0.0808  0.2041  0.0060  0 0169  0.0001  8 25  78 S        13 18 13 48-999.90  30.00  -999.90  0.20-0.463E+01  173.000  1.00 12  0.10  1.00  1.00  39.00  2.0  1.0  3 23
0.2400  0.0179  0.0153  0.0340  0.0179  0.0127  0.0840  0.2117  0.0063  0.0177  0.0001  8 25  78 S        13 48 14 18-999.90  30.00  -999 90  0.21-0.828E+01  112.000  1.00 12  0.10  1.00  1.00  39.00  2.0  1.0  3 23
0.1500  0.0178  0.0153  0.0339  0.0178  0.0133  0.0870  0.2173  0 0065  0.0184  0.0001  8 25  78 S        14 18 14 48-999.90  30.00  -999.90  0.22-0.237E+02  45.000  1.00 12  0.10  1.00  1.00  39.00  2.0  1.0  3 23
0.1500  0.0187  0.0159  0.0357  0.0187  0.0197  0.1250  0.3189  0.0095  0 0271  0.0001  8 25  78 S        14 48 15 18-999.90  30 00  -999.90  0.33-0.343E+02  105.000  1.00 12  0.10  1.00  1.00  39.00  2.0  1.0  3 23
0.1900  0 0178  0.0152  0.0339  0.0178  0.0144  0.0942  0 2384  0.0071  0.0201  0.0001  8 25  78 S        15 18 15 48-999.90  30 00  -999.90  0.24-0.136E+02  102.000  1.00 12  0.10  1.00  1.00  39.00  2.0  1.0  3 23
0.1500  0.0179  0.0153  0.0342  0.0179  0.0162  0.1042  0 2633  0.0079  0.0225  0 0001  8 25  78 S        15 48 16 18-999.90  30.00  -999.90  0.27-0.299E+02  66.000  1.00 12  0.10  1.00  1.00  39.00  2.0  1.0  3 23
0.1600  0.0187  0.0159  0.0357  0.0187  0.0197  0.1246  0.3159  0.0095  0.0271  0.0001  8 25  78 S        16 18 16 48-999.90  30.00  -999.90  0.33-0.692E+02  52.000  1.00 12  0.10  1.00  1.00  39.00  2.0  1.0  3 23
0.2900  0.0189  0.0160  0.0361  0.0189  0.0202  0.1276  0.3219  0 0098  0.0282  0.0001  8 25  78 S        16 48 17 18-999.90  30.00  -999.90  0.34-0.262E+03  15.000  1.00 12  0.10  1.00  1.00  39.00  2.0  1.0  3 23
0.2000  0.0185  0.0158  0.0354  0.0185  0.0190  0.1202  0.3006  0.0093  0.0265  0.0001  8 25  78 S        17 18 17 48-999.90  30.00  -999.90  0.32  0.234E+03  -14.000  1.00 12  0.10  1.00  1.00  39.00  2.0  1.0  3 23
0.2000  0.0178  0.0152  0.0339  0.0178  0.0150  0.0956  0.2331  0.0073  0.0208  0.0001  8 25  78 S        17 48 18 18-999.90  30.00  -999.90  0.25  0.539E+02  -29.000  1.00 12  0.10  1.00  1.00  39.00  2.0  1.0  3 23
0.2500  0.0179  0.0153  0.0341  0.0179  0.0161  0.1023  0.2503  0.0079  0.0224  0.0001  8 25  78 S        18 18 18 48-999.90  30.00  -999.90  0.27  0.481E+02  -41.000  1.00 12  0.10  1.00  1.00  39.00  2.0  1.0  3 23
0.1500  0.0180  0.0153  0.0343  0.0180  0.0167  0.1059  0.2605  0.0082  0.0232  0.0001  8 25  78 S        18 48 19 18-999.90  30.00  -999.90  0.28  0.610E+02  -36.000  1.00 12  0.10  1.00  1.00  39.00  2.0  1.0  3 23
0.0700  0.0180  0.0154  0.0341  0.0180  0.0120  0.0777  0.1833  0.0060  0.0167  0.0001  8 25  78 S        19 18 19 48-999.90  30.00  -999.90  0.20  0.229E+02  -35.000  1.00 12  0.10  1.00  1.00  39.00  2.0  1.0  3 23
0.1400  0.0184  0.0158  0.0347  0.0184  0.0109  0.0702  0.1609  0.0054  0.0150  0.0001  8 25  78 S        19 48 20 18-999.90  30.00  -999.90  0.18  0.139E+02  -42.000  1.00 12  0.10  1.00  1.00  39.00  2.0  1.0  3 23
0.1500  0.0468  0.0554  0.1667  0.0670  0.0062  0.0148  0 0382  0.0168  0.1401  0.0001  0  0  0  0 PART      0  0  0  0  1.84  17.80  -999.90  0.21 0.900E+10  0.000  28.00  6  0.50  1.00  1.00  9.80  9.0  1.0  5 24
0.0200  0.0464  0.0551  0.1706  0.0662  0.0070  0.0153  0 0436  0.0199  0.1686  0.0001  0  0  0  0 PART      0  0  0  0  2.22  17.80  -999.90  0.25 0.900E+10  0.000  28.00  6  0.50  1.00  1.00  9.80  9.0  1.0  5 24
0.0400  0.0498  0.0596  0.1942  0.0705  0.0092  0 0168  0.0579  0.0279  0.2436  0.0001  0  0  0  0 PART      0  0  0  0  3.22  17.80  -999.90  0.36 0.900E+10  0.000  28.00  6  0.50  1.00  1.00  9.80  9.0  1.0  5 24
0.1300  0.0464  0 0550  0.1686  0.0663  0.0067  0.0151  0.0414  0 0187  0 1573  0.0001  0  0  0  0 PART      0  0  0  0  2.07  17 80  -999.90  0.23 0.900E+10  0.000  28.00  6  0.50  1.00  1.00  9.80  9.0  1.0  5 24
0.1300  0.0463  0.0550  0.1698  0.0662  0.0069  0.0152  0.0427  0.0194  0.1641  0.0001  0  0  0  0 PART      0  0  0  0  2.16  17.80  -999.90  0.24 0.900E+10  0 000  28.00  6  0.50  1.00  1.00  9.80  9.0  1.0  5 24
0.1100  0.0464  0.0551  0.1713  0.0662  0.0071  0.0154  0.0442  0.0202  0.1716  0.0001  0  0  0  0 PART      0  0  0  0  2.26  17.80  -999.90  0.25 0.900E+10  0.000  28.00  6  0.50  1.00  1.00  9.80  9.0  1.0  5 24
0.1700  0.0463  0.0550  0.1690  0.0662  0.0067  0 0152  0 0419  0.0189  0.1596  0.0001  0  0  0  0 PART      0  0  0  0  2.10  17.80  -999.90  0.24 0.900E+10  0.000  28.00  6  0.50  1.00  1.00  9.80  9.0  1.0  5 24
0.2200  0.0463  0.0550  0.1698  0.0662  0.0069  0.0152  0.0427  0.0194  0.1641  0.0001  0  0  0  0 PART      0  0  0  0  2.16  17.80  -999.90  0.24 0.900E+10  0.000  28.00  6  0.50  1.00  1.00  9.80  9.0  1.0  5 24
0.1900  0.0463  0.0550  0.1699  0.0662  0.0069  0.0153  0.0429  0.0195  0.1648  0 0001  0  0  0  0 PART      0  0  0  0  2.16  17.80  -999.90  0.24 0.900E+10  0.000  28.00  6  0.50  1.00  1.00  9.80  9.0  1.0  5 24
0.1700  0.0464  0.0552  0.1716  0.0662  0.0071  0.0154  0 0444  0.0203  0.1731  0.0001  0  0  0  0 PART      0  0  0  0  2.17  17.80  -999.90  0.24 0.900E+10  0.000  28.00  6  0.50  1.00  1.00  9.80  9.0  1.0  5 24
0.1400  0.0466  0.0554  0.1735  0.0664  0 0074  0.0156  0.0460  0.0212  0.1813  0.0001  0  0  0  0 PART      0  0  0  0  2 28  17.80  -999.90  0.26 0.900E+10  0.000  28.00  6  0.50  1.00  1.00  9.80  9.0  1.0  5 24
0.1500  0.0466  0.0554  0.1733  0.0664  0.0073  0.0156  0.0459  0 0211  0 1806  0.0001  0  0  0  0 PART      0  0  0  0  2.39  17.80  -999.90  0.27 0.900E+10  0.000  28.00  6  0.50  1.00  1.00  9.80  9.0  1.0  5 24
0.2400  0.0464  0.0552  0.1714  0.0662  0.0071  0.0154  0 0443  0.0203  0.1723  0.0001  0  0  0  0 PART      0  0  0  0  2 38  17.80  -999.90  0.27 0.900E+10  0 000  28.00  6  0.50  1.00  1.00  9.80  9.0  1.0  5 24
0.2300  0 0464  0.0552  0.1721  0.0662  0.0072  0.0155  0 0449  0.0206  0.1753  0.0001  0  0  0  0 PART      0  0  0  0  2.27  17.80  -999.90  0.26 0.900E+10  0.000  28.00  6  0.50  1.00  1.00  9.80  9.0  1.0  5 24
0.3000  0.0465  0.0553  0.1724  0.0663  0.0072  0.0155  0 0452  0 0207  0.1768  0.0001  0  0  0  0 PART      0  0  0  0  2.31  17.80  -999.90  0.26 0.900E+10  0.000  28.00  6  0.50  1.00  1.00  9.80  9.0  1.0  5 24
0.3400  0.0467  0.0555  0.1743  0 0665  0.0075  0.0156  0.0466  0 0215  0 1843  0 0001  0  0  0  0 PART      0  0  0  0  2.33  17.80  -999.90  0.26 0.900E+10  0 000  28.00  6  0.50  1.00  1.00  9.80  9.0  1.0  5 24
0.2800  0.0468  0.0557  0.1753  0 0666  0.0076  0 0157  0.0473  0.0219  0.1881  0.0001  0  0  0  0 PART      0  0  0  0  2.43  17.80  -999.90  0.27 0.900E+10  0.000  28.00  6  0.50  1.00  1.00  9.80  9.0  1.0  5 24
0.3200  0 0469  0.0559  0.1763  0.0667  0.0077  0.0158  0 0480  0 0223  0 1918  0 0001  0  0  0  0 PART      0  0  0  0  2 48  17.80  -999.90  0.28 0.900E+10  0.000  28.00  6  0.50  1.00  1.00  9.80  9.0  1.0  5 24
0.2500  0.0469  0.0559  0.1765  0.0668  0.0077  0 0158  0 0481  0 0224  0.1926  0.0001  0  0  0  0 PART      0  0  0  0  2 53  17 80  -999 90  0.28 0.900E+10  0.000  28.00  6  0.50  1.00  1.00  9.80  9.0  1.0  5 24
0.1400  0.0472  0.0563  0.1787  0.0671  0.0079  0.0159  0.0496  0.0232  0 2001  0 0001  0  0  0  0 PART      0  0  0  0  2 54  17.80  -999.90  0.29 0.900E+10  0.000  28.00  6  0.50  1.00  1.00  9.80  9.0  1.0  5 24
0.1400  0.0481  0.0574  0.1843  0.0683  0.0084  0.0163  0.0529  0 0251  0.2174  0.0001  0  0  0  0 PART      0  0  0  0  2.64  17.80  -999.90  0.30 0.900E+10  0.000  28.00  6  0.50  1.00  1.00  9.80  9.0  1.0  5 24
0.3500  0.0471  0.0561  0.1776  0.0670  0.0078  0.0159  0.0489  0 0228  0 1963  0 0001  0  0  0  0 PART      0  0  0  0  2.59  17.80  -999.90  0.32 0.900E+10  0.000  28.00  6  0.50  1.00  1.00  9.80  9.0  1.0  5 24
0.3100  0.0472  0.0563  0.1787  0.0671  0.0079  0.0159  0.0496  0.0232  0.2001  0.0001  0  0  0  0 PART      0  0  0  0  2.64  17.80  -999.90  0.29 0.900E+10  0.000  28.00  6  0.50  1.00  1.00  9.80  9.0  1.0  5 24
0.2600  0.0473  0 0564  0.1792  0.0672  0.0080  0.0160  0 0499  0.0234  0.2016  0.0001  0  0  0  0 PART      0  0  0  0  2.66  17.80  -999.90  0.30 0.900E+10  0.000  28.00  6  0.50  1.00  1.00  9.80  9.0  1.0  5 24
0.2300  0.0478  0.0571  0.1828  0.0679  0.0083  0.0162  0.0520  0.0246  0.2129  0.0001  0  0  0  0 PART      0  0  0  0  2.81  17.80  -999.90  0.32 0.900E+10  0.000  28.00  6  0.50  1.00  1.00  9.80  9.0  1.0  5 24
0.2500  0.0489  0.0584  0.1889  0.0693  0 0088  0.0165  0 0553  0 0264  0.2301  0.0001  0  0  0  0 PART      0  0  0  0  3.04  17 80  -999 90  0.34 0.900E+10  0.000  28.00  6  0.50  1.00  1.00  9 80  9.0  1.0  5 24
0.2000  0.0518  0.0620  0.2044  0 0731  0.0099  0.0172  0 0625  0 0304  0.2676  0.0001  0  0  0  0 PART      0  0  0  0  3.54  17 80  -999.90  0.40 0.900E+10  0.000  28.00  6  0.50  1.00  1.00  9.80  9.0  1.0  5 24
0.4500  0.0465  0.0553  0.1723  0 0663  0.0072  0.0155  0.0450  0.0207  0.1761  0.0001  0  0  0  0 PART      0  0  0  0  2.32  17.80  -999.90  0.26 0.900E+10  0.000  28.00  6  0.50  1.00  1.00  9.80  9.0  1.0  5 24
0.4400  0.0465  0.0553  0.1730  0.0663  0.0073  0.0155  0.0456  0.0210  0.1791  0.0001  0  0  0  0 PART      0  0  0  0  2 36  17.80  -999.90  0.27 0.900E+10  0 000  28.00  6  0.50  1.00  1.00  9.80  9.0  1.0  5 24
0.5200  0.0466  0.0555  0.1739  0.0664  0.0074  0 0156  0 0463  0.0214  0.1828  0.0001  0  0  0  0 PART      0  0  0  0  2 41  17.80  -999.90  0.27 0.900E+10  0 000  28 00  6  0.50  1.00  1.00  9.80  9.0  1.0  5 24
0.4900  0.0467  0.0556  0.1749  0.0665  0 0075  0 0157  0 0470  0.0218  0.1866  0.0001  0  0  0  0 PART      0  0  0  0  2.46  17 80  -999.90  0.28 0 900E+10  0.000  28.00  6  0.50  1.00  1.00  9.80  9.0  1.0  5 24
0.5200  0 0472  0.0562  0.1783  0.0671  0 0079  0.0159  0.0493  0.0231  0.1986  0.0001  0  0  0  0 PAPT      0  0  0  0  2.62  17 80  -999 90  0.29 0 900E+10  0.000  28.00  6  0.50  1.00  1.00  9.80  9.0  1.0  5 24
0.4100  0.0472  0.0562  0.1785  0.0671  0.0079  0.0159  0 0494  0 0231  0.1993  0.0001  0  0  0  0 PART      0  0  0  0  2.63  17.80  -999.90  0 30 0.900E+10  0.000  28.00  6  0.50  1.00  1.00  9.80  9.0  1.0  5 24
0.3900  0.0474  0.0566  0 1801  0.0674  0.0080  0 0160  0.0504  0.0237  0.2046  0.0001  0  0  0  0 PART      0  0  0  0  2.70  17.80  -999.90  0.30 0.900E+10  0.000  28.00  6  0.50  1.00  1.00  9.80  9.0  1.0  5 24
0.3900  0 0475  0.0566  0.1806  0.0675  0.0081  0 0160  0.0507  0 0239  0.2061  0.0001  0  0  0  0 PART      0  0  0  0  2.72  17.80  -999.90  0.31 0.900E+10  0.000  28.00  6  0.50  1.00  1.00  9.80  9.0  1.0  5 24
0.4100  0.0478  0.0570  0.1825  0.0679  0.0083  0 0162  0.0519  0.0245  0.2121  0.0001  0  0  0  0 PART      0  0  0  0  2 80  17.80  -999.90  0.32 0.900E+10  0.000  28.00  6  0.50  1.00  1.00  9.80  9.0  1.0  5 24
1.1700  0 0464  0.0552  0.1719  0.0662  0.0072  0 0154  0 0447  0.0205  0 1746  0.0001  0  0  0  0 PART      0  0  0  0  2 30  17.80  -999.90  0 26 0.900E+10  0 000  28 00  6  0.50  1.00  1.00  9.80  9.0  1.0  5 24
0.4900  0 0481  0.0578  0.1862  0 0687  0.0086  0 0164  0.0539  0 0256  0 2226  0.0001  0  0  0  0 PART      0  0  0  0  2.94  17 80  -999.90  0.33 0.900E+10  0.000  28.00  6  0.50  1.00  1.00  9.80  9.0  1.0  5 24
0.5600  0.0493  0.0589  0 1912  0.0698  0.0090  0.0166  0.0565  0 0271  0 2361  0.0001  0  0  0  0 PART      0  0  0  0  3.12  17 80  -999.90  0.35 0.900E+10  0 000  28 00  6  0.50  1.00  1.00  9.80  9.0  1.0  5 24
0.6100  0.0493  0.0590  0.1915  0.0699  0.0090  0.0166  0 0566  0 0271  0 2369  0.0001  0  0  0  0 PART      0  0  0  0  3 13  17.80  -999 90  0.35 0 900E+10  0 000  28 00  6  0 50  1.00  1.00  9.80  9.0  1.0  5 24
0.6300  0.0487  0.0595  0.1936  0.0704  0.0091  0.0167  0.0576  0.0277  0.2421  0 0001  0  0  0  0 PART      0  0  0  0  3 20  17.80  -999 90  0.36 0.900E+10  0 000  28.00  6  0 50  1.00  1.00  9.80  9.0  1.0  5 24
0.7500  0.0502  0.0600  0.1960  0.0710  0.0093  0.0169  0 0588  0.0283  0.2481  0 0001  0  0  0  0 PART      0  0  0  0  3 28  17.80  -999.90  0.37 0.900E+10  0 000  28 00  6  0.50  1.00  1.00  9.80  9.0  1.0  5 24
0 9000  0.0499  0 0597  0 1945  0.0706  0.0092  0 0168  0 0580  0 0279  0.2444  0.0001  0  0  0  0 PART      0  0  0  0  3.23  17 80  -999.90  0.36 0.900E+10  0.000  28 00  6  0.50  1.00  1.00  9.80  9.0  1.0  5 24
0 9700  0.0498  0 0596  0.1942  0.0705  0.0092  0.0168  0 0579  0 0279  0 2436  0.0001  0  0  0  0 PART      0  0  0  0  3 22  17 80  -999.90  0 36 0.900E+10  0.000  28.00  6  0.50  1.00  1.00  9.80  9.0  1.0  5 24
0.3400  0.0492  0.0588  0.1906  0.0697  0.0089  0 0166  0.0562  0 0269  0 2346  0 0001  0  0  0  0 PART      0  0  0  0  3 10  17.80  -999.90  0.35 0.900E+10  0.000  28.00  6  0.50  1.00  1.00  9.80  9.0  1.0  5 24
0.3900  0.0500  0 0598  0.1951  0.0707  0.0092  0 0168  0.0583  0 0281  0.2459  0.0001  0  0  0  0 PAPT      0  0  0  0  3 25  17 80  -999.90  0 37 0 900E+10  0 000  28.00  6  0.50  1.00  1.00  9.80  9.0  1.0  5 24
0.4800  0 0505  0 0605  0.1979  0.0714  0.0094  0 0169  0 0596  0.0288  0.2526  0.0001  0  0  0  0 PAPT      0  0  0  0  3 34  17 80  -999 90  0.38 0 900E+10  0 000  28 00  6  0.50  1.00  1.00  9.80  9.0  1.0  5 24
0.3200  0 0515  0 0617  0 2031  0.0727  0.0098  0.0172  0 0619  0.0301  0 2646  0 0001  0  0  0  0 PART      0  0  0  0  3 50  17.80  -999.90  0.39 0 900E+10  0 000  28 00  6  0 50  1.00  1.00  9.80  9.0  1.0  5 24
0.3800  0 0524  0.0628  0.2078  0.0740  0.0101  0 0174  0 0639  0 0312  0 2751  0 0001  0  0  0  0 PART      0  0  0  0  3 64  17.80  -999.90  0.41 0 900E+10  0 000  28.00  6  0.50  1.00  1.00  9.80  9.0  1.0  5 24
0.4400  0.0530  0.0636  0.2110  0.0748  0.0103  0 0175  0.0652  0 0319  0 2819  0 0001  0  0  0  0 PAPT      0  0  0  0  3 73  17 80  -999.90  0.42 0.900E+10  0.000  28 00  6  0.50  1.00  1.00  9.80  9.0  1.0  5 24
0.4200  0 0538  0.0646  0.2149  0.0758  0.0105  0.0177  0 0668  0 0328  0 2901  0 0001  0  0  0  0 PART      0  0  0  0  3 84  17 80  -999.90  0 43 0.900E+10  0 000  28.00  6  0.50  1.00  1.00  9.80  9.0  1.0  5 24
0.3600  0 0541  0.0649  0.2164  0 0762  0.0106  0 0177  0 0674  0 0331  0 2931  0.0001  0  0  0  0 PAPT      0  0  0  0  3 88  17 80  -999 90  0 44 0 900E+10  0 000  28 00  6  0.50  1.00  1.00  9.80  9 0  1.0  5 24
0.4600  0 0552  0.0662  0.2217  0.0776  0 0109  0 0179  0 0694  0 0343  0 3037  0 0001  0  0  0  0 PAPT      0  0  0  0  4.02  17 80  -999.90  0 45 0 900E+10  0 000  28 00  6  0 50  1.00  1.00  9.80  9.0  1.0  5 24
0.5900  0 0543  0.0651  0.2171  0.0764  0.0107  0.0178  0.0677  0.0333  0 2946  0 0001  0  0  0  0 PAPT      0  0  0  0  3.90  17 80  -999 90  0.44 0 900E+10  0 000  28 00  6  0.50  1 00  1.00  9.80  9.0  1.0  5 24
0.9100  0.0542  0 0650  0 2168  0.0763  0 0106  0 0177  0 0676  0 0332  0 2939  0 0001  0  0  0  0 PART      0  0  0  0  3 89  17 80  -999 90  0 44 0.900E+10  0 000  28 00  6  0.50  1.00  1.00  9.80  9.0  1.0  5 24
```

0.7200	0.0556	0.0668	0.2240	0.0783	0.0111	0.0180	0.0703	0.0347	0.3082	0.0001	0	0	0	PART	0	0	0	0	4.08	17.80	-999.90	0.46	0.900E+10	0.000	28.00	6	0.50	1.00	1.00	9.80	9.0	1.0	5	24
0.6900	0.0582	0.0699	0.2364	0.0817	0.0117	0.0185	0.0748	0.0372	0.3314	0.0001	0	0	0	PART	0	0	0	0	4.39	17.80	-999.90	0.49	0.900E+10	0.000	28.00	6	0.50	1.00	1.00	9.80	9.0	1.0	5	24
1.3200	0.0539	0.0647	0.2153	0.0759	0.0106	0.0177	0.0670	0.0329	0.2909	0.0001	0	0	0	PART	0	0	0	0	3.85	17.80	-999.90	0.43	0.900E+10	0.000	28.00	6	0.50	1.00	1.00	9.80	9.0	1.0	5	24
0.9000	0.0583	0.0701	0.2372	0.0819	0.0118	0.0185	0.0751	0.0374	0.3329	0.0001	0	0	0	PART	0	0	0	0	4.41	17.80	-999.90	0.50	0.900E+10	0.000	28.00	6	0.50	1.00	1.00	9.80	9.0	1.0	5	24
0.0050	0.0478	0.0571	0.1828	0.0679	0.0083	0.0162	0.0520	0.0246	0.2129	0.0001	0	0	0	PART	0	0	0	0	2.81	17.80	-999.90	0.32	0.900E+10	0.000	28.00	6	0.50	1.00	1.00	9.80	9.0	1.0	5	24
0.0050	0.0508	0.0608	0.1995	0.0718	0.0096	0.0170	0.0603	0.0292	0.2564	0.0001	0	0	0	PART	0	0	0	0	3.39	17.80	-999.90	0.38	0.900E+10	0.000	28.00	6	0.50	1.00	1.00	9.80	9.0	1.0	5	24

A = month
B = day
C = year
D = pollutant
E = beginning hour
F = ending hour
G = wind speed
H = temperature
I = solar radiation
J = friction velocity
K = Monin-Obukhov length
L = mixing height
M = roughness length
N = number of diameters
O = smallest diameter
P = largest diameter
Q = density
R = reference height
S = leaf area index
T = LAI correction exponent
U = land use type
V = sample set number

```
24 ------ Total Number of Data Sets
ZnS        18 11
Doran & Horst (1985), AEnv, 19, 939-951.
DESERT GRASSES, 1-2 m HIGH SAGEBRUSH
   3.0,    140.0                - z0 (cm), zd(cm)
-999.9,      2.0                - ws measurement ht. (m), temp. meas. ht. (m)
-999.9,  2                      - LAI(estimated), vegetation state
    1   4.                      - no. of diameters, density(qm/cm**3)
   6.                           - particel diameter(microns)
```

MM-DD-YY	B HR (lst)	E HR (lst)	WS (m/s)	TEMP (C)	SW RAD (W/m**2)	USTAR (m/s)	MONIN (m)	HEAT FLUX (W/m**2)	RA (s/cm)	RD (s/cm)	RC (s/cm)	VD (cm/s)
05-18-83	22:48	23:18	7.61	14.7	-999.9	0.4	166.	-999.9	-999.9	-999.9	-999.9	4.21
05-18-83	22:48	23:18	8.53	14.7	-999.9	0.4	166.	-999.9	-999.9	-999.9	-999.9	4.05
05-18-83	22:48	23:18	9.43	14.7	-999.9	0.4	166.	-999.9	-999.9	-999.9	-999.9	3.65
05-26-83	23:24	23:54	3.23	19.5	-999.9	0.26	44.	-999.9	-999.9	-999.9	-999.9	1.93
05-26-83	23:24	23:54	3.59	19.5	-999.9	0.26	44.	-999.9	-999.9	-999.9	-999.9	1.80
05-26-83	23:24	23:54	3.83	19.5	-999.9	0.26	44.	-999.9	-999.9	-999.9	-999.9	1.74
06-05-83	22:10	22:40	4.74	17.5	-999.9	0.27	77.	-999.9	-999.9	-999.9	-999.9	3.14
06-05-83	22:10	22:40	5.40	17.5	-999.9	0.27	77.	-999.9	-999.9	-999.9	-999.9	3.02
06-05-83	22:10	22:40	6.32	17.5	-999.9	0.27	77.	-999.9	-999.9	-999.9	-999.9	2.84
06-12-83	22:43	23:13	3.00	14.9	-999.9	0.20	34.	-999.9	-999.9	-999.9	-999.9	1.75
06-12-83	22:43	23:13	3.39	14.9	-999.9	0.20	34.	-999.9	-999.9	-999.9	-999.9	1.62
06-12-83	22:43	23:13	3.75	14.9	-999.9	0.20	34.	-999.9	-999.9	-999.9	-999.9	1.31
06-24-83	23:06	23:28	3.07	14.1	-999.9	0.26	59.	-999.9	-999.9	-999.9	-999.9	1.56
06-24-83	23:06	23:28	3.24	14.1	-999.9	0.26	59.	-999.9	-999.9	-999.9	-999.9	1.47
06-24-83	23:06	23:28	3.46	14.1	-999.9	0.26	59.	-999.9	-999.9	-999.9	-999.9	1.14
06-27-83	21:31	22:01	3.17	20.5	-999.9	0.30	71.	-999.9	-999.9	-999.9	-999.9	1.17
06-27-83	21:31	22:01	3.80	20.5	-999.9	0.30	71.	-999.9	-999.9	-999.9	-999.9	1.15
06-27-83	21:31	22:01	4.37	20.5	-999.9	0.30	71.	-999.9	-999.9	-999.9	-999.9	1.10

```
ENDDATA
```

```
SO4          1  2
Nicholson and Davies (1987), AEnv, 21, 1561-1571
BARLEY
-999.7,     12.0                - z0 (cm), zd(cm)
   1.0,      1.0                - ws measurement ht. (m), temp. meas. ht. (m)
-999.9,  -999.9                 - LAI(estimated), vegetation state
   10  1.0                      - no. of diameters, density (qm/cm**3)
  0.1  0.2  0.3  0.4  0.5  0.6  0.7  0.8  0.9  1.0 - particle diameters
```

MM-DD-YY	B HR (lst)	E HR (lst)	WS (m/s)	TEMP (C)	SW RAD (W/m**2)	USTAR (m/s)	MONIN (m)	HEAT FLUX (W/m**2)	RA (s/cm)	RD (s/cm)	RC (s/cm)	VD (cm/s)	Z0 (cm)	Ri	phim	phih
06-04-79	6:00		1.71	14.2	-999.9	0.11	-999e9	-999.9	1.49	-999.9	-999.9	0.04	0.8	0.051	1.36	1.36

```
ENDDATA
```

```
SO4          6 10
Nicholson and Davies (1987), AEnv, 21, 1561-1571
ROUGH PASTURE
-999.7,     11.0                - z0 (cm), zd(cm)
   1.0,      1.0                - ws measurement ht. (m), temp. meas. ht. (m)
-999.9,  -999.9                 - LAI(estimated), vegetation state
   10  1.0                      - no. of diameters, density (qm/cm**3)
  0.1  0.2  0.3  0.4  0.5  0.6  0.7  0.8  0.9  1.0 - particle diameters
```

MM-DD-YY	B HR (lst)	E HR (lst)	WS (m/s)	TEMP (C)	SW RAD (W/m**2)	USTAR (m/s)	MONIN (m)	HEAT FLUX (W/m**2)	RA (s/cm)	RD (s/cm)	RC (s/cm)	VD (cm/s)	Z0 (cm)	Ri	phim	phih
06-21-79	2:36		1.23	8.8	-999.9	0.10	-999e9	-999.9	1.19	-999.9	-999.9	0.33	0.4	-0.054	0.86	0.73
06-21-79		4:00	2.53	21.2	-999.9	0.26	-999e9	-999.9	0.38	-999.9	-999.9	0.57	1.0	-0.042	0.88	0.77
06-21-79	3:55		1.64	8.3	-999.9	0.06	-999e9	-999.9	4.09	-999.9	-999.9	0.03	0.3	0.093	1.93	1.93
07-18-79		3:43	2.69	14.4	-999.9	0.29	-999e9	-999.9	0.33	-999.9	-999.9	0.33	2.2	0.000	1.00	1.00
07-18-79		2:34	2.84	-999.9	-999.9	0.27	-999e9	-999.9	0.39	-999.9	-999.9	0.23	1.3	-999.9	-999.9	-999.9
07-18-79	4:07		2.35	9.9	-999.9	0.27	-999e9	-999.9	0.32	-999.9	-999.9	-0.01	3.2	0.005	1.02	1.02

```
ENDDATA
```

```
SO4         12  3
Nicholson and Davies (1987), AEnv, 21, 1561-1571
SHORT GRASS
-999.7,      8.0                - z0 (cm), zd(cm)
   1.0,      1.0                - ws measurement ht. (m), temp. meas. ht. (m)
-999.9,  -999.9                 - LAI(estimated), vegetation state
   10  1.0                      - no. of diameters, density (qm/cm**3)
  0.1  0.2  0.3  0.4  0.5  0.6  0.7  0.8  0.9  1.0 - particle diameters
```

MM-DD-YY	B HR (lst)	E HR (lst)	WS (m/s)	TEMP (C)	SW RAD (W/m**2)	USTAR (m/s)	MONIN (m)	HEAT FLUX (W/m**2)	RA (s/cm)	RD (s/cm)	RC (s/cm)	VD (cm/s)	Z0 (cm)	Ri	phim	phih
10-08-79	6:59		3.09	-999.9	-999.9	0.22	-999e9	-999.9	0.61	-999.9	-999.9	0.29	0.4	-999.9	-999.9	-999.9
10-10-79		5:48	2.21	-999.9	-999.9	0.19	-999e9	-999.9	0.63	-999.9	-999.9	0.02	0.8	-999.9	-999.9	-999.9
10-17-79		5:20	2.90	9.4	-999.9	0.29	-999e9	-999.9	0.35	-999.9	-999.9	-0.19	1.4	-0.009	0.97	0.93
2-04-80		4:32	3.90	-999.9	-999.9	0.28	-999e9	-999.9	0.51	-999.9	-999.9	0.28	0.3	-999.9	-999.9	-999.9
2-06-80		4:50	1.44	-999.9	-999.9	0.10	-999e9	-999.9	1.41	-999.9	-999.9	0.19	0.3	-999.9	-999.9	-999.9
2-19-80		4:40	4.40	6.5	-999.9	0.33	-999e9	-999.9	0.41	-999.9	-999.9	-0.07	0.4	0.001	1.00	1.00
2-19-80	11:23		2.15	4.4	-999.9	0.17	-999e9	-999.9	0.73	-999.9	-999.9	0.02	0.9	0.016	1.09	1.09
2-20-80		4:40	3.73	5.9	-999.9	0.28	-999e9	-999.9	0.48	-999.9	-999.9	0.20	0.3	-0.010	0.96	0.93
2-20-80	11:22		2.98	-999.9	-999.9	0.22	-999e9	-999.9	0.61	-999.9	-999.9	-0.10	0.4	-999.9	-999.9	-999.9
2-21-80	9:55		3.13	5.0	-999.9	0.20	-999e9	-999.9	0.80	-999.9	-999.9	0.09	0.3	0.023	1.13	1.13
2-22-80		4:20	3.81	6.0	-999.9	0.25	-999e9	-999.9	0.62	-999.9	-999.9	0.04	0.2	0.000	1.00	1.00
2-26-80	9:58		1.79	3.0	-999.9	0.16	-999e9	-999.9	0.72	-999.9	-999.9	-0.02	1.0	0.002	1.01	1.01

```
ENDDATA
```

```
SO4        48 10 .
Nicholson and Davies (1987), AEnv, 21, 1561-1571
ROUGH PASTURE
-999.7,      9.0              - z0 (cm), zd(cm)
   1.0,      1.0              - ws measurement ht. (m), temp. meas. ht. (m)
-999.9,  -999.9               - LAI(estimated), vegetation state
   10  1.0                    - no. of diameters, density (gm/cm**3)
  0.1  0.2  0.3  0.4  0.5  0.6  0.7  0.8  0.9  1.0 - particle diameters
```

MM-DD-YY	B HR (lst)	E HR (lst)	WS (m/s)	TEMP (C)	SW RAD (W/m**2)	USTAR (m/s)	MONIN (m)	HEAT FLUX (W/m**2)	RA (s/cm)	RD (s/cm)	RC (s/cm)	VD (cm/s)	z0 (cm)	Ri	phim	phih
10-12-79		4:17	2.55	-999.9	-999.9	0.19	-999e9	-999.9	0.67	-999.9	-999.9	0.20	0.5	-999.9	-999.9	-999.9
10-12-79	6:59		2.92	-999.9	-999.9	0.24	-999e9	-999.9	0.52	-999.9	-999.9	0.09	0.6	-999.9	-999.9	-999.9
10-14-79		3:19	1.96	-999.9	-999.9	0.22	-999e9	-999.9	0.40	-999.9	-999.9	0.16	2.6	-999.9	-999.9	-999.9
10-17-79	6:54		3.53	7.8	-999.9	0.34	-999e9	-999.9	0.31	-999.9	-999.9	0.04	1.5	0.004	1.02	1.02
10-18-79		4:41	3.27	10.5	-999.9	0.33	-999e9	-999.9	0.29	-999.9	-999.9	-0.34	1.5	-0.014	0.95	0.90
10-18-79	7:00		1.53	5.1	-999.9	0.14	-999e9	-999.9	0.83	-999.9	-999.9	0.24	2.3	0.039	1.26	1.26
10-19-79		4:38	3.84	13.0	-999.9	0.35	-999e9	-999.9	0.31	-999.9	-999.9	0.34	1.1	-0.003	0.99	0.98
10-19-79	6:58		1.50	8.8	-999.9	0.18	-999e9	-999.9	0.48	-999.9	-999.9	0.08	4.3	0.010	1.06	1.06
11-21-79	10:50		1.48	2.9	-999.9	0.14	-999e9	-999.9	0.71	-999.9	-999.9	0.10	2.0	0.011	1.06	1.06
11-22-79		2:55	2.30	4.5	-999.9	0.19	-999e9	-999.9	0.66	-999.9	-999.9	0.07	0.6	-0.006	0.98	0.96
11-22-79	10:50		2.22	4.3	-999.9	0.17	-999e9	-999.9	0.74	-999.9	-999.9	-0.06	0.7	0.010	1.06	1.06
11-23-79		2:48	3.36	6.6	-999.9	0.27	-999e9	-999.9	0.47	-999.9	-999.9	-0.01	0.4	0.003	1.02	1.02
11-27-79		3:34	2.08	5.9	-999.9	0.15	-999e9	-999.9	0.97	-999.9	-999.9	-0.12	0.3	0.000	1.00	1.00
11-27-79	10:53		2.52	4.5	-999.9	0.17	-999e9	-999.9	0.87	-999.9	-999.9	0.15	0.6	0.034	1.21	1.21
11-28-79		4:02	3.34	6.5	-999.9	0.25	-999e9	-999.9	0.54	-999.9	-999.9	-0.21	0.5	0.006	1.03	1.03
11-28-79	11:02		2.62	3.1	-999.9	0.17	-999e9	-999.9	0.93	-999.9	-999.9	-0.03	0.6	0.042	1.28	1.28
11-29-79		4:07	2.31	5.2	-999.9	0.23	-999e9	-999.9	0.61	-999.9	-999.9	0.05	0.4	0.014	1.08	1.08
11-29-79	11:01		2.41	3.1	-999.9	0.15	-999e9	-999.9	1.05	-999.9	-999.9	0.02	0.6	0.044	1.30	1.30
11-30-79		3:55	4.30	7.0	-999.9	0.39	-999e9	-999.9	0.28	-999.9	-999.9	-0.28	1.3	0.007	1.04	1.04
12-03-79	11:09		3.45	2.9	-999.9	0.23	-999e9	-999.9	0.63	-999.9	-999.9	0.32	0.4	0.020	1.12	1.12
12-05-79		4:31	4.05	-999.9	-999.9	0.32	-999e9	-999.9	0.39	-999.9	-999.9	0.09	0.6	-999.9	-999.9	-999.9
12-06-79		5:52	1.47	6.8	-999.9	0.12	-999e9	-999.9	1.97	-999.9	-999.9	-0.11	1.4	0.023	1.14	1.14
12-06-79	11:12		1.78	7.6	-999.9	0.13	-999e9	-999.9	1.04	-999.9	-999.9	0.07	1.1	0.034	1.22	1.22
12-07-79		2:35	2.81	8.0	-999.9	0.20	-999e9	-999.9	0.70	-999.9	-999.9	0.23	0.4	0.008	1.04	1.04
12-12-79	11:20		4.72	6.7	-999.9	0.31	-999e9	-999.9	0.49	-999.9	-999.9	0.18	0.2	0.008	1.04	1.04
12-13-79	10:50		3.29	6.3	-999.9	0.23	-999e9	-999.9	0.62	-999.9	-999.9	-0.06	0.5	0.015	1.09	1.09
1-22-80		3:18	6.03	7.7	-999.9	0.41	-999e9	-999.9	0.35	-999.9	-999.9	0.41	0.3	0.004	1.02	1.02
1-23-80	10:59		2.07	1.7	-999.9	0.11	-999e9	-999.9	1.72	-999.9	-999.9	0.04	0.3	0.049	1.34	1.34
1-24-80	11:03		2.19	1.4	-999.9	0.10	-999e9	-999.9	2.00	-999.9	-999.9	0.01	0.1	0.044	1.29	1.29
1-28-80		5:04	2.75	1.2	-999.9	0.16	-999e9	-999.9	1.12	-999.9	-999.9	0.21	0.1	0.011	1.06	1.06
1-28-80	11:00		1.06	2.1	-999.9	0.07	-999e9	-999.9	2.21	-999.9	-999.9	-0.03	0.6	0.035	1.23	1.23
1-29-80		3:58	2.22	7.7	-999.9	0.14	-999e9	-999.9	1.10	-999.9	-999.9	-0.12	0.4	0.023	1.14	1.14
1-29-80	10:42		3.47	7.3	-999.9	0.22	-999e9	-999.9	0.73	-999.9	-999.9	0.22	0.2	0.004	1.02	1.02
1-30-80		4:07	5.02	8.2	-999.9	0.31	-999e9	-999.9	0.53	-999.9	-999.9	0.22	0.1	0.000	1.00	1.00
1-30-80	10:49		2.40	6.7	-999.9	0.16	-999e9	-999.9	0.95	-999.9	-999.9	0.04	0.4	0.018	1.10	1.10
1-31-80		6:25	4.18	-999.9	-999.9	0.26	-999e9	-999.9	0.63	-999.9	-999.9	-0.36	0.1	-999.9	-999.9	-999.9
2-06-80	11:16		2.43	-999.9	-999.9	0.18	-999e9	-999.9	0.76	-999.9	-999.9	0.02	0.4	-999.9	-999.9	-999.9
2-07-80		4:00	3.45	-999.9	-999.9	0.19	-999e9	-999.9	0.91	-999.9	-999.9	-0.18	0.1	-999.9	-999.9	-999.9
2-07-80	11:16		1.88	-999.9	-999.9	0.15	-999e9	-999.9	0.86	-999.9	-999.9	0.04	0.5	-999.9	-999.9	-999.9
2-08-80		3:48	4.31	-999.9	-999.9	0.28	-999e9	-999.9	0.54	-999.9	-999.9	0.08	0.2	-999.9	-999.9	-999.9
2-12-80		5:03	1.93	-999.9	-999.9	0.14	-999e9	-999.9	1.01	-999.9	-999.9	0.10	0.3	-999.9	-999.9	-999.9
2-14-80	11:22		3.46	5.9	-999.9	0.22	-999e9	-999.9	0.72	-999.9	-999.9	0.00	0.2	0.006	1.03	1.03
2-25-80		5:16	1.96	4.6	-999.9	0.15	-999e9	-999.9	0.92	-999.9	-999.9	-0.09	0.4	-0.009	0.97	0.94
3-05-80	9:59		3.12	3.2	-999.9	0.20	-999e9	-999.9	0.76	-999.9	-999.9	0.28	0.2	0.005	1.03	1.03
3-06-80		4:36	3.23	5.3	-999.9	0.21	-999e9	-999.9	0.73	-999.9	-999.9	0.51	0.2	0.000	1.00	1.00
3-06-80	9:56		2.70	4.7	-999.9	0.17	-999e9	-999.9	0.94	-999.9	-999.9	0.04	0.2	0.012	1.07	1.07
3-11-80	10:03		2.52	5.2	-999.9	0.19	-999e9	-999.9	0.67	-999.9	-999.9	0.02	0.7	0.010	1.05	1.05
3-12-80		7:03	4.94	7.4	-999.9	0.35	-999e9	-999.9	0.41	-999.9	-999.9	-0.53	0.3	0.001	1.01	1.01

```
ENDDATA
```

```
SO4         6  8
Nicholson and Davies (1987), AEnv, 21, 1561-1571
BARE SOIL
-999.7,     10.0              - z0 (cm), zd(cm)
   1.0,      1.0              - ws measurement ht. (m), temp. meas. ht. (m)
-999.9,  -999.9               - LAI(estimated), vegetation state
   10  1.0                    - no. of diameters, density (gm/cm**3)
  0.1  0.2  0.3  0.4  0.5  0.6  0.7  0.8  0.9  1.0 - particle diameters
```

MM-DD-YY	B HR (lst)	E HR (lst)	WS (m/s)	TEMP (C)	SW RAD (W/m**2)	USTAR (m/s)	MONIN (m)	HEAT FLUX (W/m**2)	RA (s/cm)	RD (s/cm)	RC (s/cm)	VD (cm/s)	z0 (cm)	Ri	phim	phih
1-25-80		4:56	2.53	2.9	-999.9	0.18	-999e9	-999.9	0.74	-999.9	-999.9	0.08	0.2	-0.016	0.94	0.89
2-15-80		5:39	3.10	7.4	-999.9	0.19	-999e9	-999.9	0.88	-999.9	-999.9	0.25	0.1	0.008	1.04	1.04
2-27-80		4:52	2.06	5.1	-999.9	0.16	-999e9	-999.9	0.80	-999.9	-999.9	0.01	0.3	-0.024	0.92	0.85
2-29-80		4:04	2.30	5.9	-999.9	0.17	-999e9	-999.9	0.78	-999.9	-999.9	0.38	0.2	-0.035	0.89	0.80
3-10-80	9:59		3.04	3.6	-999.9	0.24	-999e9	-999.9	0.55	-999.9	-999.9	0.25	0.5	0.004	1.02	1.02
3-13-80		4:31	4.01	4.3	-999.9	0.34	-999e9	-999.9	0.35	-999.9	-999.9	-0.16	0.7	-0.010	0.96	0.93

```
ENDDATA
```

```
SO4         1 10
Nicholson and Davies (1987), AEnv, 21, 1561-1571
LONG GRASS
-999.7,      6.0                - z0 (cm), zd(cm)
   1.0,      1.0                - ws measurement ht. (m), temp. meas. ht. (m)
-999.9,  -999.9                 - LAI(estimated), vegetation state
   10  1.0                      - no. of diameters, density (qm/cm**3)
  0.1  0.2  0.3  0.4  0.5  0.6  0.7  0.8  0.9  1.0 - particle diameters
MM-DD-YY   B HR  E HR     WS   TEMP    SW RAD  USTAR   MONIN   HEAT FLUX      RA      RD      RC      VD      Z0      Ri    phim    phih
          (lst) (lst)   (m/s)    (C) (W/m**2)  (m/s)     (m)   (W/m**2) (s/cm) (s/cm) (s/cm) (cm/s)    (cm)
10-21-79   6:52          1.77    6.6    -999.9   0.10 -999e9     -999.9    1.62 -999.9 -999.9   0.35     1.3   0.071    1.59    1.59
ENDDATA
-----------------------------------------------------------------------------------------------------------------------------------
SO4         4  2
Nicholson and Davies (1987), AEnv, 21, 1561-1571
TALL BARLEY ???
-999.7,      6.0                - z0 (cm), zd(cm)
   1.0,      1.0                - ws measurement ht. (m), temp. meas. ht. (m)
-999.9,  -999.9                 - LAI(estimated), vegetation state
   10  1.0                      - no. of diameters, density (qm/cm**3)
  0.1  0.2  0.3  0.4  0.5  0.6  0.7  0.8  0.9  1.0 - particle diameters
MM-DD-YY   B HR  E HR     WS   TEMP    SW RAD  USTAR   MONIN   HEAT FLUX      RA      RD      RC      VD      Z0      Ri    phim    phih
          (lst) (lst)   (m/s)    (C) (W/m**2)  (m/s)     (m)   (W/m**2) (s/cm) (s/cm) (s/cm) (cm/s)    (cm)
 6-09-80   5:11          2.45   11.2    -999.9   0.17 -999e9     -999.9    0.84 -999.9 -999.9   0.01     0.3   0.006    1.03    1.03
 6-10-80         5:05    3.58   14.7    -999.9   0.27 -999e9     -999.9    0.51 -999.9 -999.9   0.04     0.3  -0.010    0.97    0.93
 6-10-80   5:10          1.67   10.9    -999.9   0.12 -999e9     -999.9    1.15 -999.9 -999.9  -0.29     0.3  -0.010    0.97    0.93
 6-12-80   5:12          2.28   10.0    -999.9   0.17 -999e9     -999.9    0.76 -999.9 -999.9   0.21     0.4   0.000    1.00    1.00
ENDDATA
-----------------------------------------------------------------------------------------------------------------------------------
S           8  3
Hicks et al (1986), BLM, 34, 103-121
GRASSLAND
   9.4,  -999.9                 - z0 (cm), zd(cm)
   7.0,      1.0                - ws measurement ht. (m), temp. meas. ht. (m)
-999.9,  -999.9                 - LAI(estimated), vegetation state
   10  1.0                      - no. of diameters, density (qm/cm**3)
  0.1  0.2  0.3  0.4  0.5  0.6  0.7  0.8  0.9  1.0 - particle diameters
MM-DD-YY   B HR  E HR     WS   TEMP    SW RAD  USTAR   MONIN   HEAT FLUX      RA      RD      RC      VD
          (lst) (lst)   (m/s)    (C) (W/m**2)  (m/s)     (m)   (W/m**2) (s/cm) (s/cm) (s/cm) (cm/s)
09-17-79  15:05 15:30    1.83   23.6    -999.9   0.11 -999e9       51.0 -999.9 -999.9 -999.9   0.61
09-17-79  15:35 16:00    1.40   23.5    -999.9   0.11 -999e9       19.0 -999.9 -999.9 -999.9  -0.01
09-25-79  11:35 12:00    1.28   21.5    -999.9   0.15 -999e9       88.0 -999.9 -999.9 -999.9   0.72
09-25-79  12:05 12:30    1.44   22.0    -999.9   0.15 -999e9       70.0 -999.9 -999.9 -999.9   0.44
09-25-79  12:35 13:00    1.34   22.5    -999.9   0.15 -999e9       70.0 -999.9 -999.9 -999.9   0.33
09-25-79  13:05 13:30    1.29   22.9    -999.9   0.16 -999e9       41.0 -999.9 -999.9 -999.9   0.12
09-25-79  14:35 15:00    1.57   22.9    -999.9   0.15 -999e9       53.0 -999.9 -999.9 -999.9   0.00
09-25-79  15:35 16:00    1.53   22.9    -999.9   0.15 -999e9       22.0 -999.9 -999.9 -999.9   0.00
ENDDATA
-----------------------------------------------------------------------------------------------------------------------------------
Pb          1  3
Garland (1982), Conference Proceedings, 849-858
GRASS - WIND TUNNEL
   2.0,  -999.9                 - z0 estimated(cm), zd(cm)
-999.9,  -999.9                 - ws measurement ht. (m), temp. meas. ht. (m)
-999.8,  -999.9                 - LAI(estimated), vegetation state
    1  1.0                      - no. of diameters, density (qm/cm**3)
  13.                           - diameter (microns)
MM-DD-YY   B HR  E HR     WS   TEMP    SW RAD  USTAR   MONIN   HEAT FLUX      RA      RD      RC      VD
          (lst) (lst)   (m/s)    (C) (W/m**2)  (m/s)     (m)   (W/m**2) (s/cm) (s/cm) (s/cm) (cm/s)
                      -999.9    20.    -999.9   0.35  9.0e9     -999.9 -999.9 -999.9 -999.9   1.90
ENDDATA
-----------------------------------------------------------------------------------------------------------------------------------
Pb          1  3
Garland (1982), Conference Proceedings, 849-858
GRASS - WIND TUNNEL
   2.0,  -999.9                 - z0 estimated(cm), zd(cm)
-999.9,  -999.9                 - ws measurement ht. (m), temp. meas. ht. (m)
-999.8,  -999.9                 - LAI(estimated), vegetation state
    1  1.0                      - no. of diameters, density (qm/cm**3)
  10.                           - diameter (microns)
MM-DD-YY   B HR  E HR     WS   TEMP    SW RAD  USTAR   MONIN   HEAT FLUX      RA      RD      RC      VD
          (lst) (lst)   (m/s)    (C) (W/m**2)  (m/s)     (m)   (W/m**2) (s/cm) (s/cm) (s/cm) (cm/s)
                      -999.9    20.    -999.9   0.35  9.0e9     -999.9 -999.9 -999.9 -999.9   1.40
ENDDATA
```

```
Pb          1  3
Garland (1982), Conference Proceedings, 849-858
GRASS - WIND TUNNEL
   2.0,  -999.9                 - z0 estimated(cm), zd(cm)
-999.9,  -999.9                 - ws measurement ht. (m), temp. meas. ht. (m)
-999.8,  -999.9                 - LAI(estimated), vegetation state
    1  1.0                      - no. of diameters, density (qm/cm**3)
  7.5                           - diameter (microns)
MM-DD-YY   B HR  E HR      WS    TEMP    SW RAD  USTAR   MONIN   HEAT FLUX      RA      RD      RC      VD
           (lst) (lst)   (m/s)     (C) (W/m**2)  (m/s)     (m)   (W/m**2) (s/cm) (s/cm) (s/cm) (cm/s)
                       -999.9     20.   -999.9   0.35  9.0e9      -999.9 -999.9 -999.9 -999.9   1.00
ENDDATA
-------------------------------------------------------------------------------------------------------
Pb          1  3
Garland (1982), Conference Proceedings, 849-858
GRASS - WIND TUNNEL
   2.0,  -999.9                 - z0 estimated(cm), zd(cm)
-999.9,  -999.9                 - ws measurement ht. (m), temp. meas. ht. (m)
-999.8,  -999.9                 - LAI(estimated), vegetation state
    1  1.0                      - no. of diameters, density (qm/cm**3)
  5.0                           - diameter (microns)
MM-DD-YY   B HR  E HR      WS    TEMP    SW RAD  USTAR   MONIN   HEAT FLUX      RA      RD      RC      VD
           (lst) (lst)   (m/s)     (C) (W/m**2)  (m/s)     (m)   (W/m**2) (s/cm) (s/cm) (s/cm) (cm/s)
                       -999.9     20.   -999.9   0.35  9.0e9      -999.9 -999.9 -999.9 -999.9   0.45
ENDDATA
-------------------------------------------------------------------------------------------------------
Pb          1  3
Garland (1982), Conference Proceedings, 849-858
GRASS - WIND TUNNEL
   2.0,  -999.9                 - z0 estimated(cm), zd(cm)
-999.9,  -999.9                 - ws measurement ht. (m), temp. meas. ht. (m)
-999.8,  -999.9                 - LAI(estimated), vegetation state
    1  1.0                      - no. of diameters, density (qm/cm**3)
  3.2                           - diameter (microns)
MM-DD-YY   B HR  E HR      WS    TEMP    SW RAD  USTAR   MONIN   HEAT FLUX      RA      RD      RC      VD
           (lst) (lst)   (m/s)     (C) (W/m**2)  (m/s)     (m)   (W/m**2) (s/cm) (s/cm) (s/cm) (cm/s)
                       -999.9     20.   -999.9   0.35  9.0e9      -999.9 -999.9 -999.9 -999.9   0.15
ENDDATA
-------------------------------------------------------------------------------------------------------
Pb          1  3
Garland (1982), Conference Proceedings, 849-858
GRASS - WIND TUNNEL
   2.0,  -999.9                 - z0 estimated(cm), zd(cm)
-999.9,  -999.9                 - ws measurement ht. (m), temp. meas. ht. (m)
-999.8,  -999.9                 - LAI(estimated), vegetation state
    1  1.0                      - no. of diameters, density (qm/cm**3)
  1.6                           - diameter (microns)
MM-DD-YY   B HR  E HR      WS    TEMP    SW RAD  USTAR   MONIN   HEAT FLUX      RA      RD      RC      VD
           (lst) (lst)   (m/s)     (C) (W/m**2)  (m/s)     (m)   (W/m**2) (s/cm) (s/cm) (s/cm) (cm/s)
                       -999.9     20.   -999.9   0.35  9.0e9      -999.9 -999.9 -999.9 -999.9   0.04
ENDDATA
-------------------------------------------------------------------------------------------------------
Pb          1  3
Garland (1982), Conference Proceedings, 849-858
GRASS - WIND TUNNEL
   2.0,  -999.9                 - z0 estimated(cm), zd(cm)
-999.9,  -999.9                 - ws measurement ht. (m), temp. meas. ht. (m)
-999.8,  -999.9                 - LAI(estimated), vegetation state
    1  1.0                      - no. of diameters, density (qm/cm**3)
 0.75                           - diameter (microns)
MM-DD-YY   B HR  E HR      WS    TEMP    SW RAD  USTAR   MONIN   HEAT FLUX      RA      RD      RC      VD
           (lst) (lst)   (m/s)     (C) (W/m**2)  (m/s)     (m)   (W/m**2) (s/cm) (s/cm) (s/cm) (cm/s)
                       -999.9     20.   -999.9   0.35  9.0e9      -999.9 -999.9 -999.9 -999.9   0.02
ENDDATA
-------------------------------------------------------------------------------------------------------
Pb          1  3
Garland (1982), Conference Proceedings, 849-858
GRASS - WIND TUNNEL
   2.0,  -999.9                 - z0 estimated(cm), zd(cm)
-999.9,  -999.9                 - ws measurement ht. (m), temp. meas. ht. (m)
-999.8,  -999.9                 - LAI(estimated), vegetation state
    1  1.0                      - no. of diameters, density (qm/cm**3)
  0.4                           - diameter (microns)
MM-DD-YY   B HR  E HR      WS    TEMP    SW RAD  USTAR   MONIN   HEAT FLUX      RA      RD      RC      VD
           (lst) (lst)   (m/s)     (C) (W/m**2)  (m/s)     (m)   (W/m**2) (s/cm) (s/cm) (s/cm) (cm/s)
                       -999.9     20.   -999.9   0.35  9.0e9      -999.9 -999.9 -999.9 -999.9   0.02
ENDDATA
```

```
Pb          1  3
Garland (1982), Conference Proceedings, 849-858
GRASS - WIND TUNNEL
   2.0,  -999.9                - z0 estimated(cm), zd(cm)
-999.9,  -999.9                - ws measurement ht. (m), temp. meas. ht. (m)
-999.8,  -999.9                - LAI(estimated), vegetation state
    1  1.0                     - no. of diameters, density (gm/cm**3)
 0.04                          - diameter (microns)
MM-DD-YY   B HR  E HR     WS   TEMP   SW RAD  USTAR  MONIN  HEAT FLUX     RA     RD     RC     VD
           (lst) (lst)  (m/s)    (C) (W/m**2)  (m/s)    (m)   (W/m**2) (s/cm) (s/cm) (s/cm) (cm/s)
                      -999.9    20.   -999.9   0.35  9.0e9    -999.9 -999.9 -999.9 -999.9   0.09
ENDDATA
-------------------------------------------------------------------------------------------------
FEOOH       2  3
Garland (1982), Conference Proceedings, 849-858
GRASS
   2.0,  -999.9                - z0 estimated(cm), zd(cm)
  10.0,  -999.9                - estimated ws meas. ht. (m), temp. meas. ht. (m)
-999.9,  -999.9                - LAI(estimated), vegetation state
    1  1.0                     - no. of diameters, density
  2.8                          - diameter (microns)
MM-DD-YY   B HR  E HR     WS   TEMP   SW RAD  USTAR  MONIN  HEAT FLUX     RA     RD     RC     VD
           (lst) (lst)  (m/s)    (C) (W/m**2)  (m/s)    (m)   (W/m**2) (s/cm) (s/cm) (s/cm) (cm/s)
05-21-81                  2.5   20.0   -999.9 -999.9  9.0e9        0.0 -999.9 -999.9 -999.9   0.05
09-23-81                  3.0   20.0   -999.9 -999.9  9.0e9        0.0 -999.9 -999.9 -999.9   0.12
ENDDATA
-------------------------------------------------------------------------------------------------
FEOOH       2  3
Garland (1982), Conference Proceedings, 849-858
GRASS - WIND TUNNEL
   2.0,  -999.9                - z0 estimated(cm), zd(cm)
  10.0,  -999.9                - estimated ws meas. ht. (m), temp. meas. ht. (m)
-999.8,  -999.9                - LAI(estimated), vegetation state
    1  1.0                     - no. of diameters, density
  2.8                          - diameter (microns)
MM-DD-YY   B HR  E HR     WS   TEMP   SW RAD  USTAR  MONIN  HEAT FLUX     RA     RD     RC     VD
           (lst) (lst)  (m/s)    (C) (W/m**2)  (m/s)    (m)   (W/m**2) (s/cm) (s/cm) (s/cm) (cm/s)
06-01-81                  3.5   20.0   -999.9 -999.9  9.0e9        0.0 -999.9 -999.9 -999.9   0.18
08-17-81                  3.5   20.0   -999.9 -999.9  9.0e9        0.0 -999.9 -999.9 -999.9   0.12
ENDDATA
-------------------------------------------------------------------------------------------------
FEOOH       1  3
Garland (1982), Conference Proceedings, 849-858
GRASS
   2.0,  -999.9                - z0 estimated(cm), zd(cm)
  10.0,  -999.9                - estimated ws meas. ht. (m), temp. meas. ht. (m)
-999.9,  -999.9                - LAI(estimated), vegetation state
    1  1.0                     - no. of diameters, density
  3.8                          - diameter (microns)
MM-DD-YY   B HR  E HR     WS   TEMP   SW RAD  USTAR  MONIN  HEAT FLUX     RA     RD     RC     VD
           (lst) (lst)  (m/s)    (C) (W/m**2)  (m/s)    (m)   (W/m**2) (s/cm) (s/cm) (s/cm) (cm/s)
09-30-82                  2.4   20.0   -999.9 -999.9  9.0e9        0.0 -999.9 -999.9 -999.9   0.42
ENDDATA
-------------------------------------------------------------------------------------------------
Fine Prt  12  4
Wesely et al (1983), BLM, 27, 237-255.
LEAFLESS DECIDUOUS FOREST IN WINTER (North Carolina)
  100.,  -999.9                - z0 estimated(cm), zd(cm)
  39.0,    42.0                - ws measurement ht. (m), temp. meas. ht. (m)
-999.9,     3.0                - LAI(estimated), vegetation state
    6  1.0                     - no. of diameters, density (gm/cm**3)
 0.05 0.06 0.07 0.08 0.09  0.1   - particle diameters
MM-DD-YY   B HR  E HR     WS   TEMP   SW RAD  USTAR  MONIN  HEAT FLUX     RA     RD     RC     VD
           (lst) (lst)  (m/s)    (C) (W/m**2)  (m/s)    (m)   (W/m**2) (s/cm) (s/cm) (s/cm) (cm/s)
01-26-81  10:00 10:30    4.0    9.2   -999.9   0.64 -999e9       49.0 -999.9 -999.9 -999.9   0.010
01-26-81  17:30 18:00    2.1   15.4   -999.9   0.26 -999e9      -16.0 -999.9 -999.9 -999.9   0.020
01-26-81  18:00 18:30    2.5   14.8   -999.9   0.28 -999e9      -20.0 -999.9 -999.9 -999.9   0.120
01-27-81  10:30 11:00    2.5   13.2   -999.9   0.38 -999e9       85.0 -999.9 -999.9 -999.9   0.110
01-27-81  11:30 12:00    2.6   15.0   -999.9   0.38 -999e9       56.0 -999.9 -999.9 -999.9   0.070
01-27-81  12:30 13:00    1.8   15.2   -999.9   0.25 -999e9       26.0 -999.9 -999.9 -999.9   0.140
01-28-81  10:30 11:00    3.6    7.5   -999.9   0.56 -999e9       43.0 -999.9 -999.9 -999.9   0.680
01-28-81  11:30 12:00    2.7    8.4   -999.9   0.57 -999e9      209.0 -999.9 -999.9 -999.9   0.320
01-28-81  12:00 12:30    2.9    8.5   -999.9   0.48 -999e9       69.0 -999.9 -999.9 -999.9   0.800
01-28-81  12:30 13:00    3.3    9.2   -999.9   0.56 -999e9      231.0 -999.9 -999.9 -999.9   0.550
01-28-81  13:00 13:30    2.8    9.7   -999.9   0.57 -999e9      237.0 -999.9 -999.9 -999.9   0.200
01-28-81  15:00 15:30    1.5    9.7   -999.9   0.35 -999e9       55.0 -999.9 -999.9 -999.9   0.090
ENDDATA
```

```
S          18  3
Wesely et al (1982), Conference Proceedings, 943-952
SHORT GRASS, TEXAS
   1.0,  -999.9                - z0 estimated(cm), zd(cm)
  39.0,   42.0                 - ws measurement ht. (m), temp. meas. ht. (m)
-999.9,  -999.9                - LAI(estimated), vegetation state
   10  1.0                     - no. of diameters, density (qm/cm**3)
  0.1  0.2  0.3  0.4  0.5  0.6  0.7  0.8  0.9  1.0 - particle diameters
```

MM-DD-YY	B HR (lst)	E HR (lst)	WS (m/s)	TEMP (C)	SW RAD (W/m**2)	USTAR (m/s)	MONIN (m)	HEAT FLUX (W/m**2)	RA (s/cm)	RD (s/cm)	RC (s/cm)	VD (cm/s)
08-25-78	11:18	11:48	-999.9	30.	-999.9	0.24	-999e9	144.	-999.9	-999.9	-999.9	0.220
08-25-78	11:48	12:18	-999.9	30.	-999.9	0.25	-999e9	135.	-999.9	-999.9	-999.9	0.140
08-25-78	12:18	12:48	-999.9	30.	-999.9	0.26	-999e9	156.	-999.9	-999.9	-999.9	0.110
08-25-78	12:48	13:18	-999.9	30.	-999.9	0.32	-999e9	170.	-999.9	-999.9	-999.9	0.150
08-25-78	13:18	13:48	-999.9	30.	-999.9	0.20	-999e9	173.	-999.9	-999.9	-999.9	0.230
08-25-78	13:48	14:18	-999.9	30.	-999.9	0.21	-999e9	112.	-999.9	-999.9	-999.9	0.240
08-25-78	14:18	14:48	-999.9	30.	-999.9	0.22	-999e9	45.	-999.9	-999.9	-999.9	0.150
08-25-78	14:48	15:18	-999.9	30.	-999.9	0.33	-999e9	105.	-999.9	-999.9	-999.9	0.150
08-25-78	15:18	15:48	-999.9	30.	-999.9	0.24	-999e9	102.	-999.9	-999.9	-999.9	0.190
08-25-78	15:48	16:18	-999.9	30.	-999.9	0.27	-999e9	66.	-999.9	-999.9	-999.9	0.150
08-25-78	16:18	16:48	-999.9	30.	-999.9	0.33	-999e9	52.	-999.9	-999.9	-999.9	0.160
08-25-78	16:48	17:18	-999.9	30.	-999.9	0.34	-999e9	15.	-999.9	-999.9	-999.9	0.290
08-25-78	17:18	17:48	-999.9	30.	-999.9	0.32	-999e9	-14.	-999.9	-999.9	-999.9	0.200
08-25-78	17:48	18:18	-999.9	30.	-999.9	0.25	-999e9	-29.	-999.9	-999.9	-999.9	0.200
08-25-78	18:18	18:48	-999.9	30.	-999.9	0.27	-999e9	-41.	-999.9	-999.9	-999.9	0.250
08-25-78	18:48	19:18	-999.9	30.	-999.9	0.28	-999e9	-36.	-999.9	-999.9	-999.9	0.150
08-25-78	19:18	19:48	-999.9	30.	-999.9	0.20	-999e9	-35.	-999.9	-999.9	-999.9	0.070
08-25-78	19:48	20:18	-999.9	30.	-999.9	0.18	-999e9	-42.	-999.9	-999.9	-999.9	0.140

```
ENDDATA
```

```
PART       61  5
Lorenz & Murphy(1989), BLM, 46, 355-366.
PINE PLANTATION
  28.0,   790.0                - z0 (cm), zd(cm)
   9.8,  -999.9                - ws measurement ht. (m), temp. meas. ht. (m)
   9.0   -999.9                - LAI, vegetation state
    6   1.                     - no. of diameters, density (qm/cm**3)
  0.5  0.6  0.7  0.8  0.9  1.0    -  particle diameters (microns)
```

MM-DD-YY	B HR (lst)	E HR (lst)	WS (m/s)	TEMP (C)	SW RAD (W/m**2)	USTAR (m/s)	MONIN (m)	HEAT FLUX (W/m**2)	RA (s/cm)	RD (s/cm)	RC (s/cm)	VD (cm/s)
			1.84	17.8	-999.9	-999.9	9.e09	0.	-999.9	-999.9	-999.9	0.15
			2.22	17.8	-999.9	-999.9	9.e09	0.	-999.9	-999.9	-999.9	0.02
			3.22	17.8	-999.9	-999.9	9.e09	0.	-999.9	-999.9	-999.9	0.04
			2.07	17.8	-999.9	-999.9	9.e09	0.	-999.9	-999.9	-999.9	0.13
			2.16	17.8	-999.9	-999.9	9.e09	0.	-999.9	-999.9	-999.9	0.13
			2.26	17.8	-999.9	-999.9	9.e09	0.	-999.9	-999.9	-999.9	0.11
			2.10	17.8	-999.9	-999.9	9.e09	0.	-999.9	-999.9	-999.9	0.17
			2.16	17.8	-999.9	-999.9	9.e09	0.	-999.9	-999.9	-999.9	0.22
			2.17	17.8	-999.9	-999.9	9.e09	0.	-999.9	-999.9	-999.9	0.19
			2.28	17.8	-999.9	-999.9	9.e09	0.	-999.9	-999.9	-999.9	0.17
			2.39	17.8	-999.9	-999.9	9.e09	0.	-999.9	-999.9	-999.9	0.14
			2.38	17.8	-999.9	-999.9	9.e09	0.	-999.9	-999.9	-999.9	0.15
			2.27	17.8	-999.9	-999.9	9.e09	0.	-999.9	-999.9	-999.9	0.24
			2.31	17.8	-999.9	-999.9	9.e09	0.	-999.9	-999.9	-999.9	0.23
			2.33	17.8	-999.9	-999.9	9.e09	0.	-999.9	-999.9	-999.9	0.30
			2.43	17.8	-999.9	-999.9	9.e09	0.	-999.9	-999.9	-999.9	0.34
			2.48	17.8	-999.9	-999.9	9.e09	0.	-999.9	-999.9	-999.9	0.28
			2.53	17.8	-999.9	-999.9	9.e09	0.	-999.9	-999.9	-999.9	0.32
			2.54	17.8	-999.9	-999.9	9.e09	0.	-999.9	-999.9	-999.9	0.25
			2.64	17.8	-999.9	-999.9	9.e09	0.	-999.9	-999.9	-999.9	0.14
			2.87	17.8	-999.9	-999.9	9.e09	0.	-999.9	-999.9	-999.9	0.14
			2.59	17.8	-999.9	-999.9	9.e09	0.	-999.9	-999.9	-999.9	0.35
			2.64	17.8	-999.9	-999.9	9.e09	0.	-999.9	-999.9	-999.9	0.31
			2.66	17.8	-999.9	-999.9	9.e09	0.	-999.9	-999.9	-999.9	0.26
			2.81	17.8	-999.9	-999.9	9.e09	0.	-999.9	-999.9	-999.9	0.23
			3.04	17.8	-999.9	-999.9	9.e09	0.	-999.9	-999.9	-999.9	0.25
			3.54	17.8	-999.9	-999.9	9.e09	0.	-999.9	-999.9	-999.9	0.20
			2.32	17.8	-999.9	-999.9	9.e09	0.	-999.9	-999.9	-999.9	0.45
			2.36	17.8	-999.9	-999.9	9.e09	0.	-999.9	-999.9	-999.9	0.44
			2.41	17.8	-999.9	-999.9	9.e09	0.	-999.9	-999.9	-999.9	0.52
			2.46	17.8	-999.9	-999.9	9.e09	0.	-999.9	-999.9	-999.9	0.49
			2.62	17.8	-999.9	-999.9	9.e09	0.	-999.9	-999.9	-999.9	0.52
			2.63	17.8	-999.9	-999.9	9.e09	0.	-999.9	-999.9	-999.9	0.41
			2.70	17.8	-999.9	-999.9	9.e09	0.	-999.9	-999.9	-999.9	0.39
			2.72	17.8	-999.9	-999.9	9.e09	0.	-999.9	-999.9	-999.9	0.39
			2.80	17.8	-999.9	-999.9	9.e09	0.	-999.9	-999.9	-999.9	0.43
			2.30	17.8	-999.9	-999.9	9.e09	0.	-999.9	-999.9	-999.9	1.17
			2.94	17.8	-999.9	-999.9	9.e09	0.	-999.9	-999.9	-999.9	0.49
			3.12	17.8	-999.9	-999.9	9.e09	0.	-999.9	-999.9	-999.9	0.56
			3.13	17.8	-999.9	-999.9	9.e09	0.	-999.9	-999.9	-999.9	0.61
			3.20	17.8	-999.9	-999.9	9.e09	0.	-999.9	-999.9	-999.9	0.63
			3.28	17.8	-999.9	-999.9	9.e09	0.	-999.9	-999.9	-999.9	0.75
			3.23	17.8	-999.9	-999.9	9.e09	0.	-999.9	-999.9	-999.9	0.90
			3.22	17.8	-999.9	-999.9	9.e09	0.	-999.9	-999.9	-999.9	0.97
			3.10	17.8	-999.9	-999.9	9.e09	0.	-999.9	-999.9	-999.9	0.34

3.25	17.8	-999.9	-999.9	9.e09	0.	-999.9	-999.9	-999.9	0.39
3.34	17.8	-999.9	-999.9	9.e09	0.	-999.9	-999.9	-999.9	0.48
3.50	17.8	-999.9	-999.9	9.e09	0.	-999.9	-999.9	-999.9	0.32
3.64	17.8	-999.9	-999.9	9.e09	0.	-999.9	-999.9	-999.9	0.38
3.73	17.8	-999.9	-999.9	9.e09	0.	-999.9	-999.9	-999.9	0.44
3.84	17.8	-999.9	-999.9	9.e09	0.	-999.9	-999.9	-999.9	0.42
3.88	17.8	-999.9	-999.9	9.e09	0.	-999.9	-999.9	-999.9	0.36
4.02	17.8	-999.9	-999.9	9.e09	0.	-999.9	-999.9	-999.9	0.46
3.90	17.8	-999.9	-999.9	9.e09	0.	-999.9	-999.9	-999.9	0.59
3.89	17.8	-999.9	-999.9	9.e09	0.	-999.9	-999.9	-999.9	0.91
4.08	17.8	-999.9	-999.9	9.e09	0.	-999.9	-999.9	-999.9	0.72
4.39	17.8	-999.9	-999.9	9.e09	0.	-999.9	-999.9	-999.9	0.69
3.85	17.8	-999.9	-999.9	9.e09	0.	-999.9	-999.9	-999.9	1.32
4.41	17.8	-999.9	-999.9	9.e09	0.	-999.9	-999.9	-999.9	0.90
2.81	17.8	-999.9	-999.9	9.e09	0.	-999.9	-999.9	-999.9	0.00
3.39	17.8	-999.9	-999.9	9.e09	0.	-999.9	-999.9	-999.9	0.00

ENDDATA

Appendix D

Predicted Deposition Velocities vs Particle Diameter

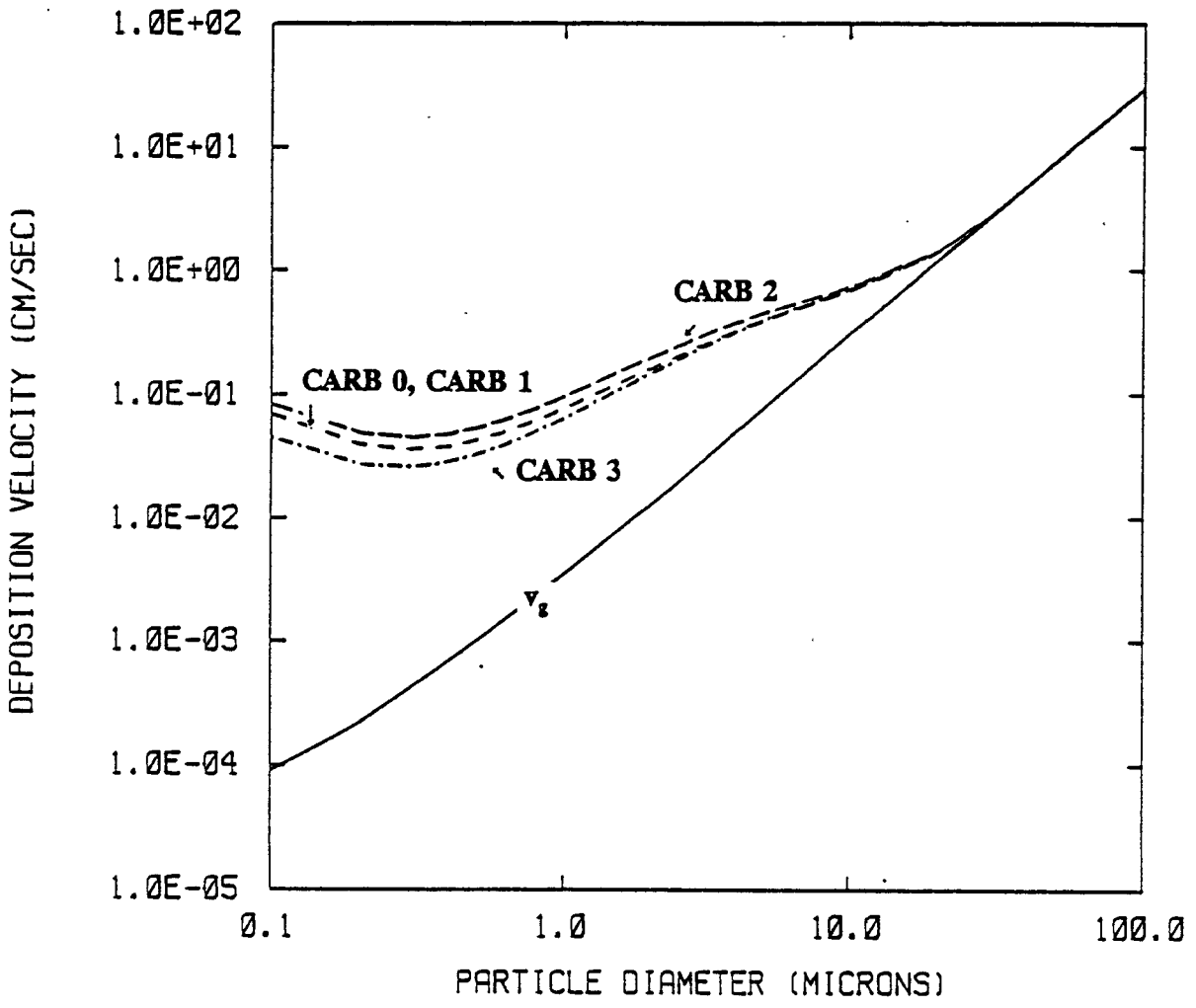

Figure D-1. Predicted deposition velocity for the CARB-based models for $u_* = 10$ cm/s, $z_o = 10$ cm, LAI = 1.0, $\rho = 1.0$ g/cm^3, and neutral stability. The gravitational settling velocity is v_g.

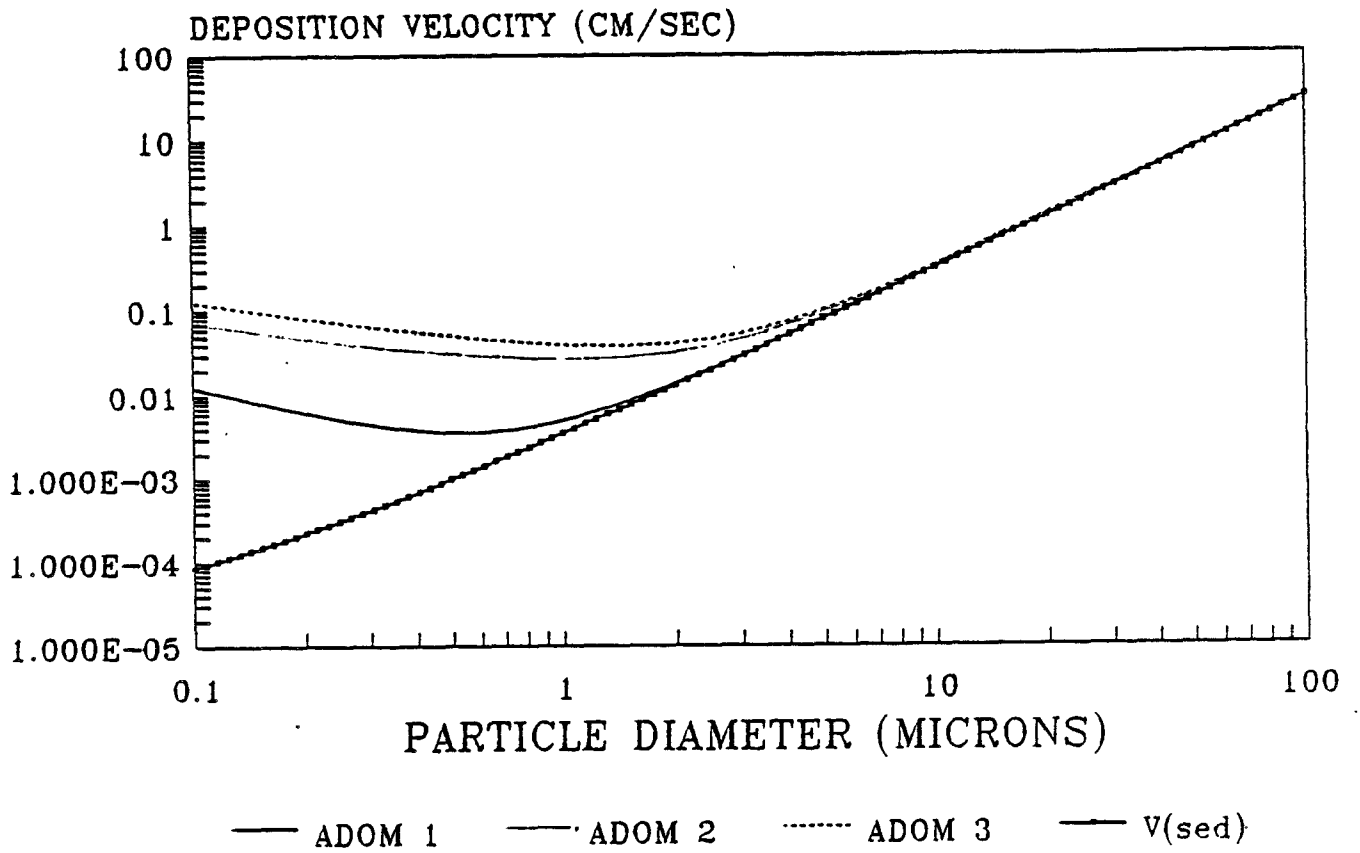

Figure D-2. Predicted deposition velocity for the ADOM-based models for $u_* = 10$ cm/s, $z_0 = 10$ cm, LAI = 1.0, $\rho = 1.0$ g/cm^3, and neutral stability. The gravitational settling velocity is v_g.

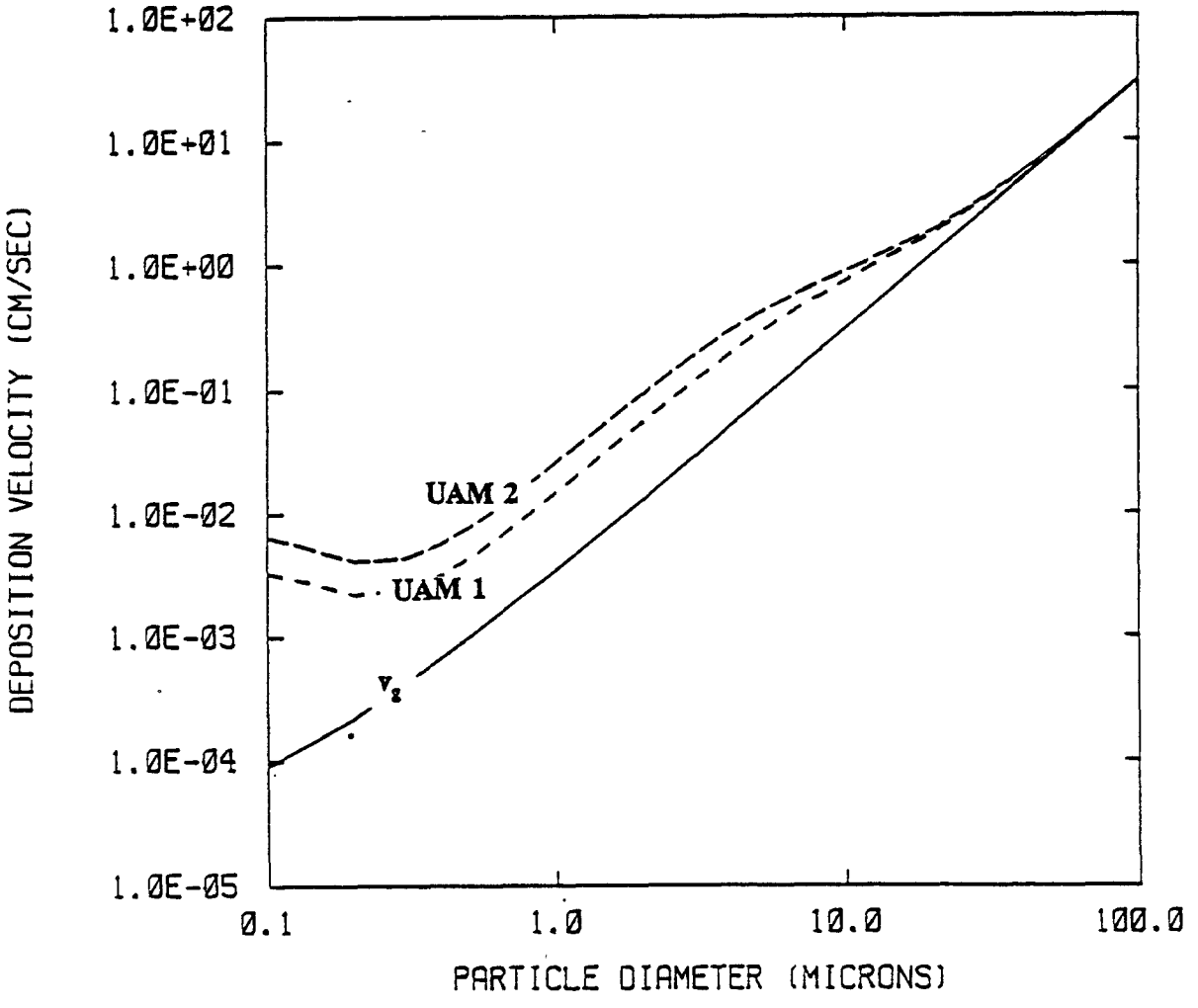

Figure D-3. Predicted deposition velocity for the UAM-based models for $u_* = 10$ cm/s, $z_o = 10$ cm, LAI = 1.0, $\rho = 1.0$ g/cm^3, and neutral stability. The gravitational settling velocity is v_g.

APPENDIX E

Implementation of the Modified Source Depletion Method in ISC2

E.1 Overview of Method

Horst (1983) describes a method for incorporating the effects of deposition on the vertical distribution of material in a plume, without resorting to a full surface depletion treatment (see the discussion of plume depletion techniques in Section 3). The method includes a vertical profile adjustment factor as well as a source depletion factor, so that concentrations in the lower portion of the plume approximate those produced by the surface depletion model. This adjustment factor is important because deposition is proportional to near-surface concentrations. The source depletion method by itself overestimates near-surface concentrations, thereby overpredicting deposition rates which hastens removal of material from the plume.

Let V(x,z,h) denote the vertical distribution of plume material in the absence of deposition. In terms of the notation used by Horst (1983),

$$V(x,z,h) = u\ D(x,z,h)\sqrt{2\pi}\ \sigma_z \qquad \text{(E-1)}$$

where D is the crosswind-integrated concentration distribution for a plume at a height h above the ground, released from a source of unit source strength. Then the vertical distribution factor that is modified to account for the depletion resulting from deposition, V_d (x,z,h), is defined to be:

$$V_d(x,z,h) = V(x,z,h)\ F_Q(x)\ P(x,z) \qquad \text{(E-2)}$$

$F_Q(x)$ is the fraction of material that remains in the plume at the downwind distance x (i.e., the mass that has not yet been deposited on the surface). This factor may be thought of as a source depletion factor, a ratio of the "current" mass emission rate to the original mass emission rate. P(x,z) is the vertical profile adjustment factor.

The effect of Equation (E-2) is illustrated in Figures E-1 and E-2. Figure (E-1) displays a depletion factor F_Q, and the corresponding profile correction factor P(x,z) for a distance at which σ_z is 1.5 times the plume height. This assures that the plume has been in contact with the ground for a long enough time that significant deposition has occurred. The depletion factor is constant with height, whereas the profile correction shows that most of the material is lost from the lower portion of the plume. Figure (E-2) compares the vertical profile of concentration both with and without deposition and the corresponding depletion of material from the plume. The depleted plume profile is computed using Equation (E-2).

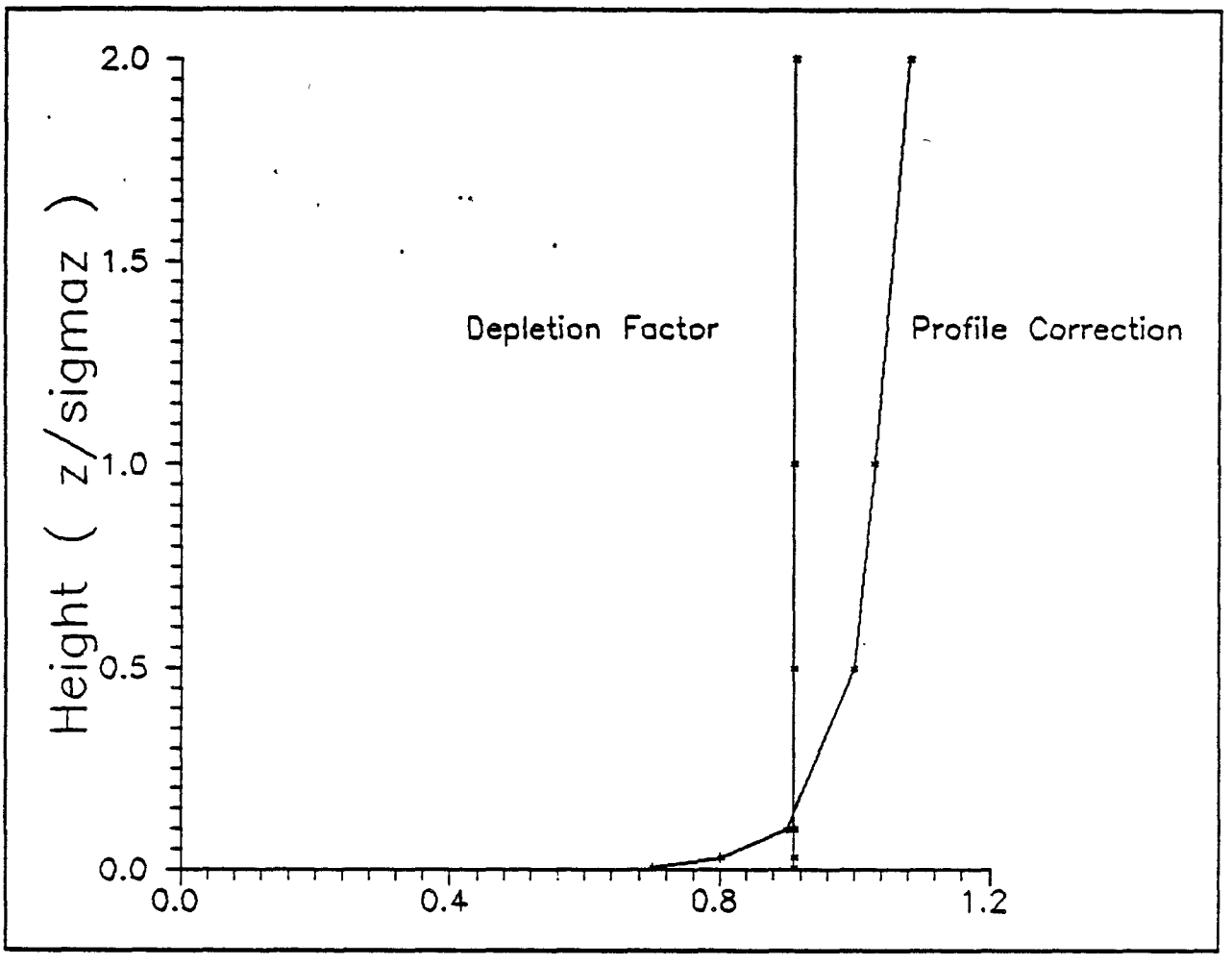

FIGURE E-1. ILLUSTRATION OF THE DEPLETION FACTOR F_Q AND THE CORRESPONDING PROFILE CORRECTION FACTOR P(x,z).

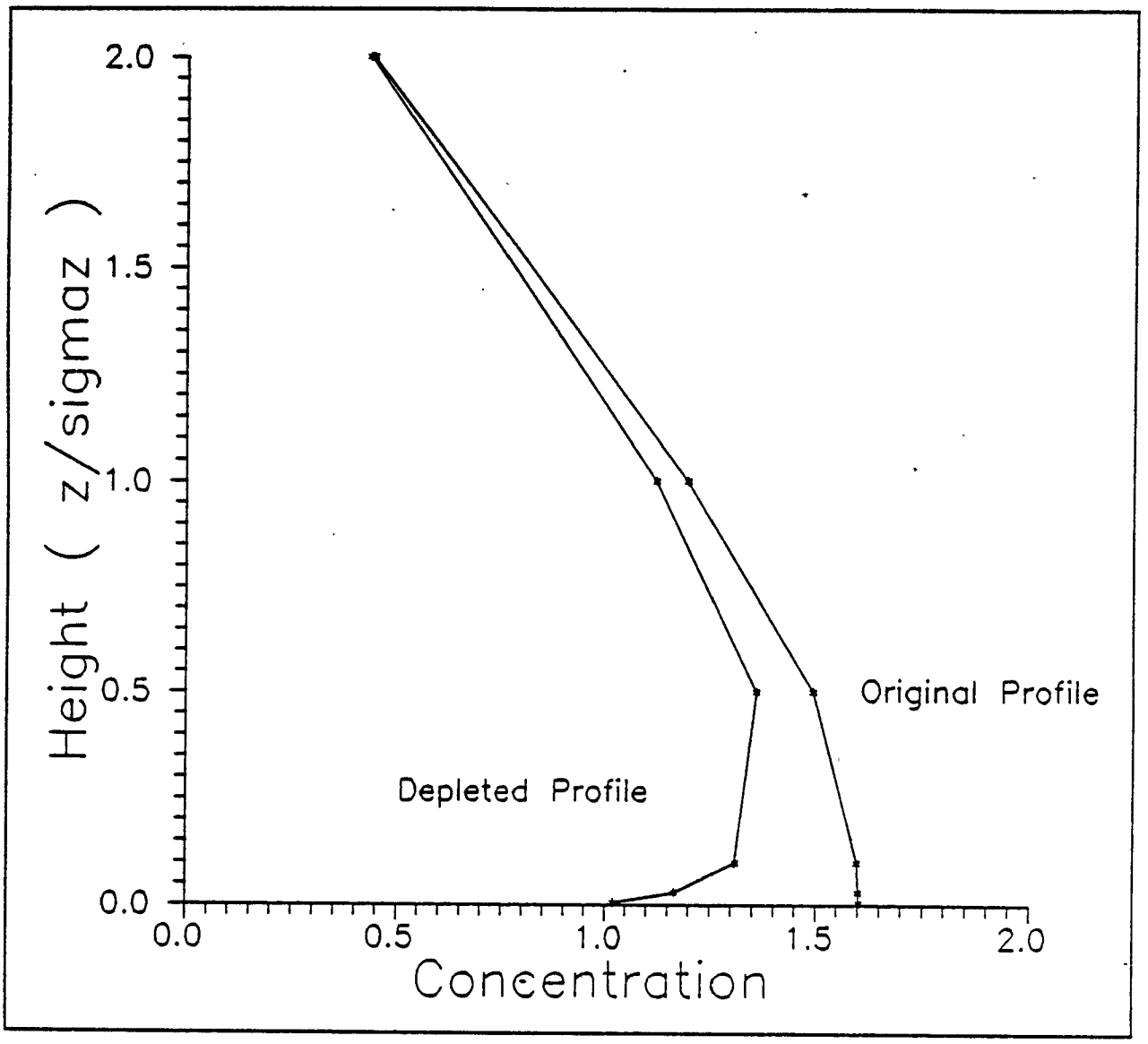

FIGURE E-2. VERTICAL PROFILE OF CONCENTRATION BEFORE AND AFTER APPLYING F_Q AND P(x,z) SHOWN IN FIGURE E-1.

$F_Q(x)$ is a function of the total deposition velocity (v_d), $V(x,z_d,h)$, and $P(x,z_d)$:

$$F_Q(x) = EXP\left[- \int_0^x v_d \, V(x',z_d,h) \, P(x',z_d) \, dx' \right] \tag{E-3}$$

where z_d is a height near the surface at which the deposition flux is calculated. This equation reflects the fact that the material removed from the plume by deposition is just the integral of the deposition flux over the distance that the plume has traveled. For general forms of V(x,z,h) and P(x,z), Equation (E-3) is evaluated numerically.

The deposition velocity for particles generally contains a component related to the settling velocity, v_s. A "tilted plume" is used to simulate the effect of gravitational settling on the plume as a whole. This approximation entails replacing the plume height, h, in Equations (E-1) and (E-2) with

$$h_s = h - \frac{x}{u} v_s \tag{E-4}$$

For large travel-times, h_s can become less than zero. However, the tilted plume approximation is not a valid approach in this region. Therefore, a minimum value of zero must be imposed on h_s. In effect, this limits the settling of the plume, although the deposition velocity continues to account for gravitational settling near the surface.

The profile correction factor P(x,z) is developed by Horst (1983) for the case in which reflection of material from the mixing lid is not important. He finds

$$\begin{aligned} P(x,z) &= P(x,z_d)\left[1 + \frac{v_d - v_s}{v_s}\left(1 - EXP\left[-v_s \, R(z,z_d)\right]\right)\right] \\ P(x,z_d) &= \left[1 + \frac{v_d - v_s}{v_s}\int_0^\infty \frac{V(x,z',o)}{\sqrt{2\pi}\,\sigma_z}\left(1 - EXP\left[-v_s R(z',z_d)\right]\right)dz'\right]^{-1} \end{aligned} \tag{E-5}$$

where $R(z,z_d)$ is an atmospheric resistance to vertical transport. When the product $v_s R(z,z_d)$ is of order 0.1 or less, the exponential function is approximated (for small argument) to simplify P(x,z):

$$\begin{aligned} P(x,z) &= P(x,z_d)\left[1 + (v_d - v_s)\, R(z,z_d)\right] \\ P(x,z_d) &= \left[1 + (v_d - v_s)\int_0^\infty \frac{V(x,z',o)}{\sqrt{2\pi}\,\sigma_z} R(z',z_d)\, dz'\right]^{-1} \end{aligned} \tag{E-6}$$

This simplification is important, since the integral in Equation (E-6) can be computed using analytical approximations for many forms of $R(z,z_d)$ that are consistent with the Briggs' formulas for σ_z (Gifford, 1976). Typically, only the largest particles may have a settling velocity v_s large enough to require the numerical integration of Equation (E-5).

The atmospheric resistance is defined as

$$R(z,z_d) = \int_{z_d}^{z} \frac{dz'}{K(z')} \tag{E-7}$$

where K(z) is the vertical eddy diffusivity. Because we will be using empirical expressions for σ_z, K(z) should be consistent with these. Horst (1983) points out that

$$K = u\ \sigma_z \frac{d\sigma_z}{dx} \tag{E-8}$$

and that

$$\bar{z} = \sqrt{2/\pi}\ \sigma_z \tag{E-9}$$

for a Gaussian plume from a ground-level source, where $\bar{z}$ is the mean height of the distribution of mass in the plume. Using Equation (E-9) to map z to σ_z, Equation (E-7) is represented by

$$R(z,z_d) = \int_{z_d/\sqrt{2/\pi}}^{z/\sqrt{2/\pi}} \frac{\sqrt{2/\pi}}{u\ \sigma_z \dfrac{d\sigma_z}{dx}}\, d\sigma_z \tag{E-10}$$

This allows $R(z,z_d)$ to be evaluated for particular forms of σ_z. Horst provides solutions for

$$\begin{aligned} \sigma_z &= ax \\ \sigma_z &= ax(1 + bx)^{-1/2} \\ \sigma_z &= ax(1 + bx)^{-1} \end{aligned} \tag{E-11}$$

which encompass the forms used for Briggs' rural dispersion curves, as well as Briggs' urban curves for stability classes C, D, E, and F. The solution for urban classes A and B,

$$\sigma_z = ax(1 + bx)^{1/2} \tag{E-12}$$

is derived in Section E-2. (Solutions to Equations (E-7) and (E-6) for each form of σ_z are listed in Section E-2).

E.2 Extension of Solutions for Urban Classes A and B

The Briggs' curves for σ_z for urban locations during stability classes A and B have the form of Equation (E-12). Therefore, Equation (E-10) becomes

$$R(z,z_d) = \sqrt{\frac{2}{\pi}}\,\frac{1}{u}\int_{x(z_d)}^{x(z)} \frac{dx'}{ax'\sqrt{1+bx'}} = \sqrt{\frac{2}{\pi}}\,\frac{1}{au}\ln\left(\frac{\sqrt{1+bx}-1}{\sqrt{1+bx}+1}\right)\Bigg|_{x(z_d)}^{x(z)} \tag{E-13}$$

The limits are implicit functions obtained from Equation (E-9):

$$\sqrt{\frac{\pi}{2}}\,z = a\,x(z)\sqrt{1+b\,x(z)} \tag{E-14}$$

That is, x(z) is the distance at which σ_z equals $z/\sqrt{2/\pi}$. If both sides are squared, x(z) can be expressed as the root of a cubic equation. In developing the FORTRAN code to implement Horst's method, we use an iterative method to solve for the root of Equation (E-14).

Adding Equation (E-13) to the solutions given by Horst for the other forms of σ_z, we have:

$\sigma_z = ax$:

$$R(z,z_d) = \sqrt{\frac{2}{\pi}}\,\frac{1}{au}\ln(z/z_d) \tag{E-15}$$

$\sigma_z = ax/(1+bx)^{1/2}$:

$$R(z,z_d) = \sqrt{\frac{2}{\pi}}\,\frac{1}{au}\left[\ln(z/z_d) + \frac{b}{a}\sqrt{\frac{\pi}{2}}\,(z-z_d)\right] \tag{E-16}$$

$\sigma_z = ax/(1 + bx)$:

$$R(z,z_d) = \sqrt{\frac{2}{\pi}}\,\frac{1}{au}\left[\ln(z/z_d) + \frac{2b}{a}\sqrt{\frac{\pi}{2}}\,(z - z_d) + \frac{3b^2}{2a^2}\sqrt{\frac{\pi}{2}}\,(z^2 - z_d^2)\right] \qquad \text{(E-17)}$$

$\sigma_z = ax(1 + bx)^{1/2}$:

$$R(z,z_d) = \sqrt{\frac{2}{\pi}}\,\frac{1}{au}\ln\left[\frac{\sqrt{1 + bx(z)} - 1}{\sqrt{1 + bx(z)} + 1}\,\frac{\sqrt{1 + bx(z_d)} + 1}{\sqrt{1 + bx(z_d)} - 1}\right] \qquad \text{(E-18)}$$

The profile correction factor, P(x,z), requires the integral of the product of $R(z,z_d)$ and the vertical distribution factor V(x,z,h), which is dominated by a series of exponential functions of height. An analytic solution to this integral is possible for the $R(z,z_d)$ terms involving $\ln(z/z_d)$, $(z-z_d)$ and $(z^2-z_d^2)$; but the complex form of Equation (E-18), coupled with the supplementary relation in Equation (E-14), precludes such a solution. After trying several approximation techniques, the solution for $P(x,z_d)$ with $R(z,z_d)$ given by Equation (E-18), was approximated as follows.

First, a program was developed that solves the integral in Equation (E-6) numerically. This not only allows us to test various approximate results, it can also serve as a numerical solver if no analytical approximations are found to be adequate. Then, we developed an approximate expression for $R(z,z_d)$ for small z, which is facilitated by the fact that the constant b = 0.001 for urban classes A and B:

$$\sqrt{1 + bx} \approx 1 + \frac{bx}{2}$$

or (E-19)

$$(1 + bx) \approx \sqrt{1 + kz}$$

where $k = \frac{2b}{a}\sqrt{\frac{\pi}{2}}$.

This allows Equation (E-18) to be written as

$$R(z,z_d) = \sqrt{\frac{2}{\pi}}\,\frac{1}{au}\,\ln\left[\frac{(1+kz)^{1/4}-1}{(1+kz)^{1/4}+1}\;\frac{(1+kz_d)^{1/4}+1}{(1+kz_d)^{1/4}-1}\right] \tag{E-20}$$

Further expanding $(1 + kz)^{1/4}$ as $1 + kz/4$, the natural log expression in Equation (E-18) becomes

$$\ln\left(\frac{z}{z_d}\right) - \ln\left(\frac{1+\frac{kz}{8}}{1+\frac{kz_d}{8}}\right) \tag{E-21}$$

This gives a leading term that is the same as Equation (E-15), for $\sigma_z = ax$, and the approximate result for P is

$$P(x,z_d) = \left[1 + (v_d - v_s)\,\frac{\sqrt{2}}{\pi}\,\frac{1}{au}\,I\right]^{-1} \tag{E-22a}$$

where

$$I = \ln\left(\frac{\sqrt{2}\,\sigma_z}{z_d}\right) - 1 + \ln\left(1+\frac{kz_d}{8}\right) - \frac{\sqrt{2}\,k\,\sigma_z}{16}\left(\frac{2}{\sqrt{\pi}} - \frac{\sqrt{2}\,k\,\sigma_z}{8}\right) \tag{E-22b}$$

Comparing Equation (E-22) with the numerical solution, the approximate form worked well for small z, but diverged from the correct solution at larger z. Several empirical adjustments produced a good fit for a full range of heights. The resulting analytic expressions for $P(x,z_d)$ for each of the σ_z functions are:

$\sigma_z = ax$:

$$P^{-1}(x,z_d) = 1 + \frac{v_d - v_s}{ua}\sqrt{\frac{2}{\pi}}\left[\ln\left(\frac{\sqrt{2}\,\sigma_z}{z_d}\right) - 1\right] \tag{E-23}$$

$\sigma_z = ax/(1 + bx)^{1/2}$:

$$P^{-1}(x,z_d) = 1 + \frac{v_d - v_s}{ua}\sqrt{\frac{2}{\pi}}\left[\ln\left(\frac{\sqrt{2}\sigma_z}{z_d}\right) - 1 + \frac{b}{a}\left(\sigma_z - \sqrt{\frac{\pi}{2}}\,z_d\right)\right] \tag{E-24}$$

$\sigma_z = ax/(1 + bx)$:

$$P^{-1}(x,z_d) = 1 + \frac{v_d - v_s}{ua}\sqrt{\frac{2}{\pi}}\left[\ln\left(\frac{\sqrt{2}\,\sigma_z}{z_d}\right) - 1 + \frac{2b}{a}\left(\sigma_z - \sqrt{\frac{\pi}{2}}\,z_d\right) + \frac{3b^2}{2a^2}\,\frac{\pi}{2}\left(\sigma_z^2 - z_d^2\right)\right] \qquad \text{(E-25)}$$

$\sigma_z = ax(1 + bx)^{1/2}$:

$$P^{-1}(x,z_d) = 1 + \frac{v_d - v_s}{ua}\sqrt{\frac{2}{\pi}}\left[\ln\left(\frac{\sqrt{2}\,\sigma_{z1}}{z_d}\right) - 1 + \ln\left(1 + \frac{k\,z_d}{8} - \sqrt{\frac{2}{\pi}}\,\frac{k\,\sigma_{z2}}{8}\right)\right] \qquad \text{(E-26)}$$

For the last form, $k = \frac{2b}{a}\sqrt{\frac{\pi}{2}}$, and

$$\sigma_{z1} = \sigma_z\left(1 - .0006\,\sigma_z\right)^2 \qquad \sigma_z \le 300m$$

$$\sigma_{z1} = 0.6724\,\sigma_z \qquad \sigma_z > 300m$$

and

$$\sigma_{z2} = \sigma_{z1} \qquad \sigma_{z1} \le 1000m$$

$$\sigma_{z2} = \sqrt{1000\,\sigma_{z1}} \qquad \sigma_{z1} > 1000m$$

The approximation to the integral in $P(x,z_d)$ for $\sigma_z = ax(1 + bx)^{1/2}$ matches the numerical solution to within 1% for $z_d = 0.03$ m and $\sigma_z \le 4000$ m, and it matches to within about 2% for $z_d = 1$ m over the same height range.

E.3 Mixing-Lid Treatment

The results presented above do not include the presence of a mixing lid. With such a lid, the profile correction factor must operate only within the mixed layer, so that the upper limit in the integral for $P(x,z_d)$ is z_i, not infinity, in Equation (E-6). Furthermore, the standard formulation of $V(x,z,h)$ is also a function of z_i, since the distribution of material in the plume is

"reflected" from $z = z_i$. In principle, the additional reflections in the $V(x,z,h,z_i)$ just add to the number of terms in $P(x,z_d)$, since the form of the integral in Equation (E-6) remains the same. However, most of the emphasis in obtaining $P(x,z_d)$ is placed near the ground, because this is where the depletion correction is most important. Therefore, in the interest of streamlining the implementation of the method, we have adopted an alternate strategy. We solve for $P(x,z_d)$ for the case of well-mixed plumes ($\sigma_z > z_i$), and compare the results with Equations (E-23) through (E-26).

In the well-mixed limit,

$$\frac{V(x,z,h)}{\sqrt{2\pi}\ \sigma_z} = \frac{1}{z_i} \tag{E-27}$$

so that $P(x,z_d)$ involves the integral of terms involving just $\ln(z/z_d)$, $(z-z_d)$, and $(z^2-z_d^2)$, since the exponentials are not present in Equation (E-27). Performing the integrations yields functions that are equivalent to Equations (E-23) through (E-25), except σ_z is replaced by a constant times z_i:

$$\ln\left(\frac{\sqrt{2}\ \sigma_z}{z_d}\right) - \ln\left(\frac{z_i}{z_d}\right) \tag{E-28}$$

$$\left(\sigma_z - \sqrt{\frac{\pi}{2}}\ z_d\right) - \left(\sqrt{\frac{\pi}{8}}\ z_i - \sqrt{\frac{\pi}{2}}\ z_d\right) \tag{E-29}$$

$$\left(\sigma_z^2 - z_d^2\right) - \sqrt{\frac{2}{\pi}}\left(\frac{1}{3}\ z_i^2 - z_d^2\right) = \left(\sqrt{\frac{2}{\pi}}\ \frac{z_i^2}{3} - z_d^2\right) \tag{E-30}$$

Therefore, the effect of the lid is to limit the size of σ_z in evaluating $P(x,z_d)$. Hence, we retain Equations (E-23) through (E-25), but restrict the use of σ_z to values no larger than those that satisfy Equations (E-28) through (E-30). In other words, caps are placed on the value of σ_z used when a mixed layer exists.

Equation (E-26), for $\sigma_z = ax(1+bx)^{1/2}$, is a special case. We were able to solve the integral for the case of complete mixing (Equation E-27), but the result involves many terms. Since the approximate form used in Equation (E-26) performed well in the absence of a mixing lid, we also tested a version in which σ_z was replaced by z_i as in Equation (E-28). This result

also performed well when compared to the numerical integration, so this more compact result was adopted.

E.4 Numerical Integration For $P(x,z_d)$

Because Equation (E-3) involves the numerical evaluation of an integral over the distance from the source to each receptor, an analytic representation of $P(x,z_d)$ is preferred in order to streamline the computations. As discussed in Section E.1, $P(x,z_d)$ can be represented by simple analytic functions so long as $v_s R(z,z_d) \leq 0.1$. However, larger and denser particles (greater than 10 μm in diameter) have settling velocities great enough to violate this condition at times. For these situations, the full expression for $P(x,z_d)$ (Equation E-5) must be solved numerically as well. This means that each point evaluated in Equation (E-3) involves a numerical evaluation of Equation (E-5). This can be time-consuming.

The subroutines developed make use of a general integration routine. It subdivides the interval into more and more equally-spaced segments until the value of the integral converges to within an imposed tolerance. Further study is recommended to optimize these integration procedures. For example, the tolerance level might be too restrictive. Or, an integration technique might be specifically designed for the integrand. We know the form of $V(x,z,h)$ and $R(z,z_d)$, and may be able to increase the efficiency of the integration by designing an algorithm that "knows" where the integrand changes most rapidly, and least rapidly. Fewer points are needed to integrate across regions in which the variation of the integrand is nearly linear.

There is also a possibility that the solution to Equation (E-5) can be approximated simply enough to avoid its numerical solution. We have been able to recast the integral in Equation (E-5) to one of the form:

$$I = \int_{z_d}^{\infty} (z/z_d)^{-v_s A} \, e^{-1/2 D^2 (z + B/D^2)^2} \, dz \qquad \text{(E-31)}$$

for $R(z,z_d)$ of the form

$$R(z,z_d) = A \ln(z/z_d) + B(z - z_d) + C(z^2 - z_d^2) \qquad \text{(E-32)}$$

With a suitable definition of a new variable of integration, it appears that Equation (E-5) could be solved to yield a representation made up of the product of a Gamma function, an exponential function, and a parabolic cylinder function. Such a solution has not been completely worked out, since it is not clear that such a representation would lead to a more efficient evaluation of the integrals.

References

Gifford, F.A., Jr., 1976: Turbulent diffusion - Typing schemes: A review. *Nucl. Saf.*, 17, 68-86.

Horst, T.W., 1983: A correction to the Gaussian source-depletion model. In *Precipitation Scavenging, Dry Deposition and Resuspension*, H.R. Pruppacher, R.G. Semonin, W.G.N. Slinn, eds., Elsevier, NY.

TECHNICAL REPORT DATA
(Please read Instructions on reverse before completing)

1. REPORT NO.	2.	3. RECIPIENT'S ACCESSION NO.
EPA-454/R-94-015		

4. TITLE AND SUBTITLE	5. REPORT DATE
Development and Testing of Dry Deposition Algorithms	April 1994
	6. PERFORMING ORGANIZATION CODE

7. AUTHOR(S)	8. PERFORMING ORGANIZATION REPORT NO.
Joseph S. Scire and Gary E. Moore, Sigma Research Corporation	

9. PERFORMING ORGANIZATION NAME AND ADDRESS	10. PROGRAM ELEMENT NO.
Sigma Research Corporation 196 Baker Avenue Concord, MA 01742	11. CONTRACT/GRANT NO. 68-D9007, Work Assignment 3-1

12. SPONSORING AGENCY NAME AND ADDRESS	13. TYPE OF REPORT AND PERIOD COVERED
U.S. Environmental Protection Agency Office of Air Quality Planning and Standards, TSD Research Triangle Park, NC 27711	Final Report
	14. SPONSORING AGENCY CODE

15. SUPPLEMENTARY NOTES
This document replaces EPA-454/R-92-017. EPA Work Assignment Manager: Jawad S. Touma

16. ABSTRACT

This study was designed to identify dry deposition models suitable for routine use, evaluate and intercompare several techniques, and select the most appropriate approach for use in the Industrial Source Complex (ISC2) model. Reviews were conducted of methods for computing dry deposition velocity, plume depletion, and certain micrometeorological parameters from routinely-available observations. Several observational data bases were identified from the literature and used in testing and evaluating ten particle deposition velocity models. Recommendations for computing particle deposition velocity, plume depletion, and micrometeorological variables were made. These techniques have been incorporated into a revised version of the ISC2 model and related processor programs.

17. KEY WORDS AND DOCUMENT ANALYSIS

a. DESCRIPTORS	b. IDENTIFIERS/OPEN ENDED TERMS	c. COSATI Field/Group
Air Pollution Dry Deposition Air Quality Dispersion Modeling Meteorology		

18. DISTRIBUTION STATEMENT	19. SECURITY CLASS (Report)	21. NO. OF PAGES
Release Unlimited	Unclassified	128
	20. SECURITY CLASS (Page)	22. PRICE
	Unclassified	

EPA Form 2220-1 (Rev. 4-77) PREVIOUS EDITION IS OBSOLETE